

# The potential of actual evaporation

A data-driven study of surface evaporation  
in the Netherlands

Femke A. Jansen



## Propositions

1. Knowledge on environmental drivers of sensible heat flux remains too latent.  
(this thesis)
2. Penman should not have used 'open water' in the title of his seminal paper on evaporation (Penman, 1948).  
(this thesis)
3. Scientific progress is driven by irrational things like humour and intuition.
4. The success of a PhD trajectory is not tied to obtaining the degree.
5. Training university students to live with nature is crucial for more effective environmental education.
6. Acknowledging that we are nature leads to a deeper understanding of environmental issues.
7. Life without death is like evaporation without rainfall.

Propositions belonging to the thesis, entitled

The potential of actual evaporation:

a data-driven study of surface evaporation in the Netherlands

Femke A. Jansen

Wageningen, 7 June 2023

# **The potential of actual evaporation: a data-driven study of surface evaporation in the Netherlands**

Femke A. Jansen

## **Thesis committee**

### **Promotors**

Dr A.J. Teuling

Associate professor, Hydrology and Quantitative Water Management Group  
Wageningen University & Research

Prof. Dr R. Uijlenhoet

Professor of Hydrology & Water Resources  
Delft University of Technology

### **Other members:**

Prof. Dr J. Vila-Guerau de Arellano, Wageningen University & Research

Dr N.E. Theeuwes, Royal Netherlands Meteorological Institute, De Bilt, The Netherlands

Dr J.R. Larsen, University of Birmingham, United Kingdom

Prof. Dr A. Verhoef, University of Reading, United Kingdom

This research was conducted under the auspices of the Graduate School for  
Socio-Economic and Natural Sciences of the Environment (SENSE)



# The potential of actual evaporation: a data-driven study of surface evaporation in the Netherlands

Femke A. Jansen

## Thesis

submitted in fulfilment of the requirements for the degree of doctor  
at Wageningen University  
by the authority of the Rector Magnificus,  
Prof. Dr A.P.J. Mol,  
in the presence of the  
Thesis Committee appointed by the Academic Board  
to be defended in public  
on Wednesday 7 June 2023  
at 4 p.m. in the Omnia Auditorium.

Femke A. Jansen

The potential of actual evaporation:

a data-driven study of surface evaporation in the Netherlands

xvi+162 pages.

PhD thesis, Wageningen University, Wageningen, the Netherlands (2023)

With references, with summary in English and Dutch

ISBN 978-94-6447-621-7

DOI 10.18174/589524

© 2023 Femke A. Jansen

# Summary

Surface evaporation is a crucial component in the global hydrological cycle. In that capacity, accurate estimates evaporation rates are of vital importance for effective water management. This becomes even more critical with the expected intensification of the hydrological cycle as a consequence of global warming. However, evaporation remains one of the most difficult hydrological processes to understand and experimentally measure. Monitoring and forecasting of evaporation has seen rapid development over the recent decades, driven by both technological and scientific developments. Traditionally, most studies have been dedicated to analysing terrestrial surface evaporation, while the study of evaporation from water bodies has lagged behind (**Chapter 1**). A thorough understanding of the dynamics and drivers of actual surface evaporation over a landscape is essential to correctly parameterize evaporation in hydrological models, to make well-supported short-term predictions and long-term projections of surface evaporation. This thesis aims to *identify the drivers of surface evaporation, including open water evaporation, based on observations conducted in the temperate maritime climate of the Netherlands*. To do so, we analysed and compared several evaporation models (Chapter 3), determined the main drivers of evaporation over a large inland water body (Chapter 4), and compared drivers of evaporation over different land cover types (Chapter 5). The focus area of this thesis is the Netherlands, which provides a unique opportunity for this study because of the relatively dense evaporation measurement network. The study area, data and measurement methods are introduced in **Chapter 2**.

In **Chapter 3**, we systematically compare estimated evaporation from six evaporation models: Penman, De Bruin-Keijman, Makkink, Hargreaves, Granger-Hedstrom and FLake. Evaporation is parameterized differently in each of these models, which makes them sensitive to different drivers. For the Lake IJssel region, we characterized the (dis)agreement between the models at various temporal scales ranging from hourly to decadal periods during the historical period (1960–2018) and the projected future period (2019–2100). We found relatively large disagreement between the models at shorter timescales, which resulted in distinct diurnal cycles of estimated evaporation. The models agreed more with longer timescales, although there were still large differences in the projected evaporation trends (2019–2100), showing a positive trend to a greater (i.e. Penman, De Bruin-Keijman, Makkink, and Hargreaves) or lesser extent (i.e. Granger-Hedstrom and FLake). As a

result of the disagreement between the models, the simulated water losses of the Lake IJssel region varied substantially. The selection of an evaporation model can thus have substantial impact on the estimated evaporation, of which water managers should be aware in their decision making.

In **Chapter 4**, we conducted a unique long-term measurement campaign to infer the principal drivers of open water evaporation. To this end, two eddy covariance systems were employed at two locations, Stavoren and Trintelhaven, at the border of Lake IJssel during two summer periods. These measurements were used to develop data-driven models for both locations. We found that wind speed and vertical vapour pressure gradient were the principal drivers of hourly open water evaporation. In other words, exchange efficiency controls the exchange processes of energy and water between the water surface and the atmosphere at this timescale. This finding is in agreement with the well-established Dalton equation. Supported by the positive results of the validation of the models, the results of Chapter 4 showed that simple data-driven models, consisting of only two variables, provide reliable estimates of open water evaporation.

Land cover is known to control the land-atmosphere exchange of water and energy through the partitioning of solar energy into latent and sensible heat. In **Chapter 5**, we study how the controls of daily and midday latent and sensible heat fluxes over different land cover types are distributed along three axes: energy availability, water availability and exchange efficiency. To do so, a multitude of (historical) flux observations, all within the same climatic zone and in relative close proximity, were required. Therefore, we used eddy covariance observations from 19 sites in the Netherlands, covering six land cover types: grass, forest, urban, open water, crop and peatland swamp. Based on regression analyses, we found a clustering of sites that belonged to the same land cover type along the three axes. This indicated that land cover can partly explain the variation of the daily and midday latent heat flux. We also found that the midday and daily sensible heat fluxes are less sensitive to land cover type. The relation found between land cover type and drivers can be used to optimise evaporation models.

**Chapter 6** synthesizes the main findings of the three core chapters. The main conclusions are: 1) there is a substantial effect of the parameterization of evaporation in hydrological models on the estimated evaporation rates; 2) wind speed and vertical vapour pressure gradient, i.e. exchange efficiency, are found to be the principal drivers of hourly and daily open water evaporation; 3) land cover partly explains the variation of daily and midday evaporation. Therefore, water bodies and land surfaces require different evaporation parameterizations in hydrological models. Based on observations, exchange efficiency is found to be the principal driver of open water evaporation. On the other hand, energy availability is found to be the main control of land surface evaporation.

In this thesis, regression models have been used to determine the explanatory variables of evaporation over different land cover types. However, there are some limitations to

using regression models. For instance, these models do not necessarily prove causal relationships between correlated variables within the coupled land-atmosphere system. In addition, long time series are required to accurately determine extreme values. The use of regression models in a changing environment, e.g. prone to climate and land cover changes, is therefore limited and caution should be taken when applying these models to regions with a different climatic, geographical and topographical setting. Despite these constraints, regression models are able to capture patterns in the data and provide the most important explanatory variables, even when the underlying physical mechanisms are not fully understood.

The distinct difference found in the dynamics of open water evaporation compared to terrestrial evaporation (see Chapters 4 and 5) is one of the main findings of this thesis and has direct implications for water management in the Netherlands. Currently, the Directorate-General for Public Works and Water Management (Rijkswaterstaat, RWS) uses the energy-driven Makkink equation, including a correction factor, to estimate open water evaporation in the Landelijk Hydrologisch Model (LHM). However, based on the results of this thesis, I would recommend implementation of a transport-driven model in the LHM to correctly estimate open water evaporation, also at the shorter timescales. Given the importance of wind speed in explaining open water evaporation, measures to reduce wind speed could be explored to decrease open water evaporation of Lake IJssel. It is more difficult to control or change the dynamics of evaporation over forests in the more elevated areas in the Netherlands, with deep groundwater levels. However, mean evaporation may be decreased through land cover conversion to deciduous trees or other plants that transpire less in the long-term. As a result, recharge of the area could increase. The impact of the proposed measures on the ecosystem should first be studied thoroughly before they are considered.





# Samenvatting

Oppervlakteverdamping is een cruciaal onderdeel van de globale hydrologische cyclus. Nauwkeurige schattingen van verdamping zijn essentieel voor effectief waterbeheer, temeer daar een intensivering van de hydrologische cyclus wordt verwacht als gevolg van de opwarming van de aarde. Verdamping blijft echter een van de moeilijkste hydrologische processen om te begrijpen en te meten. Het monitoren en voorspellen van verdamping heeft een snelle ontwikkeling doorgemaakt de afgelopen decennia, gedreven door zowel technologische als wetenschappelijke ontwikkelingen. Van oudsher zijn de meeste onderzoeken gewijd aan de analyse van verdamping van het landoppervlak, terwijl onderzoeken gericht op verdamping boven waterlichamen zijn achter gebleven (**Hoofdstuk 1**). Een grondig begrip van de dynamiek en de sturende variabelen (*drivers*) van de werkelijke oppervlakteverdamping over een heel landschap is essentieel om verdamping correct te parametriseren in hydrologische modellen. Op die manier kunnen er goed onderbouwde korte- en langetermijnverwachtingen van verdamping gemaakt worden. Het doel van dit proefschrift is om *de sturende variabelen van oppervlakteverdamping, inclusief openwaterverdamping, te identificeren op basis van observaties in het gematigde maritieme klimaat van Nederland*. Om dit doel te bereiken hebben we meerdere verdampingsmodellen geanalyseerd en met elkaar vergeleken (**Hoofdstuk 3**), de belangrijkste sturende variabelen van verdamping boven een groot binnenwater vastgesteld (**Hoofdstuk 4**) en de sturende variabelen van verdamping over verschillende landgebruikstypen vergeleken (**Hoofdstuk 5**). Als studiegebied is in dit proefschrift Nederland gekozen. Dit studiegebied biedt een uitgelezen kans voor dit onderzoek vanwege het relatief dichte netwerk van verdampingsmetingen. Het studiegebied, de data en de meetmethoden worden in **Hoofdstuk 2** geïntroduceerd.

In **Hoofdstuk 3** vergelijken we systematisch de geschatte verdamping volgens zes verdampingsmodellen: Penman, De Bruin-Keijman, Makkink, Hargreaves, Granger-Hedstrom en FLake. In elk van deze modellen wordt verdamping anders geparametriseerd. Hierdoor zijn ze gevoelig voor verschillende factoren die verdamping beïnvloeden. Voor het IJsselmeergebied hebben we de overeenkomsten en verschillen tussen de modellen gekwantificeerd. Dit hebben we gedaan op verschillende tijdschalen, variërend van uurlijkse tot tienjarige perioden, voor een historische periode (1960–2018) en een toekomstige periode (2019–2100). We vonden relatief grote verschillen tussen de modellen op de kortere tijdschalen, wat resulteerde in verschillende dagelijkse cycli van geschatte verdamping. Op

langere tijdschalen waren de modellen het meer met elkaar eens, hoewel er nog steeds grote verschillen bestonden in de geprojecteerde trends van verdamping (2019–2100), met een positieve trend in verdamping in meerdere (i.e. Penman, De Bruin-Keijman, Makkink, en Hargreaves) of mindere mate (i.e. Granger-Hedstrom en FLake). Als gevolg van de verschillen tussen de modellen varieerde het geschatte waterverlies door verdamping van het IJsselmeer aanzienlijk. De keuze van een verdampingsmodel kan dus een aanzienlijke invloed hebben op de geschatte verdamping. Hierop moeten waterbeheerders bedacht zijn bij hun besluitvorming.

In **Hoofdstuk 4** hebben we een unieke langlopende meetcampagne uitgevoerd om de belangrijkste sturende variabelen van openwaterverdamping vast te kunnen stellen. Hiertoe zijn er twee eddy-covariantiesystemen ingezet op twee locaties gelegen aan de rand van het IJsselmeer (Stavoren en Trintelhaven) gedurende twee zomerperiodes. Hun metingen zijn gebruikt om datagestuurde modellen te ontwikkelen voor beide locaties. Uit de analyses bleek dat windsnelheid en verticale dampdrukgradiënt de belangrijkste sturende variabelen waren van openwaterverdamping op uurlijkse tijdschaal. Met andere woorden: het is de efficiëntie van uitwisseling die op deze tijdschaal het uitwisselingsproces van energie en water tussen het wateroppervlak en de atmosfeer bepaalt. Deze bevinding is in overeenstemming met het bekende verdampingsmodel van Dalton. De validatie van onze datagestuurde modellen liet een positief resultaat zien. Dit ondersteunt de resultaten van Hoofdstuk 4, waarin we hebben aangetoond dat simpele datagestuurde modellen, die slechts uit twee variabelen bestaan, betrouwbare schattingen van openwaterverdamping leveren.

Het is bekend dat landgebruik de uitwisseling van water en energie tussen het land en de atmosfeer beïnvloedt via de verdeling van zonne-energie in latente en sensibele warmte. In **Hoofdstuk 5** onderzoeken we hoe de sturende variabelen van latente en sensibele warmtefluxen voor verschillende landgebruikstypen verdeeld zijn langs de volgende drie assen: energiebeschikbaarheid, waterbeschikbaarheid en uitwisselingsefficiëntie. Deze analyse is uitgevoerd op zowel dagelijkse tijdschaal als op enkel de middaguren. Hiervoor was een veelvoud aan (historische) fluxmetingen nodig, allemaal gemeten binnen dezelfde klimaatzone en op relatief korte afstand van elkaar. Daarom hebben we eddy-covariantiemetingen gebruikt van 19 meetlocaties in Nederland, die zes verschillende landgebruikstypen beslaan: grasland, bos, stedelijk gebied, water, akkerland en veenmoeras. Op basis van regressieanalyses hebben we een clustering langs de drie assen gevonden van locaties die tot hetzelfde landgebruikstype behoren. Dit duidt erop dat landgebruik de variatie van de latente warmteflux gedurende zowel het gehele etmaal als enkel de middaguren deels kan verklaren. We vonden ook dat de sensibele warmteflux minder gevoelig is voor landgebruik. De relatie tussen landgebruik en sturende variabelen van verdamping kan worden gebruikt om verdampingsmodellen te verfijnen.

**Hoofdstuk 6** vat de belangrijkste bevindingen van de drie kernhoofdstukken samen. De belangrijkste conclusies zijn: 1) er is een aanzienlijk effect van de manier waarop verdamping wordt geparametriseerd in hydrologische modellen op de geschatte verdampingswaarde; 2) windsnelheid en verticale dampdrukgradiënt, oftewel de uitwisselingsefficiëntie, zijn de belangrijkste sturende variabelen van openwaterverdamping op zowel de dagelijkse tijdschaal als op enkel de middaguren; 3) landgebruik verklaart deels de variatie van verdamping op zowel de dagelijkse tijdschaal als op enkel de middaguren. Waterlichamen en landoppervlakken vereisen daarom verschillende manieren van parametriseren van verdamping in hydrologische modellen. Op basis van metingen blijkt dat uitwisselingsefficiëntie de belangrijkste sturende factor is voor openwaterverdamping, terwijl energiebeschikbaarheid de belangrijkste sturende factor is voor de verdamping van landoppervlakken.

In dit proefschrift zijn regressiemodellen gebruikt om de sturende variabelen van verdamping te bepalen voor verschillende landgebruikstypen. Er zijn echter enkele beperkingen bij het gebruik van dergelijke modellen. Zo bewijzen deze modellen niet noodzakelijkerwijs causale verbanden tussen gecorreleerde variabelen binnen het gekoppelde land-atmosfeersysteem. Bovendien zijn er lange tijdreeksen nodig om extreme waarden nauwkeurig te kunnen bepalen. Het gebruik van regressiemodellen in een veranderende omgeving, zoals ten gevolge van veranderingen in klimaat en landgebruik, is daardoor ook beperkt. Daarom is voorzichtigheid geboden bij het toepassen van deze modellen in regio's in een andere klimatologische, geografische en topografische context. Ondanks deze beperkingen zijn regressiemodellen in staat om de patronen in de data te vatten en om de belangrijkste sturende variabelen te vinden, zelfs wanneer de onderliggende fysische mechanismen niet volledig worden begrepen.

Het opvallende verschil in de dynamiek van openwaterverdamping in vergelijking met verdamping van landoppervlakken (zie Hoofdstukken 4 en 5) is een van de belangrijkste bevindingen van dit proefschrift en heeft een directe implicatie voor het waterbeheer in Nederland. Momenteel gebruikt Rijkswaterstaat het energiestuurde model van Makkink, inclusief een correctiefactor, om openwaterverdamping in het Landelijk Hydrologisch Model (LHM) te schatten. Op basis van de resultaten van dit proefschrift zou ik echter aanbevelen om een transportgestuurd verdampingsmodel in het LHM te implementeren om zodoende openwaterverdamping ook op de kleinere tijdschalen correct te kunnen schatten. Gezien het belang van windsnelheid bij het verklaren van openwaterverdamping kunnen maatregelen onderzocht worden om de windsnelheid rondom en daarmee ook de verdamping van het IJsselmeer te verminderen. Het is minder evident om de verdampingsdynamiek van bossen in de hogergelegen delen van Nederland, met diepe grondwaterstanden, te reguleren of te veranderen. De gemiddelde verdamping kan wellicht wel worden verminderd door het landgebruik te veranderen naar loofbos of andere vegetatie die op de lange termijn minder transpireert. De wateraanvulling van het gebied zou hierdoor kunnen toenemen. De impact van dergelijke maatregelen op het ecosysteem moet echter eerst grondig worden onderzocht voordat deze overwogen worden.





# List of symbols

$\alpha$	Albedo (-)
$\beta$	Bowen ratio (-)
$\Delta e$	Vertical vapour pressure gradient (kPa)
$\epsilon_a$	Apparent emissivity (-)
$\epsilon_s$	Surface emissivity (-)
$\gamma$	Psychrometric constant (kPa °C <sup>-1</sup> )
$\mu$	Mean of variable (mm d <sup>-1</sup> )
$\rho_a$	Air density (kg m <sup>-3</sup> )
$\sigma$	Standard deviation of variable (mm d <sup>-1</sup> )
$\sigma_{\text{SB}}$	Stefan-Boltzmann constant (= $5.67 \cdot 10^{-8} \text{ W m}^{-2} \text{ K}^{-4}$ )
$c_p$	Specific heat of air (J K <sup>-1</sup> kg <sup>-1</sup> )
$E$	Evaporation (mm d <sup>-1</sup> )
$e_a$	Vapour pressure of the air (kPa)
$e_s$	Saturation vapour pressure of the air (kPa)
$E_{\text{water}}$	Open water evaporation (mm d <sup>-1</sup> )
$G$	Ground heat flux (W m <sup>-2</sup> )
$H$	Sensible heat flux (W m <sup>-2</sup> )
$K^*$	Net shortwave radiation (W m <sup>-2</sup> )
$K_{\text{in}}$	Incoming shortwave radiation (W m <sup>-2</sup> )
$L_{\text{e,out}}$	Emitted longwave radiation (W m <sup>-2</sup> )
$L_{\text{in}}$	Incoming longwave radiation (W m <sup>-2</sup> )
$L_{\text{out}}$	Outgoing longwave radiation (W m <sup>-2</sup> )
$L_v$	Latent heat of vaporization (J kg <sup>-1</sup> )
$LE$	Latent heat flux (W m <sup>-2</sup> )
$P$	Precipitation (mm d <sup>-1</sup> )
$P_a$	Air pressure (kPa)
$q$	Specific humidity of air (kg m <sup>-3</sup> )
$r_a$	Aerodynamic resistance factor (s m <sup>-1</sup> )
$R_n$	Net radiation (W m <sup>-2</sup> )
$r_s$	Surface resistance factor (s m <sup>-1</sup> )
$s$	Slope of saturated vapour pressure curve (kPa °C <sup>-1</sup> )

$T_a$	Air temperature (°C or K, depending on the equation)
$T_s$	Surface temperature (°C or K, depending on the equation)
$T_{\text{water}}$	Water temperature (°C or K, depending on the equation)
$u$	Wind speed ( $\text{m s}^{-1}$ )

# Contents

	Page
Summary	v
Samenvatting	ix
List of symbols	xiii
1   Introduction	1
2   Study area, data and methods	21
3   (Dis)agreement between evaporation models	37
4   Observed drivers of open water evaporation	59
5   Land cover control on latent and sensible heat fluxes	85
6   Synthesis	113
Appendices	127
References	137
Statement of authorship contribution	155
Acknowledgements	157
Graduate school certificate	160



# Chapter 1

## Introduction



## 1.1 Evaporation and the hydrological cycle

### 1.1.1 Evaporation in the hydrological cycle

Water is a vital element on Earth as it cycles endlessly through the atmosphere, oceans and the Earth's surface in altering states. One of the main processes in the global hydrological cycle is evaporation (Jung et al., 2010). Evaporation represents the water flux from the Earth's surface to the atmosphere as the state of the water transitions from liquid to gas. Once in the atmosphere, the water molecules will ultimately condensate and form clouds, which will eventually precipitate out again. Land evaporation is a major source of water for land precipitation. Van der Ent et al. (2010) have shown that a substantial part, nearly 60 %, of all land evaporation will return as precipitation over land. In other words, precipitation over land heavily depends on moisture recycling through land evaporation. The precipitated water can subsequently follow different pathways. Part of the water will evaporate directly after it precipitated out, either from water surfaces (*open water evaporation*) or vegetation (*interception evaporation*). The remaining part will infiltrate into the soil, from which it can either (i) evaporate (*bare soil evaporation*), (ii) be taken up by vegetation through their roots and evaporated through their stomata (*transpiration*), or (iii) percolate through to deeper soil layers thereby recharging the groundwater. Groundwater can subsequently be drained and discharged through ditches, streams and rivers to end up in the oceans.

There have been strong discussions in the hydrological community on what terminology to use for the evaporation process (Savenije, 2004; Miralles et al., 2020). *Evaporation* and *evapotranspiration* are the most common terms used. While 'evaporation' has been used for centuries (Miralles et al., 2020), 'evapotranspiration' only started to appear in scientific literature since the 1940s, referring to the integrated land surface evaporation. Nowadays, the term evapotranspiration dominates the literature (Miralles et al., 2020). However, evapotranspiration cannot appropriately be used when referring to evaporation from open water bodies, and is also less intuitive to use for evaporation from urban areas. In this thesis, therefore, evaporation is the preferred term as it is the general terminology that refers to the phase transition of water from liquid to gas. To refer to one of the components of evaporation more specific terminology will be used, e.g. open water evaporation, transpiration, etc.

### 1.1.2 The physical process of evaporation

Evaporation is the process by which water molecules escape from the surface of liquid water and enter the atmosphere as gas. Energy input is required for this phase transition of water from liquid to gas (Feynman, 1964). The energy input causes the water molecules to vibrate and move increasingly faster until they escape as water vapour molecules into the atmosphere. Evaporation is thus connecting the hydrological and the energy cycle.

The historical line of the development of hypotheses on the physical process of evaporation will be described in Section 1.2.

From a hydrological perspective, a distinction can be made between evaporation from water bodies, such as oceans and inland lakes, and evaporation from terrestrial surfaces. The latter is often referred to as evapotranspiration, which includes multiple surface evaporation components as described in Section 1.1.1: transpiration, interception and bare soil evaporation. An important difference between open water evaporation and land surface evaporation is the location and capacity of heat storage. As solar radiation can penetrate the water surface, energy can be delivered and stored in the whole volume of the water body (Brutsaert, 1982; Kleidon and Renner, 2017). This means that heat storage takes places below the atmosphere-water interface (see Fig. 1.1). Heat storage on a land surface, by contrast, takes place in the lower atmosphere, vegetation and the upper soil layer. Furthermore, the specific heat capacity of a water body ( $4.2 \text{ kJ kg}^{-1} \text{ }^{\circ}\text{C}^{-1}$ ) is much larger than that of a land surface ( $< 1 \text{ kJ kg}^{-1} \text{ }^{\circ}\text{C}^{-1}$ ). These distinct characteristics of water compared to land result in different dynamics of water and heat exchange between the atmosphere and the surface, which is reflected in both the seasonal and daily cycle of evaporation (Brutsaert, 1982). The large heat capacity of a water body causes a delay in the release of energy. At night-time, the water remains warmer compared to the more rapidly cooling air above it. As a consequence, heat stored in the water is released into the air, thereby warming the air above the lake. This warming causes the air to be less stable than the surrounding air, which reinforces evaporation (Kleidon and Renner, 2017). These unstable conditions during the night, result in continued night-time evaporation (see Fig. 1.1). Evaporation over land surfaces responds more directly to input of solar radiation and often without noticeable delay compared to water bodies.

### 1.1.3 Drivers of evaporation: water, energy and transport

Evaporation requires three principal elements: water, the supply of energy required for the phase transition and a transport mechanism to transport water away from the evaporating surface.

- **WATER**

There are several reservoirs of water within the hydrological cycle: intercepted precipitation, soil water, water in vegetation, and surface water of lakes, oceans, rivers, wetlands, and ponds on impervious surface layers.

- **ENERGY**

The energy required for the phase transition of water is also known as the latent heat of vaporization. The supply of energy originates from the sun, which drives the hydrological and energy cycles. When solar radiation reaches the Earth's surface it is partially absorbed and partially reflected back. The net radiation, which is the

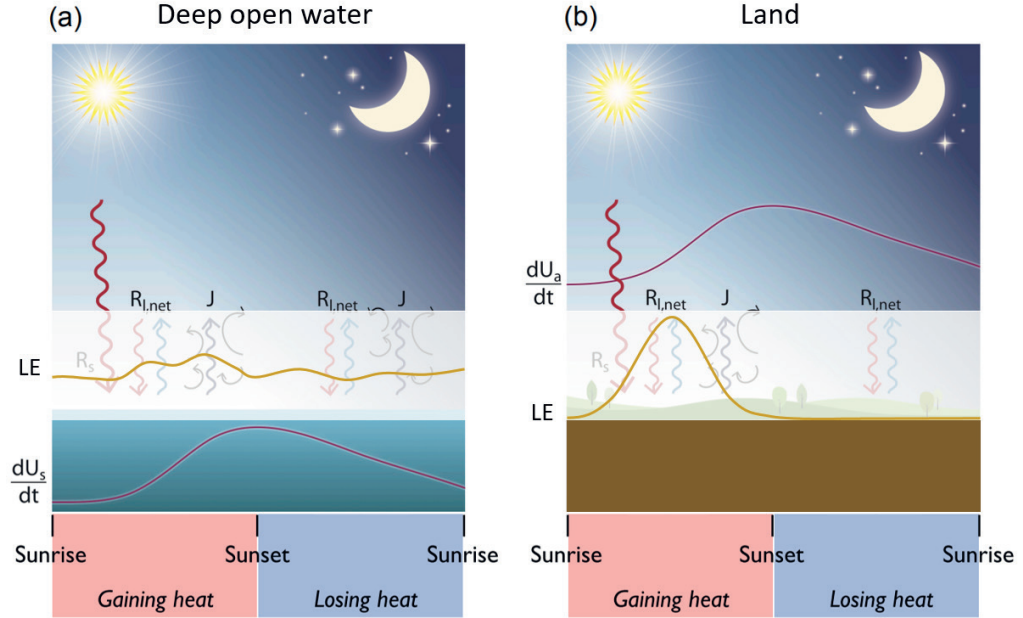


**Figure 1.1:** Schematic diagram of the diurnal cycle of heat storage changes and evaporation of (a) a deep open water surface and (b) a land surface. Adjusted after Kleidon and Renner (2017). Heat storage change ( $dU/dt$ ) takes place below the water-atmosphere surface, while above a land surface it takes place in the lower atmosphere. The resulting stable conditions above the land surface prevent evaporation ( $LE$ ), while evaporation continues during day and night above a water surface. In the background the following elements of the energy balance are shown:  $R_{l,net}$  is the net long-wave radiation,  $R_s$  the incoming shortwave radiation, and  $J$  refers to turbulent fluxes.

net balance between incoming and outgoing radiation, is partitioned into the latent heat flux (evaporation), sensible heat flux, and the ground heat flux.

- **TRANSPORT**

There are different mechanisms through which water vapour can be transferred away from the surface into the atmosphere. Evaporation through the mechanism of diffusion occurs through random movement of water molecules, which is the result of concentration gradients, e.g. the vapour pressure gradient. A more effective vertical exchange of water vapour than diffusion is through turbulence. Advection is the transport of water vapour as a result of mass motion of the atmosphere driven by wind or other large-scale atmospheric motions. In meteorology, advection often refers to the horizontal component of motion. Advection helps to prevent the air above the surface-atmosphere interface from becoming saturated, which would otherwise stagnate the evaporation process.

Environmental factors such as soil moisture content, vegetation type, land cover and atmospheric conditions are linked to these drivers of evaporation. Potential evaporation is the evaporation that theoretically can take place given the actual meteorological conditions, the land cover, and under conditions with sufficient water availability. Hence, potential evaporation is a measure of the atmospheric demand for water. Atmospheric demand refers to the capacity of the atmosphere to hold water and is determined by air temperature, solar radiation, relative humidity and wind speed. When atmospheric demand is high, potential evaporation increases. Actual evaporation is the evaporation that occurs in reality, given the meteorological conditions, the land cover, and the actual water availability at the time. Therefore, under water-limited conditions actual evaporation does not meet the potential evaporation.

Under water-limited conditions at a land surface, soil moisture can be directly linked to evaporation rates (Seneviratne et al., 2010; Dirmeyer, 2011). When soil moisture is reduced plants may close their stomata, thereby increasing the stomatal resistance and reducing the transpiration to regulate their water loss, i.e. a positive land-atmosphere feedback loop. Vegetation affects evaporation also through other characteristics such as the rooting depth, aerodynamic roughness, albedo and leaf area index (Pielke and Avissar, 1990; Hoek van Dijke et al., 2019; Breil et al., 2021). When soil moisture is plentiful, a system is assumed to be energy-limited, in which evaporation meets its potential rates. However, a transport mechanism remains required to prevent the air from becoming saturated, thereby reducing evaporation.

In case of a water body, water availability will by definition not be limited. This implies that open water evaporation is determined by the other two principal elements: energy availability and transport. Yet, as already mentioned in Section 1.1.2, the large heat storage capacity of water and related delay of energy release, results in different evaporation dynamics compared to land surfaces (Brutsaert, 1982). This suggests that at relatively short timescales, transport is a more important driver for evaporation, as was already proposed by Dalton (1802) (see Sect. 1.2).

#### 1.1.4 Changes in evaporation

The land surface and the atmosphere are closely coupled across a continuum of spatial and temporal scales. Surface properties (e.g. soil moisture, land cover, and heat storage capacity) and atmospheric conditions (e.g. vapour pressure deficit, net radiation) determine the strength of this coupling. The complexity of the interaction and feedbacks between the surface and the atmosphere, e.g. between soil moisture and evaporation (see Sect. 1.1.3), makes it challenging to study changes in states (e.g. soil moisture) and fluxes (e.g. evaporation). Hence, it is not straightforward to determine how evaporation will change under changing surface characteristics or atmospheric conditions.

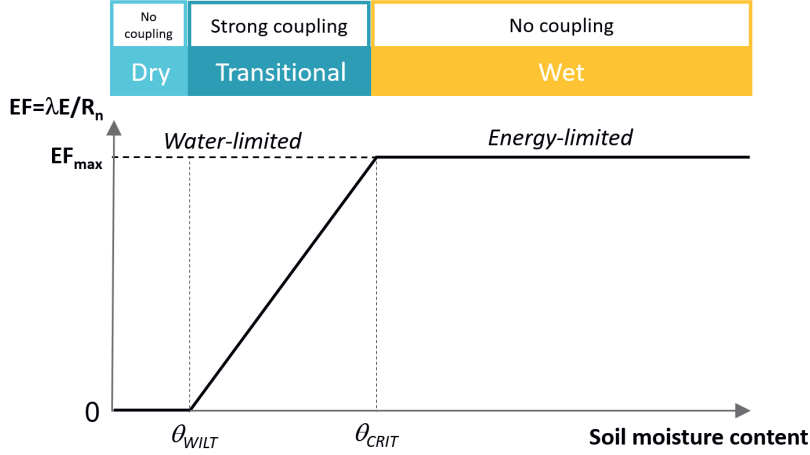


**Figure 1.2:** Conceptual framework for the impact of soil moisture on evaporation and the corresponding soil moisture and evaporation regimes. Adapted from Seneviratne et al. (2010). EF denotes the evaporative fraction and  $\theta_{wilt}$  and  $\theta_{crit}$  the soil moisture content at wilting point and critical point, respectively. Coupling refers to the land-atmosphere coupling through the impact of soil moisture content on evaporation variations.

#### *The role of soil moisture*

Through its coupling to evaporation, soil moisture is an important part of the energy and water cycle (Seneviratne et al., 2010). The role of soil moisture content and its impact on evaporation is especially strong for (soil) water-limited regimes. In these regimes, transpiration through vegetation will be reduced in the case of low soil moisture contents. The relation between soil moisture content and evaporation fraction (EF) as described by Seneviratne et al. (2010) (see Fig. 1.2), can be used to determine whether a system can be defined as energy-limited or soil moisture-limited (Feldman et al., 2019). Above a critical moisture content the EF is insensitive to moisture content, i.e. the system is energy-limited. Below this critical threshold the system is soil moisture-limited. The EF linearly decreases with soil moisture content, until the wilting point is reached, in which wilting point refers to the soil moisture content below which water is not accessible to plants anymore. In this transitional regime, soil moisture impacts the coupling between the land surface and the atmosphere through evaporation strongest. Below wilting point, i.e. the dry regime, the EF becomes zero.

#### *The role of climate change*

The hydrological cycle is projected to intensify as a consequence of global warming (Huntington, 2006; Oki and Kanae, 2006; Jung et al., 2010). As a result, the mean soil moisture content and evaporation are projected to change. These changes vary regionally

depending on the combination of dominant evaporation drivers and changes in forcings. For the Boreal summer months (JJA) soil moisture is projected to decrease in Europe and the Southern U.S., which can be related to decreased precipitation during those months and to dry conditions (i.e. low precipitation, high evaporation) during the preceding months (Seneviratne et al., 2006; Seneviratne et al., 2010). The projected decrease in soil moisture results in decreased evaporation for the Southern U.S. and the Mediterranean area. However, this is not the case for Central Europe. These regional differences can be related to the spatial distribution of energy-limited and water-limited regimes, or, more specifically the transitional regimes (Teuling et al., 2009; Seneviratne et al., 2010).

The projected changes in mean soil moisture content can also explain the projected interannual variability in evaporation during summer periods in Europe (Seneviratne et al., 2006; Seneviratne et al., 2010). The mean climate regime in Central Europe is projected to shift from a wet to a transitional regime. As a result, evaporation becomes more sensitive to mean soil moisture changes (see Fig. 1.2), and thus the projected temporal variability of evaporation increases in those regions in Central Europe with a transitional regime. The perturbations in the land surface energy caused by changes in soil moisture content, also impact atmospheric temperatures, as more energy is dissipated in the form of sensible heat. Increased air temperature in turn enhances the atmospheric demand for evaporation (Teuling, 2018a; Miralles et al., 2019). Increased climate variability results in summers with increasing air temperatures, increasing evaporative demand and increasing precipitation deficits. It has been shown that this will inevitably result in more frequent and more intense droughts and heatwaves, which will have a large impact on society and ecosystems (Schär et al., 2004; Seneviratne et al., 2006; Fischer and Schär, 2010; Miralles et al., 2014; Teuling et al., 2010; Teuling, 2018b; Miralles et al., 2019).

#### *The role of land cover change*

Besides climate factors, changes in land cover also affect evaporation. Focusing on Europe, Teuling et al. (2019) found that changes in both climate (represented by precipitation and potential evaporation) and land use (indicated by forest cover and urban fraction) affect the amount and spatial distribution of evaporation at a decadal time scale. The resulting difference in evaporation from 1960 to 2010 shows a strong latitudinal gradient, from increased evaporation in Northern Europe, towards decreased evaporation in Southern Europe (see Fig. 1.3).

Land use and climate factors contribute in a comparable manner to the net changes of evaporation over the whole continent (Teuling et al., 2019). However, locally and regionally, the absolute impact of land use and climate on changes in evaporation differs, illustrating the regional differences in water flux partitioning. For instance, the effect of urbanization around Paris has led to a decrease in evaporation, while the net effect of land use change and climate combined, has led to a small increase in evaporation. In

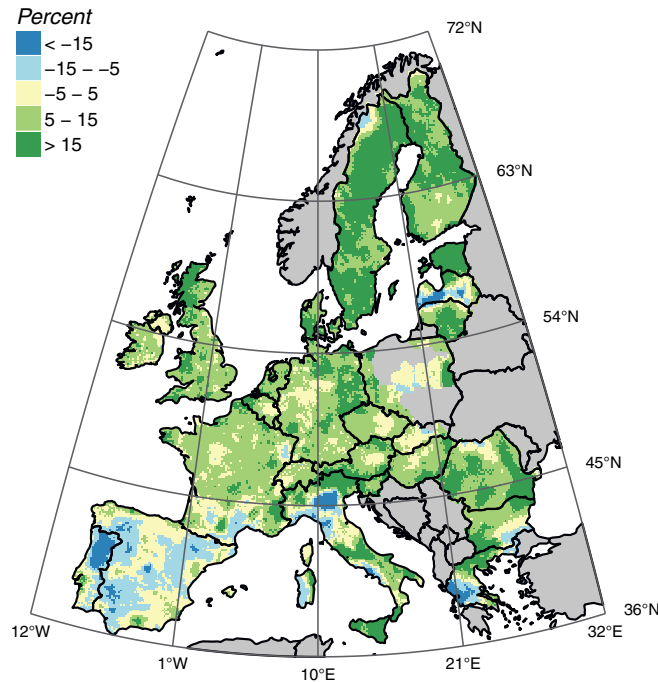


**Figure 1.3:** Change in evaporation over the period 1960–2010. Copied from Teuling et al. (2019). Blue colours indicate a decrease of evaporation for that period, while green colours indicate an increase in evaporation.

the highlands of Scotland, afforestation has led to increased evaporation rates (Teuling et al., 2019). Afforestation in the Seville region, however, does not result in a net increase evaporation because it is counteracted by a strong decline in precipitation (Teuling et al., 2019). So, the dry conditions limit actual evaporation. These examples highlight that locally the effect of changes in land use on changes in evaporation, can be amplified or counteracted by the effect of changes in climate.

## 1.2 From theory to observations

### HISTORY OF EVAPORATION THEORIES: 12TH–17TH CENTURY

Historically, studies on the evaporation process were at first not based on observations, but rather were only hypotheses. Already in very early years (BC), scientists and philosophers came up with speculations on the physics of evaporation as they were trying to understand what drives evaporation. Around 350 BC Aristotle understood that a source of heat (e.g. solar radiation) was required, but he denied that wind was to be directly affecting evaporation (Brutsaert, 1982; McMahon et al., 2016). At the time, Aristotle’s theory

was accepted by colleagues. However, it was only in the 17th century when Descartes deviated from the theory presented by Aristotle. Descartes hypothesized that all matter in the environment consists of particles. Evaporation could be explained by the existence of these small particles as they could move apart and away from the surface under the influence of heat from the sun. However, so far these hypotheses were not yet supported by experiments.

#### THE FIRST EXPERIMENT

Perrault (1674) was the first to experimentally support the hypothesis that heat and wind are required for the evaporation of water particles, although at the time he argued cold also to be a driver of evaporation. The integration of experiments and theoretical hypotheses as a scientific approach created opportunities to improve our understanding of the evaporation process.

#### FROM DALTON TO PENMAN

A clear mark and crucial step in the history of the development of evaporation theory was made by Dalton (1802). His experiments led to his finding that evaporation can be estimated based on the vapour pressure gradient and wind speed. It was Stelling (1882) who was the first to formulate the findings by Dalton in the following manner:

$$LE_{\text{Dalton}} = f(u)(e_s(T_s) - e_a) \quad (1.1)$$

in which  $e_a$  is the vapour pressure at 2 m height,  $e_s(T_s)$  is the saturation vapour pressure at the surface temperature, and  $f(u)$  is an empirical function of the mean wind speed, which was later adjusted to take the following form (Penman, 1956; De Bruin, 1979):

$$f(u) = a + bu_2, \quad (1.2)$$

in which  $u_2$  is the wind speed at 2 m height and  $a$  and  $b$  are constants.

The Dalton equation (which actually was not formulated by Dalton himself) was found to be suitable for estimating open water evaporation (Brutsaert, 1982; McMahon et al., 2016). In 1926 the Bowen ratio ( $\beta$ ) was introduced, which is the ratio of sensible to latent heat fluxes describing the loss of energy from the surface to the atmosphere. By combining the Bowen ratio with the energy balance equation Cummings and Richardson (1927) developed the so-called Bowen ratio-energy balance (BREB) equation, which can be written as follows:

$$LE_{\text{BREB}} = \frac{R_n - G}{1 + \beta} \quad (1.3)$$

in which  $R_n$  is the net radiation and  $G$  is the ground heat flux.

An important next step was taken by Penman (1948), who introduced the combination of the energy balance (radiation component) with the Dalton equation (aerodynamic component) to estimate evaporation from wet surfaces. Penman was able to eliminate the surface temperature by assuming that the surface temperature could be replaced



by a temperature at reference height through linearisation of the vapour pressure curve (Brutsaert, 1982). So while Dalton uses a vertical vapour pressure gradient, which requires observations of the surface temperature, which are often difficult to acquire, Penman uses the vapour pressure deficit. Penman's equation can be written as:

$$LE_{\text{Penman}} = \frac{s}{s + \gamma}(R_n - G) + \frac{\gamma}{s + \gamma}f(u)(e_s(T_a) - e_a), \quad (1.4)$$

in which  $s$  is the slope of the saturated vapour pressure curve at air temperature,  $\gamma$  the psychrometric constant, and  $e_s(T_a) - e_a$  the vapour pressure deficit (VPD) of the air. The first term is referred to as the radiation term and the second as the aerodynamic term. From Penman's equation several other more simplified evaporation models were derived, requiring less input data. One of these is Priestley-Taylor model, where the aerodynamic term of the Penman equation was taken to be a constant proportion of the radiation term (Priestley and Taylor, 1972):

$$LE_{\text{PT}} = \alpha \frac{s}{s + \gamma}(R_n - G) \quad (1.5)$$

in which  $\alpha$  is an empirical constant. An even simpler form was already formulated by Makkink (1957), who assumed that the net radiation is about half of the global radiation and that the ground heat flux can be neglected:

$$LE_{\text{Makkink}} = 0.65 \frac{s}{s + \gamma} K_{\text{in}}, \quad (1.6)$$

in which  $K_{\text{in}}$  is the global radiation. Makkink's model was developed for Dutch grasslands during summer and it requires only data of global radiation and air temperature.

#### PENMAN-MONTEITH

To represent the effect of plants on evaporation over vegetated surfaces in the Penman equation, Monteith (1965) introduced a surface resistance factor ( $r_s$ ) in the so-called Penman-Monteith (PM) equation:

$$LE_{\text{PM}} = \frac{s(R_n - G) + \frac{\rho_a c_p}{r_a}(e_s(T_a) - e_a)}{s + \gamma(1 + \frac{r_s}{r_a})} \quad (1.7)$$

in which  $\rho_a$  is the air density,  $c_p$  the specific heat of air, and  $r_a$  the aerodynamic resistance factor. The surface resistance factor describes the stomatal resistance to evaporation and is a function of meteorological variables. This has proved to work well in estimating the potential evaporation for vegetation that is not water-stressed. However,  $r_s$  does not integrate the active response of the vegetation to changes in these atmospheric variables or stomatal properties, as was proposed by Jarvis (1976). Jarvis (1976) proposed a model that includes the active stomatal response to unfavourable environmental conditions. As a result, for instance the effect of soil moisture limitation on transpiration can be modeled, as well as other stress factors that reduce the potential evaporation. However, nowadays the PM equation still forms the base for estimating evaporation in many studies and hydrological models.

## 1.3 Observation techniques

All aforementioned models (see Sect. 1.2) use (standard) meteorological and other environmental data to estimate potential evaporation. However, direct observations of evaporation are required to start understanding the dynamics of actual evaporation. In this section, a short overview will be provided of available techniques to estimate actual evaporation. Generally, two points of view can be distinguished when measuring surface evaporation, namely how much water leaves the surface or how much water vapour is mixed-in with the lower atmosphere.

### 1.3.1 Evaporation pan

One of the first types of evaporation estimates were performed using evaporation pans. An evaporation pan is filled with water to a predefined water level. At regular time intervals the water level in the pan is measured. The resulting change of water level, after accounting for precipitation, provides an indication of the amount of water that has left the pan as a result of evaporation from this open water surface. The first record of evaporation through measurements of loss of weight of a pan with water, dates back to the late 17th century (McMahon et al., 2016). Evaporation from a pan is a result of the integrated effects of temperature, humidity, wind speed, and (global) radiation.

Evaporation pans have been widely used because they represent a relatively simple and cheap method to use, with only moderate data and installation requirements. This method, however, also faces some drawbacks such as: undesirable effects of heat exchange through the side walls, heat storage properties that are incomparable to that of a bigger body of water such as a lake or ocean, limited temporal resolution, and entering or exiting of water caused by wind and rain (Allen et al., 1998; Sumner and Jacobs, 2005; Masoner and Stannard, 2010). Furthermore, inherently, the effects of water stress on evaporation cannot be determined. Once the pan evaporation is known it can be converted to reference evaporation using a pan coefficient (Grismar et al., 2002).

A decline in pan evaporation is reported globally, while global precipitation and cloudiness increase. This increase requires more water to enter the atmosphere through evaporation, not less. This is known as the ‘pan evaporation paradox’ (Brutsaert and Parlange, 1998). This paradox can be explained in the following manner. In a water-stressed environment, actual evaporation decreases and falls below potential evaporation. More energy will be available for the sensible heat flux, which will therefore increase. As a result, pan evaporation will no longer be a direct measurement of potential evaporation. The increased sensible heat flux results in the drying and warming of the air, which increases the pan evaporation. So, if actual evaporation of the regional area is small, pan evaporation will be large. This mechanism works the other way too: if actual evaporation of the regional

environment is large, pan evaporation will be small. This explains the observed decreased pan evaporation.

### 1.3.2 Lysimeter

Lysimeters are large cylinders filled with soil, either covered with vegetation or left bare. By measuring its mass or volume change over time lysimeters provide a direct observation of actual evaporation (Pruitt and Angus, 1960; Fisher, 2012). The first lysimeters were developed in the late 19th century (Fank, 2011). The size, shape and vegetation cover of a lysimeter can vary depending on the intended use. There exist weighing and non-weighing lysimeters. Non-weighing lysimeters determine actual evaporation as the residual of the soil water balance, for which all the other components such as precipitation, drainage and storage change are measured on a daily or weekly base. Weighing lysimeters determine the change of water content over time by weighing the lysimeter. As a result, the total evaporation between precipitation events can be determined. A disadvantage of lysimeters is that the soil is disturbed when installing it. However, a weighing lysimeter is considered to be one of the best ways to measure actual evaporation over a small area. An example of the use of non-weighing lysimeters, are the ones installed in the dunes near Castricum, the Netherlands, in 1943. The long-term data from this site has proven to be valuable for evaporation analyses (De Laat and Varoonchotikul, 1996; Teuling, 2018a).

### 1.3.3 Eddy covariance

Currently, the eddy covariance (EC) measurement technique, proposed for the first time in the early 1950's by Swinbank (1951), is seen as the most direct micro-meteorological method available to measure the latent heat flux ( $LE$ ) and the sensible heat flux ( $H$ ) at the same time. EC is based on high-frequency measurements (e.g. 20 Hz) of the vertical wind direction and speed, humidity and temperature. It can be shown mathematically that  $LE$  and  $H$  can be approximated as the covariance between the turbulent fluctuations of vertical wind speed and specific humidity ( $LE$ ), and the covariance between the turbulent fluctuations of vertical wind speed and temperature ( $H$ ):

$$LE = \rho_a L_v \overline{w'q'}, \quad (1.8)$$

$$H = \rho_a c_p \overline{w'T'_a}, \quad (1.9)$$

where  $L_v$  is the latent heat of vaporization,  $w'$  the vertical wind speed,  $q'$  the specific humidity, and  $T'_a$  the air temperature. Primes in these equations represent the fluctuations from the mean.

The raw EC data require substantial processing steps to compute reliable fluxes over the chosen averaging interval, frequently taken as 30 minutes. The area that is sampled, i.e. the

footprint, upwind of the EC measurements is affected by the measurement height, surface roughness, and atmospheric stability (McGloin et al., 2014) (a more elaborate description will be provided in Sect. 2.4.4). There are a couple of limitations to this technique. For instance, during precipitation events no accurate measurements can be made and the data should therefore be removed. Like other methods that measure turbulent fluxes from experimental data, the measurements often show a lack of energy balance closure (Foken and Oncley, 1995). The sum of the net radiation and the ground heat flux is found to be larger than the sum of the measured latent and sensible heat fluxes (Foken et al., 2012). In the Netherlands, the EC flux sites in Cabauw (grass) (Beljaars and Bosveld, 1997; Bosveld et al., 2020), Veenkampen (grass) (Jacobs et al., 2003; Jacobs et al., 2010), and Loobos (forest) (Dolman et al., 2002; Moors, 2012) provide a unique set of long-term observations that are used for studying surface-atmosphere interactions. These observations are used for, amongst others, climate modelling, monitoring long-term trends, and validation of space-born observations.

Since the majority of the research in this thesis is based on the EC technique, a more extensive description of this method will be provided in Section 2.4.

### 1.3.4 More recently developed observation techniques

#### *Scintillometry*

This ground-based remote sensing technique makes use of a light source (transmitter) and a detector (receiver) to measure evaporation over the scintillometer path (Hartogensis et al., 2003). The transmitter emits a beam of light of a certain wave length and the detector measures and analyses the intensity fluctuations of that beam caused by refractive index variations due to turbulent eddies along the scintillometer path. Since the measured variance of intensity fluctuations is a measure for the turbulent behaviour of the atmosphere, it can indirectly be related to the transport of heat and water vapour and thus to the sensible and latent heat fluxes. To measure both fluxes the method should be employed at two-wavelengths (i.e. within the optical and microwave range, respectively) simultaneously, either integrated within one device, or using two separate scintillometer instruments that are tuned to each other (Andreas, 1989; Meijninger et al., 2002). Under certain conditions, evaporation can also be estimated from a microwave link in combination with an energy budget constraint (Leijnse et al., 2007). The scintillometer path can range from a couple of hundred metres to a few kilometers. This way, area-averaged fluxes will be obtained. This makes the technique especially suitable for measuring over heterogeneous areas and for comparison with data obtained from satellites (McJannet et al., 2011).

#### *Distributed Temperature Sensing*

The Distributed Temperature Sensing (DTS) method can be used to determine the latent and sensible heat fluxes through the BREB method (see Sect. 1.2) (Euser et al., 2014;

Schilperoort et al., 2018). The DTS method uses a fibre-optic cable that allows to measure temperature every few centimeters. A vertical temperature profile can be acquired by placing the cable vertically along a structure. Installing two cables along each other, of which one is wrapped with a wet cloth, offers the opportunity to measure both the vertical dry and wet-bulb temperature gradients. From this, both the temperature and vapour pressure gradients can be inferred. Subsequently, these gradients can be used to determine the Bowen ratio and by combining it with the energy balance, the latent and sensible heat fluxes can be calculated using the BREB method. This method was successfully applied to measure open water evaporation from a pond and a lake (Van Emmerik et al., 2013; Solcerova et al., 2019).

### *Earth observation*

Satellite remote sensing products provide the opportunity to spatially extrapolate ground-based evaporation measurements. This is of particular interest when studying regional or global evaporation dynamics and trends and it provides an opportunity to study evaporation in regions with none or little ground-based observations available. Satellite products that make use of sensors in the visible or thermal infrared spectrum are only available under cloudless conditions. This is a major limitation of these satellite products (Holmes et al., 2016; Martens et al., 2018).

Different methods exist to retrieve evaporation rates from satellite observations. One commonly used method uses surface temperatures obtained from infrared radiation measurements to estimate the sensible heat flux and to subsequently estimate the actual evaporation as a residual of the surface energy balance (Bastiaanssen et al., 1998). Based on this principle, a number of algorithms have been developed that include surface meteorological parameters to account for spatially heterogeneous hydrological conditions and can therefore be used for estimating evaporation from complex landscapes. Examples of such algorithms are SEBAL (Bastiaanssen et al., 1998) and SEBS (Su, 2002; Gokmen et al., 2012). There are other methods that are based on the Penman-Monteith equation (e.g. Zhang et al. (2009)), optionally in combination with remotely sensed vegetation indices to include information on the water availability in the model (Cleugh et al., 2007). Another promising global land-surface evaporation product based on satellite observations is GLEAM (Global Land surface Evaporation: the Amsterdam Methodology), which uses the Priestley-Taylor evaporation model (see Eq. 1.5) as it requires a relatively small number of inputs (Miralles et al., 2011). In the surface energy balance model ALEXI by Anderson et al. (2011), a multi-sensor thermal infrared approach is used to assess the surface moisture conditions to generate evaporation products. The model uses a two-source energy balance model to distinguish between soil and canopy temperatures. This two-source land-surface models is then coupled to an atmospheric boundary layer model to simulate land-atmosphere feedbacks.

## 1.4 The relevance of studying actual evaporation dynamics and its drivers

### 1.4.1 Water management and climate change

Evaporation is the largest loss term of the land surface water balance. Therefore, it is of great importance for water managers to know how much water evaporates and to understand its dynamics over different time scales. This is especially important during summer periods when most water is lost through evaporation, while at the same time the water demand is highest. The projected intensification of the hydrologic cycle as a consequence of global warming, with projected increased drought and heatwave events (Seneviratne et al., 2012b; Miralles et al., 2019), poses an even bigger challenge to operational water management. Teuling (2018b) argues for including the evaporation process adequately in models to improve the projection of droughts and heatwaves, because the evaporation response in such conditions may vary significantly as a function of vegetation properties (Teuling et al., 2010).

The projected hot future raises the question how the quality of life in urban areas will be affected. What impact will the urban heat island effect have on urban societies? What measures can be taken to alleviate the detrimental effects of increasing temperatures and dry conditions not only in cities, but in natural ecosystems as well? More and more attempts are taken to mitigate and regulate the climate to a certain degree, by letting the water and the soil be the key guide in spatial planning decisions (e.g. create more water retention reservoirs, invest in healthy soils that can retain more water). Such a policy, in which water and soil are the key guide, was for instance recently proposed by the Dutch government (Rijksoverheid, 2022). To understand what measures will help to avoid or alleviate adverse consequences of droughts (or floods), a good understanding of the processes and feedbacks involved is required. Since evaporation is a key process in the water and energy cycle, a correct parameterization of evaporation in operational hydrological models is required. Only if the impact of different drivers is included correctly, will we be able to correctly predict and project evaporation rates.

### 1.4.2 Evaporation in the context of the Netherlands

Effective and adequate water management is of vital importance in a low-lying and densely populated delta such as the Netherlands (see Fig. 1.4 for a map of the geographical setting). The Netherlands is a hydrologically sensitive area with a long history of managing the water flows to guarantee ample access to high-quality fresh water and to avoid or reduce the frequency and intensity of droughts and floods. Historically, a significant focus of water management in the Netherlands has been geared towards discharging water as quickly as possible to prevent floods and adverse effects of too much water. However, with droughts becoming more frequent and more intense, the challenge increases to provide sufficient

fresh water during the warm summer period for multiple sectors such as: agriculture, navigation, drinking water, and the industry (Prinsen et al., 2015). At the same time, floods should still be prevented during wetter periods. This requires a solid and integral approach towards the spatial planning in which water is used as a guiding principle. The so-called Freshwater Delta Decision, which is part of the Dutch Delta Programme by the Dutch government, is initiated to address these issues (Rijksoverheid, 2022).

As mentioned in Section 1.4.1, the use of water and soil as guiding principles has now been advocated for in policies in the Netherlands (Rijksoverheid, 2022). This has, for instance, already led to decisions of allowing a flexible water level in the biggest fresh water reservoir of the country: Lake IJssel (see Sect. 2.2 for a more detailed description). Lake IJssel serves as the most important fresh water storage reservoir of the Netherlands, providing water for surrounding agricultural areas and for drinking water. Another critically important area is the Veluwe area, the largest nature reserve of the country, which serves as a groundwater recharge area (Verhagen et al., 2014). The recharge of sufficient water in this area is jeopardized, despite the above-average precipitation rates in this slightly elevated area (see Fig. 1.4). The decreased recharge is a consequence of increased groundwater abstractions and drainage of surrounding areas (Van Engelenburg, 2020). Additionally, the effect of increased evaporation caused by a substantial land cover change from bare soil and heather to mostly coniferous forest contributes to decreased recharge of groundwater as well (Witte et al., 2019). The effect of land cover change on evaporation was also observed in the dunes near Castricum based on lysimeter data (Teuling, 2018a). Evaporation was observed to increase with the gradual afforestation of the land in the decades after installation of the lysimeters.

So far, most studies in the Netherlands have been dedicated to analysing terrestrial surface evaporation. Apart from several short-term studies (Keijman and Koopmans, 1973; De Bruin and Keijman, 1979; Abdelrady et al., 2016; Solcerova et al., 2019; Wieringa, 2019), no long-term measurement campaigns have been conducted up till now to measure open water evaporation in the Netherlands. However, if we are to understand better the surface evaporation as a whole over the complexity of the water-rich landscape of the Netherlands, it is essential to learn more about the dynamics and drivers of open water evaporation as well. This can be used to improve the estimation of total surface evaporation using hydrological models.

## 1.5 Research objectives and thesis outline

A thorough understanding of the dynamics and drivers of actual surface evaporation over a landscape is essential to make well-supported short-term predictions and long-term projections of surface evaporation at the relevant temporal and spatial resolutions. A correct parameterization of evaporation in operational hydrological models is particularly

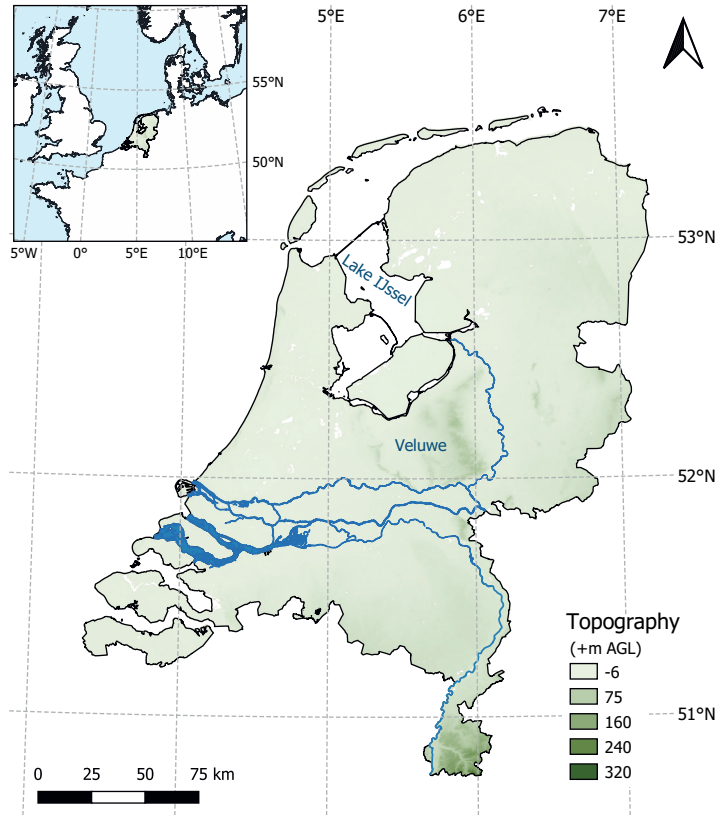


**Figure 1.4:** Map of the geographical setting of the Netherlands. Topography is indicated in shades of green.

crucial during the warm summer periods, especially in the light of the ongoing intensification of the hydrologic cycle as a consequence of global warming.

A distinction should be made between evaporation from land surfaces and water bodies, since different drivers underlie the process of water vapour exchange between the Earth surface and the atmosphere. Inland water bodies form an important component in regional hydrological systems ( $\sim 17\%$  of the total area in the Netherlands consists of inland water bodies, Huisman, 1998). However, previous studies, so far, have predominantly focused on the monitoring and analysis of terrestrial evaporation dynamics as opposed to open water evaporation. Therefore, the aim of this thesis is to *identify the drivers of surface evaporation, including open water evaporation, based on observations*. The focus area of this thesis is the Netherlands. The Netherlands provides a great opportunity for this study because of the availability of a multitude of evaporation measurements conducted in the past over different land cover types. This relatively dense measurement network provides the opportunity to directly compare dynamics and drivers of evaporation from



different land cover types, all within a small region with a temperate marine climate. All measurements used in this thesis are conducted in the Netherlands. While the approaches and methods might be transferable to regions with a different climate, topography or geographical setting, regional conditions should be taken into account before transferring the results of this thesis. To meet the objective of this thesis, the following three questions were identified:

- What are the effects of crucial assumptions made in various evaporation parameterizations on simulating open water evaporation from a large lowland reservoir at different temporal scales?
- What are the main drivers of evaporation from a large lowland reservoir during the warm season?
- How do drivers of latent and sensible heat fluxes over different land cover types compare during the warm season?

Chapters 3, 4 and 5 are linked to the three research questions, respectively, and form the core chapters of this thesis. Figure 1.5 shows how the chapters are related to each other.

Chapter 2 introduces the study area used in this thesis, i.e. the Netherlands. Additionally, this chapter describes the eddy covariance measurement technique in greater detail because most of the observations used in this thesis are based on this technique.

Many models are available to estimate evaporation based on meteorological and environmental variables. In Chapter 3 several evaporation models are selected to compare their resulting estimates of evaporation from hourly to decadal timescales.

In order to contribute to reducing the existing gap on the analysis and observations of open water evaporation dynamics in the Netherlands Chapter 4 discusses the measurement campaign we have conducted over Lake IJssel. The observations obtained over two summer periods are used in this chapter to study the drivers ( $x$ ,  $y$ ,  $z$  in Fig. 1.5) of hourly and daily evaporation and create regression models.

In Chapter 5 historical flux tower measurements of 19 sites covering six land cover types within the Netherlands are used. These observations are used to explore how the control of daily and midday latent and sensible heat fluxes over different land cover types is distributed along three axes: energy availability, water availability and exchange efficiency. At the same time, this study provides a synthesis of historical observations of latent and sensible heat fluxes measured within the Netherlands.

The concluding Chapter 6 synthesises the main findings of this thesis and reflects on the main objective. Additionally, it provides an outlook on future opportunities for further analysis on the drivers and dynamics over a landscape, and on the implementation of the findings in this thesis for operational water management.

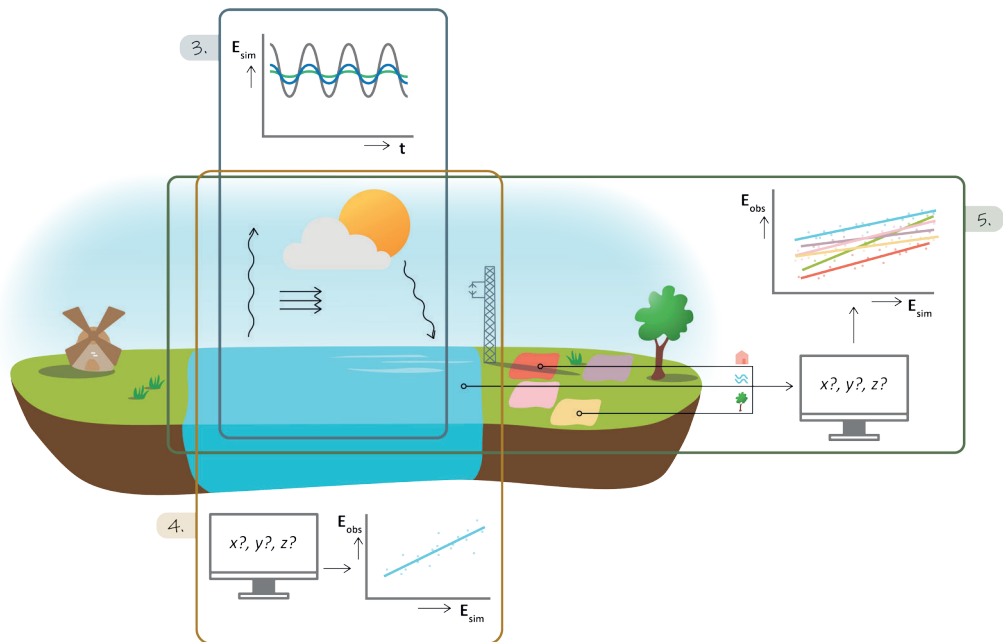
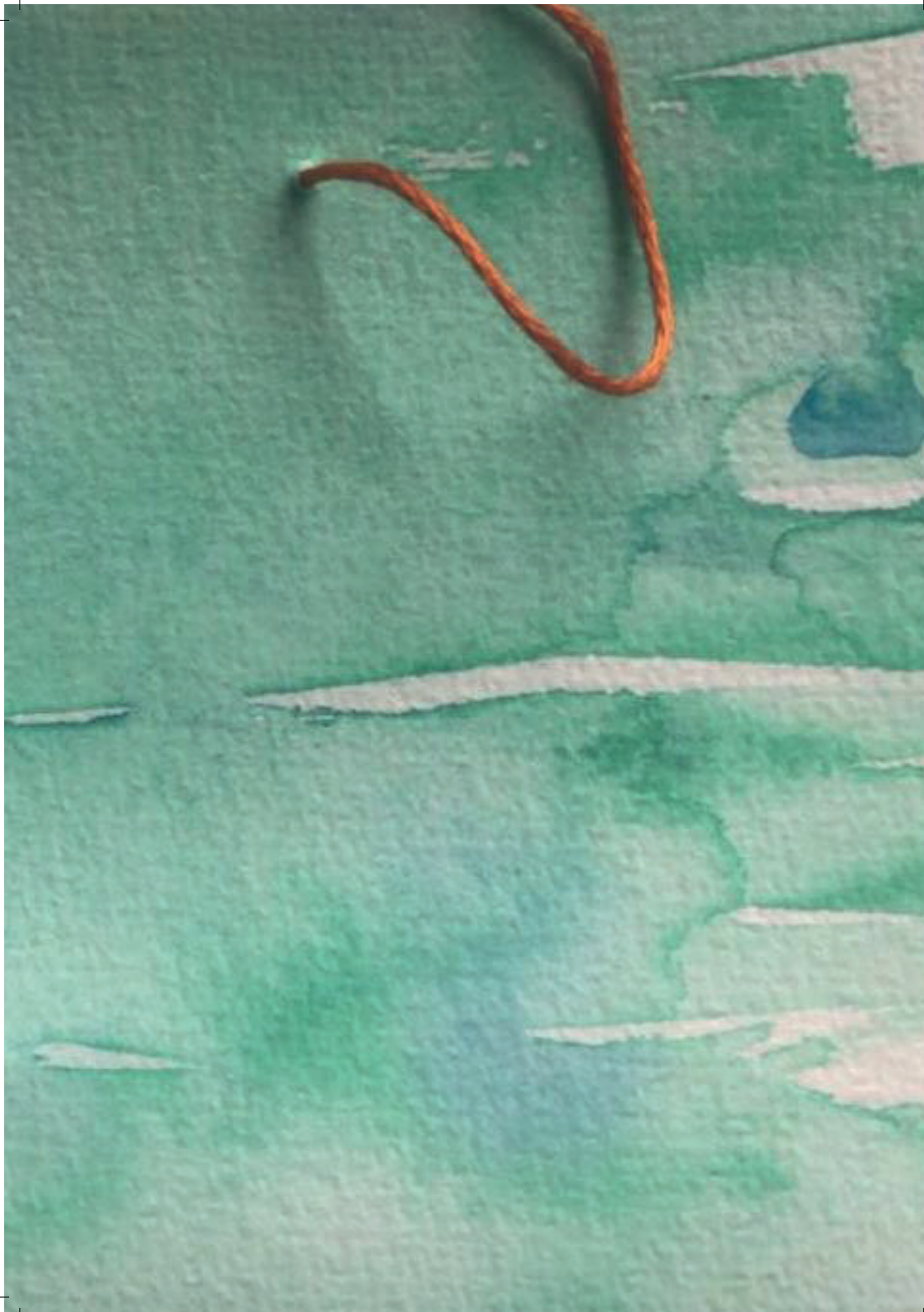


**Figure 1.5:** Schematic overview of the contents of this thesis (image created by Susan Klinkert). The numbered frames provide an overview of the relations between the core chapters of this thesis.



## Chapter 2

### Study area, data and methods

## 2.1 Introduction

Several observation methods, evaporation models and data products are used multiple times in this thesis. Therefore, I will provide a description of these aspects here in this chapter. Furthermore, since this thesis is focused on the Netherlands, a description of the study area will be provided here as well. In Section 2.2 the study area will be introduced, with a particular focus on the Lake IJssel region as this is the study area in Chapters 3 and 4. Section 2.3 introduces a couple of well-known and frequently-used evaporation models that are used in Chapter 3, as well as on several occasions in Chapters 4 and 5. The eddy covariance measurement technique on which the analyses in Chapters 4 and 5 are based, will be described in Section 2.4. Lastly, Section 2.5 describes the environmental data that has been used additionally to the flux observations, as input for the evaporation models used in Chapter 3 and for the regression analyses performed in Chapters 4 and 5.

## 2.2 Study area

The Netherlands is a delta located in north-western Europe and is bordered in the west and north by the North Sea (see Fig. 1.4). The Netherlands has a warm temperate humid climate with prevailing south-westerly winds, a long-term average yearly temperature of 10.5°C, precipitation sum of 855 mm and evaporation of 581 mm (KNMI, 2022). Orographic differences are almost absent, with mostly some topography in the very south-west of the country of which the highest point reaches 322 m above NAP (Normaal Amsterdams Peil, or Amsterdam Ordnance Datum, the local sea level reference). More than a quarter of the country is situated below sea level (De Vries, 2007). In the low-lying areas, with mostly clay or peat soils, groundwater levels are shallow, ranging from two meters deep to a few centimeters or less. In the somewhat elevated ice-pushed ridge areas in the middle, east and the far south of the country the groundwater levels are deeper (up to 20 meters deep), but also highly spatially variable (TNO, 2022).

In Chapters 3 and 4, the Lake IJssel region is studied. Lake IJssel, also referred to as “IJsselmeer” in Dutch, is the largest freshwater lake in the Netherlands, bordering the provinces of Flevoland, Friesland, and North Holland (see Fig. 2.1). The lake covers an area of 1100 km<sup>2</sup> and is enclosed by the Afsluitdijk embankment to the north and by the Houtribdijk embankment to the south-west. With an average depth of 5.5 m and a maximum depth of 7 m, the lake can be considered a large shallow lake. The IJssel River is the main vein that supplies the lake with freshwater. Together with the inflow from the neighbouring polder systems, the lake receives an average of 340 m<sup>3</sup> s<sup>-1</sup>. Its main outflow occurs under gravity at the sluices of the Afsluitdijk, where water is discharged to the Wadden Sea. During summertime, a flexible water level is used, which can vary between -0.10 m NAP and -0.30 m NAP. In winter, the lake level should not be lower than -0.40 m NAP. Lake IJssel fulfils an important hydrological role in the low-lying

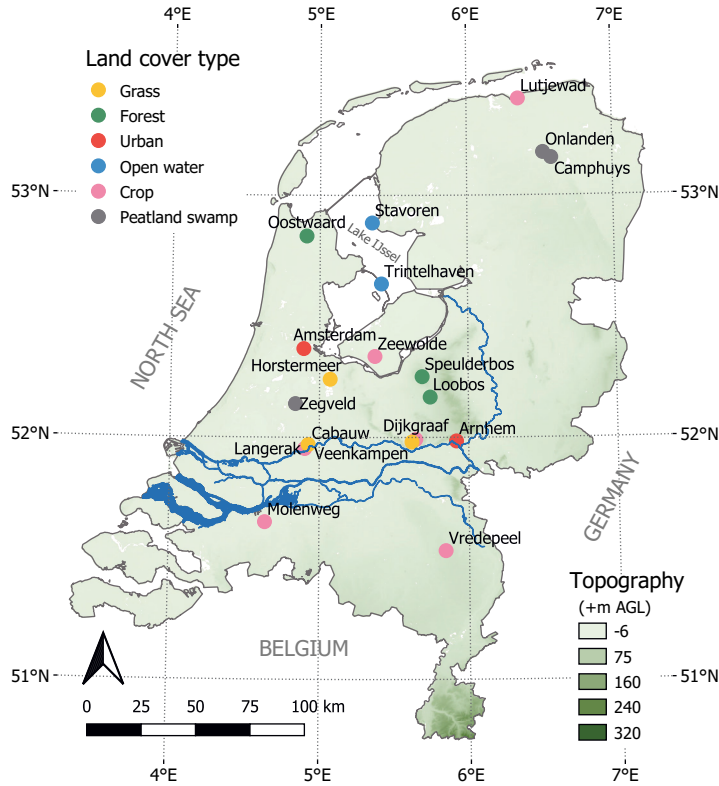


**Figure 2.1:** Map of the study area, including the location and land cover type of the measurement sites (see Chapter 5) and the topography of the Netherlands in meters above surface level. The dots on the map represent the locations of the flux tower observations, where the colours indicate the land cover type.

Netherlands with respect to both flood mitigation and freshwater supply for agricultural and drinking water purposes. The flexible management of the lake level during the year provides water managers with a tool to respond to the meteorological conditions and the need for fresh water.

In Chapter 4, data from two eddy covariance (EC) systems (see Sect. 2.4) that we have employed at two locations along Lake IJssel, namely Stavoren and Trintelhaven (see Fig. 2.1), are used in the analyses. More detailed information about the setup of these measurement locations is provided in Section 2.4.2. In addition to our own measurements, we gathered historical measurements from 17 more EC flux towers within the Netherlands, containing data of latent heat flux, sensible heat flux and auxiliary meteorological observations. In Chapter 5, observations from the in total 19 flux sites covering six land cover types were analysed. The six land cover types studied are grass (GR), forest (FO), urban (UR), open water (WA), crop (CR) and peatland swamp (PS).

Figure 2.1 provides an overview of the study region with the locations of the flux tower sites and the topographical setting.

Table 2.1 provides an overview of all the sites including the land cover classification, period over which measurements were performed, climatological yearly means of air temperature and precipitation, and the key references of each measurement site. The 19 sites were selected based on measurement method (i.e. eddy covariance), data availability of latent and sensible heat fluxes and auxiliary meteorological observations, and the requirement of a minimum length of the data record of one warm season (MJJA). The majority of the sites have been operated on a campaign basis for only a relatively short period of one or two years. However, there are also sites where a long-term measurement effort has been made or is still continued, such as locations Cabauw (grass), Veenkampen (grass), Horstermeer (grass), Loobos (forest), Speulderbos (forest) and Arnhem (urban). Evaporation has been measured at other sites as well using EC, however we have not been able to obtain these data (see Table C1 in Appendix C for an overview of these sites).

## 2.3 Evaporation models

A wide variety of models is available to estimate evaporation. In this Section, I will list the evaporation models that are used in Chapters 3 and 4, in which the focus was on open water evaporation from Lake IJssel. This section provides a more elaborate description of the models than already provided in the Introduction chapter of this thesis. The six evaporation models described below are commonly used to estimate surface evaporation and are sensitive to a variety of forcings (Table 2.2; see Table A1b in Appendix A for explanations of all the variables).

The Penman method (Penman, 1948) has been used because it was originally developed for wet surfaces and because it is the most commonly used method globally to estimate evaporation. The method developed by De Bruin (1979) finds its origin in Penman's method, but has been based on observations conducted at Lake Flevo, the Netherlands (see Fig. 2.4). Makkink's method (Makkink, 1957) is an even more simplified derivation of Penman's equation and is currently used in operational hydrological models in the Netherlands, which is why it is included in our analyses. For comparison, methods that use other forcing variables are included in the analyses of Chapter 3 as well. These include the methods of Granger and Hedstrom (2011), using wind speed as the main forcing, the Hargreaves (1975) method, using solely air temperature, and the more physically based method, FLake (Mironov, 2008). Below a short description of the models that are used is given, and in Appendix A a more detailed description is given of the methods, including the assumptions that are made and the input data required (see Table A1a in Appendix A).

**Table 2.1:** Site characteristics, including key references and climatological yearly means of air temperature and precipitation based on the nearest automatic meteorological KNMI station.

Measurement site	Code	Land cover	Location (lat/lon)	Period (used in this study)	Avg. $T_a$ (°C)	Avg. $P$ (mm)	Energy balance*	Key reference
Cabauw	GR1	Grass	51.970 / 4.926	2003 – 2020	10.4	770	0.85	Beljaars and Bosveld (1997); Bosveld et al. (2020)
Veenkampen	GR2	Grass	51.981 / 5.620	2014 – 2021	10.1	868	0.81	Jacobs et al. (2003); Jacobs et al. (2010)
Horstermeer	GR3	Grass	52.240 / 5.071	2004 – 2011	10.5	855	0.78	Jacobs et al. (2007); Hendriks et al. (2007)
Loobos	FO1	Forest	52.167 / 5.744	2003 – 2018	10.1	868	0.74	Dolman et al. (2002); Elbers et al. (2011) and Moors (2012)
Oostwaard	FO2	Forest	52.832 / 4.909	2008	10.5	787	0.88	Elbers et al. (2009)
Speulderbos	FO3	Forest	52.251 / 5.690	2015 & 2020	10.1	868	0.94	Cisneros Vaca et al. (2018); Schilperoort et al. (2018)
Stavoren	WA1	Open water	52.886 / 5.355	2019 – 2020	10.2	755	0.61	Jansen et al. (2022)
Trintellhaven	WA2	Open water	52.634 / 5.417	2019 – 2020	10.2	824	0.81	Jansen et al. (2022)
Arnhem	UR1	Urban	51.985 / 5.918	2012 – 2016	10.1	868	0.99	Jacobs et al. (2015)
Amsterdam	UR2	Urban	52.367 / 4.893	2018 – 2020	10.7	850	1.23	Steenneveld et al. (2020)
Dijkgraaf	CR1	Crop (maize)	51.992 / 5.646	2007	10.1	868	0.89	Elbers et al. (2009); Moors et al. (2012)
Langerak	CR2	Crop (maize)	51.954 / 4.903	2005	10.7	770	0.77	Elbers et al. (2009); Moors et al. (2012)
Lutjewad	CR3	Crop (wheat)	53.399 / 6.356	2006	9.9	829	0.84	Van der Laan (2010)
Molenweg	CR4	Crop (potato)	51.65 / 4.639	2005	10.6	799	0.25	Elbers et al. (2009); Moors et al. (2012)
Vredepeel	CR5	Crop (beet)	51.532 / 5.844	2006	10.5	739	0.81	Elbers et al. (2009); Moors et al. (2012)
Zeewolde	CR6	Crop (maize)	52.335 / 5.373	2008	10.2	824	0.98	Moors et al. (2012)
Onlanden	PS1	Peatland swamp	53.177 / 6.524	2020	9.8	805	0.84	Kruijt et al. (2020)
Camphuis	PS2	Peatland swamp	53.155 / 6.580	2020	9.8	805	0.80	Kruijt et al. (2020)
Zegveld	PS3	Peatland swamp	52.139 / 4.839	2020 – 2021	10.4	770	1.34	Buzacott et al. (2022)

\*Energy balance here defined as the average of the sum of  $LE$  and  $H$  divided by  $R_n$  based on hourly data.



### *Penman*

The Penman method is a combination equation and is based on the two fundamental factors that determine evaporation, namely, available energy and atmospheric demand (see Table 2.2). The effect of these factors combined is captured by the turbulent transfer and energy balance equations for a wet surface (Brutsaert, 1982; Tanny et al., 2008; Moene and van Dam, 2014). Starting from the energy balance principle combined with the flux-gradient approach, the following form of Penman's equation is derived:

$$LE = \frac{s}{s + \gamma}(R_n - G) + \frac{\frac{\rho_a c_p}{r_a}(e_s(T_a) - e_a)}{s + \gamma}, \quad (2.1)$$

in which  $s$  is the slope of the saturated vapour pressure curve,  $\gamma$  the psychrometric constant,  $R_n$  the net radiation,  $G$  the water heat flux,  $\rho_a$  air density,  $c_p$  the specific heat of air,  $r_a$  the aerodynamic resistance, and  $(e_s(T_a) - e_a)$  the vapour pressure deficit of the air. In Penman's derivation, it was assumed that the available energy  $(R_n - G)$  is equal to the net radiation, assuming other terms of the energy budget equation into the water body to be negligible, e.g. the water heat flux. This flux is difficult to measure, especially at smaller timescales, and is therefore often ignored (Van Emmerik et al., 2013). However, for water bodies it is essential to account for heat storage changes as its storage capacity is significantly larger compared to land surfaces. Not accounting for heat storage changes can lead to (i) overestimation of  $E_{\text{water}}$  in spring (Northern Hemisphere) when incoming radiation is used to warm up the water body instead of immediate release through  $E_{\text{water}}$  and (ii) underestimation of  $E_{\text{water}}$  during autumn (Northern Hemisphere) when additional heat that was stored in the water body is released through  $E_{\text{water}}$ . The Penman equation requires standard meteorological variables (net radiation, air temperature, wind speed, and humidity) at one height.

### *De Bruin-Keijman*

A similar expression to determine reference evaporation was proposed by De Bruin and Keijman (1979). They applied the Priestley–Taylor method to the former Lake Flevo (see Fig. 2.4) in the Netherlands. The Priestley–Taylor method is a derivation of Penman's method where the aerodynamic term in Penman's equation was found to be a constant proportion of the radiation term (Priestley and Taylor, 1972). De Bruin and Keijman (1979) adjusted this empirical relation to determine evaporation, namely, that the aerodynamic term is linearly proportional to the radiation term with an additional constant. These two parameters were found to vary during the year, but they are mostly taken as constants.

*Makkink*

Another method that is based on Priestley–Taylor is the method of Makkink, which was developed for grassland areas in summertime in the Netherlands (Makkink, 1957). It only requires observations of global radiation and temperature, since it assumes that the water heat flux can be neglected with respect to net radiation and that net radiation is about half of global radiation. The first assumption is only valid for land surfaces, and the second assumption considers average summers in the Netherlands. Makkink is currently used in operational hydrological models in the Netherlands and is applied to open water using a correction factor.

*Granger-Hedstrom*

None of the methods described above includes wind explicitly, although wind speed is recognized as an important driving factor for evaporation. Granger and Hedstrom (2011) found the most significant correlation to exist between  $E_{\text{water}}$  and wind speed at hourly timescales, and no direct relation was found with net radiation. The authors developed a simple model to quantify  $E_{\text{water}}$  in which the key variables and parameters are wind speed, land–water contrasts in temperature and humidity, and downwind distance from the shore.

*Hargreaves*

The Hargreaves method is an example of a simple and highly empirical temperature-based model (Hargreaves, 1975; Hargreaves and Allen, 2003). Global surface radiation is frequently not readily available; therefore, the Hargreaves method uses the extra-terrestrial radiation, which depends on the angle between the direction of solar rays and the axis perpendicular to the atmosphere’s surface, to simulate its seasonality. Furthermore, it incorporates the range in maximum and minimum temperatures as a proxy to estimate the level of cloudiness. The method was originally designed for land surfaces at longer temporal scales and does not account for lake heat storage. However, previous studies have also shown that temperature-based evaporation methods can perform reasonably well over lake surfaces at larger timescales (Rosenberry et al., 2007).

*FLake*

A more physically oriented model is FLake, which has been developed by Mironov (2008). This one-dimensional freshwater model is designed to simulate the vertical temperature structure and the energy budget of a lake. It consists of an upper mixed layer, of which the temperature is assumed to be uniform, and an underlying stratified layer of which the curve is parameterized using the concept of self-similarity (assumed shape) (Kitaigorodskii and Miropolskii, 1970). The same concept is used to represent the thermal structure of the ice and snow cover and of the thermally active layer of the bottom sediments.

**Table 2.2:** Methods used to calculate open water evaporation. Explanation of all variables can be found in Table A1(b).

Method	Short description	Equation	Reference
Penman	Combines a radiation term and an aerodynamic term.	$LE = \frac{s}{s+\gamma} Q_n + \frac{\gamma}{s+\gamma} E_a$	Penman (1948)
Makkink	Based on same principles as Priestley-Taylor using only temperature and global radiation	$LE = 0.65 \frac{s}{s+\gamma} K_{in}$	Makkink (1957)
De Bruin - Keijman	Alternative to Penman's equation using data from Lake Flevo experiments (1967).	$LE = \alpha_{BK} \frac{s}{s+\gamma} (R_n - G) + \beta_{BK}$	De Bruin and Keijman (1979)
Granger & Hedstrom	A simple hourly $E_{water}$ model using the relationship with wind.	$E = a * u$ $a = f(\Delta T, \Delta e, X)$	Granger and Hedstrom (2011)
Hargreaves	Temperature-based method	$E_{ref} = 0.0023 R_a (TC + 17.8) TR^{0.50}$	Hargreaves and Allen (2003)
FLake	A two-layer parametric fresh water model. Capable to predict the vertical temperature structure.	$LE = -(q_z - q_s) \frac{u_* k}{Sc_n} \frac{Lv \rho_a}{(\ln(\frac{z}{z_0}) + \psi_q(z/L))}$	Mironov (2008)

## 2.4 Eddy covariance

The analyses of the drivers of latent and sensible heat fluxes in Chapters 4 and 5 are all based on eddy covariance (EC) flux tower observations. This section provides a description of the method, the two measurement locations where we employed EC systems to measure evaporation from Lake IJssel, as well as the processing steps required to convert the raw data to fluxes, and the footprint analysis.

### 2.4.1 The method explained

The EC method is used to measure the exchange of heat, mass and momentum between the earth's surface and the atmosphere. An EC instrument consists of a sonic anemometer that measures the wind direction in three dimensions and an infrared gas analyser that measures the concentration of water vapour and other trace gases. Based on these high frequent measurements (e.g. 20 Hz), the covariance between turbulent fluctuations of the vertical wind speed and specific humidity is used to calculate the latent heat flux ( $LE$ ), while for the sensible heat flux ( $H$ ) the covariance between turbulent fluctuations of the vertical wind speed and temperature is used:

$$LE = \rho_a L_v \overline{w'q'}, \quad (2.2)$$

$$H = \rho_a c_p \overline{w'T'_a}, \quad (2.3)$$

The area that is sampled, i.e. the footprint, upwind of the flux tower is affected by the measurement height, surface roughness, and atmospheric stability (McGloin et al., 2014) (see Sect. 2.4.4). There are a number of assumptions that have to be met to properly employ the EC method. These include the assumptions of footprint matching the area of

interest, horizontal homogeneity of the terrain, steady state conditions, and turbulent flow. Often these assumptions cannot be met, which can result in erroneous flux calculations. Therefore, the processing of the raw fluxes requires some correction steps. Following a description of the measurement systems we employed in Stavoren and Trintelhaven to measure open water evaporation (Sect. 2.4.2), a description of the steps taken to process these raw data will be provided (see Sect. 2.4.3).

### 2.4.2 Measurement locations

During the summer periods of 2019 and 2020, an EC measurement system was mounted in a telecommunication tower that is located at the shoreline in the city of Stavoren on the north-east coast of the lake (see Figs. 2.2a and 2.3a). Its favourable position in relation to the predominant south-westerly wind direction in combination with a pre-existing telecommunication tower renders this location suitable for the measurements needed to analyse the dynamics of open water evaporation. An additional benefit of this location is that it allows a comparison between the dynamics of terrestrial evaporation and open water evaporation by selecting time intervals based on the footprint of the flux tower (see Section 2.4.4 for the flux footprint analysis). An integrated open-path infrared gas analyser and 3D sonic anemometer (IRGASON) instrument (Campbell Scientific) was installed at a height of 7.5 m above the land surface and was pointed towards a heading of 220°. The IRGASON measures the water vapour and CO<sub>2</sub> concentration, air temperature (by the sonic anemometer), barometric pressure, and the three wind components at a sampling frequency of 20 Hz. Additional data of air temperature and relative humidity were both measured at 5.9 and 7.4 m height using HMP155A sensors (Campbell Scientific).

In the harbour of Trintelhaven, located in the middle of the Houtribdijk embankment, another telecommunication tower was equipped with the same EC system, installed at a height of 10.8 m above the surface (see Figs. 2.2b and 2.3a). This location is surrounded by water, with Lake IJssel on the east of the embankment and lake Marker on the west. The IRGASON pointed in a 240° direction for the summer period of 2019 and in a 92° direction as of January 2020. The latter change maximized the suitable viewing angle of the IRGASON, considering the dominant wind direction and the position of the telecommunication tower and Lake IJssel. HMP155A sensors were used to measure the air temperature and relative humidity at two heights, namely 9.1 and 10.9 m. The measurement height at the two locations (Stavoren and Trintelhaven) differ. In our analysis, we have not adjusted the measurements to an equivalent height. In theory, the small height difference will not affect the heat fluxes under the assumption of a constant turbulent flux layer.

As a short side note I would like to remark that, originally, we had the plan to compare our point EC measurements to path-averaged fluxes of open water evaporation using a combination of two scintillometers. We installed these scintillometers, consisting of

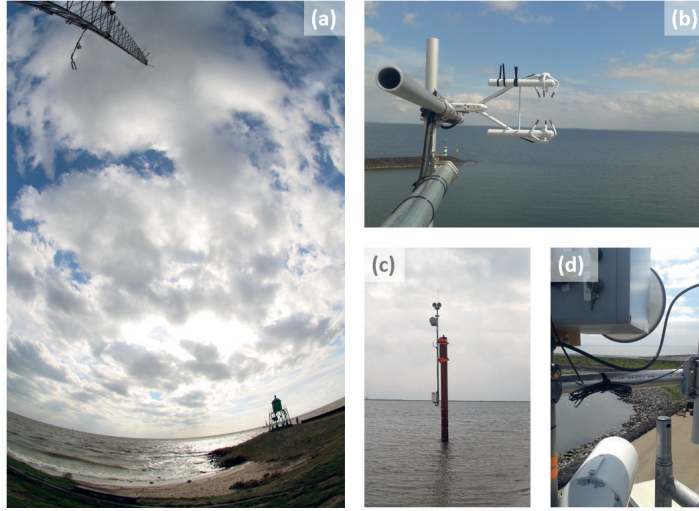


**Figure 2.2:** Pictures of the installed eddy covariance systems at Stavoren (a, picture by Ryan Teuling) and Trintelhaven (b), and the two scintillometer links between Marker Wadden islands (c) and the Trintelhaven (d).

a microwave link and an optical scintillometer, between the Trintelhaven harbour and the Marker Wadden islands (see Figs. 2.2c and d). Hence, the heading of  $240^\circ$  of the IRGASON during the first measurement period in 2019 for intended comparison reasons. Unfortunately, the scintillometer instruments failed as they, amongst other issues, suffered from water damage.

### 2.4.3 Processing steps

The raw EC data collected with our EC measurement systems during the summer periods of 2019 and 2020 were processed according to Foken et al. (2012). The processing steps were performed using the EddyPro software (EddyPro, 2021). This software package was chosen because it is widely used for processing eddy covariance measurements. The results compare well with the results directly obtained through the incorporated EasyFlux DL software created for the IRGASON instrument (EasyFlux, 2017).

Firstly, the raw data underwent quality control using several criteria in order to remove faulty or corrupt data. This included testing for completeness. If more than 5 % of the expected high-frequency data within the chosen averaging interval were missing, the interval was flagged. Unrealistic values for each variable based on fixed individual thresholds were removed. Spikes were detected and eliminated in accordance with the algorithm of (Mauder et al., 2013). Furthermore, according to the approach of Vickers and Mahrt (1997), the data were screened for too many poor-resolution records and for too many so-called ‘dropouts’, referring to jumps in the data that continue over a longer period

and are consequently not recognized as spikes. Density fluctuations were compensated for using the Webb–Pearman–Leuning (WPL) approach (Webb et al., 1980). If the signal strength of the gas analyser fell below 70 %, the data were also removed. Secondly, this quality-checked dataset was further processed to obtain calculated raw fluxes. Next, coordinate rotation of the sonic anemometer using the double-rotation method (Wilczak et al., 2001) was applied to correct for an imperfectly levelled sonic anemometer, and trends were removed using block averaging.

From this point, the final covariances were calculated and were subject to two essential tests, as described by Foken et al. (2004): (i) a test of stationarity during the averaging interval (30 min) and (ii) a test of whether there were well-developed turbulent conditions such as those required for proper usage of the Monin–Obukhov similarity theory. This yielded time series containing raw fluxes. As a final step, spectral corrections were applied to account for high- and low-frequency losses (Massman, 2000; Moncrieff et al., 2004), and the correction developed by Schotanus et al. (1983) was also applied to account for the humidity effect on the sonic temperature, which becomes specifically important for locations near waterbodies. After iterating the last steps and incorporating the quality tests, a fully quality-checked half-hourly flux dataset was obtained. Within this dataset, gaps of a maximum of one data point (i.e. half an hour) were linearly interpolated. Larger gaps were intentionally not gap filled, as this would create too many synthetic results which would interfere with our aim of performing a process-oriented study. Hourly data were obtained by aggregating the half-hourly dataset with no further gap-filling action taken. Daily averages were only calculated from the half-hourly dataset if valid data were available for at least 66 % of the time.

#### 2.4.4 Flux footprint analysis

The flux footprint is computed to quantify the sampling area that contains the sinks and sources contributing to the measurement point. Additionally, the relative contribution of each upwind location to the measured flux is quantified. In Fig. 2.3b and c, the contour lines represent 20 %, 40 %, 60 %, and 80 % of the footprint area, where the 20 % line is located closest to the measurement tower. This footprint analysis helps to decide which wind directions to include in the analysis based on the area of interest. The size of the footprint depends on the measurement height, atmospheric stability, and surface roughness (McGloin et al., 2014). In this study, we used the footprint model developed by Kljun et al. (2004) with the Flux Footprint Prediction (FFP) R code (Kljun et al., 2015). For Stavoren, this footprint analysis showed that the flux data for wind directions between 163 and 349° are available for analysis of  $E_{\text{water}}$ , whereas the remaining wind directions represent the fetch over land and could, therefore, be used for comparison with terrestrial evaporation. At Trintelhaven, we were only interested in the fetch over Lake IJssel. Therefore, the flux data for Trintelhaven were disregarded for wind directions between 170 and 70° for the summer of 2019. After changing the direction of the IRGASON, this yielded a larger angle

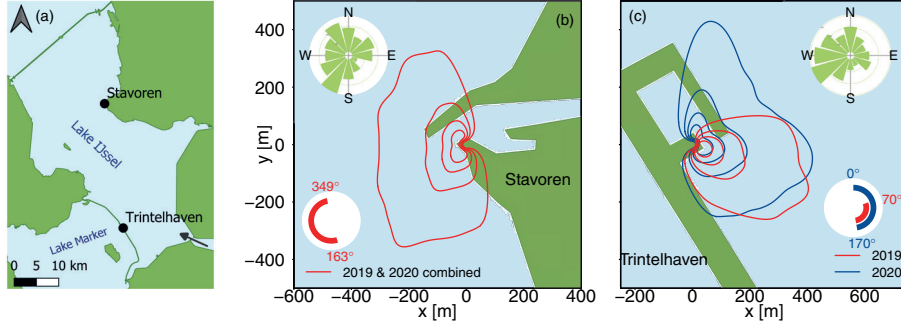


**Figure 2.3:** Map of the Lake IJssel study region and location of the eddy covariance measurement sites. The black dots in panel (a) represent the locations of the turbulent flux observations (Stavoren and Trintelhaven). Black arrow indicates the location where water from the IJssel river enters Lake IJssel. Panels (b) and (c) illustrate the sampling area that is measured by the flux tower for onshore wind conditions by contour lines (20, 40, 60, and 80 % from inside to outside). This was based on a flux footprint analysis using the model of Kljun et al. (2015). The circular inset on the bottom side of both panels indicates the wind directions that are included in the analysis of open water evaporation. At location Trintelhaven (c) this angle has shifted from the year 2019 to 2020 following the change of direction of the eddy-covariance instrument (see Sect. 2.4.4). The circular inset at the top of both panels represents the average wind conditions as illustrated by a windrose.

from which data could be used during the summer of 2020, namely for wind directions between 0 and 170°. Given the dominant south-westerly wind direction, visualized with a wind rose (inset at the top of Fig. 2.3b and c), this means that a large part of the data unfortunately had to be rejected at Trintelhaven.

## 2.5 Data products

Besides data obtained with EC systems, other environmental variables were required throughout Chapters 3, 4, and 5. Therefore, other sources of routinely measured variables were used in these chapter. Below, a description of these data sources is provided per chapter.

The evaporation models used in Chapter 3 were forced with observed historical hourly data (1960–2018) and systematically compared. Therefore, we chose to give preference to a long-term dataset of observed meteorological variables above land, rather than a shorter-term dataset of the same variables in closer proximity to Lake IJssel. As a consequence, we used long-term hourly meteorological data observed in De Bilt, the Netherlands, situated at approximately 50 km distance from Lake IJssel, rather than using the stations nearby in Stavoren or Lelystad (see Fig. 2.4. At the latter stations all required variables have been

measured only since the end of 2002, and in Stavoren air pressure was never measured, while in De Bilt all variables required have been measured since 1960. We compared the stations of Stavoren and Lelystad to station De Bilt. This showed that temperature, relative humidity, air pressure, and global radiation are comparable, while the wind speed is lower in De Bilt compared to Stavoren and Lelystad. However, there is no substantial difference in the daily cycle and frequency distribution of wind speed between the locations (not shown).

Depending on each evaporation model (see Table A1 in Appendix A), data that was used from station De Bilt includes air temperature ( $T_a$ ), global radiation ( $K_{in}$ ), air pressure ( $P_a$ ), wind speed ( $u$ ), wind direction, relative humidity (RH) and cloud cover. Furthermore, water surface temperature (WST) is required as a variable in the Granger-Hedstrom model, as well as to calculate outgoing longwave radiation. WST is not operationally measured at a regular base in The Netherlands, however the Directorate-General for Public Works and Water Management (Rijkswaterstaat, RWS) measures hourly water temperature at several locations, e.g. Friese Kust and Marker Wadden, at a depth of approximately 1.5 metre in the Lake IJssel since 2014 (see Fig. 2.4). Another source of WST measurements is an experiment done in 1967 (Keijman and Koopmans, 1973; Wieringa, 2019) in former Lake Flevo before that part of Lake IJssel was reclaimed (see Fig. 2.4). This experiment includes four weeks of data of amongst others WST, average water temperature, and  $T_{air}$  and vapour pressure at 2 and 4 m height. Yet another WST product is estimated by the FLake model. Remotely sensed satellite products inferring WST were not considered in the analyses of Chapter 3 because of its low temporal resolution. Comparing the different water temperature sources (not shown) and considering the availability of the data, it has been chosen to use the FLake simulations of WST for further analysis.

To quantify the (dis)agreement between the models on the long-term, 3-hourly realizations resulting from the regional climate model (RCM) RACMO2 (Van Meijgaard et al., 2008) driven by the global climate model (GCM) EC-EARTH 2.3 (Hazeleger et al., 2012) were used in Chapter 3. This long-term RCM simulation covers the period 1950–2100 and consists of 16 ensemble members at a spatial resolution of  $0.11^\circ$  ( $\sim 12$  km) available at 3-hourly timesteps (Aalbers et al., 2017). Each member of the ensemble has a slightly different atmospheric initial state perturbed in 1850, and the members can thus be considered as independent realizations. EC-EARTH was forced with historical emissions until 2005 and future projections (2006–2100) were generated using a substantial greenhouse gas emission scenario (RCP8.5). We used the grid cell representing location De Bilt. Direct evaporation observations from an EC instrument at 10-min time resolution made in Cabauw (see Fig. 2.4) from 1986–2018 (Beljaars and Bosveld, 1997) are used to validate the climate change signal of estimated evaporation.

For a thorough understanding of the drivers of open water evaporation, as analysed in Chapter 4, observations of variables additional to the ones we measured using the EC



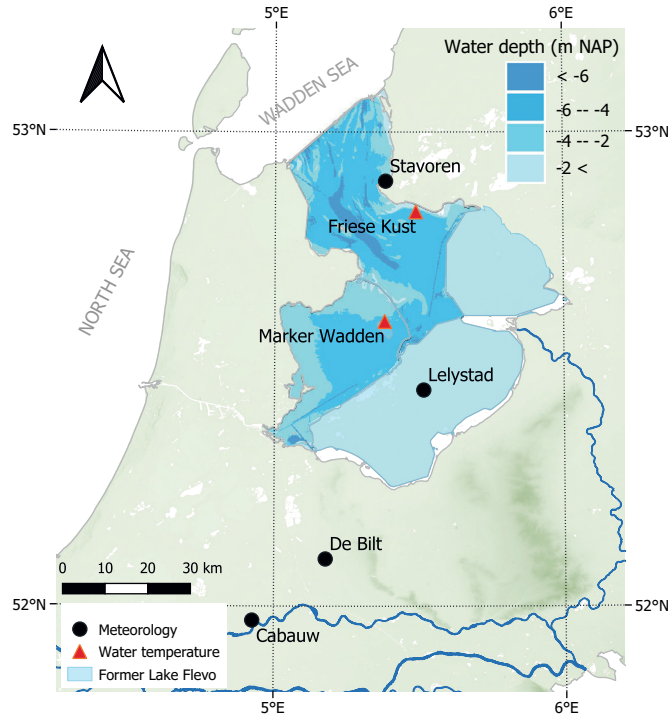
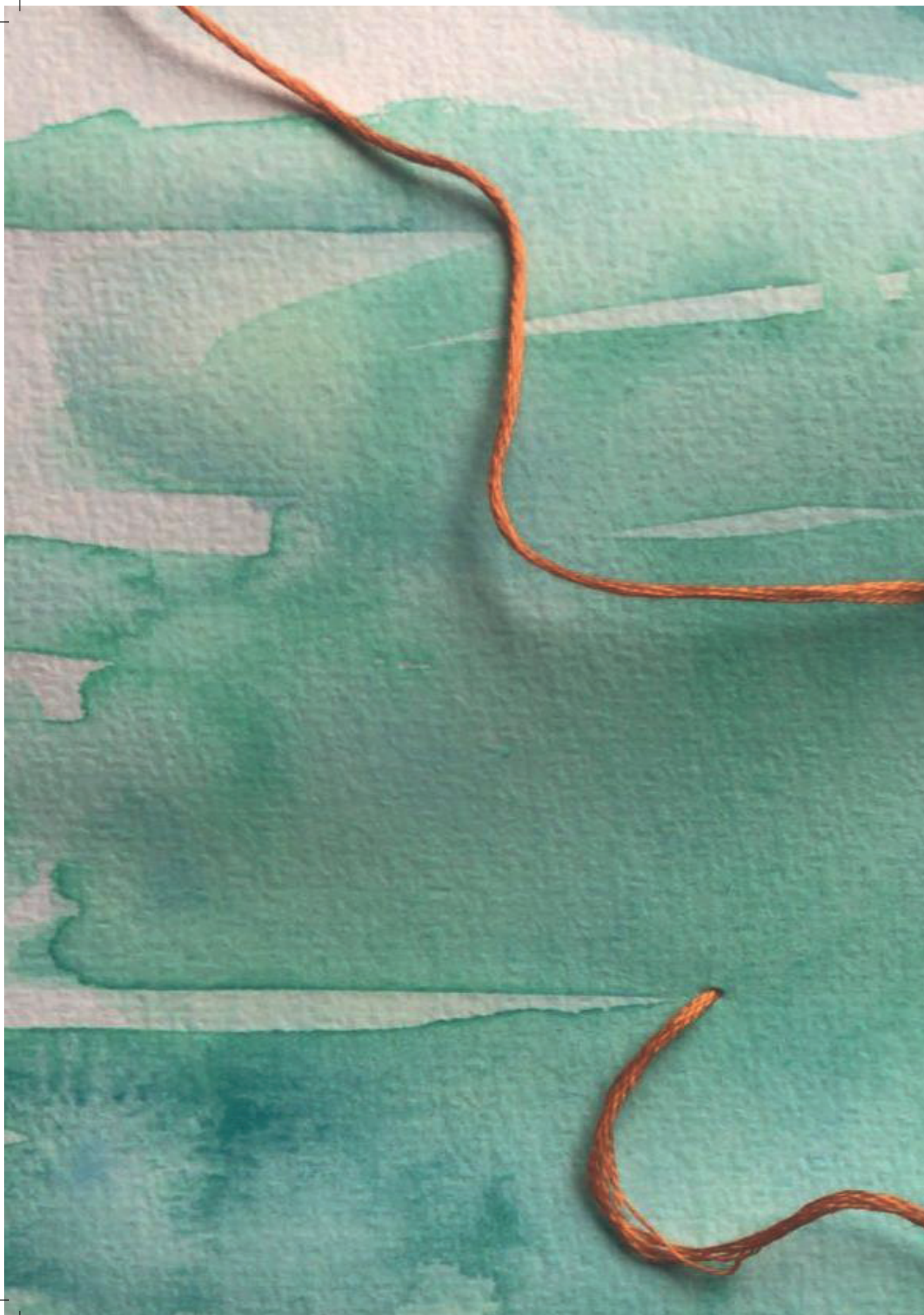


**Figure 2.4:** Overview of the Lake IJssel region with the locations of the KNMI weather stations (black dots) and the Rijkswaterstaat water temperature stations (red triangles). Furthermore, the water depth of the Lake IJssel region is depicted in four classes of blue, and the region of former Lake Flevo is marked in light blue.

systems were required, such as radiation and water temperature. Unfortunately, practical issues precluded observations of the four radiation components and water temperature at the EC sites. Therefore, observations of global radiation were obtained from the automated weather stations employed by the Royal Netherlands Meteorological Institute (KNMI) in Stavoren and Lelystad (see Fig. 2.4). The KNMI weather station in Lelystad is assumed to be representative of Trintelhaven. The sub-skin water temperature, used to estimate the water vapour pressure at the air–water surface, was retrieved from the hourly sub-skin Sea Surface Temperature product with a  $0.05^\circ$  spatial resolution derived from the Meteosat-11 satellite. The product specifications describe a target accuracy with a bias of  $0.5^\circ\text{C}$  and a standard deviation of  $1.0^\circ\text{C}$ . From this product, the grids belonging to the locations of Stavoren ( $52^\circ53'06.2''\text{N}$   $5^\circ21'04.1''\text{E}$ ) and Trintelhaven ( $52^\circ38'03.8''\text{N}$   $5^\circ25'03.8''\text{E}$ ) were retrieved. Data were only available during cloudless days. Furthermore, routinely measured water temperatures of Lake IJssel were retrieved from Rijkswaterstaat measuring stations. For this, the Friese Kust and Marker Wadden stations (red triangles in Fig. 2.4) were used; the water temperature at these stations is measured at a depth of  $-1.5\text{ m}$  NAP and

–1.2 m NAP respectively. Although a strong vertical water temperature gradient typically exists near the water surface, a good correlation ( $R^2 = 0.71$  and  $R^2 = 0.94$  for the summer period of 2019 at Stavoren and Trintelhaven respectively) was found between the sub-skin water temperature from the satellite product and the water temperature measured at the larger depths.

In Chapter 5, the drivers of evaporation of 19 different EC flux sites covering six land cover types were studied. For each site the following variables were required: latent heat flux, global radiation, net radiation, air temperature, wind speed, vapour pressure deficit (VPD), precipitation ( $P$ ) and soil moisture (SM). Soil moisture data for all sites originate from the ERA5-Land reanalysis dataset, which is based on the land component of the ECMWF ERA5 climate reanalysis (Muñoz Sabater, 2021). It is a gridded global dataset with a spatial resolution of  $0.1^\circ \times 0.1^\circ$  and an hourly temporal resolution. Soil moisture from the first and shallowest layer between 0 and 7 cm was used. The majority of the other meteorological variables was measured at the site. However, in some cases precipitation (Stavoren, Trintelhaven, Amsterdam, Speulderbos) and radiation data (Stavoren, Trintelhaven) were not available. In those cases data from the nearest automatic meteorological station operated by the Royal Netherlands Meteorological Institute (KNMI) were used. Similarly, if one of the variables was missing for more than 60 % of the time, with latent heat flux as reference, data from the nearest station were used to fill the gaps using linear regression. In case of small gaps of at most one hour, the gap was linearly interpolated. Daily averages were only calculated if valid data were available for at least 70 % of the time.



## Chapter 3

# (Dis)agreement between evaporation models

This chapter is based on:

Jansen, F. A. and Teuling, A. J. (2020). Evaporation from a large lowland reservoir – (Dis)Agreement between evaporation models from hourly to decadal timescales, *Hydrology and Earth System Sciences*, 24, 1055–1072. doi: 10.5194/hess-24-1055-2020.

## Abstract

Accurate monitoring and prediction of surface evaporation become more crucial for adequate water management in a changing climate. Given the distinct differences between characteristics of a land surface and a water body, evaporation from water bodies requires a different parameterization in hydrological models. In this chapter, we compare six commonly used evaporation models that are sensitive to different drivers of evaporation, brought about by a different choice of parameterization. We characterize the (dis)agreement between the models at various temporal scales ranging from hourly to 10-yearly periods, and we evaluate how this reflects in differences in estimated water losses through evaporation of Lake IJssel in the Netherlands. At smaller timescales the models correlate less ( $r = 0.72$ ) than at larger timescales ( $r = 0.97$ ). The disagreement at the hourly timescale results in distinct diurnal cycles of estimated evaporation for each model. Although the models agree more at larger timescales (i.e. yearly and 10-yearly), there are still large differences in the projected evaporation trends for the future period 2019–2100, showing a positive evaporation trend to a greater (i.e. Penman, De Bruin–Keijman, Makkink, and Hargreaves) or lesser extent (i.e. Granger–Hedstrom and FLake). The resulting discrepancy between the models in estimated water losses of the Lake IJssel region due to evaporation ranges from 4 mm (Granger–Hedstrom) to 94 mm (Penman) between the models. This difference emphasizes the importance and consequence of the evaporation model selection for water managers in their decision making.

## 3.1 Introduction

Evaporation is the largest loss term of the land surface water balance, and it couples the Earth's water and energy cycle (Beer et al., 2018). This hydrological cycle is projected to intensify in the future as a consequence of global warming (Huntington, 2006; Oki and Kanae, 2006; Jung et al., 2010). This intensification will result in higher and more extreme precipitation and enhanced surface evaporation, which can threaten our drinking water resources and increase the vulnerability of natural ecosystems and agricultural production (Arnell, 1999; Vörösmarty, 2000; Middelkoop et al., 2001; Verburg and Hecky, 2009; Trenberth et al., 2014). To avoid or alleviate negative consequences of droughts and floods and to guarantee ample access to high-quality freshwater resources, an efficient water management system is required. In a changing climate, the ability to accurately monitor and predict surface evaporation therefore becomes even more crucial for adequate water management. However, there can be considerable uncertainty even in the signs of hydrological projections depending on model parameterization or structure (Melsen et al., 2018). Accurate evaporation estimates are particularly important in densely populated and hydrologically sensitive areas such as the low-lying Netherlands.

The Netherlands is an example of a region for which many studies have been dedicated to a better understanding of the processes driving the terrestrial part of surface evaporation, including forested, agricultural, and urban areas (De Bruin and Lablans, 1998; Dolman et al., 1998; Elbers et al., 2009; Vermeulen et al., 2015; Teuling, 2018a). Resulting from the differences in surface characteristics, the dynamics of surface evaporation, as well as its sensitivity to different atmospheric drivers, will differ over various land use types. For forests, Moors (2012) found that surface evaporation is mainly driven by the vapour pressure deficit (VPD). In contrast, surface evaporation over grasslands is typically driven by available energy through radiation, with little to no sensitivity to VPD (Makkink, 1957). This direct relation between net radiation and surface evaporation was also found by Beljaars and Bosveld (1997) for the grassland area around Cabauw, the Netherlands. For urban areas, Jacobs et al. (2015) found a clear negative relation between observed surface evaporation and days since the last precipitation event. This can be attributed to the almost immediate drying of the vast impermeable surfaces, suggesting that urban environments are strongly water-limited. In the case of open water bodies wind speed was found to be the most important driver of evaporation according to Granger and Hedstrom (2011). Despite the fact that water bodies comprise a large share of the total area in the Netherlands ( $\sim 17\%$ , Huisman, 1998) and therefore form a crucial element in our water management system, in the past only a few studies in the Netherlands focussed on open water evaporation (Keijman and Koopmans, 1973; De Bruin and Keijman, 1979; Abdelrady et al., 2016; Solcerova et al., 2019), and few observations of open water evaporation are available.

Water surfaces have different surface properties than land surfaces, which leads to a difference in behaviour of the turbulent exchange, which can be seen from the main drivers of this exchange, namely the temperature and vapour pressure gradient (see Fig. 3.1). One important difference is that solar radiation is able to penetrate a water surface, in contrast to a land surface, which is not transparent. Therefore the energy balance is not preserved at the water surface, which entails heat storage in the water body. As a consequence of this thermal inertia, it was found that on shorter timescales the turbulent fluxes are not directly coupled to global radiation and that the diurnal cycle of turbulent fluxes is smaller (Kleidon and Renner, 2017) and shifted in time compared to land surfaces (Venäläinen et al., 1999; Blanken et al., 2011). Blanken et al. (2000) found, similarly to Granger and Hedstrom (2011), a relation between evaporation and the product of horizontal wind speed and vapour pressure gradient on daily timescales. In contrast, Nordbo et al. (2011) found the vapour pressure deficit alone to be more strongly correlated with evaporation rather than the product of wind speed and vapour pressure deficit. On intraseasonal timescales, Lenters et al. (2005) found evaporation to be a function of the thermal lag between temperatures of air and water. Resulting from the difference in properties, and consequently its behaviour, the estimation of evaporation from lakes requires a different parameterization than land surface evaporation in hydrological models to account for the relevant driving processes at the timescale of interest.

To illustrate the difference between open water evaporation and evaporation above land surfaces, we used observations from a short measurement campaign. During this measurement campaign in August/September 1967 the vertical gradients of vapour pressure and temperature were measured at the water surface and at 2 and 4 m above the former Lake Flevo (Wieringa, 2019). It is assumed that the sign of these gradients can be used as a proxy for the sign of the latent and sensible heat exchange between the surface and the atmosphere. This proxy is used because there are no direct measurements available of open water evaporation ( $E_{\text{water}}$ ) during the 1967 measurement campaign. To analyse the difference between latent and sensible heat fluxes above land surface and open water, the observations of this measurement campaign above Lake Flevo were compared to observations conducted above a grassland in Cabauw. The results show distinct differences despite the similar behaviour of global radiation. The latter generally regarded as the main driver of evaporation. It demonstrates that both the temperature and vapour pressure gradients above the lake are positive throughout most of the day and night. This refers to unstable situations which become strongest during the night when the air cools faster than the water surface. The continuous positive gradient of vapour pressure above the lake indicates that evaporation continues during the night, which is in contrast to what is found above land. Another distinct difference between land and lake surfaces can be found in the timing of the peak of the temperature and vapour pressure gradients, which are a few hours earlier above land than over the lake. From this experiment it directly becomes clear that we can distinguish a difference in behaviour of the latent and sensible

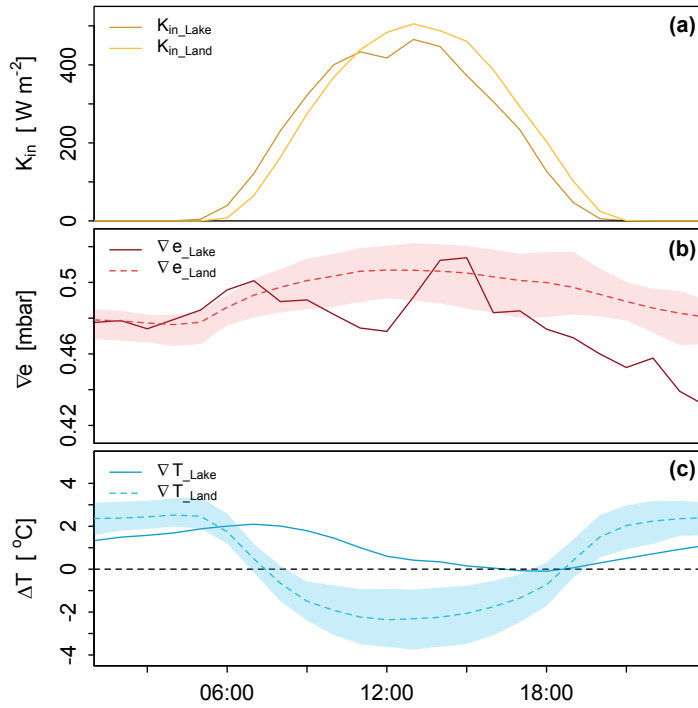


**Figure 3.1:** Illustration of the mean diurnal cycle of proxies for latent and sensible heat fluxes over land compared to open water. Lake data is obtained above Lake Flevo during the Flevo experiment in Aug/Sept 1967 (Wieringa, 2019). Data above land originates from observations in Cabauw, and is based on ten Aug/Sept months of consecutive years (2009–2018); the solid line represents the average and the shaded bands represent the range in these ten years. The top panel presents the diurnal cycle of global radiation (a). The middle and bottom panel display the vertical gradients of vapour pressure and temperature for the lake and land surface (b and c, respectively).

heat fluxes above land compared to over a lake, which therefore should be acknowledged in hydrological models.

Given the importance of open-water evaporation in short-term predictions and long-term projections, the process should be parameterized realistically in operational hydrological models. Depending on the parameterization strategy of a model to capture the process of evaporation at the relevant timescale, different decisions are made to parameterize evaporation. In the past, most studies have focussed on the parameterization of open-water evaporation on weekly or even longer timescales (Finch, 2001; Zhan et al., 2019), where often potential evaporation is improperly used as a proxy for lake evaporation, neglecting heat storage (Lazhu et al., 2016; Duan and Bastiaanssen, 2017). However, parameterizations at the hourly and daily timescales have remained underexplored. The effect of the



parameterization strategy on the short-term prediction and long-term projection of evaporation can likely lead to profound differences in model results (Melsen et al., 2018) and therefore in (local) water management decisions. Our aim therefore is to study the effects of various parameterizations of evaporation on shorter-term local water management and to investigate how these parameterization decisions affect long-term hydrologic projections. To this end, we compare to what extent six commonly used evaporation models (dis)agree at various temporal scales and look at the impact of the different parameterizations of evaporation under projected climate change.

## 3.2 Methods and data

### 3.2.1 Evaporation models

A wide variety of models exist that can be used to estimate evaporation from water bodies. In this chapter, six commonly used evaporation models, that are sensitive to a variety of forcings, are systematically compared. We compare the radiation-driven models of Penman (1948), De Bruin and Keijman (1979) and Makkink (1957), the temperature-driven Hargreaves (1975) model, the transport-driven model developed by Granger and Hedstrom (2011), and the more physical model FLake developed by Mironov (2008). The choice for these models, as well as a detailed description of these models is provided in Section 2.3. An overview of the model equations and the required input data is shown in Table 2.2 and Table A1 in Appendix A.

### 3.2.2 Study area

In this chapter, the (dis)agreement of evaporation models is studied for the Lake IJssel region. Lake IJssel, located in the north of the Netherlands, is the largest freshwater lake in the Netherlands, bordering the provinces of Flevoland, Friesland, and North Holland (see Fig. 2.4 and Sect. 2.2). Covering an area of 1100 km<sup>2</sup> with an average depth of 5.5 m and a maximum depth of 7 m, the lake can be considered a large shallow lake. The lake receives its freshwater supply ( $\sim 340 \text{ m}^3 \text{ s}^{-1}$ ) from the IJssel River and from the neighbouring polder systems. The main outflow from the lake occurs under gravity at the sluices of the Afsluitdijk embankment. The lake has an important hydrological function in the low-lying Netherlands in both flood prevention and freshwater supply for agricultural and drinking water purposes. For more information about the study area, we refer to Section 2.2.

### 3.2.3 Data input sources

The six evaporation models are compared during a long-term historical period (1960–2018) and a projected future period (2019–2100). The observed historical input data for the models were obtained from the automated weather station De Bilt (see Fig. 2.4),

employed by the Royal Netherlands Meteorological Institute (KNMI), and situated at approximately 50 km distance from Lake IJssel. We gave preference to a long-term dataset of observed meteorological variables above land, rather than a shorter-term dataset of the same variables in closer proximity to Lake IJssel for this comparison study. Besides the meteorological data, some of the evaporation models also require water surface temperature data. Considering the data availability and the temporal resolution of different water temperature data sources (e.g. satellite, observations by Rijkswaterstaat), we have chosen to use the FLake estimations of WST for further analysis. To quantify the (dis)agreement between the models on the long-term, 3-hourly realizations resulting from the regional climate model (RCM) RACMO2 (Van Meijgaard et al., 2008) driven by the global climate model (GCM) EC-EARTH 2.3 (Hazeleger et al., 2012) were used. In Section 2.5 a more elaborate explanation of the input data used for the models is given.

### 3.2.4 Diurnal cycle

Models that are sensitive to different types of forcings show a distinct diurnal signal of estimated evaporation. A wide variety of evaporation models uses  $K_{in}$  as forcing variable to estimate the diurnal cycle of evaporation, partly because  $K_{in}$  affects temperature, vapour pressure deficit (VPD), and wind speed, which are all driving forces of evaporation. Therefore, an analysis of the diurnal signals and possible phase shift of these variables provides information on how these driving forces relate to each other and to the estimated evaporation.

We depict the diurnal cycle as function of time for 1 specific day where no clouds were present, as well as for the average diurnal cycle for the period 1960–2018 using data from De Bilt, the Netherlands (see Fig. 2.4 and Sect. 3.2.3). Another way that we will use to analyse and illustrate the diurnal cycle and the relation to other evaporation models is to plot evaporation as a function of  $K_{in}$  similarly to Renner et al. (2019). When the diurnal cycle appears as a hysteresis loop, it indicates a phase difference between the addressed variable and  $K_{in}$ . The size of the loop quantifies the magnitude of the phase lag, and the direction of the loop denotes whether the phase lag is negative or positive. The model of Hargreaves will be omitted in these diurnal cycle analyses. This model requires a temperature maximum and minimum (see Appendix A) over the considered time period. Therefore, it is not possible to calculate hourly estimated evaporation for this model with the given hourly observations of temperature.

### 3.2.5 Long-term trends

To explore how evaporation has been changing in the last decades (1960–2018) and how it is projected to change in the future (2019–2100) in a changing climate, we will force the evaporation models with realizations resulting from the regional climate model (RCM) RACMO2 over these periods. The spatial grid cell that represents De Bilt in the RACMO

model is used (Sect. 2.5). The trend of the yearly averaged estimated evaporation rates will be detected based on weighted local regression, using the LOcally WEighted Scatterplot Smoother (LOWESS) method (Cleveland, 1979). This method is applied to the observational data for the historical period and to the average of the 16 RACMO members for the future period. Mean and standard deviation are calculated using the average of the RACMO members, where the standard deviation is calculated based on the de-trended time series.

### 3.2.6 Model (dis)agreement

A difference in sensitivity of the models to drivers of evaporation can help to explain the (dis)agreement found in the behaviour of estimated evaporation. To compare this sensitivity a perturbation of 1 % will be imposed one by one on the daily observational data from De Bilt of four key variables, namely air temperature, solar radiation, wind speed, and vapour pressure, without changing the other variables. For this, the percentage difference of estimated evaporation with perturbation of one of the variables to the estimation of the baseline situation without any perturbation will be calculated.

The correlations between the estimated evaporation using the different models and various meteorological variables using data from De Bilt will be calculated based on Pearson's parametric correlation method, measuring the linear dependency between two variables. We will calculate the correlations for all the timescales ranging from hourly to 10-yearly periods, all based on hourly data. To ensure that the number of data points in the calculation does not influence the results, we will apply bootstrapping to artificially create the same number of data points for each timescale.

## 3.3 Results and discussion

### 3.3.1 estimation of the diurnal cycle

The diurnal signals of several meteorological variables and estimated and observed evaporation are depicted in Fig. 3.2. The solid lines are the results from a sunny day without any clouds in March 2016, while the dotted lines reflect the average diurnal cycles. It can be seen that net radiation ( $R_n$ ) peaks between 13:00 and 14:00 LT, which coincides with the peaks of evaporation estimated using the radiation-based models, i.e. Penman (PN), De Bruin–Keijman (BK), and Makkink (MK). The peaks of these radiation-based models are estimated 2 hr later than the observed evaporation peak in Cabauw. estimated evaporation becomes negative during the night following net radiation in the cases of the PN and BK models. However, this is not realistic given the fact that the energy balance is not preserved at the water surface, which is assumed by these models, and the energy released from heat stored in the water can exceed the net radiation at night. This will drive both a positive latent and sensible heat flux. Evaporation estimated with the wind-driven

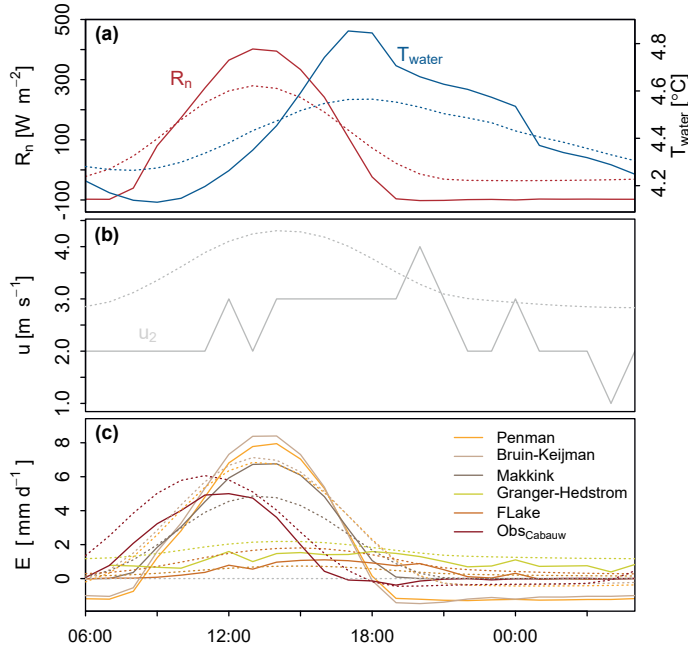


**Figure 3.2:** Illustration of the diurnal response of estimated evaporation. (a) Diurnal cycle of net radiation and water temperature (b) of wind speed, and (c) of the different evaporation models. Solid lines represent a sunny day in March 2016, while the dotted lines indicate the average diurnal cycle based on the years 1960–2018, and for observed values in Cabauw this is based on the years 1986–1997 and 2001–2018. The dotted line was lowered by  $7.5^{\circ}\text{C}$  to facilitate comparison of its dynamics to the cycle of the single sunny day.

Granger–Hedstrom (GH) model is damped relative to the radiation-based models, and it is rather constant throughout the day, with a small peak following the signal of the wind speed. The signal of evaporation resulting from FLake (FL) is damped as well, and its peak lags 2 hr behind relative to  $R_n$ , induced by a combination of  $K_{\text{in}}$ ,  $u$ , and  $T_a$ . The total average diurnal evaporation is significantly lower than for the radiation-based models. This can be explained by the remaining heat storage term of the energy balance in FL, which is used to warm up the water. This heat storage capacity is explicitly accounted for in FL. Hargreaves’ temperature-based model (HA) is not depicted in the graph because the model does not allow us to calculate evaporation at hourly timescales given the available data (see Sect. 3.2.4). The diurnal range of the water temperature ( $T_{\text{water}}$ ) is small but shows a distinct peak 4 hr lagging behind the peak of  $R_n$ , which indicates that during the day heat is stored in the water, which partly is released back during the night. The dotted line illustrating the average diurnal cycle of  $T_{\text{water}}$  was artificially lowered by  $7.5^{\circ}\text{C}$  in this graph, merely to show its diurnal course and the timing of the peak.

Figure 3.3 illustrates the diurnal cycle of the (a) latent heat flux, (b) vapour pressure, and (c) temperature, which are plotted as a function of  $K_{\text{in}}$  for a sunny day without any clouds in March 2007. It can be seen that evaporation estimated using the MK model is almost in phase with  $K_{\text{in}}$  (phase lag is 7 min), which may be expected from a model that uses  $K_{\text{in}}$  as the main driving force of evaporation. The largest phase lag (= 114 min) results from the estimation with FL; this can be explained by the fact that this model explicitly accounts for heat storage changes, resulting in a less direct response of evaporation to  $K_{\text{in}}$ . The analysis of diurnal patterns thus shows that  $K_{\text{in}}$  explains most of the variance in evaporation for models PN, BK, and MK. However, the models that incorporate WST (model GH) and heat storage capacity (FL) as explaining variables show less variation in evaporation during the day and therefore do not relate directly to  $K_{\text{in}}$ .

Air temperature shows a pronounced anti-clockwise (ACW) loop when plotted as a function of global radiation, which indicates that heat is stored in the lower part of the atmospheric boundary layer. However, the water surface temperature shows very little response to  $K_{\text{in}}$ . This combination leads to another distinct hysteresis loop of the driving force of sensible heat flux, namely, the gradient  $T_s - T_a$ , which has a clockwise (CW) direction. This implies that the latent heat flux is preceded by the sensible heat flux. The vapour pressure is rather constant throughout the day and does not display a clear hysteresis loop. However, the saturated vapour pressure, which is a function of  $T_a$ , displays pronounced ACW hysteresis. As a result, VPD also has a large ACW hysteresis loop, which is the key driver of evaporation in the PN model.

Following the analyses of the diurnal cycle, the occurrence of heat storage and release in the water body is demonstrated through the diurnal cycle of  $T_{\text{water}}$ . The capacity of heat storage should therefore be accounted for by an evaporation model. FL is the model that mimics this thermal inertia effect most clearly in its diurnal cycle, which is also supported through its phase lag to  $K_{\text{in}}$ . This makes the FL model the most realistic model to use at this timescale.

### 3.3.2 Long-term estimations and projections

For each model the estimated evaporation rates based either on observations in De Bilt or on RACMO realizations are shown in Fig. 3.4 for the historical (1960–2018) and future (2019–2100) period (note that the values on the y-axes differ). The grey lines indicate the 16 realizations of the RCM RACMO members, while the black line is the estimation resulting from observational data measured in De Bilt. The dotted blue line represents the trend of this black line. Following the positive trend of evaporation as was observed in Cabauw (red line in the lowest panel), all the models, except for the GH model, also estimate a positive trend in the historical time period when using observations from De Bilt (black line). Apart from models GH, HA, and FL, the RACMO realizations resulting from the RCM estimations also show positive trends in the historical period. However, these

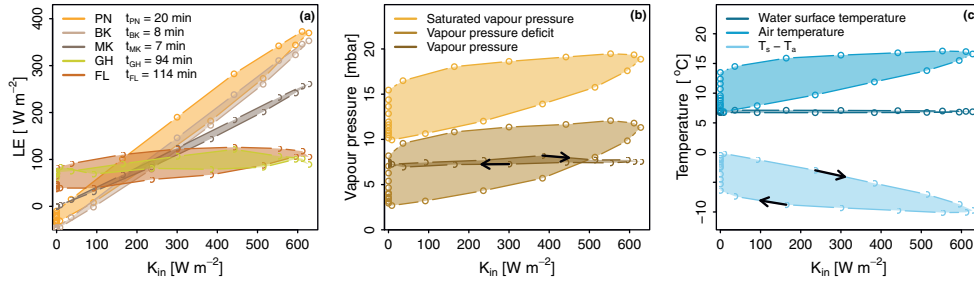


**Figure 3.3:** Phase difference of evaporation variables in response to global radiation, illustrating latent heat flux (a), vapour pressure (b), and temperature (c) responses to global radiation. Differences are calculated for one day in March 2007. The legend displays the daily phase lag in minutes. The direction of all hysteresis loops are counter-clockwise, indicating a positive phase lag with respect to global radiation, except for the two loops that have a clockwise direction indicated by a black arrow.

trends are not as strong as the trends resulting from the estimations which use observations from De Bilt. For the future period these RACMO realizations have a stronger positive trend compared to the historical period for all the models, again except for GH and FL. This implies that the RACMO estimations do not always agree with the estimations which are based on observations; however, they do demonstrate the differences between the six models regarding predicted future trends.

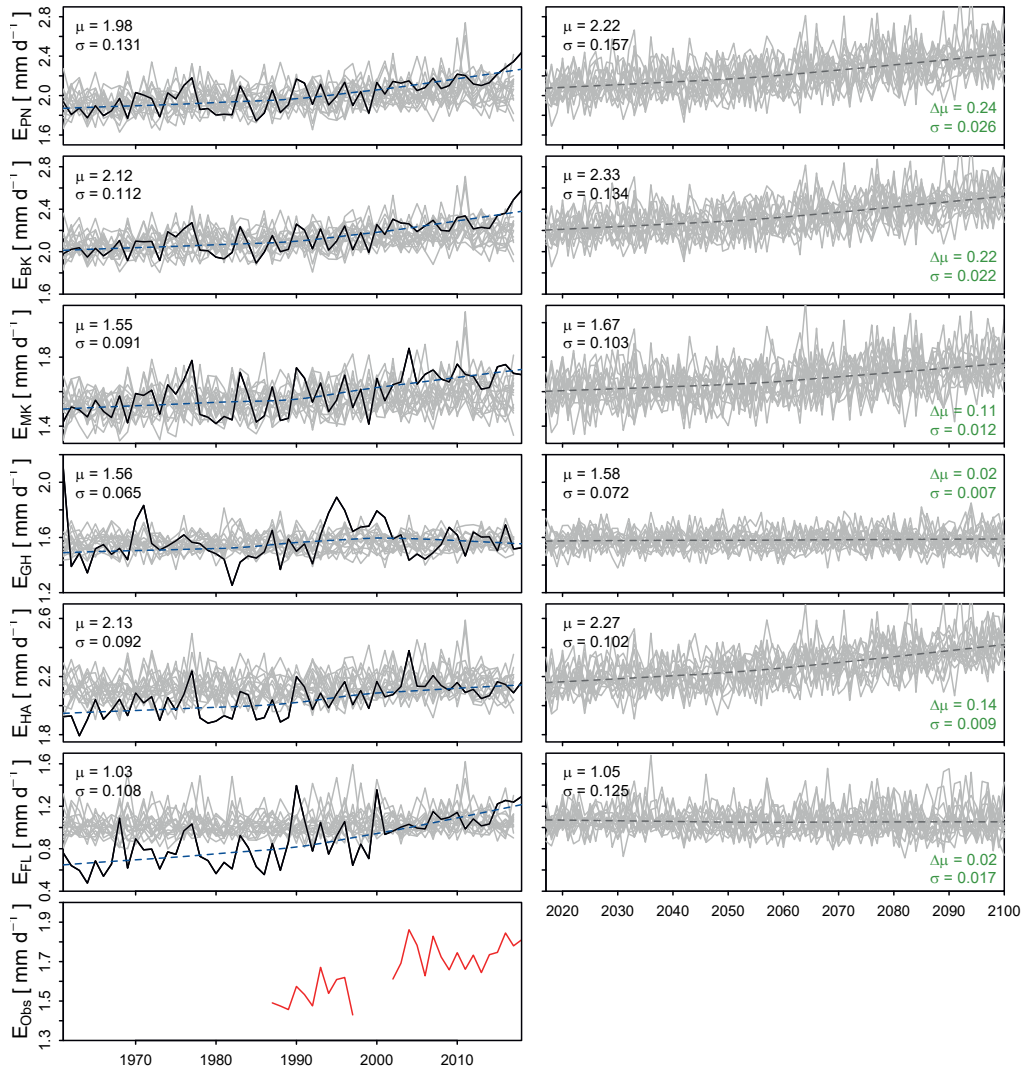
The results from the GH and FL models differ from the other models in the sense that the RACMO realizations do not result in a significant trend in either the estimated historical or projected future periods, while in the historical period the estimation based on observations presents a positive trend when using the FL model. The latter can be explained by the fact that the FL model is most sensitive to  $K_{in}$ ,  $T_a$ , and  $u$ , of which for both  $K_{in}$  and  $u$  the RACMO realizations do not show any trend (not shown here). The mismatch in the historical period for FL between the estimations based on observations and the estimations based on RACMO realizations can be attributed to the inability of RACMO to capture the trend in  $K_{in}$ . This inability will also influence the estimations made by the radiation-based models, which implies that for these models estimated trends in the future period are likely to be stronger than demonstrated in Fig. 3.4. This will lead to even larger disagreement of estimated evaporation between the six models.

Comparison between the models of the overall positive trend that is projected to continue in the future period reveals that not only the average estimated evaporation of all RACMO members ( $\mu$ ) will increase in the future for all the models, ranging from an increase of  $0.02 \text{ mm d}^{-1}$  (GH and FL) to  $0.24 \text{ mm d}^{-1}$  (PN), but also that the variability ( $\sigma$ ) is projected to increase (see Fig. 3.4). This is also demonstrated in Fig. 3.5 for both the historical (orange) and future (blue) periods. Here the spread is defined as the difference between the yearly average maximum and minimum values of the 16 RACMO members based on daily evaporation rates. For each model the average and the spread are projected to increase in the future; however, the rates at which this happens differ substantially between the models. The largest difference in spread can be found between the GH model, which has a spread of  $0.32 \text{ mm d}^{-1}$ , and the PN model with a spread of  $0.69 \text{ mm d}^{-1}$  in the historical period, and increases to a range that varies from  $0.36 \text{ mm d}^{-1}$  (GH) to  $0.94 \text{ mm d}^{-1}$  (PN) in the future period. The models that resemble each other most, and differ least in spread, are the PN and BK models during both the historical and future periods.

### 3.3.3 Model (dis)agreement at various timescales

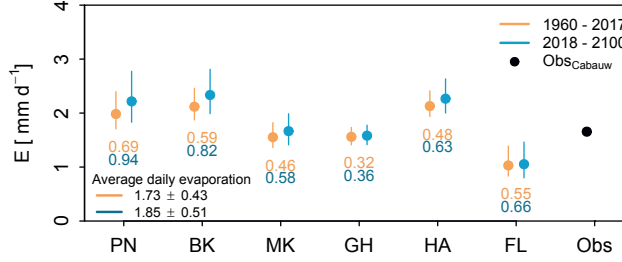
Figure 3.6 displays the difference in percentage of estimated evaporation with the baseline situation without any perturbation. The upper and lower sets of panels depict the same information arranged per variable or per model, respectively. Most of the models show the largest sensitivity to  $T_a$  and  $K_{in}$ . The purely temperature-driven HA model is only sensitive to  $T_a$ . The wind-driven GH model is the model most sensitive to wind speed (1 % difference), which is expected, but FL is also sensitive to wind speed, showing a difference of 0.5 % compared to the baseline situation without any perturbation. This implies that the behaviour of these models would start to deviate more from the other models if for instance the wind speed regime were to change in the future. In general FL is the most sensitive model, and therefore this model will start to differentiate more from the other models when these four meteorological variables were to change in the future.

Figure 3.7 displays to what extent the evaporation models and four meteorological variables correlate at (a) hourly, (b) daily, (c) weekly, (d) monthly, (e) yearly, and (f) 10-yearly timescales based on observed data from De Bilt. The colours indicate the direction and magnitude of the correlations. From our data the HA model can only be calculated at a daily timescale or coarser, hence the empty boxes at the hourly timescale. It becomes apparent that at hourly timescales there is a positive correlation between wind speed and estimated evaporation ranging from 0.12 for the MK model to 0.84 for the GH model. At larger timescales, this correlation becomes negative, except for the wind-driven GH model, and for FL it remains positive until a daily timescale. At the two largest timescales considered here (Fig. 3.7e and f), the correlation with wind speed increases again, but these are statistically insignificant except for the GH model. The correlation between  $R_n$  and estimated evaporation remains high at all timescales, except for the GH model. The latter



**Figure 3.4:** Trends of estimated evaporation for the historical and future periods. Black line indicates yearly averaged estimated historical evaporation rates based on data from De Bilt. The dotted blue line represents the trend in this line. The grey lines indicate the yearly averaged estimations from RACMO climate projections. Mean and standard deviation of the RACMO estimations are given in each panel in black. The differences of these statistics between the historical and future periods are given in green. In the lowest panel the yearly averaged observed evaporation at meteorological site Cabauw is presented in red.





**Figure 3.5:** Impact of parameterization on mean current and future evaporation. Coloured dots indicate the mean of all RACMO members for each model for both the historical and future periods. Coloured numbers below each model indicate the spread within the model. Here spread within the models is defined as the difference between the average maximum and minimum values of all RACMO members for both periods, based on yearly average daily evaporation rates (see Fig. 3.4). The black dot represents the averaged observed evaporation in Cabauw over the period 1986–2017.

model shows low correlations with the other models and most meteorological variables, which mostly become statistically insignificant (indicated by the numbers in grey) from weekly timescales and larger. The correlation between  $R_n$  and evaporation estimated using FL increases steadily from 0.63 to 0.94 with an increasing timescale. Regarding the correlation between evaporation and  $T_a$ , and evaporation and VPD, the matrices show that the correlations increase steadily for all evaporation models, again with the exception of the GH model. However, it should be noticed that there is a dip in the correlation at yearly timescales. Furthermore, the correlation between the meteorological variables  $R_n$ ,  $T_a$ , and VPD was found to increase with an increasing timescale.

The radiation-based models agree highly with each other, as can be expected, over the entire range of timescales, with correlation values above 0.9. The GH model deviates most in terms of correlation from the other models, which could be attributed to the difference in sensitivity to wind speed. The HA model shows the largest increase in agreement with the radiation-based models with increasing timescales. This can be attributed to the increasing correlation between temperature and  $R_n$ , which are the main driving forces of the HA and the radiation-based models, respectively. Comparing the average correlations between the models for each timescale reveals that the correlation increases with increasing timescale from 0.72 at an hourly timescale to 0.97 at a 10-yearly timescale. This increase implies that the models on average tend to agree more with each other at coarser timescales, which means that at smaller timescales the consequence of model choice becomes more apparent. The average correlation at the daily timescale is lowered mainly as a consequence of the low correlations of the GH model with the radiation-based models. It should be noted that insignificant values were not incorporated in the calculation of the average correlations.

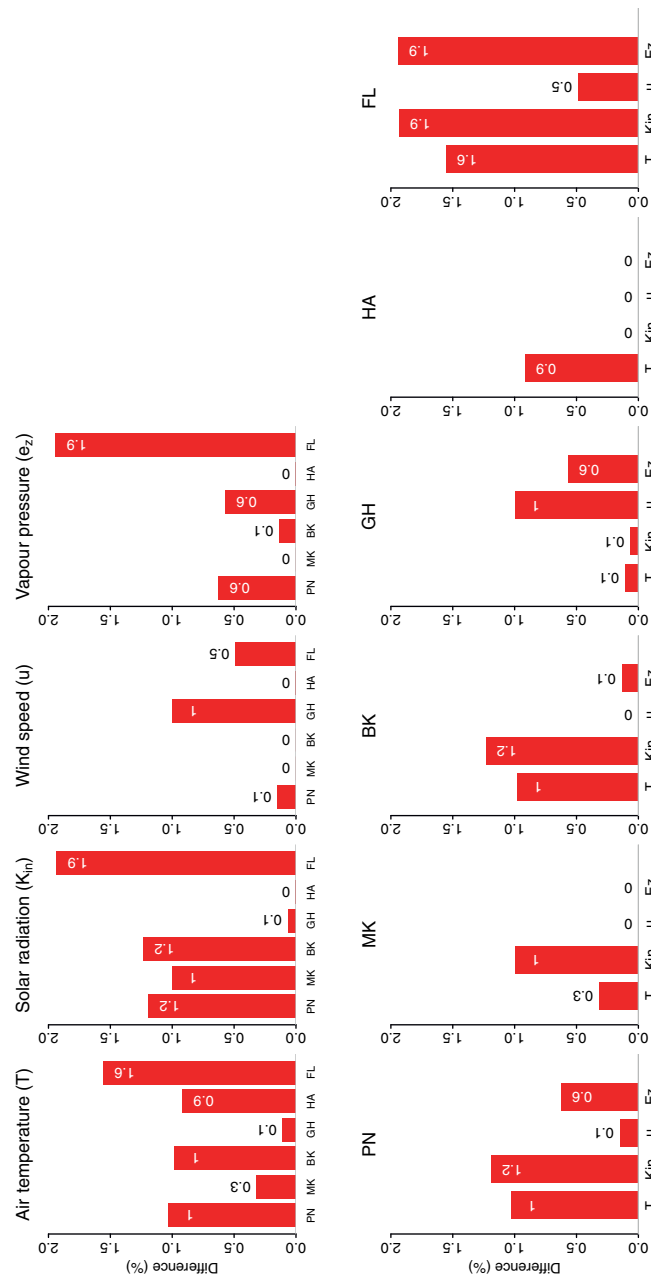


**Figure 3.6:** Sensitivity of estimated evaporation to meteorological drivers. This effect is expressed as the percentual difference between a perturbed estimation and the baseline as indicated by the white numbers plotted in the bars (rounded to one decimal). Upper set of panels arranged per variable. The lower set of panels displays the same information but clustered per model.

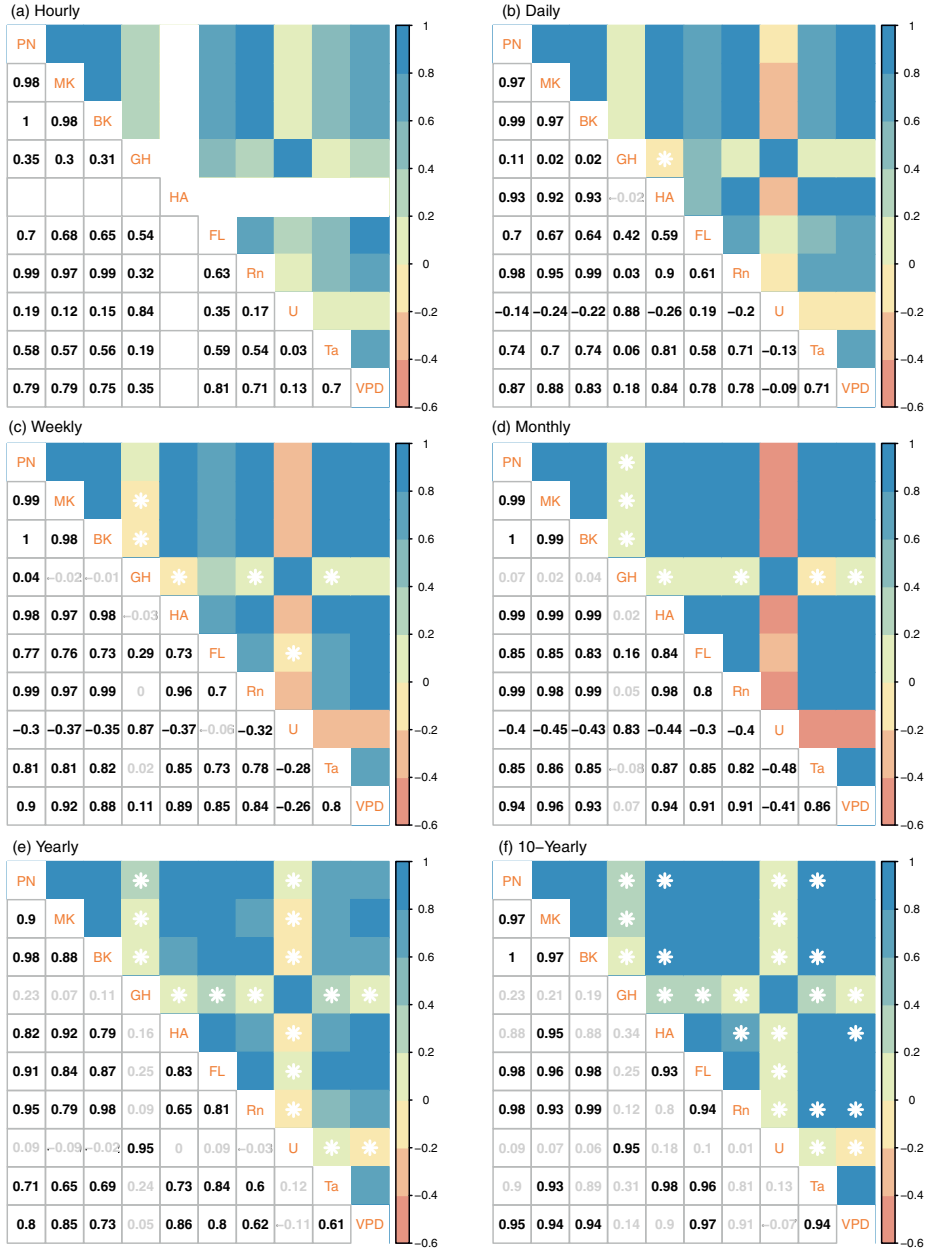


**Figure 3.7:** Correlation between estimated evaporation and meteorological variables at different timescales. Correlations are shown for (a) hourly, (b) daily, (c) weekly, (d) monthly, (e) yearly and (f) 10-yearly timescales. The colours indicate the sign and strength of the correlation. A white star and the corresponding grey number mark insignificant correlations ( $\alpha = 0.01$ ).

In Fig. 3.8 the correlations ( $r$ ) between estimated evaporation and VPD,  $T_a$ , and  $R_n$ , respectively, are depicted to further explore the (dis)agreement between the models over the range of timescales. This correlation has been calculated based on observational data from De Bilt. In general there is a high correlation ( $r > 0.75$ ) between estimated evaporation and VPD, which increases with increasing timescales, up to a correlation of 0.97 at the 10-yearly timescale. However, there is a small drop at the yearly timescale, which is also visible in Fig. 3.7. We were not able to determine the exact cause of this, but it could be a result of cross-correlation in the data. The GH model deviates in behaviour compared to the other five models, since it is the only model that does not explicitly include  $T_a$ , and with that VPD through the saturated vapour pressure, which is a function of temperature. The GH model only includes a temperature gradient, which is determined using  $T_{\text{water}}$  estimated from the FL model and  $T_a$  from De Bilt, as additional information to wind speed. The correlation between estimated evaporation and  $T_a$  increases from 0.57 at the hourly timescale up to 0.98 at the 10-yearly timescale, again with a small drop at the yearly timescale. Furthermore, similar to the correlation with VPD, the GH model again demonstrates a different behaviour compared to the other models. There is a strong increase in the correlation at the yearly and 10-yearly timescales for this model, which could be related to a change in the sign to positive values for the correlation between wind speed and  $T_a$  at these timescales (see Fig. 3.7). The correlations with  $R_n$  demonstrate clearly the resemblance between the radiation-based models PN, BK, and MK. The HA model shows similar correlations as well, except for the largest two timescales where the correlation is lower. The FL model correlates better with  $R_n$  with increasing timescales, confirming that at small timescales  $R_n$  is not a direct driver of evaporation as a result of heat storage. The correlation between  $R_n$  and evaporation estimated by the GH model is close to zero for daily timescales and larger. However, at the hourly timescale the correlation is 0.32. This corresponds to the larger correlation between wind speed and  $R_n$  at this timescale.

The general increase in the correlations with the meteorological variables that was found with increasing timescales implies that ultimately these variables act as driving forces of potential evaporation. However, at the shorter timescales some of these models may fail because the wrong controlling variables are used to estimate actual evaporation. This is especially the case for models that use  $R_n$  as a driver of evaporation and that omit the effect of thermal inertia as a result of heat storage.

Table 3.2 presents for several years the water loss through evaporation expressed as water depths in millimetres for the Lake IJssel region. Meteorological data from De Bilt were used to force the evaporation models, and although there likely will be variation in the spatial distribution of the evaporation rate over the lake, until now it is unknown to which degree this variation exists. The following results thus will merely show the difference between the models rather than the spatial distribution when applied to the Lake IJssel region. For this we considered two average years (1986 and 2009) and the two dry years

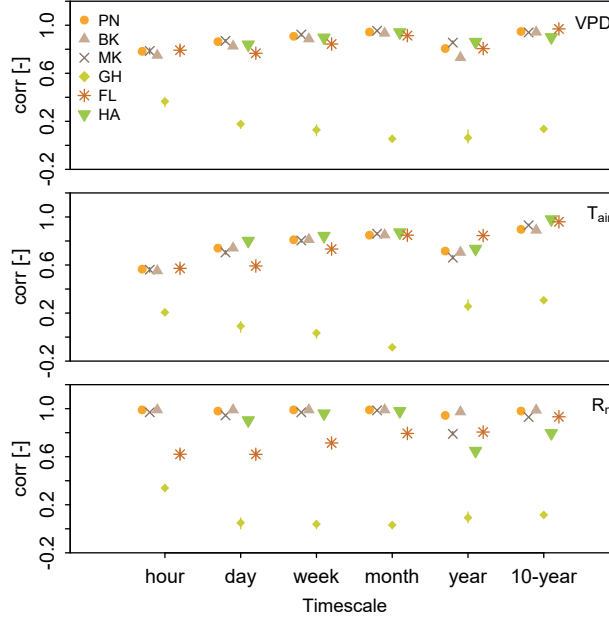


**Figure 3.8:** (Dis)agreement between estimated evaporation and meteorological forcings at different timescales. This correlation is shown for VPD (top panel),  $T_a$  (middle panel), and  $R_n$  (bottom panel).

**Table 3.1:** Average annual inputs and outputs for the Lake IJssel region in millimetres. Values are obtained from operational LHM model simulations. Note that  $Q_{\text{river}}$  can be much smaller during dry summer periods.

	P	$Q_{\text{river}}$	$Q_{\text{prov}}$	$Q_{\text{Wad}}$
Flux	+821	+7036	−99	−6996

(1976 and 2003). For the years 2000 and 2100 projected evaporation was based on the 16 RACMO members. During average years the water level of Lake IJssel would decrease by 649 mm on average as a result of evaporation only; in the case it would not be compensated by incoming fluxes through precipitation ( $P$ ) and water supply by rivers ( $Q_{\text{river}}$ ). Except for evaporation other sources of output are the discharge of water towards the surrounding provinces ( $Q_{\text{prov}}$ ) for agricultural purposes and discharge to the Waddenzee ( $Q_{\text{Wad}}$ ) for water-level regulations. Values of these annual inputs and outputs are obtained from operational LHM model simulations (De Lange et al., 2014) and are used as a reference only (see Table 3.1).

Large differences were found between the evaporation models in terms of the amount of water losses through evaporation annually. HA and FL are at both ends of the spectrum,

**Table 3.2:** Water losses through evaporation for the Lake IJssel region under different conditions. Water losses are expressed as water depths in millimetres.

	Observations				Model projections		
	Average year		Dry year		$\Delta$ Water depth		
	1986	2009	1976	2003	2000	2100	2000–2100
Penman	678	781	760	761	$733 \pm 50$	$827 \pm 62$	$-94 \pm 80$
De Bruin-Keijman	706	817	791	799	$751 \pm 41$	$830 \pm 49$	$-79 \pm 64$
Makkink	594	642	652	676	$591 \pm 33$	$652 \pm 39$	$-61 \pm 51$
Granger-Hedstrom	683	628	676	565	$732 \pm 32$	$736 \pm 38$	$-4 \pm 49$
Hargreaves	745	788	819	868	$677 \pm 31$	$751 \pm 33$	$-74 \pm 45$
FLake	310	417	378	376	$503 \pm 36$	$508 \pm 50$	$-5 \pm 62$

where HA estimates the largest losses through evaporation (745 mm), while FL estimates less than half of that (310 mm) in 1986. During dry years the total water loss through evaporation increases to on average 677 mm, but within a specific year, e.g. 2003, it ranges from 868 mm using HA to 376 mm using FL to estimate evaporation. Due to the large differences in estimated evaporation between the various models, the result of the estimated water balance of the lake could be positive or negative. This means that based on the model used to estimate evaporation, the water managers would make different decisions on whether to stop the water inlet to the surrounding land for agricultural purposes or not, for instance, or whether more or less water needs to be discharged to the Waddenzee to keep the level of the Lake IJssel region within a safe range. Since there are no direct operational measurements of evaporation available in the Lake IJssel region, this stresses even more that the knowledge of the discrepancy between the models is of great importance for water managers in their decision making.

Based on the results of the RACMO realizations, it is demonstrated that the discrepancy between the models is projected to increase from the years 2000 to 2100. The radiation-based and temperature models show a growing water loss through evaporation, while for GH and FL the water loss remains similar. All the models show increasing evaporation rates leading to lower water availability in the region, where the change in mean water depth from the years 2000 to 2100 ranges from  $-4$  mm (GH) to  $-94$  mm (PN). This implies that if water managers rely on the PN model rather than on the GH model for instance, they might have to decide to supply less water to the surrounding agricultural land.

The effect of the projected changes in evaporation in the future was found to be largest in summer (Fig. 3.9), which coincides with the period that has the highest evaporation rates. This summer period is therefore most critical regarding water resource management, also considering the fact that more extreme periods of drought are expected to occur more frequently. During summer, evaporation is thus projected to increase, and at the same time it is likely that with increasing temperatures the river discharge from the IJssel will decrease (Görgen et al., 2010). So less water will be available during summer, while the

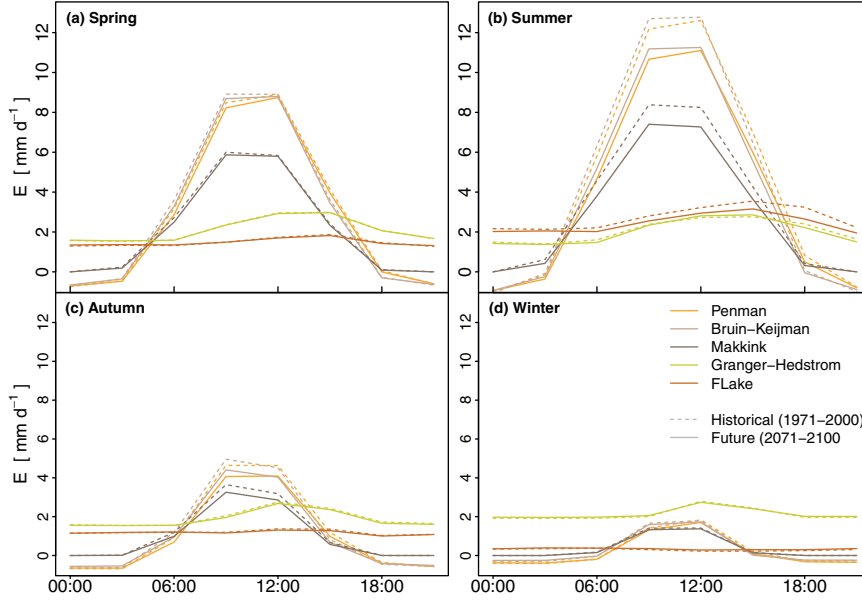


**Figure 3.9:** Projected seasonal change in the diurnal cycle of evaporation. Solid lines represent the historical period and the dotted lines the future period.

water demand from the surrounding land surfaces will increase for agricultural purposes. Therefore, the trade-offs that water managers need to make become very precarious, especially knowing that their decision is based on a certain chosen model that can differ significantly from another model in total estimated evaporation.

### 3.4 Conclusions

The aim of this chapter was to explore the effect of various conceptualizations of evaporation on shorter-term local water management and long-term hydrologic projections. We focussed on timescales ranging from hourly to 10-yearly periods, where we have (i) elaborated on the differences found in the diurnal cycle but also (ii) quantified the (dis)agreement between the models over the range of timescales in terms of correlations. Moreover, we studied how the evaporation rates according to the various models are projected to change in the future.

Our study characterized that there is a large effect of the type of forcing that is used in the evaporation model, especially on the estimated diurnal cycle. This difference is reflected in the total average daily evaporation, the timing of the evaporation peak, and

the day–night cycle. The models that use the radiation approach (PN, BK, and MK) follow the diurnal cycle of the net radiation, where MK becomes zero at night, and PN and BK negative. The estimated evaporation resulting from the GH and FL models is more constant throughout the day, and on average they show a continuation of evaporation during the night. Data of  $T_{\text{water}}$  demonstrated heat storage during the day and release of heat during the night. FL is the model that mimics this effect of thermal inertia most clearly in its diurnal cycle. This makes the FL model the most realistic model to use at this timescale. At larger timescales we found a disagreement between the models in the trend of yearly averaged daily evaporation rates for both the historical (1960–2018) and future (2019–2100) periods. Although both the average and the variability of all models are projected to increase in the future, the rate at which this happens differs substantially between the models. The average evaporation rate increase ranges from 0.02 mm d<sup>-1</sup> (GH and FL) to 0.24 mm d<sup>-1</sup> (PN).

A discrepancy at the whole range of evaluated timescales, from hourly to 10-yearly, is especially present between the radiation and temperature models (PN, BK, MK, and HA), and the wind-driven (GH) and physically based lake (FL) models. However, this disagreement generally decreases with increasing timescale, which is to be expected considering that ultimately evaporation is constrained by the energy input in the system and the transport of water vapour. However, the difference at yearly timescales is still significant. The difference between the models at yearly timescales is also demonstrated when the total yearly water losses through evaporation for Lake IJssel are calculated. For an average year this can range between 417 mm (FL) and 817 mm (BK). During a sensitive dry year this discrepancy can result in water levels being estimated to either rise or drop, solely depending on the evaporation model that is used. When considering future estimations, the projected change in mean water losses through evaporation, expressed as water depths, ranges from 4 mm (GH) to 94 mm (PN) when comparing the years 2000 to 2100. This means that if water managers would rely on the PN model rather than on the GH model, they might have to decide to supply less water to the surrounding land in the future. Therefore, owing to the disagreement between the models, it reveals that the choice of model is of great importance for water managers in their decision making. To gain confidence in which model is most reliable to use, now and in the future, we suggest performing long-term direct observations of  $E_{\text{water}}$  at high temporal resolution. This will help to improve optimal parameterization of  $E_{\text{water}}$  in hydrological models.





# Chapter 4

## Observed drivers of open water evaporation

This chapter is based on:

Jansen, F. A., Uijlenhoet, R., Jacobs, C. M. J., and Teuling, A. J. (2022). Evaporation from a large lowland reservoir – Observed dynamics and drivers during a warm summer, *Hydrology and Earth System Sciences*, 26, 2875–2898. doi: 10.5194/hess-26-2875-2022

## Abstract

We study the controls on open water evaporation of a large lowland reservoir in the Netherlands. To this end, we analyse the dynamics of open water evaporation at two locations, Stavoren and Trintelhaven, at the border of Lake IJssel (1000 km<sup>2</sup>). Eddy covariance systems were installed at these locations during the summer seasons of 2019 and 2020. The measurements were used to develop data-driven models for both locations. Such a statistical model is a clean and simple approach that can provide a direct indication of (and insight into) the most relevant input parameters involved in explaining the variance in open water evaporation, without making a priori assumptions regarding the process itself. We found that a combination of wind speed and the vertical vapour pressure gradient can explain most of the variability in observed hourly open water evaporation. This is in agreement with Dalton's model, which is a well-established model often used in oceanographic studies for calculating open water evaporation.

Validation of the data-driven models demonstrates that a simple model using only two variables yields satisfactory results at Stavoren, with  $R^2$  values of 0.84 and 0.78 for hourly and daily data, respectively. However, the validation results for Trintelhaven fall short, with  $R^2$  values of 0.67 and 0.65 for hourly and daily data, respectively. Validation of the simple models that only use routinely measured meteorological variables shows adequate performance at hourly ( $R^2 = 0.78$  at Stavoren and  $R^2 = 0.51$  at Trintelhaven) and daily ( $R^2 = 0.82$  at Stavoren and  $R^2 = 0.87$  at Trintelhaven) timescales. These results for the summer periods show that open water evaporation is not directly coupled to global radiation at the hourly or daily timescale. Rather a combination of wind speed and vertical gradient of vapour pressure is the main driver at these timescales. We would like to stress the importance of including the correct drivers of open water evaporation in the parametrization in hydrological models in order to adequately represent the role of evaporation in the surface–atmosphere coupling of inland water bodies.

## 4.1 Introduction

Inland water bodies are known to interact with the local, regional, and even global climate; thus, they are highly sensitive to climate change (Adrian et al., 2009; Liu et al., 2009; Le Moigne et al., 2016; Wang et al., 2018; Woolway et al., 2020). Evaporation is a sink in the water balance of inland water bodies; therefore, it becomes most critical to understand how open water evaporation ( $E_{\text{water}}$ ) will respond to these changing conditions. It is expected that changes in long-wave radiation, the Bowen ratio, ice cover, and thermal stratification will affect the dynamics of  $E_{\text{water}}$  in the long term (Wang et al., 2018; Woolway et al., 2020). At the shorter decadal timescale, in contrast, a contribution to trends and variations in  $E_{\text{water}}$  is expected as a result of changes in wind speed and humidity as well as due to global and regional solar dimming and brightening and their effect on water surface temperature (Desai et al., 2009; McVicar et al., 2012; Schmid and Köster, 2016; Wang et al., 2018; Woolway et al., 2020). During the summer season, evaporation rates are highest and, depending on the functions of the water body, the water demand is largest for other purposes such as drinking water extraction and agricultural irrigation practices. Summer seasons are projected to become warmer in the Netherlands, with more severe and prolonged periods of drought (Seneviratne et al., 2006; Seneviratne et al., 2012a; KNMI, 2015; Teuling, 2018b; Christidis and Stott, 2021). Only if we are able to correctly parameterize  $E_{\text{water}}$ , implying that the employed model is right for the right reasons, is it possible to make well-supported short-term predictions and long-term projections of  $E_{\text{water}}$  during these critical summer periods. These predictions and projections could assist water managers to make the appropriate decisions to guarantee ample access to freshwater.

In terms of thermodynamics, a shallow inland water body that is only a few metres deep can be considered as a system that can be placed somewhere between an ocean system (or another deep water body) and an infinite shallow water surface that behaves almost like a land surface. An important difference between these two systems at both ends of the spectrum is the location where heat is stored (Brutsaert, 1982; Kleidon and Renner, 2017). In the case of water bodies, heat storage takes place below the atmosphere–water interface and is generally mixed away from the surface. This is different for a land surface, where heat is stored in the lower atmosphere, vegetation, and the upper soil layers. This leads to larger temperature amplitudes under sunny conditions, with strongly increasing surface temperatures and warming of the lower atmosphere during daytime and strong decreases during night-time. This difference is rooted in the distinct surface properties and heat capacity of a water body and a land surface that lead to different dynamics of turbulent exchange with the atmosphere, which are reflected in both the seasonal and daily cycle of latent heat flux (Brutsaert, 1982). In contrast to a land surface, solar radiation is able to penetrate through the water surface, thereby delivering and storing its energy down in deeper water layers, depending on the light absorption characteristics of the water. There, subsurface redistribution of energy can take place through turbulent mixing and

non-turbulent flow of the water, and the energy can be released back into the atmosphere through sensible and latent heat fluxes. The subsurface energy budget implies that lake depth controls the dynamical range of lake temperature amplitudes on a diurnal timescale. Thus, instead of focusing solely on the surface, the whole volume of the system should be considered. It is essential to understand how differences in the properties of a system result in distinct drivers of evaporation and to include and represent those drivers in the parameterization of evaporation in hydrological models.

The frequently used model of Penman (1948) is widely recognized as the standard for calculating both terrestrial evaporation and  $E_{\text{water}}$  for shallow water surfaces, for which the model was originally developed. Penman (1948) based his model on the historical model originally developed by Dalton in 1802. The latter model (and variations of it in the form of bulk transfer models) has been adopted and reviewed by many oceanographic studies and has been found to perform well in estimating  $E_{\text{water}}$  from oceans (Brutsaert, 1982; Josey et al., 2013; Pinker et al., 2014; Bentamy et al., 2017; Cronin et al., 2019). Dalton (1802) recognized the importance of using the difference in vapour pressure at the water–air interface, where the exchange of water takes place, to model  $E_{\text{water}}$ . This difference is subject to change when energy enters the water body, is stored, and is then released again, thereby changing the temperature and, in turn, the vapour pressure at the water surface. Dalton (1802) proposed that  $E_{\text{water}}$  can best be described by the product of a wind function, acting as a transport mechanism, and the difference between the saturation vapour pressure at the water surface and the vapour pressure at 2 m above the water surface. Penman (1948) eliminated the surface temperature, which is often difficult to determine, by assuming that it could be replaced by temperature and vapour pressure at a reference height via linearization of the vapour pressure curve (Brutsaert, 1982). This assumption results in the essential difference between the models of Dalton and Penman: Dalton uses the vertical difference in vapour pressure, whereas Penman uses the vapour pressure deficit at 2 m height (Brutsaert, 1982). Omitting the water heat flux ( $G$ ) for infinitely shallow water surfaces reduces Penman’s model to a combination of a radiation term that is driven by net radiation and an aerodynamic term.

Most studies in the past have been dedicated to measuring terrestrial evaporation to understand its driving variables. However, significantly fewer studies have performed measurements of  $E_{\text{water}}$  from inland water bodies. This can partly be attributed to practical difficulties when measuring above or close to a water body. There are numerous methods available to measure  $E_{\text{water}}$  using either indirect estimations (e.g. the water balance method, the energy budget approach, the bulk transfer method, or complementary approaches) or more direct measurements (e.g. scintillometry, the eddy covariance technique, or the evaporation pan method) (Finch and Calver, 2008; Abtew and Melesse, 2013). Historically, evaporation pans have been widely employed because of their relatively simple use and moderate data and installation requirements. However, depending on the installation method of the pan, the following drawbacks might be encountered: adverse effects of heat

exchange through the side walls, incomparable heat storage properties of the pan and a lake, limited temporal resolution, and entering or exiting of water caused by wind and rain (Allen et al., 1998; Sumner and Jacobs, 2005; Masoner and Stannard, 2010). Furthermore, inherently, the effects of water stress on evaporation cannot be determined. Scintillometry, a technique that was developed more recently, enables us to quantify  $E_{\text{water}}$  integrated over larger surfaces. Therefore, scintillometers offer the possibility to account for spatial variability and allow for comparisons with data obtained from satellite images (McJannet et al., 2011). However, scintillometers only indirectly measure the turbulent fluxes through the use of the Monin–Obukhov similarity theory (MOST), and the assumptions of this theory do not always hold (Beyrich et al., 2012). In general, the eddy covariance technique is considered to be the most accurate method to quantify  $E_{\text{water}}$  (Lenters et al., 2005). In contrast to scintillometry, eddy covariance is based on a point measurement with a smaller footprint at the hectare to square kilometre scale, depending on the meteorological conditions and the height of the sensor. It measures the vertical moisture flux through the covariance of turbulent fluctuations of vertical wind speed and the concentration of water vapour. This concept renders this method the most direct flux measurement technique available, and it provides continuous observations suitable for studying the evaporation process.

In the past, a number of studies have reported measurements of  $E_{\text{water}}$  from which modelling concepts to estimate  $E_{\text{water}}$  have been developed. Some of these concepts are based on different drivers of evaporation, and they disagree regarding the meteorological variables that should be included. Some studies have, for instance, found that global radiation is not a direct driver of  $E_{\text{water}}$  at shorter timescales and should, therefore, not be included in the parameterization (Venäläinen et al., 1999; Blanken et al., 2011; Kleidon and Renner, 2017); rather, the product of the vapour pressure deficit (VPD) and wind speed should be used, as argued by Blanken et al. (2000) and Granger and Hedstrom (2011). At larger timescales, a spatial coupling was found between  $E_{\text{water}}$  and precipitation minus land surface evaporation (Zhou et al., 2021). In Chapter 3 we studied the (dis)agreement among a number of concepts that are commonly used. We found that the models of Penman (1948), Makkink (1957), De Bruin and Keijman (1979), Granger and Hedstrom (2011), Hargreaves (1975), and Mironov (2008) result in different representations of especially the diurnal cycle of evaporation. Additionally, at the yearly timescale, the models disagree on the average increasing historical trend of the evaporation rate as well as on the projected future trends. At longer timescales (i.e. seasonal and yearly), it is important to include the interdependency between lake temperature and evaporation (Woolway et al., 2018; Wang et al., 2018). This requires a concept in which the water body energy balance is represented adequately in order to ensure the correct modelling of the  $E_{\text{water}}$  process.

In the Netherlands, measurements of  $E_{\text{water}}$  have been under-represented. However, measured by their extent ( $\sim 17\%$  of the total area; Huisman, 1998) inland water bodies form a crucial element in the country's water management system (Buitelaar et al., 2015).

Thus, adequate estimations of  $E_{\text{water}}$  are important in this context, as there is a strong coupling between  $E_{\text{water}}$  and, for instance, lake level and extent, the lake ecosystem, and lake stratification and mixing regimes (Woolway et al., 2020; Jenny et al., 2020). Lake IJssel is the largest freshwater reservoir in the Netherlands and fulfils crucial hydrological functions with respect to both flood prevention and freshwater supply for agricultural irrigation and drinking water extraction. The water level of the lake is managed, and it has a distinct summer and winter level. This flexibility provides the opportunity to raise the water level before the start of the summer, which typically has higher evaporation rates. In this way, a buffer can be created to ensure that the lake’s functions can be fulfilled continuously throughout the summer season. Currently, the Dutch operational hydrological models use Makkink’s equation (Makkink, 1957) to quantify  $E_{\text{water}}$  for Lake IJssel. Makkink is a radiation-based model, which finds its origin in Penman’s equation through the Priestley–Taylor equation (explained in Sect. 4.2.5), and has been developed to estimate evaporation over well-watered grasslands at a daily timescale. Although a correction factor is applied to account for the difference between land surface evaporation and  $E_{\text{water}}$ , Makkink’s equation is not able to capture the dynamics of  $E_{\text{water}}$  compared with what has been found by the aforementioned observational studies on  $E_{\text{water}}$  and compared with estimations from physically based lake models such as FLake (see Chapter 3). This calls for improvement and implementation of our understanding of the driving process of  $E_{\text{water}}$  by building on previous studies of  $E_{\text{water}}$  for Lake IJssel (Keijman and Koopmans, 1973; De Bruin and Keijman, 1979; Abdelrady et al., 2016; Wieringa, 2019). Therefore, the goal of our study is to analyse the dynamics of  $E_{\text{water}}$  for Lake IJssel using a data-driven analysis with the aim of parameterizing  $E_{\text{water}}$  based on its main drivers. To this end, we performed a long-term measurement campaign focusing on two summer periods (2019 and 2020) at two locations over Lake IJssel in the Netherlands; during this campaign, the eddy covariance technique was used to measure  $E_{\text{water}}$ , and observations of related meteorological variables were made.

## 4.2 Data, materials, and methods

### 4.2.1 Study area

In this chapter, the drivers of latent heat flux of Lake IJssel (see Fig. 2.4), the largest lake in the Netherlands, was analysed. The lake covers an area of 1100 km<sup>2</sup> and with an average depth of 5.5 m and a maximum depth of 7 m, the lake can be considered a large shallow lake. During summertime, a flexible water level is used, which can vary between −0.10 m NAP (Normaal Amsterdams Peil, or Amsterdam Ordnance Datum, the local sea level reference) and −0.30 m NAP. In winter, the lake level should not be lower than −0.40 m NAP. A more elaborate description of lake and its location in the Netherlands is provided in Section 2.2. Lake IJssel fulfils an important hydrological role in the low-lying Netherlands with respect to both flood mitigation and freshwater supply for agricultural

and drinking water purposes. The flexible management of the lake level during the year provides water managers with a tool to respond to the meteorological conditions and the need for fresh water.

#### 4.2.2 Site description, instrumentation, and data

During the summer periods of 2019 and 2020 we employed two EC systems. A full description of the eddy covariance measurement sites and systems is provided in Section 2.4.2. Both locations, Stavoren and Trintelhaven, were chosen based on the position relative to the studied lake region considering the dominant south-westerly winds, as well as on the practicality of the site in terms of available infrastructure. Unfortunately, due to practical constraints we were not able to measure all variables of interest ourselves. Section 2.5 includes a description of the data sources that were used to obtain data of global radiation and water surface temperature.

#### 4.2.3 Data processing

Processing of the raw data obtained from the EC systems requires a number of processing steps to obtain reliable flux data. These processing steps include raw data quality checks, checks on assumed conditions, and application of corrections. The processing steps were performed using the EddyPro software (EddyPro, 2021) and are described in Section 2.4.3. As a result, fully quality-checked half-hourly flux datasets were obtained and processed further into hourly and daily datasets as described in Section 2.4.3 as well.

#### 4.2.4 Flux footprint analysis

To quantify the sampling area of the EC measurements, a flux footprint analysis was performed. This footprint analysis helps to decide which wind directions to include in the analysis based on the area of interest. The size of the footprint depends on the measurement height, atmospheric stability, and surface roughness (McGloin et al., 2014). In this chapter, we used the footprint model developed by Kljun et al. (2004) with the Flux Footprint Prediction (FFP) R code (Kljun et al., 2015). Figure 2.3b and c displays the results of the footprint analyses of locations Stavoren and Trintelhaven, as described in Section 2.4.4.

#### 4.2.5 Regression model

A regression analysis was performed to explore which variable or combination of variables could best explain the dynamics of  $E_{\text{water}}$ . The ‘leaps’ package in R was used to identify the best regression model, and the residual sum of squares was used as a metric to find the best model given the predictors. The variables included in this analysis were wind speed, VPD, global radiation, vertical vapour pressure gradient, and water temperature. These variables are generally considered to be important in describing  $E_{\text{water}}$  and are partially



included in the models of Dalton and Penman. To be specific, the choice of including VPD and vertical vapour pressure gradient in the regression analysis was motivated by the apparent drivers of the Dalton and Penman equations. VPD was given preference over air temperature as the dependent variable in the regression analysis due to its explicit mention in the Penman equation, whereas air temperature only features implicitly in the definition of the slope of the vapour pressure gradient ( $s$ ) and in the definition of VPD. From the regression analysis, a data-driven model was developed to estimate  $E_{\text{water}}$  of Lake IJssel. This was done for both locations, Stavoren and Trintelhaven. For each individual variable, as well as for all combinations of variables, both the sum and product, a regression model was created. In the regression analysis simple linear regression models (Eq. 4.1), multiple linear regression models (Eq. 4.2), and quadratic regression models (Eq. 4.3) were considered. The equations of these models are prescribed as:

$$Y = \beta_0 + \beta_1 X_1 + \epsilon, \quad (4.1)$$

$$Y = \beta_0 + \beta_1 X_1 + \beta_2 X_2 + \dots + \beta_i X_i + \epsilon, \quad (4.2)$$

$$Y = \beta_0 + \beta_1 X_1 + \beta_2 X_1^2 + \epsilon, \quad (4.3)$$

where  $Y$  is the dependent variable,  $X_i$  the explanatory variable(s),  $\beta_0$  the intercept,  $\beta_i$  the parameter(s), and  $\epsilon$  the error term. The explanatory variable(s)  $X_i$  was prescribed to be either a single variable or the product of multiple variables, except for equation 4.2, where  $X_i$  can only be a single variable. Statistical significance ( $p < 0.05$ ) was tested. From the multitude of regression models that resulted from the regression analysis, the best model was chosen by using the adjusted  $R^2$  and RMSE metrics to evaluate the fit of each regression model. We aimed to find the best model; however, we were also interested in finding the best simple model that used a maximum of two variables while still being able to explain the dynamics of  $E_{\text{water}}$  well. The summer season of 2019, here taken as 1 May to 31 August, was used as the training dataset to calibrate the data-driven model, and the dataset of the summer of 2020 was used for validation. The analysis was performed at hourly and daily timescales.

The above-mentioned procedure was repeated using only routinely measured observations. This was done to explore the possibility of using routine observations to make accurate estimations of  $E_{\text{water}}$ , instead of continuing the labour-intensive and expensive measurements with the eddy covariance systems. As described previously (see Sect. 2.5), data from automatic meteorological stations of the KNMI were used to obtain global radiation measurements and were complemented by air temperature, wind speed, and relative humidity, which are routinely measured at these stations. There are no available routine observations of the skin water temperature of the lake. As an alternative, the use of water temperature data routinely measured by Rijkswaterstaat at depths ranging from 1.2 to 1.5 m was explored.

The resulting regression model was compared to the models of Dalton, Penman, and Makkink (see Eqs. 4.4, 4.6, and 4.10) to give an indication of the (dis)agreement of the variables involved in explaining the dynamics of  $E_{\text{water}}$  and its form. Dalton's model is based on the empirical relationship that was found between evaporation and the product of a wind function and the vertical vapour pressure difference, which can be written as follows:

$$LE_{\text{Dalton}} = f(u)(e_s(T_s) - e_a), \quad (4.4)$$

in which  $e_a$  is the vapour pressure at 2 m height,  $e_s(T_s)$  is the saturation vapour pressure at the surface, and  $f(u)$  is the wind function which takes the following form (Penman, 1956; De Bruin, 1979):

$$f(u) = 37 + 40u_2, \quad (4.5)$$

in which  $u_2$  is the wind speed at 2 m height. Although the representation of the Dalton models may seem simple, obtaining reliable measurements of surface temperature is challenging.

Similarly, Penman's equation, which is derived from Dalton's equation, can be written as:

$$LE_{\text{Penman}} = \frac{\gamma}{s + \gamma} f(u)(e_s(T_a) - e_a) + \frac{s}{s + \gamma} (R_n - G), \quad (4.6)$$

in which  $s$  is the slope of the saturated vapour pressure curve at air temperature,  $\gamma$  the psychrometric constant,  $e_s(T_a) - e_a$  the vapour pressure deficit of the air, and  $R_n - G$  the available energy at the surface, where  $R_n$  is net radiation and  $G$  is the downward heat flux from the water surface. Net longwave radiation was calculated following equations 2.24 and 2.28 from Moene and van Dam (2014):

$$L_{\text{in}} = \epsilon_a \sigma_{\text{SB}} T_a^4, \quad (4.7)$$

$$L_{\text{out}} = L_{e,\text{out}} + (1 - \epsilon_s) L_{\text{in}}, \quad (4.8)$$

in which  $L_{\text{in}}$  is the incoming longwave radiation,  $L_{\text{out}}$  is the outgoing longwave radiation,  $\epsilon_a$  is the apparent emissivity that is a function of the fraction of cloud cover,  $\sigma_{\text{SB}}$  the Stefan-Boltzmann constant,  $T_a$  the air temperature,  $L_{e,\text{out}}$  is the emitted longwave radiation, and  $\epsilon_s$  the surface emissivity. Net shortwave radiation was calculated as (Allen et al., 1998):

$$K^* = (1 - \alpha) K_{\text{in}}, \quad (4.9)$$

in which  $K^*$  is the net shortwave radiation,  $K_{\text{in}}$  the global radiation, and  $\alpha$  the albedo values for which monthly values were calculated as a function of latitude (Cogley, 1979).

Priestley and Taylor (1972) found that the aerodynamic term of Penman's equation is approximately one-fourth of the radiation term. Makkink (1957) found that this equation

could be simplified even more for estimating daily evaporation from well-watered surfaces. Under these conditions  $G$  is assumed to be negligible and a constant ratio between net radiation and global radiation of on average 0.5 can be assumed, which results in the following equation (Makkink, 1957):

$$LE_{\text{Makkink}} = 0.65 \frac{s}{s + \gamma} K_{\text{in}}, \quad (4.10)$$

According to Penman's derivation,  $G$  is assumed to be negligible for timescales of a day to several days for shallow water surfaces, similar to land surfaces, and the term is often ignored because of the difficulty involved with measuring it. However, for water bodies that are several metres deep, the impact of neglecting  $G$  on the energy balance can be considerable (Keijman, 1974; De Bruin, 1982; Tanny et al., 2008; Van Emmerik et al., 2013). For these water bodies,  $G$  should be considered as a result of temperature changes integrated over the volume of the water column, in contrast to a land surface where the impact of  $G$  is more superficial. It should be clearly noted that, although Lake IJssel is a lake that is several metres deep, we have neglected  $G$  in the following analyses for the following two reasons: (i) we were not able to measure it, and (ii) we wished to adhere to how Penman's equation is typically employed for shallow water surfaces.

## 4.3 Results

### 4.3.1 Data quality and quantity

To guarantee the data quality of the flux measurements, quality checks were performed, as described in Sect. 2.4.3. After the quality control, 66 % and 64 % of the latent heat flux data were available in 2019 for Stavoren and Trintelhaven, respectively. In 2020, this number was lower: 49 % and 59 % for Stavoren and Trintelhaven, respectively. Part of the available quality-checked data needed to be rejected based on the flux footprint analysis. This led to a further reduced number of available data for 2019: 42 % and 13 % of the total data for Stavoren and Trintelhaven, respectively. In 2020, the total available latent heat flux data was 33 % and 19 % for Stavoren and Trintelhaven, respectively. The reduction of the available data at Trintelhaven was larger given the combination of dominant south-westerly winds and the location of the instrument at the south-west border of Lake IJssel (see Fig. 2.3a). The number of total available flux data is at the lower end (although not unusual) of data availability reported in other studies on lakes, which is typically in the range of 16 %–59 % (Vesala et al., 2006; Nordbo et al., 2011; Bouin et al., 2012; Mammarella et al., 2015; Metzger et al., 2018).

No clustering was found in the availability of latent heat flux data during daylight hours (06:00–21:00 LT) compared to the night (21:00–06:00 LT). In the final half-hourly dataset, latent heat flux data were available during 56 % of the total half-hour daytime periods

in Stavoren in the summer of 2019 and during 49 % of the periods during night-time. In the summer of 2020, this was 49 % and 40 % for daytime and night-time, respectively. For Trintelhaven, the corresponding fractions were 10 % and 18 % during daytime and night-time in the summer of 2019, respectively. The difference between the daytime and night-time fractions was smaller during the summer of 2020, with 18 % and 21 % of data available, respectively.

#### 4.3.2 Meteorological conditions

Similar dynamics were observed at both locations (Stavoren and Trintelhaven). Here, we only show the meteorological conditions observed in Stavoren during the period from 1 May to 30 September 2019 (Fig. 4.1; see Figure B1 in Appendix B for the meteorological conditions in Stavoren in the summer period of 2020). Figure 4.1 illustrates the dynamics and trends of the meteorological variables and the heat fluxes before, during, and after the summer period, and it explores if any visible lags, for instance, would occur at this timescale. Table 4.1 provides an indication of the source of the data for the variables that will be elaborated on in this section. According to the measurements of the KNMI, both measurement stations received on average the same amount of global radiation for the period from 1 May to 30 September 2019, namely  $208 \text{ W m}^{-2}$  in Stavoren and  $204 \text{ W m}^{-2}$  at Lelystad, with the latter assumed to be representative of Trintelhaven. The average air temperature that we measured with the HMP155A sensor is lower in Stavoren ( $16.4^\circ\text{C}$ ) than in Trintelhaven ( $18.0^\circ\text{C}$ ). These temperatures are higher than the climatological mean observed by the KNMI (period 1991–2020) for the same months:  $15.9^\circ\text{C}$  in Stavoren and  $16.1^\circ\text{C}$  at Lelystad (KNMI, 2022). The water temperature measured by Rijkswaterstaat in the vicinity of Stavoren was on average  $17.9^\circ\text{C}$ , and the water temperature at Marker Wadden close to Trintelhaven was on average  $18.3^\circ\text{C}$ . The time series of water temperature shows a more smooth, attenuated, and lagged signal compared with the air temperature. At both measurement locations, the measured wind speed observed with the IRGASON is similar, with an average wind speed of  $5.8 \text{ m s}^{-1}$  in Stavoren and  $5.6 \text{ m s}^{-1}$  at Trintelhaven, without a distinct seasonal pattern. The vapour pressure that we measured follows the seasonal cycle of the air temperature and has a mean value of 1.4 kPa in Stavoren and 1.6 kPa at Trintelhaven. Figure 4.1e shows the observed turbulent fluxes. The sensible heat flux remains consistently low throughout the summer period, with an average value of  $17 \text{ W m}^{-2}$  in Stavoren and  $25 \text{ W m}^{-2}$  at Trintelhaven. The latent heat flux is more than 4 times as high on average, with mean values of  $88 \text{ W m}^{-2}$  in Stavoren and  $91 \text{ W m}^{-2}$  in Trintelhaven. Basic statistics on the observed latent heat flux can be found in Table B1 in Appendix B. The latent heat flux displays trends similar to those for the measured wind speed, indicating that the two variables are correlated ( $R^2 = 0.61$ ). Based on the average rates of sensible and latent heat flux, the Bowen ratio is 0.19 in Stavoren and 0.27 at Trintelhaven.

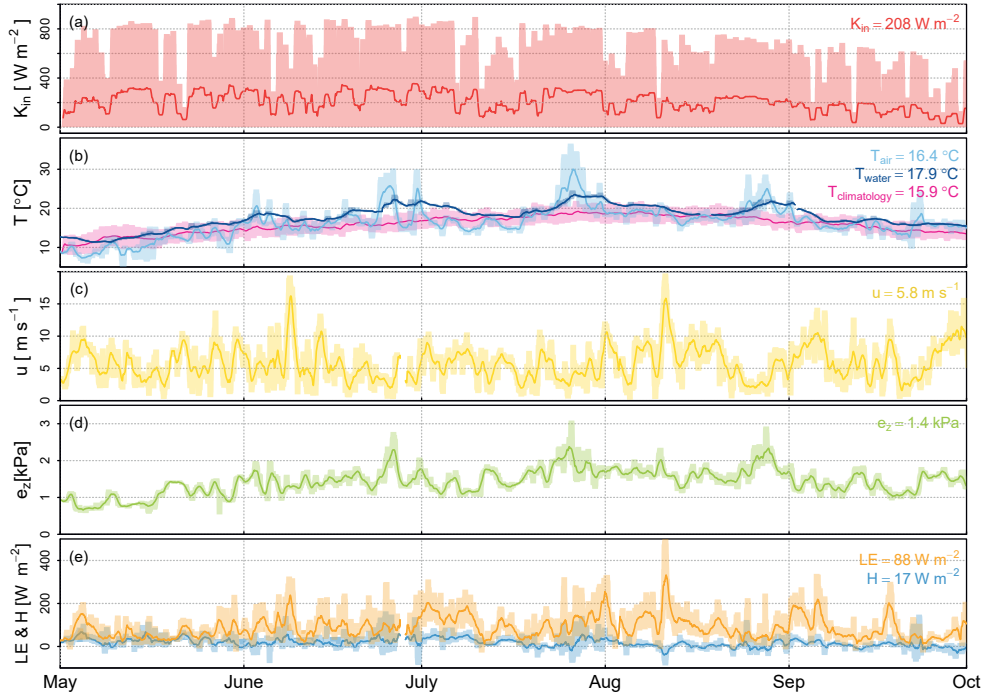


**Figure 4.1:** Meteorological conditions in Stavoren in 2019 showing running daily means of global radiation (a), air temperature (current and climatology) and water temperature (b), wind speed (c), vapour pressure (d), and turbulent fluxes (e). The shaded area represents the range between minimum and maximum observed values and the numbers reported at the top right of each panel provide the average values of the respective variables during the presented months.

#### 4.3.3 Diurnal and intra-seasonal variability in latent heat flux

The monthly average diurnal variability in observed  $LE$ , based on hourly data, is shown in the top panels of Figure 4.2 for Stavoren for the same period as in Figure 4.1 (i.e. 1 May–30 September 2019). The diurnal variability in  $LE$  does not have a strong diurnal cycle; rather, it is constant throughout the day and night, which is in contrast to terrestrial evaporation that typically peaks during the day. However, in August, the  $LE$  signal shows a distinct peak during the late afternoon and lower values during the night and early morning. The highest average diurnal  $LE$  is reached in July, as indicated by the number in the top left corner of each panel in Figure 4.2. Global radiation measured at the KNMI meteorological stations in Stavoren is shown in the middle panels. A clear distinctive diurnal cycle is visible with a peak in the afternoon, and the highest average value is found in June at both locations. The global radiation has served as input for the commonly used radiation-based models of Penman (1948) and Makkink (1957), of which

**Table 4.1:** Sources of data used in this study. The variables measured at our locations in Stavoren at 7.5 m and Trintelhaven at 10.8 m were sampled at high frequency (20 Hz) and aggregated to hourly data. The data retrieved from KNMI stations in Stavoren and Lelystad are provided at hourly timescales and were measured at 1.5 m height above the land surface, and 10-minute water temperature data measured by Rijkswaterstaat at Friese Kust at  $-1.5$  m NAP and Marker Wadden at  $-1.2$  m NAP were aggregated to hourly timescales.

	Own observations	KNMI	Rijkswaterstaat
$K_{in}$		×	
$T$			
- $T_a$	×		
- $T_{a,climatology}$		×	
- $T_{water}$			×
$u$	×		
$e_a$	×		
$LE$	×		
$H$	×		

the average diurnal cycles are shown in the lower panels of the same figures. Recall that  $G$  was omitted in Penman's model in this analysis (see Sect. 4.2.5). The diurnal cycles of the models of Penman and Makkink closely follow the pattern of the global radiation but with a lower amplitude. The highest average  $LE$  values are found in June for these models, in contrast to observed  $LE$  which is found to be highest a month later. In the lower panels, the average diurnal cycle of  $LE$  that follows from Dalton's model is shown as well. There is no strong diurnal cycle visible, similar to the observed  $LE$ , but rates are generally highest during daytime. The highest average  $LE$  values are found in August. The observed monthly average diurnal dynamics were found to be similar in Trintelhaven (see Figure B2 in Appendix B).

The extension of the time series to a complete year in order to visualize the seasonal variability shows a clear seasonal cycle that is reminiscent of the influence of a radiation component on  $E_{water}$  (see Fig. 4.3). The bars represent the monthly average  $E_{water}$  rate based on half-hourly data. For the year 2019, the evaporation rate is highest in July for both locations:  $4.3 \text{ mm d}^{-1}$  in Stavoren and  $3.8 \text{ mm d}^{-1}$  in Trintelhaven. The lowest values are  $0.2 \text{ mm d}^{-1}$  in Stavoren (February) and  $0.6 \text{ mm d}^{-1}$  in Trintelhaven (December); note that data from January–February 2019 are lacking for the latter location. In 2020, similar rates are found in winter,  $0.1 \text{ mm d}^{-1}$  in Stavoren (December) and  $0.5 \text{ mm d}^{-1}$  in Trintelhaven (November), while the summer of 2020 now has a dip in July instead of being the peak.

#### 4.3.4 Drivers of open water evaporation

Based on historical theory, it is known that governing factors of  $E_{water}$  include the gradient of vapour pressure above the water surface and some measure of the strength of the turbulence (Dalton, 1802; Penman, 1948; De Bruin, 1979; Brutsaert, 1982). These variables form the ingredients of the so-called 'aerodynamic method' or 'mass transfer

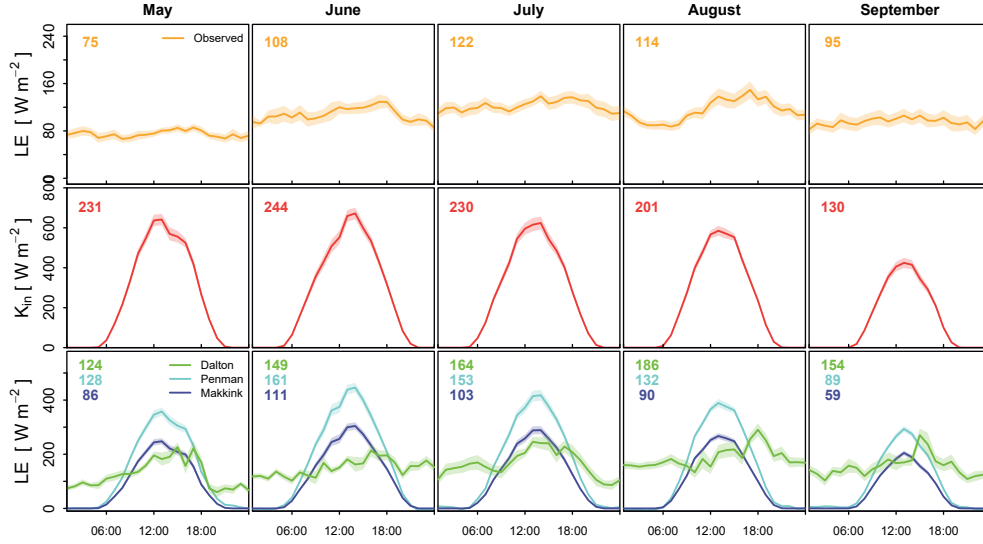


**Figure 4.2:** An illustration of the decoupling in Stavoren in 2019 between the monthly average diurnal cycles of observed latent heat flux (top panels) and global radiation (middle panels), with the latter forming the basis of the frequently used evaporation models of Penman (1948) and Makkink (1957). These models are shown together with the model of Dalton (1802) at the bottom panels. Note that some variables included in the evaporation models are measured at heights above the 2 m that is prescribed (see Eq. 4.4–4.10). Additionally, all three models are generally used on a daily basis, but they are presented here to show the underlying daily cycle. The shaded area represents the uncertainty, which is defined as the standard deviation divided by the square root of the number of observations. Average daily means of the respective variables are indicated by the number in the top left of each panel and display the average course over the summer period.

approach’ (Brutsaert, 1982). Here, we tested which variable or combination of variables can best explain the dynamics of observed  $E_{\text{water}}$  at Lake IJssel at both an hourly and daily temporal resolution. The variables included in this analysis are global radiation, vertical gradient of vapour pressure, vapour pressure deficit, sub-skin water temperature, and wind speed. Recall that air temperature was not explicitly included in the regression analysis, as explained in Sect. 4.2.5. We expect that including air temperature as a separate dependent variable might have explained a part of the evaporation dynamics, as air temperature affects surface temperature through the sensible heat flux. The surface temperature, in turn, affects the vapour pressure gradient and, thus, evaporation. However, due to the large thermal buffer of a water body, we expect that there is a less direct coupling between the sensible heat flux and evaporation at short timescales.

The proportion of the dynamics of  $E_{\text{water}}$  that can be explained by the variable or combination of variables is shown in Venn diagrams, with the adjusted coefficient of

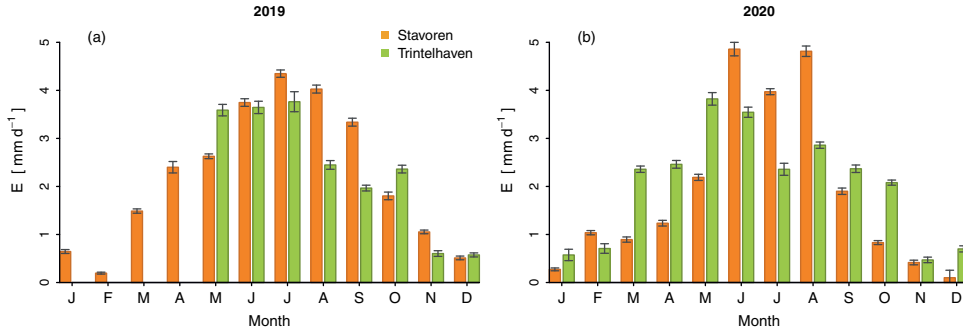


**Figure 4.3:** Yearly cycle of observed open water evaporation in Stavoren (orange) and Trintelhaven (green) based on half-hourly data for both of the respective years, 2019 and 2020. The bars indicate the monthly average evaporation, and the whiskers represent the uncertainty, which is defined as the standard deviation divided by the square root of the number of observations.

determination ( $R^2$ ) written inside (see Fig. 4.4). The higher the adjusted  $R^2$ , the darker blue the colour in the figure. Adding a variable will not always result in a higher adjusted  $R^2$  value, as the adjusted  $R^2$  takes the degrees of freedom into account; therefore, if an added variable only slightly correlates with the dependent variable, it can lead to a decrease in the adjusted  $R^2$  value. Values of the adjusted  $R^2$  were removed if the model fit was found to be insignificant ( $p < 0.05$ ). Venn diagrams a and c on the left-hand side of Fig. 4.4 illustrate the analysis based on hourly data, and diagrams b and d on the right-hand side of Fig. 4.4 are based on daily data. The outer ‘leaves’ of the diagram represent the single variables, whereas combinations of variables are taken into account towards the centre of the diagram in order to explain the dynamics of  $E_{\text{water}}$ . Both the sums and the products of the combined variables are analysed (Fig. 4.4 and Fig. B3 in Appendix B, respectively). Based on these diagrams, a decision was made regarding which variables to include in the data-driven model to estimate  $E_{\text{water}}$ . The prominent blue colour connected to wind speed already tells us that this is an important variable to include, which is in agreement with Dalton’s model and was also visible from Fig. 4.1 ( $R^2 = 0.61$ ). Global radiation has the lowest adjusted coefficient of determination, which agrees with our findings in Figs. 4.1 and 4.2.

#### Calibration

For both locations, two models were developed: (i) a model that included the variable or variables that explain most of the variability in  $E_{\text{water}}$  (and, thus, had the highest adjusted  $R^2$ ), and (ii) a model that only used one or two variables that were still able to explain a significant portion of the variability in  $E_{\text{water}}$  (the number depicted in red in the Venn diagrams in Fig. 4.4 and Fig. B3 in Appendix B). At the hourly timescale, the



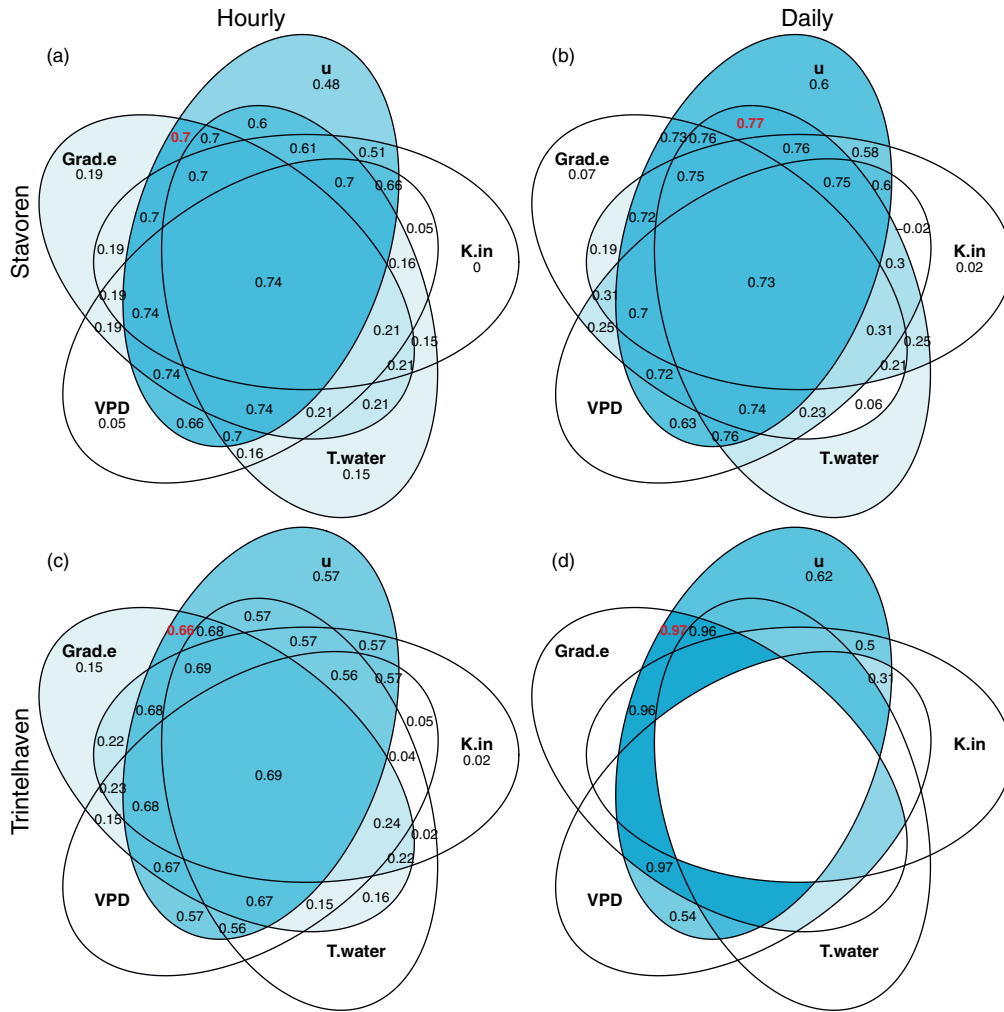


**Figure 4.4:** A systematic exploration of which variable or combination of variables (sums) can best explain the dynamics of open water evaporation. The outer “leaves” of the Venn diagram represent the model fit based on the single variables, whereas the summed combinations of variables are represented towards the centre of the diagram. Within each leaf, the adjusted  $R^2$  value is depicted. The higher this value, the bluer the colour of the leaf. The red number indicates the highest  $R^2$  value, indicating the best combination found for a maximum of two variables, i.e. the best “simple” model. The  $R^2$  values were removed if the model fit was found to be insignificant ( $p < 0.05$ ). The analysis is based on data from the summer of 2019 and is performed at an hourly timescale – Stavoren (a) and Trintelhaven (c) – and a daily timescale – Stavoren (b) and Trintelhaven (d).

best model fit, indicated by the highest  $R^2$  value, is reached when the sum of (almost) all five variables are included ( $R^2 = 0.74$  and  $R^2 = 0.69$  at Stavoren and Trintelhaven, respectively). Moving from the outer leaves towards the centre of the diagram, we find that the most simple hourly model that still explains a large portion of the variance (i.e. the red numbers) includes only wind speed and the vertical gradient of vapour pressure:  $R^2 = 0.70$  in Stavoren (see Fig. 4.4) and  $R^2 = 0.69$  in Trintelhaven (see Fig. B3 in Appendix B). This is in agreement with Dalton's model. At the daily timescale in Stavoren, we see a shift in the variables that are included in the 'simple' model. The sum of wind speed and water temperature reaches the highest  $R^2$  value ( $R^2 = 0.77$ ). Unfortunately, very few data points ( $N = 10$ ) were left at the daily timescale at Trintelhaven, which led to many insignificant model fits (values were removed from those intersecting areas). However, a couple of models were found to be significant, and the sum of wind speed and the vertical gradient of vapour pressure again showed the highest  $R^2$  value ( $R^2 = 0.97$ ). The relatively high adjusted  $R^2$  values of these simple model fits, compared with models including more than two variables, indicate that the added value of using more than two variables is virtually nil. The results from the Venn diagrams form the base to create the data-driven models for which the data collected in 2019 are used. Both linear and quadratic regression models were considered, as explained in Sect. 4.2.5.

The results presented in the Venn diagrams are used to formulate the regression models. Both the 'simple' and 'best' fitted model were evaluated, based on hourly and daily data, and are presented in panels a and b of Fig. 4.5 (Stavoren) and Fig. 4.6 (Trintelhaven). At both locations, the simple models were also found to be the best models. For both locations, the regression analysis based on hourly data showed that the combination of wind speed and vertical gradient of vapour pressure explains most of the variability in  $E_{\text{water}}$ , leading to  $R^2$  values of 0.74 and 0.70 at Stavoren and Trintelhaven, respectively. The sum of wind speed and the vertical gradient of vapour pressure was the most important ingredient to explain  $E_{\text{water}}$  at a daily timescale at Trintelhaven ( $R^2 = 0.98$ ). In Stavoren, the sum of wind speed and water temperature resulted in an  $R^2$  value of 0.8. Without predetermination of the variables, we found the same ingredients as used in the Dalton model to be the most important drivers of  $E_{\text{water}}$  at hourly timescales. To determine if the coefficients that were found for the hourly regression models of the two measurements locations differ significantly, an ANOVA (analysis of variance) statistical test was performed (see Table B2 in Appendix B). This analysis showed that the inclusion of the measurement site matters ( $p < 0.05$ ). Therefore, we cannot rule out that the sites are different.

#### *Validation*

The models are validated using the data collected in 2020, and the results are presented in panels c and d of Figs. 4.5 (Stavoren) and 4.6 (Trintelhaven). The adequate  $R^2$  values in the validation give confidence in the performance of the models. Validation of the hourly regression model in Stavoren has a higher  $R^2$  value ( $R^2 = 0.84$ ) compared with

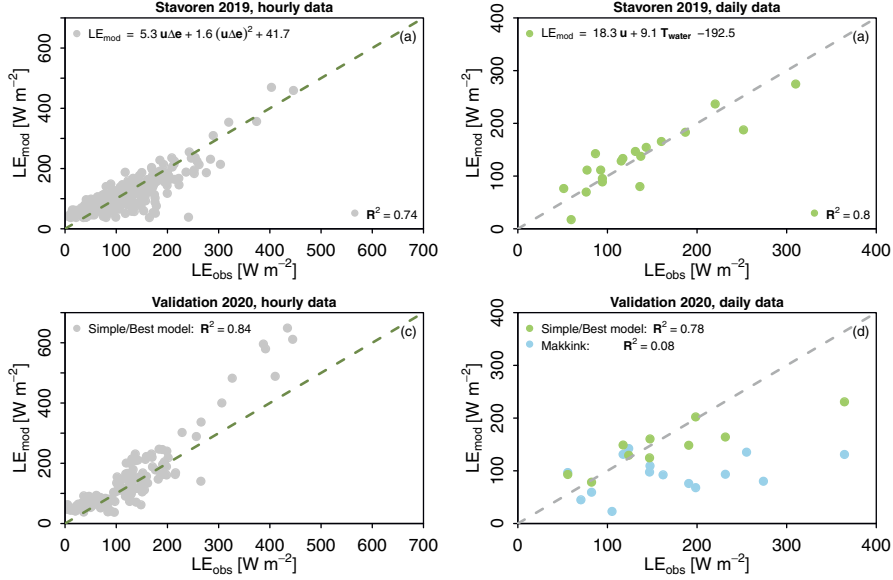


**Figure 4.5:** Evaluation of the developed ‘simple’ and ‘best’ data-driven models based on our own observations during the summer of 2019 (calibration) and 2020 (validation) to estimate open water evaporation in Stavoren at hourly (a) and daily (b) timescales. The model equations are shown in panels (a) and (b) and differ from the models found based on routinely measured observations (see Table 4.2a). The results of the validation of the models are presented in panels (c) and (d) for hourly and daily timescales, respectively. The simple model was also found to be the best model. The results of estimated evaporation using Makkink’s model (light blue) are added to the validation plots as a reference. Model performance is indicated by the values of the coefficient of determination ( $R^2$ ) shown in each panel.

the calibration period ( $R^2 = 0.74$ ). In an attempt to explain why a higher  $R^2$  value occurs during the validation of the model, we swapped the calibration (now summer of 2020) and validation (summer of 2019) periods. The coefficients of the regression model were recalculated. The  $R^2$  value of the validation was now found to be smaller than during the calibration. This provides an indication that the difference in  $R^2$  values during calibration and validation seems to be related to the conditions during the two distinct summer periods, and it gives confidence that the model performs well. In addition to the data-driven models, the estimated daily evaporation rates using Makkink’s model are plotted for reference, as this model is currently used in the operational water management of Lake IJssel. Makkink’s model fails to explain the dynamics of  $E_{water}$  at a daily temporal resolution, with  $R^2$  values near zero.

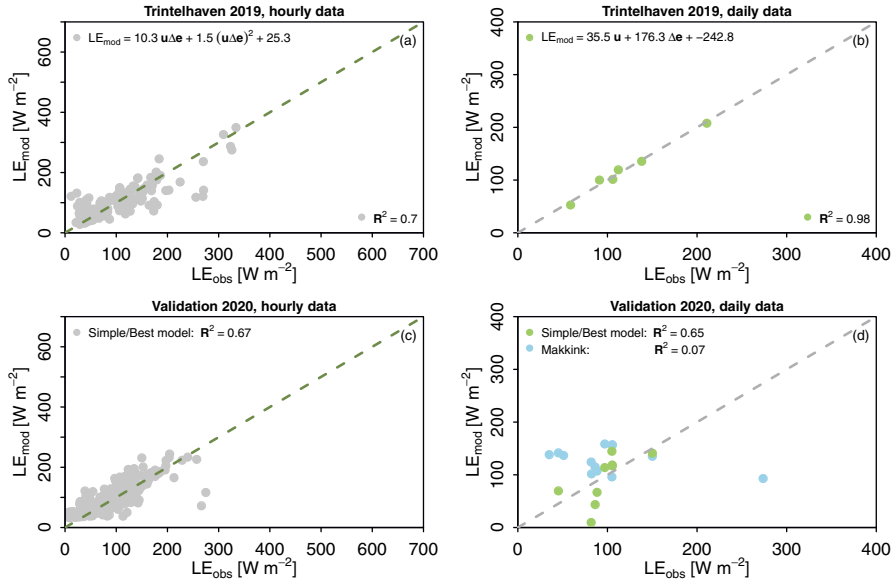


**Figure 4.6:** Evaluation of the developed ‘simple’ and ‘best’ data-driven models based on our own observations during the summer of 2019 (calibration) and 2020 (validation) to estimate open water evaporation in Trintelhaven at hourly (a) and daily (b) timescales. The simple model was found to be the best model and is shown using light coloured dots. The model equations are shown in panels (a) and (b) and differ from the models found based on routinely measured observations (see Table 4.2b). The results of the validation of the models are presented in panels (c) and (d) for hourly and daily timescales, respectively. The results of estimated evaporation using Makkink’s model (light blue) are added to the validation plots as a reference. Model performance is indicated by the values of the coefficient of determination ( $R^2$ ) shown in each panel.

#### *Models based on routinely measured variables*

The analysis described above was repeated using only routinely measured observations of meteorological variables at 2 m height by KNMI and observations of water temperatures by Rijkswaterstaat (Table 4.2a and b). This was done to explore the possibility of using these routine measurement to estimate  $E_{\text{water}}$ , instead of using the expensive and labour-intensive eddy covariance instruments. The regression models found using these routine observations are, especially for Stavoren, able to explain the dynamics of  $E_{\text{water}}$  relatively well, and wind speed and the vertical gradient of vapour pressure were the main ingredients for the simple model ( $R^2 = 0.83$  using hourly data and  $R^2 = 0.86$  using daily data). Validation using data from summer 2020 also yields satisfactory results, with high  $R^2$  values of 0.78 and 0.82 for hourly and daily data, respectively. The results of the simple model for

**Table 4.2:** Evaluation of the developed ‘simple’ and ‘best’ data-driven models based on routinely measured observations (see Section 4.3.4) during the summer of 2019 (calibration) and 2020 (validation) to estimate open water evaporation in Stavoren (Table 4.2a) and Trintelhaven (Table 4.2b) at hourly and daily timescales. The models presented here are independent of the results found based on our own observations. The results of estimated evaporation using Makkink’s model are provided as a reference. Model performance is indicated by the values of the coefficient of determination ( $R^2$ ).

(a) Stavoren	Model equation for calculating $LE_{mod}$	$R^2_{calibration}$	$R^2_{validation}$
<u>Hourly</u>			
Simple data-driven model	$29.4 u \Delta e - 4.1$	0.83	0.78
Best data-driven model	$1.4 u \Delta e T_{water} + 2.8$	0.84	0.81
<u>Daily</u>			
Simple data-driven model	$30.8 u \Delta e - 9.2$	0.86	0.82
Best data-driven model	$1.5 u \Delta e T_{water} - 3.8$	0.91	0.80
Makkink	$0.65 \frac{s}{s+\gamma} K_{in}$	–	–0.02

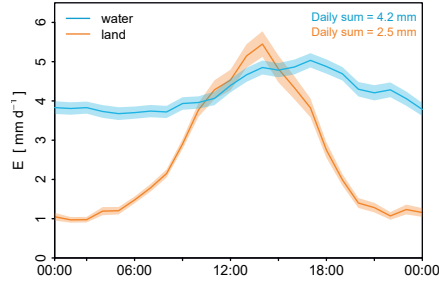
  

(b) Trintelhaven	Model equation for calculating $LE_{mod}$	$R^2_{calibration}$	$R^2_{validation}$
<u>Hourly</u>			
Simple data-driven model	$13.0 u + 98.1 \Delta e - 21.8$	0.29	0.51
Best data-driven model	$18.5 u + 128.6 \Delta e - 29.0 VPD - 42.0$	0.42	0.54
<u>Daily</u>			
Simple/Best data-driven model	$28.9 u \Delta e + 22.7$	0.48	0.87
Makkink	$0.65 \frac{s}{s+\gamma} K_{in}$	–	0.003

Trintelhaven fall short compared with Stavoren, with  $R^2$  values of 0.29 and 0.48 for hourly and daily data, respectively. An explanation for this may be that the location of the routine observations is situated further from the target location (Trintelhaven) compared with the observation location for Stavoren (Figs. 2.3a and 2.4). At Trintelhaven,  $R^2$  values during the validation period are again found to be higher than during the calibration period, which seem to be related to the different conditions during the two summers.

## 4.4 Discussion

Our results have shown that the diurnal cycle of observed  $E_{water}$  shows a distinctively different pattern compared with evaporation estimated using the evaporation models of Penman (1948) and Makkink (1957). Recall that we omitted  $G$  in Penman’s model in this study. The estimated evaporation using the models of Penman and Makkink better resembles the cycle that was observed at our station in Stavoren when we selected wind directions coming from the land surface, i.e. representing terrestrial evaporation (see Fig. 4.7). In contrast to the observed terrestrial evaporation, the observed  $E_{water}$  is not directly coupled to global radiation at these timescales, which is demonstrated by the difference in diurnal variability between global radiation and observed  $LE$  (middle and



**Figure 4.7:** Comparison of the average diurnal cycle of open water evaporation (blue) and terrestrial evaporation (orange) observed during the summer period 2019 in Stavoren. The shaded area represents the uncertainty band, which is defined as the standard deviation divided by the square root of the number of observations.

upper panels of Fig. 4.2). Note that the relation between  $E_{\text{water}}$  and other components of the radiation budget could not be studied because of the lack of observations of these components. In combination with a lack of data on  $G$ , this prevented us from fully capturing the role of net radiation in the energy balance of the lake and, thus, in the warming and cooling of the lake, which relates to evaporation through the water surface temperature. A better agreement with the observed diurnal cycle was found for Dalton's model, which is more constant throughout the day. Nevertheless, to date, Makkink's model has been used as a base for calculating  $E_{\text{water}}$  at Lake IJssel (see Chapter 3). We have shown that Makkink's model is not able to explain the dynamics of  $E_{\text{water}}$  for the summer period at the daily timescale. Such a radiation-based approach (including a potential linear correction factor) might lead to the correct daily or monthly evaporation sums, but it will be for the wrong reason.

From the data-driven modelling that was performed, we found that not radiation but a combination of wind speed and vapour pressure gradient is the most important ingredient to explain the variance in  $E_{\text{water}}$  at short timescales. This is similar to what has been found by studies such as Blanken et al. (2011) and McGloin et al. (2014). It was also noticed that intraseasonal variations in  $E_{\text{water}}$  can be linked to synoptic weather variations through these variables (Lenters et al., 2005; MacIntyre et al., 2009; Liu et al., 2011a; Woolway et al., 2020). The same ingredients, wind speed and the vapour pressure gradient, were used in the model by Dalton (1802). By combining and rearranging Eqs. (4.4) and (4.5), we can write Dalton's model in the following form:

$$LE_{\text{Dalton}} = 37\Delta e + 40u_2\Delta e, \quad (4.11)$$

in which  $\Delta e$  is  $e_s(T_s) - e_a$ . This highlights the similarity of the functional form of Dalton's model and our data-driven model that resulted from the regression analysis (see Figs. 4.5 and 4.6). When the exact functional form of Eq. (4.11), i.e.  $LE = a\Delta e + bu_2\Delta e$ , is fitted

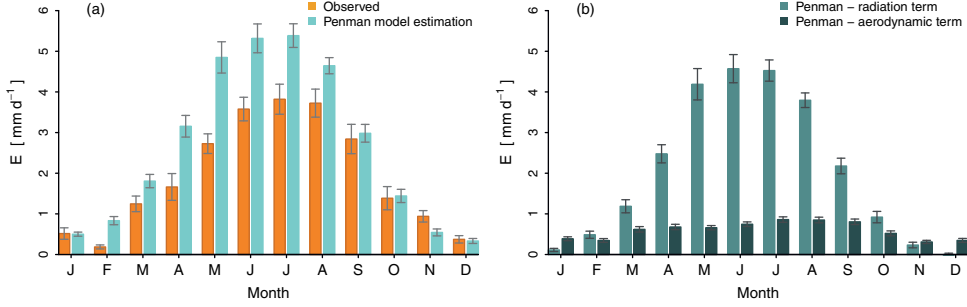


**Figure 4.8:** Comparison of the annual cycle of observed open water evaporation (orange) in Stavoren and estimated evaporation (blue) using Penman's model (a) based on daily data in 2019. The individual terms of Penman's model are displayed in the right panel (b), which shows the similarity of the annual cycle between observed open water evaporation and the radiation term of Penman's model. The bars indicate the monthly average evaporation, and the whiskers represent the uncertainty, which is defined as the standard deviation divided by the square root of the number of observations.

to our hourly observations of 2019, we find that coefficients  $a$  and  $b$  differ (not shown here). This difference is likely related to the height at which our measurements were done (10.8 and 7.5 m above the surface in Stavoren and Trintelhaven, respectively) compared with the standard height of 2 m. We found that Penman's model seemed unsuitable for estimating  $E_{\text{water}}$  over the summer period in the form in which we have employed it (i.e. with  $G$  omitted). However, when we extended the time series from only the summer period to the whole year, a clear yearly cycle was visible, with a peak in summer that is similar to the cycle of (available) radiation and, thus, to estimates of evaporation using Penman's model (see Fig. 4.8a). The benefit of Penman's model in this case is that it can easily be decomposed into an aerodynamic term and a radiation term. The individual terms are presented in Fig. 4.8b. Here, a clear distinction between the yearly cycle of the two Penman terms is visible: the radiation term has a distinct cycle with a peak in June, whereas the aerodynamic term is more constant over the year. This resembles the constancy of observed  $E_{\text{water}}$  found in the diurnal cycle (see Fig. 4.2).

Another phenomenon that could affect the yearly cycle of evaporation is lake water stability and, thus, mixing depth within the lake. Seasonal changes in lake water stability affect the surface temperature and, therefore, evaporation rates via the vapour pressure gradient. Evaporation, in turn, has a cooling effect on the surface temperature, which increases potential mixing. Supported by a preliminary study where mixing depths were estimated using the FLake model (Voskamp, 2018), we assume that Lake IJssel is fully mixed 70 % of the time. This number is not surprising given the fact that evaporation continues during night-time and with wind speeds that are on average  $5.8 \text{ m s}^{-1}$ . In addition, the inflow of

**Table 4.3:** Regression analysis between observed open water evaporation and estimated evaporation using Penman’s model, also broken down into the two individual terms of Penman’s model, i.e. the aerodynamic and radiation term. Analysis is performed for the summer period in 2019 using hourly observations of Stavoren.

Penman	Regression model	$R^2$
Full Penman model	$0.08 \text{ Penman} + 93.5$	0.03
Aerodynamic term	$4.3 \text{ Penman}_{\text{aerodynamic}} - 13$	0.75
Radiation term	$0.05 \text{ Penman}_{\text{radiation}} + 99.1$	0.01

the IJssel River into the lake is also likely to support mixing. During summer, it is more likely that stable conditions occur, and we cannot directly assume fully mixed conditions. However, we considered a full analysis of this phenomenon to be beyond the scope of the current study.

Linking back to the shorter time series spanning the summer months of 1 May to 31 August, we can see that a simple linear relationship exists between observed  $E_{\text{water}}$  and the aerodynamic term of Penman’s model. In contrast, the variability in radiation is uncorrelated with observed  $E_{\text{water}}$  (see Table 4.3). The high correlation between the aerodynamic term of Penman, which includes similar variables to Dalton’s model, and observed  $E_{\text{water}}$  strengthens the finding that our data-driven model is embedded into the well-known theory. We are aware that using a statistical modelling approach has its limitations, as it does not account for the actual physical processes in the way that they might be included in physically based models such as FLake (Mironov, 2008) for estimating lake evaporation. However, in such physically based models, empirical relations are also included (e.g. the wind function in Dalton’s and Penman’s model), and parameters need to be statistically estimated. Furthermore, if drivers of open water evaporation appear to be a function of the temporal resolution, it should be concluded that models, including physical models, can only be properly used at the right temporal resolution. Considering this, we think that statistical modelling is a clean and simple approach that can provide a direct indication of (and insight into) the most relevant input parameters involved in explaining the variation in evaporation, without making a priori assumptions regarding the processes or relations that might be relevant. Therefore, we argue that our model is robust with respect to an application to Lake IJssel and to other inland reservoirs that are several metres deep and in a similar climatic setting.

The dynamics of the observed diurnal cycle of  $E_{\text{water}}$  agree with what has been found in studies such as Tanny et al. (2008), Venäläinen et al. (1999), Granger and Hedstrom (2011), Nordbo et al. (2011), and Potes et al. (2017). Additionally, the estimated diurnal cycle from the FLake lake model (Mironov, 2008) resembles our observed  $E_{\text{water}}$  relatively well (see Chapter 3). All of the aforementioned studies have also found the occurrence of night-time evaporation. This indicates that heat which has been stored during the day is being released during the night when the lake temperature exceeds the air temperature. The  $LE$  and  $H$  fluxes are a function of surface and air temperature, and, through the



outgoing and incoming long-wave radiation,  $R_n$  is a function of surface and air temperature as well. As a consequence of the energy balance, this means that  $G$  is also a function of temperature. The large heat capacity of a water body, controlled by the depth of the water column, provides the system with a ‘memory’. As a result, the water temperature at the surface is not directly related to the instantaneous energy balance at the surface, where net radiation is divided over the turbulent fluxes and a water heat flux; rather, water temperature is subject to a delay and results from the heat storage that is integrated over a longer timescale. We argue that the effect of this delay also leads to the different drivers that have been found at hourly and daily timescales in Stavoren. The volume of a water body that is several metres deep with a large heat capacity and 3D heat transfer through mixing results in a fundamentally different system compared with a shallow water surface or land surface with different factors that drive evaporation (McMahon et al., 2013).

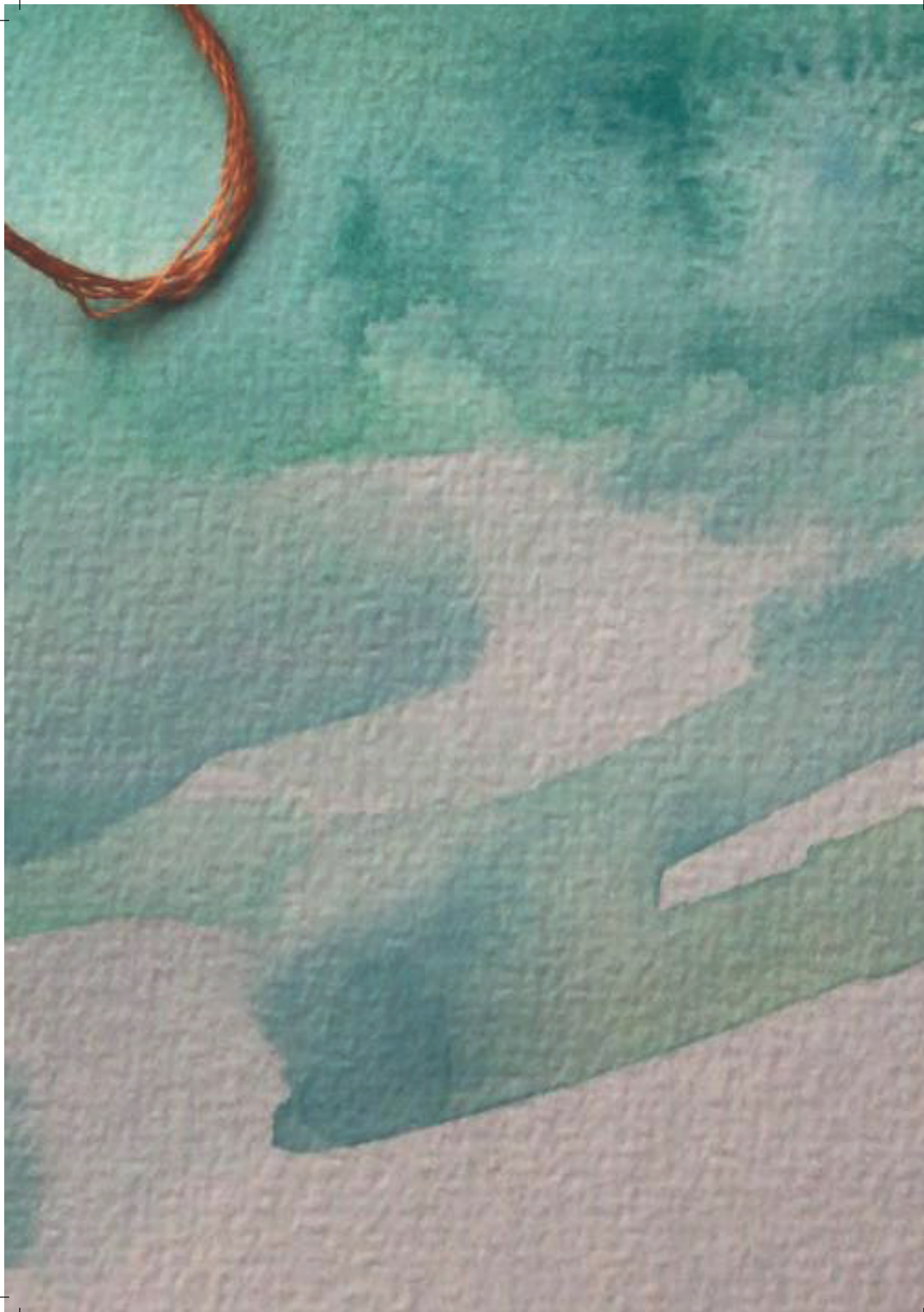
In other studies, the dynamics of  $E_{\text{water}}$  have been found to vary spatially over an inland water body due to advection and the fetch distance from the upwind shore (Weisman and Brutsaert, 1973). More specifically, Granger and Hedstrom (2011) found that  $E_{\text{water}}$  is a function of the lake–land contrast of temperature and vapour pressure. Another source of spatially varying  $E_{\text{water}}$  is the water surface temperature, which can be affected by the spatial variability in the water depth (Wang et al., 2014b) or, for instance, by the supply of water with a different temperature from rivers. Therefore, the fact that our measurement sites are located (i) at the shore in the north of the lake (Stavoren) and (ii) on the dike in the middle of the lake (Trintelhaven) could potentially lead to differences in observed  $E_{\text{water}}$  dynamics between the two measurement sites. The coefficients of the hourly regression models were found to be significantly different between the two locations (Sect. 4.3.4). This difference might be attributed to the difference in location (i.e. at the shore and in the middle of the lake, respectively). Other reasons might be the difference in the measurement height or the inherently different meteorological conditions that we measure, as the two measurement sites are located on opposite sides of the lake.

Not all of the components of the energy balance could be measured during our field campaign. Therefore, the closure of the energy balance, which can be calculated as the ratio between the turbulent fluxes and available energy, could not be analysed. Other studies that have been able to assess the energy balance closure (EBC) over lakes and/or reservoirs have found imbalances in the energy balance that were within a narrow range and were similar to those over land (Wilson et al., 2002a). McGloin et al. (2014) found an average EBC value of 76 % over a year as well as little variation over the seasons, with a value of 77 % for the summer season. Similar respective values of 82 % and 72 % for the summer seasons of 2006 and 2007 were found by Nordbo et al. (2011). A reasonable EBC of 91 % was found by Tanny et al. (2008), although this was for a short period of 14 days. The measured imbalance suggests a general underestimation of the turbulent fluxes. Factors that could contribute to this imbalance are large-scale transport (advection) of heat and water vapour, a systematic instrument bias, mismatch between the frequency

of sampling and the turbulent eddies, mismatch of the measurement footprint of the individual terms, and neglected energy sources or sinks (Wilson et al., 2002a; Foken, 2008; Mauder et al., 2013; Mauder et al., 2020). Despite this likely underestimation of observed  $E_{\text{water}}$  following the imbalance of the energy budget, we believe that this bias will not influence the dynamics of  $E_{\text{water}}$  or the correlations found with other meteorological variables.

## 4.5 Conclusions

In this study, we investigated the dynamics and drivers of open water evaporation of Lake IJssel in the Netherlands via the development of a data-driven model. To this end, open water evaporation was measured during two summer periods at two locations using eddy covariance instruments. Based on the results of regression analysis, it was found that wind speed and vertical water vapour pressure gradient are the main drivers of open water evaporation at hourly timescales during the observed summer periods of 2019 and 2020. These variables are the same as those used in Dalton's model, which is often used for estimating evaporation from deep water bodies. Using the data collected in 2019, simple data-driven models for both locations were developed based on the aforementioned variables. At an hourly timescale, this resulted in  $R^2 = 0.74$  and  $R^2 = 0.70$  for Stavoren and Trintelhaven, respectively. Validation of these hourly simple models using the data collected during the summer of 2020 showed that a simple data-driven model is able to explain large parts of the hourly dynamics of open water evaporation ( $R^2 = 0.84$  and  $R^2 = 0.67$  for Stavoren and Trintelhaven, respectively). The absence of a correlation between observed daily open water evaporation and estimated evaporation using Makkink's model indicates that this radiation-based model is unable to explain the dynamics of  $E_{\text{water}}$ , although this is current practice in the operational water management of Lake IJssel. Given the importance of  $E_{\text{water}}$  in the large-scale water balance, it is necessary to correctly incorporate this process in hydrological models.



# Chapter 5

## Land cover control on latent and sensible heat fluxes

This chapter is based on:

Jansen, F. A., Jongen, H. J., Jacobs, C. M. J., Bosveld, F. C., Buzacott, A. J. V., Heusinkveld, B. G., Kruijt, B., Van der Molen, M., Moors, E., Steeneveld, G-J., Van der Tol, C., Van der Velde, Y., Voortman, B., Uijlenhoet, R., and Teuling, A. J. (2022). Land cover control on evaporation and sensible heat flux dynamics: an observation-based synthesis for the Netherlands, *Water Resources Research* (manuscript under review).

## Abstract

Land cover is known to control the land-atmosphere exchange of water and energy through the partitioning of solar energy into latent and sensible heat. Observations over all land cover types at the regional scale are required to study the variability of these latent and sensible heat fluxes over a landscape. Here, we aim to study how the control of daily and midday latent and sensible heat fluxes over different land cover types is distributed along three axes: energy availability, water availability and exchange efficiency. To this end, observations from 19 eddy covariance flux tower sites in the Netherlands, covering six land cover types located within the same climatic zone, were used in a regression analysis. The resulting relative position of these study sites along the three axes suggests that land cover can partly explain the variance of daily and midday latent and sensible heat fluxes. We found that evaporation dynamics from grassland, peatland swamp and cropland sites could mostly be explained by energy availability. Forest evaporation can mainly be explained by water availability, urban evaporation by water availability and exchange efficiency, and open water evaporation can almost entirely be explained by exchange efficiency. We also found that the sensible heat flux is less sensitive to land cover type. This demonstrates that the land-atmosphere interface plays an active role in the shedding of sensible heat. Our results contribute to a better understanding of the dynamics of evaporation over different land cover types and may help to optimise, and potentially simplify, models to predict evaporation.

## 5.1 Introduction

## 5.2 Introduction

Partitioning of solar energy at the land surface into latent heat (or evaporation) and sensible heat is a key process in the climate system, and a main control on the terrestrial part of the hydrological cycle (Seneviratne et al., 2010). The partitioning is strongly controlled by vegetation and soil moisture, resulting in reduced evaporation during droughts due to soil moisture limitation. The associated higher sensible heat fluxes can amplify heatwave temperatures (Miralles et al., 2014; Miralles et al., 2019). In a warming climate, it is projected that many regions will face increased water limitation, with important implications for heatwaves and ecosystem functioning (Denissen et al., 2022). Within hydrology, the total evaporation from the vegetated land surface is commonly referred to as evapotranspiration. Since the use of this term has come under scrutiny for various reasons (Savenije, 2004; Miralles et al., 2020), we will simply use ‘evaporation’ in this study to refer to the total flux of water from the (land) surface to the atmosphere. Generally, there is a focus on understanding the dynamics and drivers of evaporation rather than the sensible heat flux when analysing land surface-atmosphere exchange processes (Brutsaert, 1982). Observations of the sensible heat flux are predominantly made to serve the aim of energy balance closure (Katul and Parlange, 1992; Vercauteren et al., 2009). As a result, the active role of the land surface in driving the sensible heat flux has remained under-explored (Wilson et al., 2002b). Over the past years, however, interest in the use of land use management as a tool to optimize not only local water but also local climate services has been growing. In addition to the role of evaporation in controlling water availability, sensible heat fluxes can be used to control near-surface temperature in particular during the warm season when energy balance partitioning at the land surface has the largest impact on atmospheric conditions. So far, however, few studies have investigated the variability of flux partitioning and its drivers in a climatologically homogeneous region such as the low-lying countries of the Rhine-Meuse delta with a temperate marine climate.

Historically, studies on the exchange of water and heat at the land surface were based on hypotheses rather than observations. Already in the 12th century, hypotheses were presented in which possible explanations for evaporation were given (Brutsaert, 1982). The integration of experiments and hypotheses as a scientific approach created opportunities to improve our understanding of the evaporation process. The findings by Dalton (1802), who was able to relate evaporation to wind speed and vapour pressure gradient, formed a crucial step in the development of evaporation theory. More than a century later, Thornthwaite (1948) introduced the concept of potential evaporation, which describes the atmospheric evaporative ability over large uniform surfaces (implying no effects of local advection), in which evaporation rates rise to their maximum depending solely on the climatic setting, thereby assuming unlimited water access. A more elaborate method,

which considers additional meteorological input, was developed by Penman (1948). He described potential evaporation from a wet surface as the sum of a radiation and an aerodynamic term, both expressed in terms of energy. This suggests that these two terms could also compensate each other's effects and could therefore be interchangeable. To estimate potential evaporation for vegetated surfaces, Monteith (1965) introduced a surface resistance factor ( $r_s$ ) to represent plant physiological processes in the so-called Penman-Monteith (PM) equation. This resistance is a function of atmospheric variables such as radiation, air temperature and vapour pressure deficit (VPD), but it does not integrate the active response of the vegetation to changes in these atmospheric variables, as was proposed by Jarvis (1976). This dependency of  $r_s$  on atmospheric variables in a coupled biological system makes it challenging to understand the exact role of  $r_s$  on the dynamics of evaporation. In fact,  $r_s$  can compensate for all the processes and mechanisms that are included in the PM equation. The interchangeability between the two PM terms is therefore questionable for biological systems. Nevertheless, many studies have found the PM equation to correctly describe evaporation rates. Therefore, the physically-oriented PM equation is nowadays the default model to estimate evaporation based on standard meteorological data.

Parallel to the development of the physically-oriented theoretical approaches to approximate evaporation, another branch of studies was emerging, which explored simplifications of these physically-oriented theories. This quest for simplification partly originated from limited data availability. This has led to the development of several simpler models to estimate potential evaporation compared to the PM equation. For example, Priestley and Taylor (1972) showed that in a land surface-atmosphere system, in which many feedbacks are present, the evaporation tends to reach an equilibrium. This equilibrium evaporation represents the lower limit of evaporation when the air is saturated and thus the drying power of the air is reduced to zero. This would eliminate the second term of the Penman equation. However, conditions without any advection are rare. Therefore, Priestley and Taylor (1972) added a constant ( $\alpha$ ) to the first Penman term to account for conditions of minimal advection. Other simplified models were developed for specific regions. For instance, the temperature- and global radiation-based model of Makkink (1957) has been successfully employed in operational water and drought management in the Netherlands since 1987. Makkink (1957) developed this pragmatic model based on the same principles as Priestley and Taylor (1972), but it was specified to conditions in the Netherlands in an attempt to find a model that only includes meteorological variables that were readily available. If global radiation observations are not available either, the highly empirical temperature-based model developed by Hargreaves (1975) is often chosen. This model can be used at longer temporal scales and it accounts for seasonality by using location-specific extra-terrestrial, i.e. top-of-the-atmosphere, radiation data estimated from the solar constant, the solar declination and the time of the year. In the aforementioned examples of simplified evaporation models, not all terms of the

PM equation are represented. Recently, Maes et al. (2019) demonstrated using eddy covariance (EC) observations that the more complex approaches such as the PM model perform consistently poorer than simpler approaches at daily timescales. By using this modern flux dataset, Maes et al. (2019) support the idea that  $r_s$  is highly dynamic and that it might compensate for many atmospheric feedbacks, rather than being a constant as was originally proposed by Monteith (1965). So where physically-oriented approaches might suffer from over-parametrization, EC observations can provide invaluable insight into the control of both vegetation-related processes and atmospheric feedbacks on water and energy exchange at the land surface.

The gradually increasing availability of observations and new measurement techniques allowed to not only study potential evaporation, but it also created a shift to start analysing the role and impact of water limitation on actual evaporation. Initially, observations of evaporation could only be determined indirectly through long-term average discharge measurements, from which systems at the larger temporal and spatial scale could be analysed. This does not allow studying the drivers of evaporation in detail, but it can inform us more on the transition from energy to water limitation within a larger river catchment. Budyko (1974) recognized that the long-term water balance of river catchments has two limiting regimes, namely a regime where evaporation is limited by the available energy and a regime where it is limited by water availability. Whether catchments are closer to one than to the other regime depends on the partitioning of precipitation between evaporation and discharge. The so-called Budyko curve can thus be used to identify how water limitation influences the energy partitioning at relatively large scales. Later, more recently developed measurement methods, such as the Bowen ratio method and EC, were used to analyse the effect of water limitation on the reduction of evaporation. Brutsaert and Chen (1995) and Williams and Albertson (2004) found a clear relation between soil moisture depletion and the reduction of evaporation rates during experiments performed over a prairie and a savanna landscape, respectively. Studies performed in urban areas using EC and scintillometry measurement techniques found that evaporation in these systems is strongly water limited within days during a drydown and that interception plays an important role in the timing of the total urban evaporation rate (Jacobs et al., 2015; Jongen et al., 2022). Originating from the initial focus of the role of energy availability as a driver of evaporation, these more recent observations on the role of water limitation supported the integration of a second dimension to the evaporation limitation concept and to start studying the actual evaporation (Budyko, 1974; Seneviratne et al., 2010). The two-dimensional evaporation limitation concept, where evaporation is constrained by water and energy availability, currently appears to be the common way to present and categorize the drivers of evaporation. The ever-increasing availability of more direct evaporation observations enhances the potential to evaluate the current framework and to continue to study the energy partitioning and drivers of evaporation for different scales, environmental conditions and land cover types.



Over the past decades, advances in sensor and computer technology have turned EC flux measurements from a highly specialized endeavour, used mainly during dedicated field campaigns, into a more routine observation method. Starting from the mid-1990's, this has allowed researchers to routinely measure fluxes of water, energy, and carbon over a range of ecosystems around the world. The FLUXNET initiative (Baldocchi et al., 2001) brought together many of these observations, and has since served as a valuable dataset for the study of flux responses to extreme events such as heatwaves and droughts (e.g. Ciais et al., 2005; Teuling et al., 2010), for the study of land cover impacts on land-atmosphere exchange and atmospheric conditions (e.g. Lee et al., 2011; Lansu et al., 2020; Hoek van Dijke et al., 2020; Xu et al., 2022), and to study long-term changes in land surface evaporation (e.g. Teuling et al., 2009; Jung et al., 2010). The location of the flux towers in FLUXNET is however far from random, with a tendency for sites to be located in carbon-rich ecosystems in wealthier countries, and less so in dryland ecosystems or for instance in cities. The FLUXNET database is not a comprehensive archive of EC observations either. In many regions, the Netherlands being a good example, only a small minority of the EC sites contributes to the FLUXNET database. In conclusion, while the abundance of EC observations that became available through FLUXNET has provided a tremendous opportunity for global and continental analysis on the drivers of land-atmosphere exchange over different climate zones, the current number of sites is insufficient to study variability of evaporation at the regional scale, and over all land cover types that make up real-world landscapes.

We aim to study the drivers of latent and sensible heat exchange over land cover types that are less or not represented in FLUXNET. Results from case studies where other land cover types, such as urban areas, peatland swamps and inland water bodies, are analysed indicate that our knowledge on the drivers of evaporation and the role of land cover type can be further increased. As mentioned earlier, urban areas can be considered water-limited systems. Linked to the vast impervious surfaces in urban areas, it is shown that evaporation in cities is closely linked to precipitation events, or more specifically to the time since precipitation (Jacobs et al., 2015; Jongen et al., 2022). During drydowns less water is available for evaporation, which leads to increased air temperatures and thus an increased sensible heat flux ( $H$ ). Van der Velde et al. (2013) showed that peatland swamps use significantly less energy and water for evaporation compared to open water, thereby maintaining or even creating new peatland swamps. The reduced evaporation from peatland swamps compared to open water, could potentially be related to the stronger stomatal control and a lower decoupling factor (Jarvis and McNaughton, 1986) as a result of the higher surface roughness caused by the vegetation. Furthermore, the lower albedo and the reduced air exchange as a result of stable and moist air created in between the peatland swamp vegetation can also contribute to reduced evaporation. Based on regression analysis daily open water evaporation from inland water bodies was found to be dominantly transport-limited and could be explained by a combination of wind speed

and a vapour pressure gradient (see Chapter 4). Similarly, Lobos-Roco et al. (2021) found that transport in addition to radiative energy are the principle components to explain the dynamics of evaporation for a saline lake in the Atacama desert. This transport mechanism, consisting of wind speed and a vapour pressure gradient, could be considered a mechanical energy term, similar to the aerodynamic term in the PM equation. However, it can also be looked upon as an exchange efficiency term that controls the exchange processes of energy and water between the land surface and the atmosphere, in which  $r_s$ , with its biological controls, is eliminated. This exchange efficiency can be weaker or stronger and with that it can explain part of the variance of evaporation. This suggests that the exchange efficiency can be seen as a third dimension, next to energy availability and water availability, to explain evaporation dynamics over different land cover types.

One way to better understand the complexity of latent and sensible heat exchange over different systems is by comparing sites of various land cover types located within the same region and climatic setting. By including EC sites beyond the FLUXNET database, we can increase the density of EC sites within a region and thus improve the representation of different land cover such as wetlands and urban areas with respect to FLUXNET. The multitude of EC measurements conducted over different land cover types in the Netherlands provides the opportunity to perform a direct comparison of drivers of evaporation over land cover types within the same climatic zone, and largely in the absence of orographic differences. The landscape of the Netherlands is almost completely anthropogenically managed, resulting in a mosaic of urban areas, forest, grassland, agriculture, peatland swamps and open water areas, all in close proximity. Long-term EC measurements of latent and sensible heat exchange have been performed over the grassland areas Cabauw, Veenkampen and Horstermeer (Hendriks et al., 2007; Jacobs et al., 2010; Bosveld et al., 2020). The coniferous forests of Loobos (Dolman et al., 1998; Moors, 2012) and Speulderbos (Bosveld and Bouten, 2001; Cisneros Vaca et al., 2018) both have a long history of EC measurements as well, while in Oostwaard there was a short measurement campaign over a willow forest (Elbers et al., 2009). In the past, various croplands have been studied, i.e. locations Dijkgraaf, Langerak, Lutjewad, Molenweg, Vredepeel and Zeewolde (Elbers et al., 2009; Moors et al., 2012). More recently, open water evaporation from Lake IJssel was studied at two locations: Stavoren and Trintelhaven (see Chapter 4). Furthermore, evaporation in the urban areas of Arnhem and Amsterdam has been studied (Jacobs et al., 2015; Steeneveld et al., 2020; Jongen et al., 2022), and in recent years measurement campaigns over the peatland swamps Onlanden, Camphuys and Zegveld have been performed (Kruijt et al., 2020; Buzacott et al., 2022). Additional evaporation observations in the Netherlands have been made based on other techniques, including lysimeters (Voortman et al., 2015; Teuling, 2018a), scintillometry (Meijninger et al., 2002; Leijnse et al., 2007; Steeneveld et al., 2011; Jacobs et al., 2015), Bowen ratio method (Moors, 2012) and distributed temperature sensing (Schilperoort et al., 2018). However, these methods are either unable to resolve diurnal or even day-to-day variability, or they

do not (currently) allow for a comparison between different land cover types. Therefore, EC measurements are currently the best basis for a synthesis of the drivers of evaporation dynamics over different land cover types.

In this study, we aim to compare the external drivers of daily and midday evaporation, expressed in terms of energy, i.e. the latent heat flux ( $LE$ ), and sensible heat flux over different land cover types within a climatic zone during the warm season. As a case, we will use EC observations obtained in the Netherlands (i.e. temperate marine climate) over 19 forest, grassland, urban area, open water, cropland and peatland swamp sites (see Fig. 2.1). These include sites that are part of FLUXNET, but also sites outside that network. This study provides a first synthesis presenting the drivers of observed evaporation dynamics over complex landscapes, which we will express as a three-dimensional framework in which evaporation is found to be limited by either energy availability, water availability or exchange efficiency depending on land cover.

## 5.3 Data and Methods

### 5.3.1 Measurement sites

In this chapter we analysed historical measurements of latent heat flux, sensible heat flux and auxiliary meteorological observations from EC flux towers at 19 sites in the Netherlands, covering six land cover types within the same temperate marine climate zone (see Fig. 2.1 and Sect. 2.2). Table 2.1 provides an overview of all the flux sites including the land cover classification, period over which measurements were performed, climatological yearly means of air temperature and precipitation, and the key references of each measurement site. The 19 sites were selected based on measurement method (i.e. eddy covariance), data availability of latent and sensible heat fluxes and auxiliary meteorological observations, and the requirement of a minimum length of the data record of one warm season (May–August). The six land cover types considered are: grass (GR), forest (FO), urban (UR), open water (WA), crop (CR) and peatland swamp (PS). Peatland swamps are vegetated peat areas covered with reed-like vegetation (among others: *Phragmites* spp, *Typha* spp) which are inundated year-round with a shallow standing water level of a few centimetres. This differs from open water bodies, which do not have a significant vegetation cover and typically have deeper water levels. Peatland swamps also differ from grasslands on peat soils in terms of groundwater levels.

### 5.3.2 Data processing

All latent and sensible heat flux data used in this study were measured with the EC technique, which is considered one of the most direct methods for quantifying latent and sensible heat fluxes. This technique is based on simultaneous measurements of the vertical wind speed and gas concentration (including water vapour) and temperature measurements.

From this the heat fluxes can be derived as the covariance of turbulent fluctuations of vertical wind speed and specific humidity (latent heat flux) and the covariance of turbulent fluctuations of vertical wind speed and temperature (sensible heat flux). Raw fluxes were quality-controlled and processed by the individual researchers responsible for their site, respecting and complying with the generally accepted procedures (Aubinet et al., 2012). Fluxes were provided at 30-min or hourly averaging intervals with accompanying quality flags for the heat fluxes. In Section 2.4, we provide a more elaborate description of the EC technique and processing steps involved. Since we are interested in the process of the turbulent fluxes we chose to only use the best quality data, which means quality flags 1, 2 and 3 in case of the 9 quality flag system of Foken et al. (2004), and quality flag 0 in case of the 0-1-2 system of Mauder and Foken (2004). The use of EC in urban areas is known to be especially challenging (Feigenwinter et al., 2012). Therefore, an exception was made for Amsterdam where also flag 1 was allowed, because otherwise no data would be left for further analysis. Data of all sites are given in UTC+1.

From the processed datasets, only the warm season was selected for further analysis. Here we defined the warm season as the four months with the highest incoming short-wave radiation, i.e. May–August. Hereafter, the terms warm season and year are used interchangeably, but we always refer to the months May–August, if not stated otherwise. In case of Stavoren, Trintelhaven and Lutjewad, wind direction was employed as an additional selection criterion to ensure representation of the aimed land cover type. Furthermore, the analysis was performed on two timescales, namely daily and midday. Midday hours were taken as 11am–3pm UTC+1. This period is considered long enough to reduce the noise of half-hourly fluxes from the actual signal. Studying the midday evaporation provides the opportunity to study the difference in land-atmosphere coupling over the various land cover types, while the daily timescale is commonly used in water resources management modelling.

For each site the following variables were used to study the drivers of latent heat flux: global radiation ( $K_{in}$ ), net radiation ( $R_n$ ), air temperature ( $T_a$ ), wind speed ( $u$ ), vapour pressure deficit (VPD), precipitation ( $P$ ) and soil moisture (SM). Most variables were measured at the EC site. However, some variables were obtained from other data sources, which we explained in Section 2.5.

### 5.3.3 Regression analysis

A regression analysis with nine input variables was performed to try to explain the dynamics of evaporation for each measurement site. By using a regression method we draw conclusions that are informed by the data instead of implementing process-based assumptions. The nine potential driving variables included in the analysis are the following:

- Energy availability: global radiation, net radiation and air temperature.

- Water availability: soil moisture, hours since precipitation (HSP), cumulative precipitation over 3 days (Prec3, characteristic for urban response times (Jacobs et al., 2015; Jongen et al., 2022)) and cumulative precipitation over 10 days (Prec10, characteristic for rootzone responses (Teuling et al., 2006)).
- Exchange efficiency: wind speed and vapour pressure deficit.

The ‘all subset selection’ regression method was used in this chapter because this method is suitable for analysing large datasets in which it is attempted to explain the dynamics of a dependent variable, here evaporation, with relatively few independent variables (Kutner et al., 2005). Other regression techniques such as Lasso regression or stepwise regression methods would typically be used when there are relatively many input variables with respect to the number of data points. In our case, having large datasets with relatively few input variables it is worth examining all possible combinations from the set of independent variables (i.e. with  $n$  independent variables there are  $2^n - 1$  possible combinations).

For this analysis all input variables were normalized to range between 0–100. Furthermore, the regression method requires all variables to be available for each timestep. In case of a missing value, the timestep is removed from the dataset. Additionally, temporal independence of each input variable is required. Although we are using time series of environmental variables autocorrelation analysis showed that the temporal dependence in the data is not strong. Apparently the memory of the system is too small to have a large time dependency. To reduce the temporal dependency that is still present, we sampled every other day and used that as a training dataset. This way, the autocorrelation falls below the limit of 0.4 within 2 lags for all input variables, except for SM. To eliminate multicollinearity within the model one of the predicting variables would be removed from the subset selection method if it had a higher cross-correlation than 0.7 with other variables. For all sites, high correlations were found between global radiation and net radiation (see Fig. 5.1 for site GR1 as an example). Therefore, the analysis was continued without net radiation as a potential predictor.

Based on the remaining eight predictors all possible (multiple) linear regression models are identified of which the form is prescribed as:

$$Y = \beta_0 + \beta_1 X_1 + \beta_2 X_2 + \dots + \beta_i X_i + \epsilon \quad (5.1)$$

where  $Y$  is the dependent variable,  $X_i$  the explanatory variable(s),  $\beta_0$  the intercept,  $\beta_i$  the parameter(s), and  $\epsilon$  the error term. From all the potential subsets the best model for each subset size is returned based on objective statistical criteria, which in this study was chosen to be based on Mallow’s Cp value and the AIC (Akaike Information Criterion) value (Kutner et al., 2005). These resulting group of best models are ordered by increasing subset size. In the search for the best parsimonious model from these best models, each of different size, the best model was chosen based on the first instance when (i) both the

Cp value would be lower than the sum of the total number of predictors (eight in this study:  $K_{in}$ ,  $T_a$ , SM, HSP, Prec3, Prec10, u and VPD) plus one, (ii) as well as the difference between the AIC values of the subsequent best models of increasing size would be less than five. Following this procedure, the number of predictors included in each model for the individual measurement sites can vary.

The best regression model found by the subset selection method was tested for Variance Inflation Factors (VIF), which report whether each predictor in the model is statistically significantly contributing to explaining the dynamics of the dependent variable (Kutner et al., 2005). Because the input data was normalized, the resulting model coefficients provide the relative contribution of each predictor in explaining the dynamics of evaporation. The coefficients of the multiple linear regression model predictors were normalized so they sum up to 100. Originating from our aim to express drivers of evaporation in a three-dimensional framework in which evaporation can be limited by energy availability, water availability or exchange efficiency, the input variables are now grouped according to the categories listed above. The variables belonging to each group have been predefined according to the aforementioned bullet list. The coefficients of the model predictors are summed per category, which then provides the information on the relative contribution of that category in explaining the dynamics of evaporation. Note that a total summation of the coefficients of 100 does not mean that the regression model explains 100% of the variance of the evaporation dynamics; rather, it is used to express the relative contribution of the three limitation categories. The regression procedure described is used as a data analysis technique and is not aimed to have predictive value. Furthermore, since the input data was normalized, the resulting regression models cannot directly be used as predictive models for other sites with potentially different ranges in the input variables. The whole regression analysis procedure was performed for the sensible heat flux as the dependent variable as well, using the same categories of independent variables to explain its dynamics.

## 5.4 Results

### 5.4.1 Evaporation dynamics

A clear distinction is found in the diurnal cycle of the latent heat flux ( $LE$ ) between sites of different land cover types (Fig. 5.2). The figure displays the average diurnal cycle for all individual measurement sites, categorized by their land cover types. Especially open water (Fig. 5.2c) and urban areas (Fig. 5.2d) show a distinctively different diurnal cycle of  $LE$ , which does not follow the radiation cycle as strongly as  $LE$  from other land cover types, but is rather more constant throughout the day. In case of open water evaporation, this effect can be related to the relatively large thermal inertia of water compared to the vegetated terrestrial surfaces. This large heat capacity also leads to relatively high  $LE$

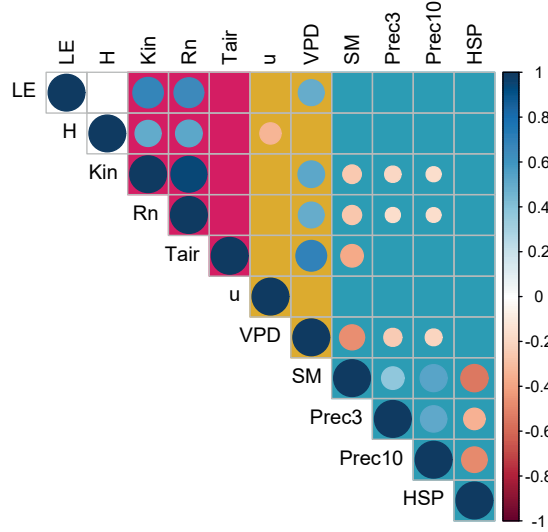


**Figure 5.1:** Correlation between observed latent heat flux, sensible heat flux and meteorological variables for site GR1 (i.e. Cabauw) at the daily timescale. The size and colour of the circles both refer to the correlation strength and sign. Circles are only provided for significant correlations. The background colour indicates the grouping of the variables, where pink relates to energy availability, yellow relates to exchange efficiency, and blue relates to water availability.

rates during the night, whereas  $LE$  from other land cover types tends to become zero during the night. At the urban sites, a peak can be found at noon following the radiation cycle, but the amplitude is much smaller compared to the vegetated terrestrial sites. However, the dynamics of sensible heat flux ( $H$ ) shows the reverse behaviour (Fig. 5.3), where the peak of urban  $H$  is highest. This is the result of the close relation between  $LE$  and  $H$  through the energy balance. As a first approximation, for closure of the energy balance, all available energy not contributing to  $LE$  and heating of the surface must be converted to  $H$ , thereby warming the air.

#### 5.4.2 Drivers of evaporation

Using the regression method we were able to study the relative contribution of each of the three groups of variables in explaining the variance of evaporation for each measurement site. These results are presented using a triangular plot, of which each of the three axes represents a group of variables related to energy availability, water availability and exchange efficiency, respectively (Fig. 5.4). If a site is located in one of the far corners of the triangle, it means that the variance explained by the regression model can be entirely explained by the variables belonging to one category. However, this does not mean that

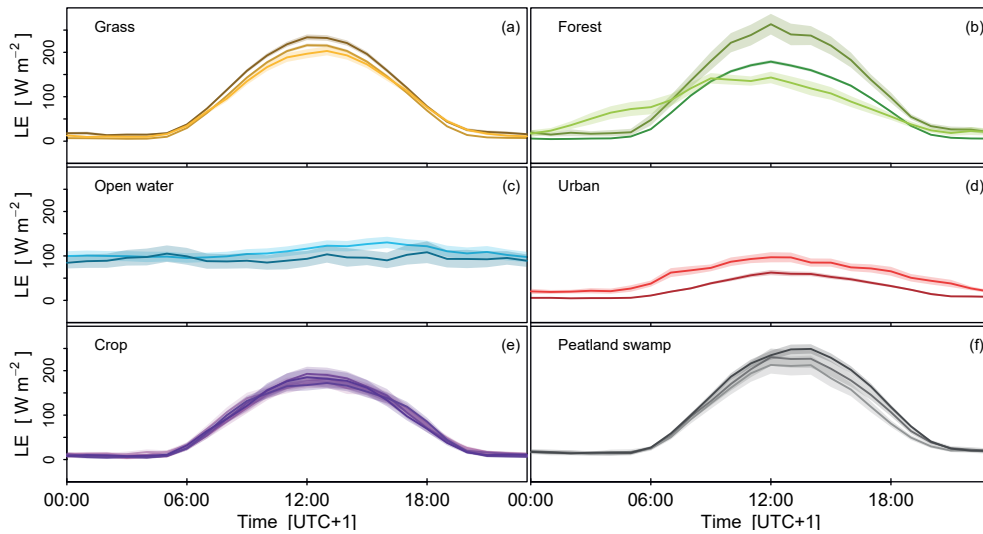


**Figure 5.2:** Average diurnal cycle of the latent heat flux in the warm season grouped per land cover type, indicating a difference in sensitivity to environmental drivers. Each coloured line represents a measurement site. The uncertainty, here defined as twice the standard error, is presented as the shaded area around the solid lines.

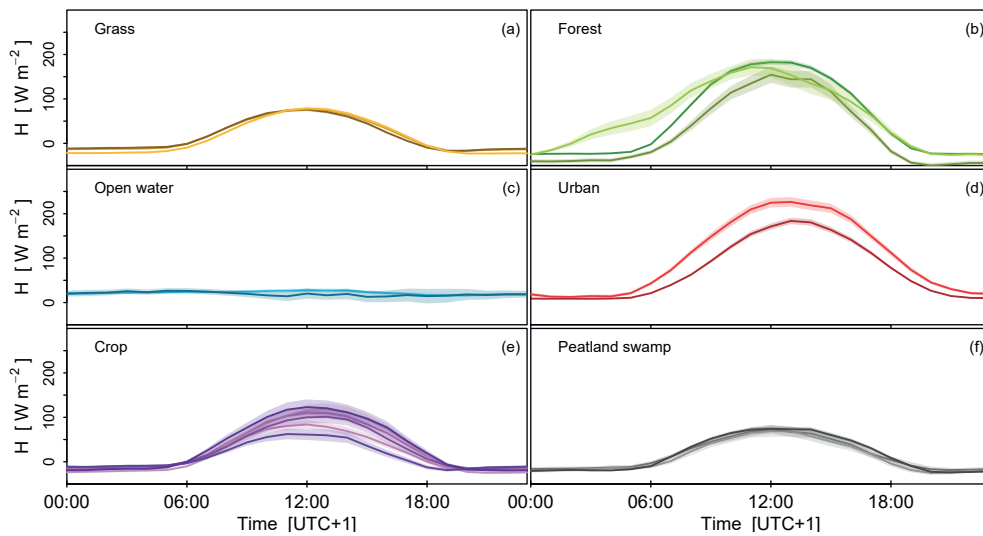


**Figure 5.3:** Average diurnal cycle of the sensible heat flux in the warm season grouped per land cover type, indicating a difference in sensitivity to environmental drivers. Each coloured line represents a measurement site. The uncertainty, here defined as twice the standard error, is presented as the shaded area around the solid lines.



100 % of the variance is explained (see Section 5.3.3). Similarly, the position of the black dot in Figure 5.4 indicates that exchange efficiency contributes for 55 % to the explained variance of evaporation for that site, while 30 % of the explained variance can be attributed to energy availability and 15 % to water availability. The variables which are able to explain a portion of the variance in the output signal, can be called driver, given the assumption that the system is sensitive and the driver itself varies and is not constant. In other words, we assume that if variation in the input signal leads to variation in output signal we can call the input variable a driver. In Table C2 in Appendix C the mean and standard deviation of the input variables for each site is shown.

By placing each site within the triangle plot a direct comparison between the sites of different land cover types is possible. Figure 5.5a shows the results at the daily timescale. In general, the sites are clustered per land cover type. For instance, the open water sites can be found in the lower left corner of the triangle, indicating that exchange efficiency is highly important in explaining evaporation, while energy availability and water availability are contributing less. On a daily timescale this means that if wind speed and/or VPD is low, evaporation will also be less. However, if energy availability is limited, the effect on evaporation will be less strong. The urban areas are found in the lower middle to right part of the triangle. This implies that the variables in the energy availability group are not explaining much of the evaporation dynamics, but rather water availability and exchange efficiency are important drivers of urban evaporation. The other land cover types, i.e. grass, forest, crop and peatland swamp, are mostly situated in the top part of the triangle, indicating the importance of energy availability in driving evaporation. The forest sites tend to be more sensitive to water availability, while for the peatland swamps water is not limiting evaporation at all, as we would expect for inundated vegetated cover. There is one outlier among the crop sites, i.e. CR4, which is located in the lower left corner.

In Figure 5.5b the results of the regression analysis based on midday hours is shown. The positioning of the land cover types is similar to the analysis based on a daily timescale, although the individual sites slightly shift. We find that the urban site UR2 moves slightly towards the left, increasing the importance of exchange efficiency at this shorter timescale in the middle of the day at the cost of water availability. The same holds for site WA2. The configuration of the grassland sites changes slightly and a slight shift towards the right can be seen, which means a decrease in the explanatory value of exchange efficiency. A similar behaviour is found for the peatland swamp and crop sites. Also for the forest sites the relative contribution of energy availability to explaining evaporation remains similar at this timescale, but there is some shift on the exchange efficiency and water availability axes. Since the results at both timescales are similar, we will focus on the daily timescale in the following analyses.

The results of the regression analysis to explain the driving mechanism of  $H$  differ from that of  $LE$ . The resulting configuration of  $H$  does not resemble that of  $LE$ . Although

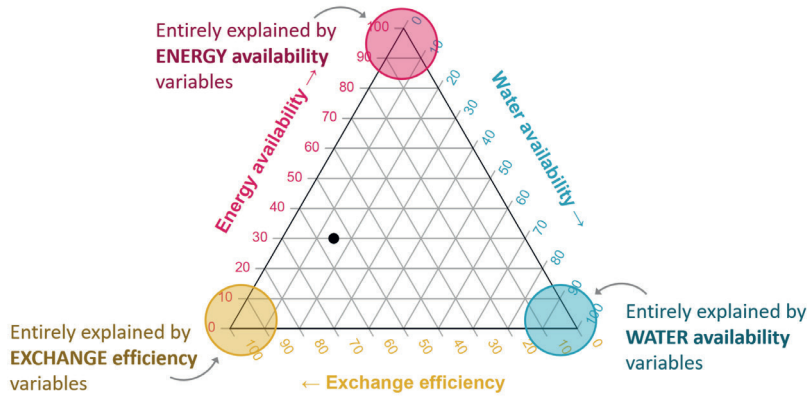


**Figure 5.4:** Explanation of the triangular plot in which each of the three axes represents one of the limitation categories: energy availability, water availability and exchange efficiency. The position of a measurement site within the triangle (for example the black dot) shows the relative contribution of each category in explaining the variance of evaporation for that measurement site. In case of the black dot, the largest portion of the explained variance can be attributed to exchange efficiency (55%), while 30 % of the explained variance can be attributed to energy availability and 15 % to water availability. If a measurement site ends up in one of the corners of the triangle, it means that all variance explained by the regression model can be attributed to the corresponding category.

turbulent eddies are able to transport water vapour and heat, these results imply that the land-atmosphere interface must play an active role in what actually is transported. At the daily timescale almost all sites end up in the top left corner of the triangle, indicating that energy availability is the main driver of  $H$  and that water availability and exchange efficiency are less involved in explaining the dynamics of  $H$ . WA1 is the only site to end up in the lower right corner. Since it is an open water site, it is physically not possible that water availability would be the limiting factor. Therefore, we consider it to be a faulty result from the regression analysis. Some clustering is visible for the land cover types grass, forest and peatland swamp. At the midday timescale the sites end up even more close to each other in the far top corner of the triangle, indicating that  $H$  can mostly be explained by energy availability during midday hours.

The datasets of the sites differ in length and period measured. In Figure 5.6a the variation between years was explored by plotting the result of the regression analysis for all individual warm seasons ( $N = 1$ , where  $N$  refers to the number of seasons) of one site with a long monitoring period of 18 years, i.e. GR1. GR1 was used as the reference site because of its well maintained long dataset and land cover, i.e. well-watered short grass, which is often used to estimate reference crop evaporation estimation (Allen et al., 1998; McMahon et al., 2013). Note that multiple warm seasons end up in the top corner of the triangle (energy

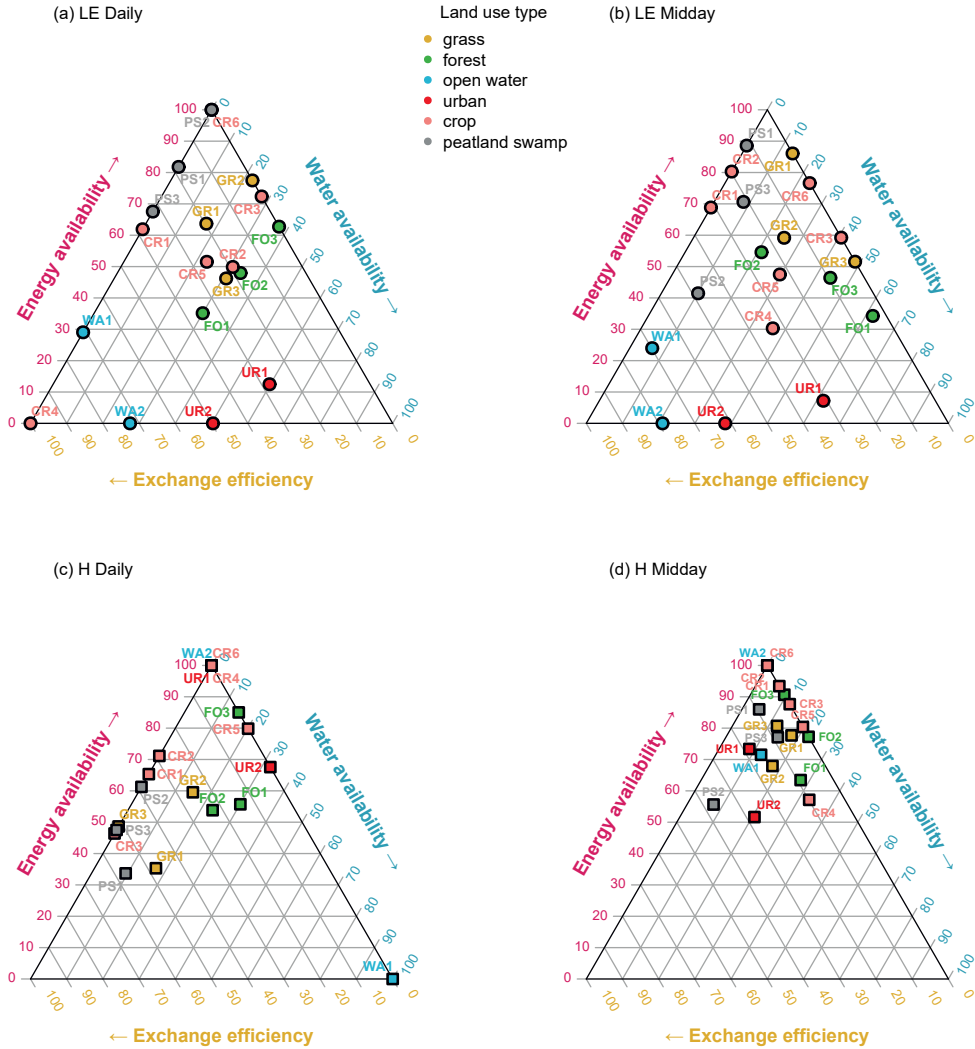


**Figure 5.5:** A direct comparison of the relative contribution of the variables grouped by energy availability, water availability and exchange efficiency in explaining the dynamics of  $LE$  (a,b) and  $H$  (c,d) for sites of different land cover type. Panels (a) and (c) show the results at the daily timescale and panels (b) and (d) for midday hours. The three axes of the triangle each represent a group. For each site the sum of the contributions of the three axes adds to 100 %.

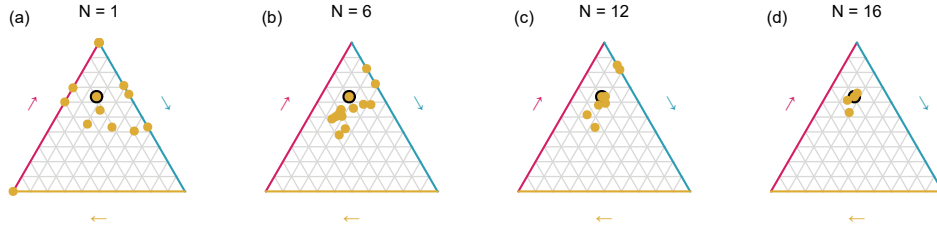


**Figure 5.6:** Exploration of the effect of inter-annual variability on the positioning within the triangle for the site GR1 at daily timescale. This was used as a reference for identifying the uncertainty ranges for the other sites with shorter monitoring periods. Each yellow dot represents the position based on a moving window of  $N$  aggregated consecutive warm seasons. The black-rimmed yellow dot represents the position when all years are included.

availability = 100, water availability and exchange efficiency = 0), therefore multiple dots overlap. By plotting all individual years separately we can analyse the influence of the conditions of an individual year on the position of the point in the triangle. Similarly, we can identify the position within the triangle when merging two consecutive years, or merging any number of consecutive years. Note that the points are therefore not fully independent of each other. This strategy was chosen over random sampling without replacement, based on the constraints of the dataset length. The analysis shows that as more years are included, the points start to converge, reducing the uncertainty, until a single point when all available years within the dataset are included (i.e. the points in Fig. 5.5). The results of this analysis are assumed to be suitable as a reference to identify uncertainty ranges for the other sites with shorter monitoring periods. The uncertainty in the three directions of the three axes has been calculated as the standard deviation with the GR1 dataset as reference. This has been done for all numbers of years. In that way, the calculated uncertainty ranges can be applied to other datasets where a given number of years of data is available.

In Figure 5.7 the uncertainty per site is shown categorized per land cover type. The uncertainty bar for each axis is placed perpendicular to the lines belonging to that axis. Note that this is not the same as the direction of the outer lines of the triangle. For instance, the lines belonging to the energy availability axis run horizontally through the triangle, hence the uncertainty bar runs vertically (see inset top-right of Fig. 5.7). Measurement sites with longer time series, e.g. FO1, have smaller uncertainty bars, meaning we are more confident in the location within the triangle. For sites with shorter time series, the impact of varying conditions from year to year on the placement within the triangle will likely be larger. Therefore, those sites could be positioned anywhere within the polygon defined by the uncertainty bars. GR1 has no uncertainty bars as this site was used as

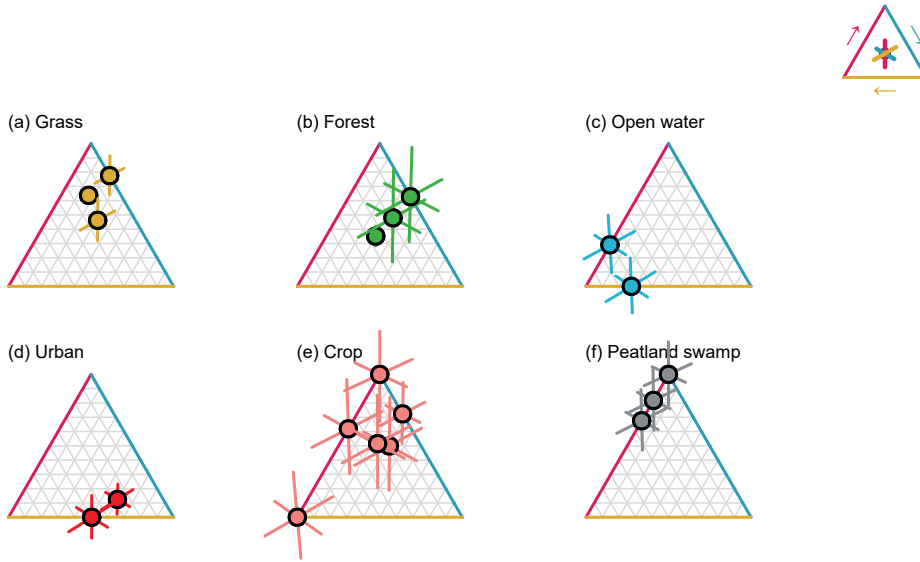


**Figure 5.7:** Uncertainty analysis per site categorized per land cover type at a daily timescale. The uncertainty bar is the standard deviation calculated for the given number of years of data availability. For these calculations the GR1 dataset acted as the reference. The inset on the top-right shows which uncertainty bar belongs to which axis.

reference. Given the uncertainty, there is a clear distribution of the land cover types within the triangle.

Figure 5.8 provides a synthesis of the results per land cover type. Here, the individual site-level is now disregarded and the input data from all sites belonging to a land cover type are merged for the regression analysis. This results in more data and thus less uncertainty of the position of the point (not shown). The resulting distinct placement of the six land cover types within the triangle, taking into account the uncertainty, indicates that evaporation drivers are sensitive to land cover type. These drivers can be grouped into three categories, namely energy availability, water availability and exchange efficiency. The terrestrial surfaces covered with short vegetation, i.e. grass and crop, are found in the top part of the triangle (energy availability  $> 50\%$ ), which indicates the importance of energy availability as the driver of evaporation over these surfaces. Additionally, peatland swamp is found in the same region within the triangle, indicating that the dynamics of evaporation can be explained by similar drivers as to grass and crop, despite the vegetated surface being inundated. The largest relative contribution to explaining the dynamics of evaporation from a forest surface is by water availability (50%), but also energy availability (33%) is an important driver. Water availability and exchange efficiency are contributing almost the same amount ( $\sim 40\%$ ) in explaining the dynamics of urban evaporation. Open water

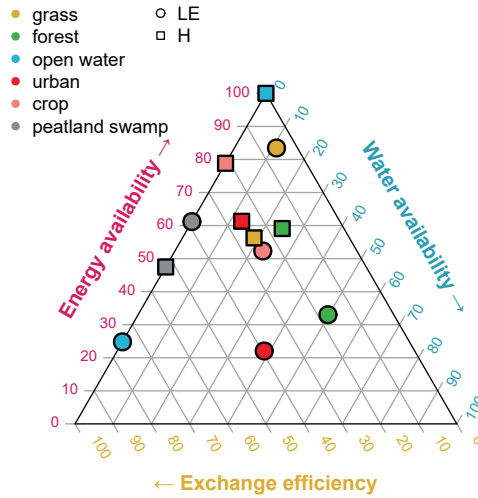


**Figure 5.8:** Synthesis of the drivers of latent heat flux (circles) and sensible heat flux (squares) per land cover type at a daily timescale. The data of all sites are merged per land cover type.

evaporation is mostly driven by exchange efficiency (75 %). The remainder of the dynamics of open water evaporation can be attributed to the energy availability category. The synthesis of the results for  $H$  emphasizes the difference with evaporation. The clustering of all sites, independent of their land cover type, in the top corner indicates that  $H$  is less sensitive to land cover type than evaporation. Interestingly, the difference between the controls for latent and sensible heat fluxes is largest for the land cover types with the smallest potential for biological control (i.e. open water and urban).

The warm season of 2018 was chosen as a case study for a direct comparison of sites under the same meteorological conditions and to study their behaviour during a warm and dry season (see Fig. 5.9). Data of three sites, i.e. GR1, GR2 and FO1 were available during that year. The summer of 2018 was the hottest in the Netherlands since 1706, with an average temperature of 18.9 °C (KNMI, 2018), where the climatological average (i.e. reference period 1991–2020) summer temperature is 17.5 °C. Additionally, it was a very dry summer with only 105 mm of precipitation, whilst the average precipitation over a summer is 240 mm. Given these conditions it can be seen that for evaporation site FO1 shifts mainly on the water availability axis relative to its yearly average position. This indicates that the site becomes more sensitive to water availability as a driver of evaporation. The terrain around FO1 is relatively hilly (i.e. ~10 m), with parts where the groundwater is shallower and trees are rooting shallower as well. When the groundwater starts to drop, the trees will soon be unable to reach it, thereby reducing evaporation. In the case of both GR sites the main shift occurs over the energy availability and exchange efficiency axis,

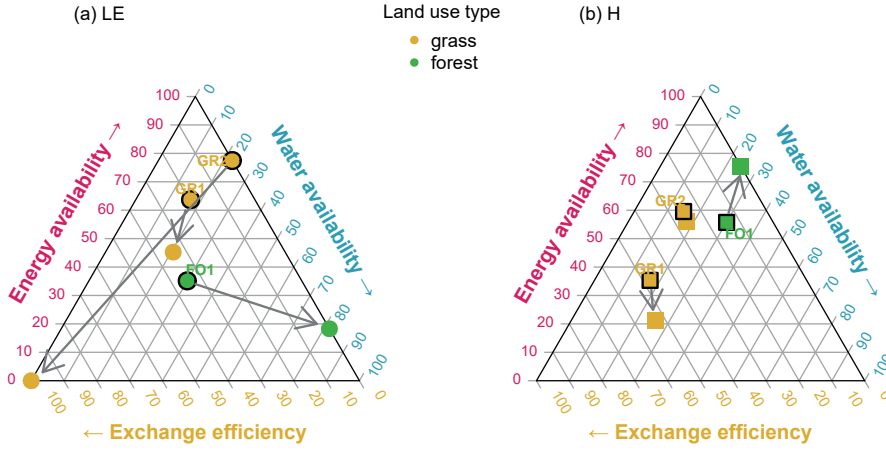


**Figure 5.9:** Direct comparison of three sites during the drought of 2018 at a daily timescale. The black-rimmed symbols represent the position when all years are included, while the symbols without black represent the warm season 2018. The arrows indicate the shift of the symbol from the yearly average position to the position in 2018. The analysis was performed for both  $LE$  (a) and  $H$  (b).

while there is hardly any change in the relative contribution of water availability. Both GR1 and GR2 have shallow groundwater levels. Water availability therefore seems to not be limiting evaporation even during a very dry year. For  $H$  the shifts are less strong during this dry year, especially site GR2 hardly shifts. GR1 mainly shifts downward over the energy availability axis, while FO1 shifts upward on the energy availability axis.

## 5.5 Discussion

Traditionally, evaporation has been defined in terms of energy- and water-limited regimes (Budyko, 1974; Koster et al., 2009; Teuling et al., 2009; Seneviratne et al., 2010; Denissen et al., 2020). This concept also forms the basis of the widely-used Budyko framework. However, studies over inland water bodies have already suggested the existence of a third type of evaporation limitation, namely exchange efficiency-limitation (Granger and Hedstrom, 2011; Lobos-Roco et al., 2021; Jansen et al., 2022). Our study, in which a direct comparison of EC measurement sites above different land cover types was performed, supports the existence of a three-dimensional system. We found that evaporation can be limited by energy availability, water availability or exchange efficiency. Therefore, we argue that the widely adopted two-dimensional system of energy and water-limitation

is a simplification of a system which is actually three-dimensional. The idea of a three-dimensional limitation system is not new as we can see the analogy with the concept of a fire triangle where the elements heat, fuel and oxygen determine the conditions under which a fire can exist or not (see Fig. 5.10). If one of these elements is absent, there will be no fire. Similar to the concept of the fire triangle, the position of a site with a certain land cover type in the ‘evaporation triangle’ identifies whether the system is (mainly) limited by energy availability, water availability or exchange efficiency. Interestingly, this study shows that these regimes can co-exist within a relatively small and climatologically homogeneous region.

At both the daily and midday timescales, exchange efficiency-limitation was found to be strongest for the inland water body sites. Evaporation from this type of land cover is not directly responding to changes in incoming global energy because of its large heat capacity, it rather responds more directly to the atmospheric demand. There are also other types of land cover that are confronted with exchange efficiency-limitation, albeit to a lesser extent. This is for instance the case for urban environments with fast impermeable surfaces, where the largest fraction of the evaporation dynamics can be explained by water availability ( $\sim 55\%$ ), but the other fraction can mainly be explained by exchange efficiency. The variance in evaporation from peatland swamps at both daily and midday timescales can be explained to a lesser extent by exchange efficiency and to a greater extent by energy availability compared to open water bodies, while both are covered by surface water. This might be explained by the stable and moist layer of air that can be created by the layer of vegetation, thereby reducing the coupling between the water layer and the atmosphere and thus decreasing the importance of exchange efficiency in explaining the evaporation dynamics. At the same time, the vascular vegetation in peatland swamps can still regulate their transpiration through their stomata which can be more related to energy availability. On the contrary, it could also be argued that the increased roughness of the vegetation in peatland swamps compared to open water would lead to a stronger coupling (Jarvis and McNaughton, 1986), which would actually mean a decreased control of evaporation by energy availability and rather a stronger control by changes in stomatal resistance. However, this effect was not shown in this study. The data-driven analysis in this study relies solely on standard meteorological variables, without explicitly considering the active role of vegetation. It can therefore be seen as a statistical analysis of the correlation between evaporation and the meteorological drivers, rather than a causal description of the processes that link the meteorological drivers to evaporation through for instance the role of vegetation.

Based on Figure 5.5a the relative contribution of the individual variables to explain the dynamics of evaporation was specified in Figure 5.11. We find that, especially for the sites with short vegetation, energy availability is important in explaining the dynamics of evaporation and in particular global radiation is the main contributor. This is in agreement with other studies over grasslands (Makkink, 1957; Teuling et al., 2010). Our results



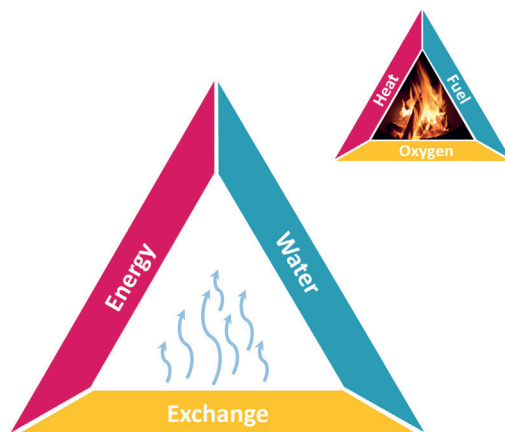


**Figure 5.10:** Conceptual illustration of the evaporation triangle. This concept is similar to the fire triangle (picture of the fire by Janneke Remmers).

showed that VPD cannot explain any variance of forest evaporation at sites FO2 and FO3. In the dry year of 2018 our analysis even showed that VPD could not be appointed as driver at any of the three forest sites (see Fig. C1 in Appendix C), which is in direct contrast to what was found by Moors (2012) and Lansu et al. (2020). They found VPD to be the main driver of forest evaporation during dry and warm summer conditions. For both grassland sites GR1 and GR2 VPD explains a larger portion during the dry year of 2018 compared to when all available years are included in the regression analysis. However, the result for Veenkampen in 2018 is more uncertain as only 18 data points were left in the dataset. In general, we found a limited role for VPD as driver for evaporation when all years were included. Although there is variability in the input signal of VPD, and thus it potentially could be a driver according to our definition, the limited portion of explained variance by VPD for the different sites may be a limitation of the statistical data approach we used.

As was already noticed in Section 5.4.2, CR4 seems to be an outlier as it shows that solely wind speed drives evaporation at that site. This outlier position relative to the other crop sites could be due to a lack of data in the dataset of CR4 to distinguish between the diurnal cycle of radiation and wind speed. The other crop sites are mostly driven by the energy variables, in particular global radiation, while wind speed is contributing less. A surprising result is found for WA2 where Prec10 partly explains open water evaporation at this site. Since it is a water body, it is impossible from a physical point of view that water availability in any way would be of importance in driving open water evaporation. This indicates a limitation to our data-driven approach combined with the number of data points available to capture and explain the diurnal dynamics. The fact that Prec3 is partly driving evaporation at urban sites is in agreement with what was found in literature

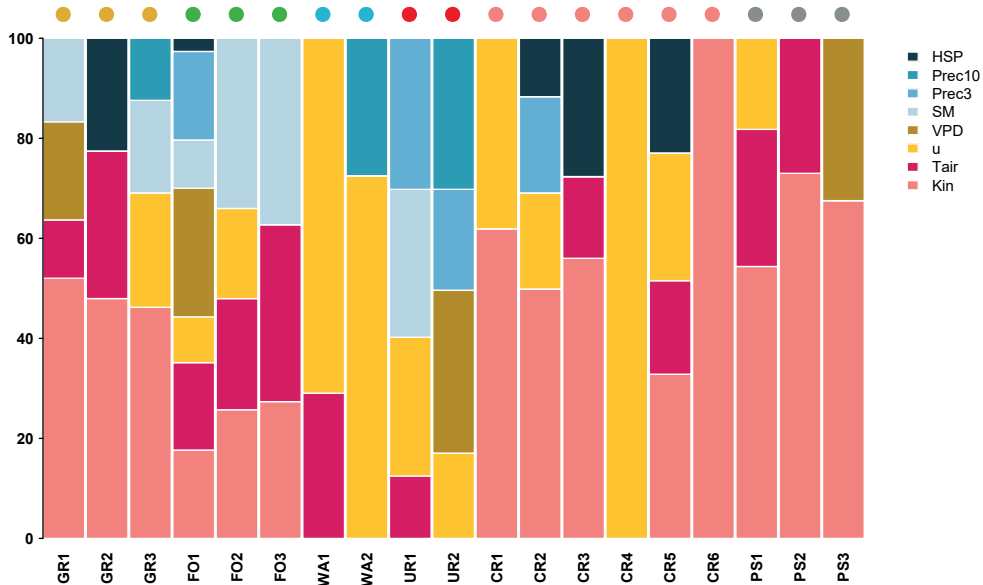


**Figure 5.11:** Relative contribution of the individual variables in explaining the dynamics of latent heat flux per site at a daily timescale. The coloured dots above the bars indicate the land cover type.

(Jacobs et al., 2015; Jongen et al., 2022). Our results also show the importance of wind speed and VPD at the urban sites, which could be explained by the response of evaporation to the atmospheric demand when the streets are wet after precipitation. It should be noted that the EC footprint of urban sites reflects the entire urban landscape that exists of a mosaic of different surfaces. Depending on the ratio of impervious and vegetated surfaces a shift in the drivers may be visible, where evaporation dynamics from ‘greener’ urban areas could be expected to behave more similar to evaporation from vegetated surfaces in which energy availability plays a more important role (Loridan and Grimmond, 2012; Jacobs et al., 2015).

Our analysis showed that different drivers explain  $H$  compared to  $LE$ . This suggests that the land-atmosphere interface plays an active role in the shedding of  $H$ . Sensible heat is often assumed to follow the latent heat flux because turbulent eddies transport both water vapour and heat, but this is not reflected in our results. Rather, we might argue the opposite to occur if we look at it from a plant physiological point of view:  $LE$  might actually be the resultant of the coping mechanism of how plants deal with heat and moisture stress by regulating their leaf temperature through transpiration (Gates, 1968;

Lin et al., 2017). Thus, our understanding of the drivers of  $H$  and the interplay with the active land surface and vegetation are still not complete.

The warm season months were analysed in this study. This means that it is not known to what extent these results might be representative for a whole year. The winter season is accompanied by more precipitation and lower temperatures, which might shift the position of sites on the evaporation triangle. Energy availability could become a more prominent limitation for evaporation in that season for the vegetated terrestrial sites. The release of heat during winter that was stored during summer in open water bodies and in urban areas, albeit differently, provides an additional energy source for evaporation. It was not studied if and how this might shift the location of the open water and urban sites within the daily and midday evaporation triangles, but it could be argued that energy availability would explain less of the variance of evaporation during winter compared to the vegetated terrestrial sites because more energy is available and thus not limiting evaporation.

The length of the datasets of the measurement sites included in this study vary. As the uncertainty bars in Fig 5.7 illustrate, data of multiple warm seasons leads to more confidence on the position of a site within the suggested three-dimensional evaporation limitation diagram. If only one warm season of data is available, the effect of the meteorological conditions will likely play a larger role on the positioning within the evaporation triangle compared to a multi-year dataset. This was for instance visible in the case study of the extremely dry and warm year 2018 (see Fig. 5.9) where a shift of the position within the triangle occurs. Ideally, a multi-year dataset and multiple sites per land cover type are used to determine the evaporation regime of that land cover type.

This study was performed in the setting of the Netherlands, which is a country with strong water and land cover management. In general, sufficient water is supplied from upstream catchments to the delta of the Netherlands. The water is mostly drained as much as possible in this lowland deltaic setting. Other pieces of land are kept artificially wet by inundating the area, which is for example the case for the peatland swamps. There is a general trend towards retaining more water for periods of drought in the warm season. These artificial settings are the boundary conditions in which this study was performed. The trivial hypothesis in this generally wet lowland country with a humid climate would be that water availability will not be a limiting factor for evaporation from terrestrial vegetated surfaces, but rather that these systems would be energy-limited. However, this study has shown that the water availability axis within the three-dimensional evaporation limitation concept does play a role in the urban, crop, grass and forest sites. Former urban studies have provided a clear indication for this by showing water availability to be a key factor in determining the timing and decay of evaporation rates around a rainfall event (Jacobs et al., 2015; Jongen et al., 2022). In forest systems the role of water availability is not trivial because of the role and contribution of interception evaporation during wet conditions to the total daily evaporation (Bosveld and Bouten, 2003; van Dijk et al., 2015).

Through observations it has been shown that transpiration reduces to zero during wet conditions, whereas interception will become the largest contributor to total evaporation during wet conditions and can continue to be high at night (Moors, 2012; Wang-Erlandsson et al., 2014). This in its turn strongly affects the sensible heat flux, which can even become negative and becoming the main energy source for evaporation (De Bruin et al., 1989). The temporal development of the different evaporation fluxes in alternating wet and dry conditions argues for including water availability as a factor to explain the dynamics of total forest evaporation.

Unfortunately, using the EC method to measure latent and sensible heat fluxes comes with limitations. One of the best known limitations of the EC method is the problem with a non-closed surface energy balance (SEB). Four topics have been identified to likely contribute to the SEB closure problem, namely instrumental errors, data processing errors, additional sources of energy and sub-mesoscale transport processes (Mauder et al., 2020). It has been shown in several experiments that especially in forests heat storage within the canopy acts as additional energy source or sink, thereby contributing to the SEB closure. In short vegetations this non-closure will be less prominent. Furthermore, the released heat stored in urban areas and open water bodies similarly act as an additional source of energy. The neglected effects and uncertainties of the SEB have been shown to be most significant during the transitions of day and night, which would therefore not be as strong for the daily and midday analyses.

## 5.6 Conclusions

In this study we analysed the dynamics of the latent and sensible heat fluxes of 19 flux tower sites in the Netherlands, covering six land cover types located within the same climatic zone. The results of the regression analysis performed over the warm season showed that daily and midday evaporation can be mainly limited by energy availability, water availability or exchange efficiency depending on the land cover type. The added value of explicitly including exchange efficiency in explaining the evaporation process, suggests that we could shift from the commonly used two-dimensional system, in which only energy and water-limitation are considered, to a three-dimensional evaporation limitation concept. Merging of the data per land cover type showed that evaporation from grassland, peatland swamp and cropland can be categorized as mainly energy-limited. Additionally, exchange efficiency-limitation plays a role in describing the dynamics of evaporation from wet peatland swamps, while exchange efficiency and water availability equally contribute to explaining the remainder of crop evaporation dynamics. The dynamics of forest evaporation can be explained for the largest part by water availability. Unexpectedly, we found exchange efficiency, which includes VPD, to contribute to a minor degree only. Open water evaporation is almost entirely explained by exchange efficiency and for the remaining

minor part by energy availability. This is in agreement with the findings in previous studies. Urban evaporation is equally explained by water availability and exchange efficiency, while energy availability contributes to a lesser extent. Given the number of years included in the datasets of individual sites and given the meteorological conditions during that period, the relative contributions of the three limitation categories can shift to some extent. However, the results of the merged data per land cover type provide confidence to the finding that land cover type plays a role in determining the drivers of daily and midday evaporation during the warm season, while  $H$  is found to be less sensitive to land cover type. The results of this study can contribute to a better understanding of the dynamics of evaporation over different land cover types and may help to optimise, and potentially simplify, models to predict evaporation.





# Chapter 6

## Synthesis



## 6.1 Introduction

Surface evaporation is a crucial component in the land surface water balance. Therefore, accurate estimates of evaporation rates are of vital importance for effective water management. This becomes even more critical with the expected intensification of the hydrological cycle as a consequence of global warming. However, evaporation remains one of the most difficult hydrological processes to understand and experimentally measure. Monitoring and forecasting of evaporation has seen rapid development over the recent decades driven by both technological and scientific developments. Traditionally, most studies have been dedicated to analysing terrestrial surface evaporation, while evaporation from water bodies has lagged behind.

The understanding of evaporation dynamics and identifying the environmental variables that are able to explain these dynamics formed the central theme of this thesis. The first part of this thesis focussed on the analysis of existing models to estimate evaporation. Next, eddy covariance (EC) flux tower observations were used to statistically derive the main drivers of open water evaporation, as well as terrestrial evaporation from five other land cover types. These land cover types included: forest, grassland, urban areas, cropland, and peatland swamp. In this final chapter, the main findings of my thesis will be discussed. Furthermore, I will discuss the potential of actual evaporation, and reflect and look ahead based on the key findings.

## 6.2 Main findings

### 6.2.1 Model (dis)agreement to estimate evaporation

A common way to infer evaporation rates is through parameterization of the relation between evaporation and other environmental variables. Using six commonly used evaporation models forced by different drivers, the (dis)agreement among the models was characterized in Chapter 3. The analysis on the model (dis)agreement was performed for a large lowland reservoir, namely Lake IJssel in the Netherlands, at various temporal scales ranging from hourly to decadal periods.

The models generally disagreed with each other at the hourly timescale, which was reflected in the simulated diurnal cycles. The most profound differences were found between the radiation-based models, i.e. Penman (1948), De Bruin and Keijman (1979), and Makkink (1957) and the models based on different drivers, i.e. the temperature-based Hargreaves (1975) model, the wind-based Granger and Hedstrom (2011) model, and the physical-oriented model FLake (Mironov, 2008). We found that at longer timescales, i.e. yearly and decadal, the models tended to agree better, which was to be expected considering that evaporation is ultimately constrained by the energy input in the system and the transport of water vapour. However, the projected evaporation trends for the future period

2019–2100, as simulated with projected meteorological variables resulting from the regional climate model RACMO, differed substantially. The evaporation trends for this future period were projected to be positive for all models, although the extent of the positive trend was greater (Penman, De Bruin-Keijman, Makkink, and Hargreaves) or lesser (i.e. Granger–Hedstrom and FLake). We showed that the simulated water losses of the Lake IJssel region due to evaporation differed between the models. The simulated water losses ranged from 4 mm (Granger-Hedstrom) to 94 mm (Penman). These variations can be attributed to the different assumptions, and connected parameterizations, on which the models are based. Generally, the sources of uncertainty related to hydrological projections involve uncertainties related with the model structure, forcing data and model parameters (Melsen et al., 2018). Our results highlight that the choice of a model should be appropriate for the land cover system of interest and the aim of the modeller, so as to ensure that the employed model is right for the right reason. Additionally, correctly including the impact of different drivers becomes especially crucial when working towards long-term future projections.

### 6.2.2 Drivers of surface evaporation

#### *Open water evaporation*

Direct observations of actual evaporation are essential to validate model estimates of evaporation. Chapter 4 is based on EC observations that we have measured over two summer periods at two locations along the border of Lake IJssel (1100 km<sup>2</sup>). These observations were used to analyse the open water evaporation ( $E_{\text{water}}$ ) dynamics and to infer its principal drivers.  $E_{\text{water}}$  did not show a strong diurnal cycle, but was rather constant throughout the day and night. This resembled the diurnal cycle simulated by the FLake and Granger-Hedstrom models that were studied in Chapter 3.

Based on the EC observations, data-driven models were developed for both measurement locations, Stavoren and Trintelhaven, to explore the most important environmental variables involved in explaining the variance of  $E_{\text{water}}$ . A combination of wind speed and the vertical vapour pressure gradient was found to best explain the dynamics of  $E_{\text{water}}$  at the hourly timescale. In other words, exchange efficiency controls the exchange processes of energy and water between the water surface and the atmosphere. This finding is in agreement with the well-established Dalton model that is often used for  $E_{\text{water}}$  estimations. At the daily timescale, the same principal drivers were found for location Trintelhaven. In Stavoren, a combination of wind speed and water temperature explained most of the variance. Supported by the satisfactory model validation, the results of Chapter 4 showed that simple data-driven models, consisting of only two explanatory variables, provide useful estimations of hourly and daily  $E_{\text{water}}$ . The use of simple models requires the correct principal drivers to be included in the model. It was shown, for instance, that the simple evaporation model of Makkink (1957), was not able to explain the observed

daily  $E_{\text{water}}$ . Despite this, Makkink's model, with a simple correction factor for open water evaporation, is currently used in operational hydrological models in the Netherlands. Chapter 4 highlights the potential of using simple statistical models to provide a direct indication of the most relevant variables to correctly estimate  $E_{\text{water}}$ .

### *Land evaporation*

Differences in surface characteristics between water bodies and terrestrial surfaces, e.g. heat storage capacity, capacity of solar radiation to penetrate the surface, and albedo, result in a different partitioning of solar energy into latent and sensible heat fluxes at the surface-atmosphere interface. In Chapter 5, a systematic comparison of the drivers of latent and sensible heat fluxes over six dominant land cover types in the Netherlands (i.e. grass, forest, open water, urban, crop, peatland swamp) was performed. To this end, available historical EC observations for 19 sites in the Netherlands were gathered. Based on regression analyses, the drivers were expressed along three axes: energy availability, water availability and exchange efficiency. Within this three-dimensional system, clusters of sites belonging to the same land cover type were found. This indicated that land cover can partly explain the variance of the daily and midday latent heat flux. We also found that the midday and daily sensible heat flux are less sensitive to land cover type. The novelty of the analysis shown in Chapter 5 is the systematic comparison of many flux sites located within the same region while covering different land cover types. This provided the opportunity to study the role of land cover on the drivers of the latent heat flux and to present this direct comparison in a three-dimensional system. The relation found between land cover type and drivers can be used to improve evaporation models.

## 6.3 The potential of actual evaporation

Actual evaporation is controlled by the tightly coupled land-atmosphere system. Studying actual evaporation dynamics can therefore inform us on land-atmosphere interactions, by analyzing how changes in the land surface (e.g. land cover, soil moisture conditions, vegetation type) affect the actual evaporation dynamics in a coupled system. So, actual evaporation integrates and reflects the effect of the active role of the land surface, which is not the case with potential evaporation. Observations of actual evaporation are therefore key to keep advancing our understanding of its role in the coupled land-atmosphere system and its associated processes and feedbacks.

Observations of actual evaporation over different land cover types allow us to study the difference in drivers over these surfaces, as shown in Chapter 5. Through our systematic data-driven analysis we were able to show that land cover type can explain part of the evaporation dynamics. We found a large difference in dynamics and drivers that exists between evaporation from an open water body and terrestrial surfaces. Only through analysis of the dynamics of actual evaporation, there is the potential to correctly include

the evaporation process in hydrological models. We have shown that using an observation-based approach can lead to well-defined simple evaporation models, requiring little input data.

There is a variety of purposes for which actual evaporation data can be used. For instance, anomalies of actual evaporation observations can be used for studying the role of evaporation in the onset and evolution of droughts as well as heatwaves (Teuling et al., 2010; Miralles et al., 2019; Senay et al., 2020). Furthermore, observations of actual evaporation can be used to validate output from climate and land-atmosphere models, as well as to study the water balance of catchments with the purpose of optimising water management, irrigation schemes, and construction of reservoirs (Wannasin et al., 2021).

## 6.4 Lessons learned and recommendations

### 6.4.1 Eddy covariance: challenges and opportunities

The eddy covariance (EC) technique is currently considered one of the best techniques to measure evaporation through continuous high-frequency measurements of wind speed, humidity and air temperature. EC has been widely applied to evaluate and understand water and energy fluxes at the ecosystem scale. Initiatives have been taken to bring together time series of individual flux towers into global (e.g. FLUXNET) and regional (e.g. AmeriFlux, AsiaFlux, ICOS) EC networks (Baldocchi et al., 2001; AmeriFlux, 2023; AsiaFlux, 2023; ICOS, 2023).

The continuously growing flux networks provide the opportunity to compare flux sites, to study the surface energy balance response to land cover changes (Bright et al., 2017; Chen et al., 2018; Yuan et al., 2021) and extreme events (Teuling et al., 2010; Teuling et al., 2013; Lansu et al., 2020), as well as to identify trends as a result of climate change (Teuling et al., 2009; Jung et al., 2010; Williams et al., 2012; Baldocchi, 2020). However, the locations of the sites in the global network FLUXNET are biased (see Chapter 5), with a tendency towards carbon-rich ecosystems in wealthier countries. This limits the statistical power to explain spatiotemporal changes of the fluxes over heterogeneous landscapes, even more so because generally single towers are employed. To reduce this limitation, Cunliffe et al. (2022) have suggested to employ clusters of lower-cost EC systems, as opposed to the more conventional systems, to quantify spatial variability and estimate biases and uncertainties at the landscape-scale (i.e. scales larger than the single flux footprint). These lower-cost type EC systems can also be employed to reduce the biased spatial sampling of fluxes in existing EC networks. Based on the results of Cunliffe et al. (2022) and on the findings in Chapter 5, I would like to argue that great benefits can be found in the use of all EC observations available in a region (though this most likely will be limited to wealthier countries), not only the sites that are contributing to global or regional databases. In Chapter 5, I have shown that a wealth of information about spatial

variability of evaporation can be retrieved from the numerous historical flux sites that are locally available.

One of the most well-known challenges concerning the use of experimental data, e.g. EC data, is the surface energy balance closure problem (Foken and Oncley, 1995). The energy balance closure problem refers to the phenomenon that the measured latent and sensible heat fluxes are smaller than expected relative to estimates of available energy, which results in non-closure of the energy balance (Foken et al., 2012). The root of this problem can be found in (i) sampling errors: the mismatch in scales and volumes that are measured, (ii) measurement errors and (iii) errors due to additional energy sources that can be related to large-scale turbulent transport or to heat storage (Foken, 2008; Mauder et al., 2020; Liu et al., 2011b). As a consequence of the energy balance closure problem, the assumption of perfect energy budget closure in commonly used numerical land-surface models is not met (Mauder et al., 2020), which may lead to incorrect model predictions. This energy balance closure problem has been known for decades (Foken, 2008) and since then several correction methods have been suggested, e.g. partitioning of the energy balance residues while preserving the Bowen ratio (Mauder et al., 2013), or correction for increased sensible heat fluxes accompanying large scale convective transport by assigning most of the energy residues to the sensible heat flux (Charuchittipan et al., 2014).

Despite the challenge of the energy balance closure problem, the effect of potentially underestimated latent and sensible heat fluxes on the results of our regression analyses is considered to be relatively small. The effect of heat storage, acting as an additional energy source in the lake and urban environments, will likely have a larger effect on the resulting estimates of latent and sensible heat fluxes and requires further analysis. Yet, I expect that the direct linkage of environmental variables to evaporation dynamics through regression analysis still provides a strong idea of the most important drivers. This is supported by the differentiation found in drivers of evaporation between different land cover types (see Chapter 5).

To maximize and upscale the potential information contained in flux networks, EC data can be extrapolated using satellite observations in combination with evaporation models (Bastiaanssen et al., 1998; Running et al., 1999; Su, 2002; Xiao et al., 2011; Jiménez et al., 2018; Jung et al., 2019). These can even be simple regression models comparable to those derived in Chapter 4. The integrated evaporation product could serve as input data as well as ground-truth data for land-atmosphere models to estimate evaporation trends and temporal variability under changing environmental conditions.

#### **6.4.2 The active role of the land surface**

In Chapter 5 it was shown that land cover can explain a part of the evaporation dynamics through the surface energy partitioning. Not only land cover, but also other surface characteristics are found to be linked to the energy partitioning, such as vegetation type,

soil moisture, and the transparency and heat storage capacity of the land surface or water body (Grimmond and Oke, 1999; Wilson et al., 2000; Seneviratne et al., 2010; Wang et al., 2014a; Vilà-Guerau de Arellano et al., 2023). Through this link with the energy partitioning, these surface characteristics play an active role in determining the rate and dynamics of the surface fluxes. In turn, the surface fluxes will affect some of the surface characteristics.

Under dry conditions with limited soil moisture, evaporation will decrease, while more energy will be shed towards the sensible heat flux, thereby controlling the near-surface temperature and thus impacting atmospheric conditions (Feldman et al., 2019; Seneviratne et al., 2010). Therefore, in a water-limited regime the soil moisture-evaporation relationship should be well represented in land-atmosphere models to estimate water and energy exchange. A link between vegetation and energy partitioning has been found, although the exact effect under different environmental conditions is not well understood (Teuling et al., 2010; Hoek van Dijke et al., 2020; Vilà-Guerau de Arellano et al., 2023). Williams et al. (2012) found that the degree of vegetation control on the surface fluxes depends on climate and vegetation type, linked to the strong stomatal control. Williams et al. (2020) found that an improved set of soil and stomatal parameters will better capture the spatial heterogeneity of evaporation and sensible heat fluxes. This spatial heterogeneity would enhance convective atmospheric conditions and thus the formation of clouds (McPherson, 2007). Therefore, local interactions between vegetation and clouds through the latent and sensible heat fluxes and partitioning of water and energy should be represented in large-scale weather and climate models (Vilà-Guerau de Arellano et al., 2023). Explicit representation of the spatial variability of surface characteristics and their interactions with surface fluxes could reduce the uncertainty of estimated spatial heterogeneity of the surface fluxes and the development of clouds.

### 6.4.3 Water availability in a changing climate

Climate change affects the amount and distribution of water availability in space and time through changes in evaporation and precipitation (Seneviratne et al., 2006; Teuling et al., 2019; Konapala et al., 2020). Limited access to water resources will impact society, agriculture and ecosystems. Changes in both the mean and variability of evaporation, which will affect precipitation through regional moisture recycling (Van der Ent et al., 2010), may lead to droughts and heatwaves in one region, while other regions will become more vulnerable to floods. Several global model studies project that wet areas are likely to become wetter, while dry areas are likely to become even drier (Held and Soden, 2006; Durack et al., 2012; Liu and Allan, 2013). However, most of the studies that have supported this paradigm are based on oceanic evidence. Greve et al. (2014) have shown that the paradigm therefore may be true over oceans, but that it is an oversimplification for land surfaces because the complexity of the system and the hydroclimatological conditions over

land are not considered. This implies that strong regional differences of water availability in response to climate change may occur.

For policy and operational water management it will be important to know what measures can be taken to reduce the impact of changes in mean and seasonal variations of water availability in a region. In the context of the Netherlands, there are several measures that could be taken to alleviate negative consequences of periods of too little or too much water. On the one hand the deltaic setting sometimes leads to high water levels during winter which requires quick discharge of water. However, water discharged during winter may actually be needed during the warm season, when evaporation rates and water demands are high, and should therefore ideally have been retained during the winter season. This means that some flexibility in the water storage system is required. One way to achieve this would be to adapt the water level of the biggest water reservoir in the country, namely Lake IJssel. By increasing the water levels during the winter period a buffer is created for the summer period, when evaporation rates are higher. The lake is supplied with water from the river IJssel, which is a tributary of the river Rhine. Therefore, to optimally manage the water levels of the lake an adequate forecasting system of the discharge in the area upstream of the delta would be necessary, in combination with adequate distribution of the water from the main rivers. Hurkmans et al. (2022) have attempted to increase the forecast skill of Rhine river discharge by optimizing the land surface parameters and initial conditions of several forecast systems. The skill ranges from one up to four months during spring, when discharge is driven by snow melt, and decreases to one to two months during the summer, when rainfall dominates discharge. The skill of discharge forecasts remains high for a longer time period compared to other components of the water balance of the lake, i.e. precipitation (Lucatero et al., 2018) and open water evaporation. Therefore, it may help water managers to include discharge forecasts to base their decisions on with respect to lake water level adjustments. Accurate discharge forecasts would be especially useful prior to the onset of a period of drought (accompanied with high open water evaporation rates), when a large part of the country depends on water from the lake.

Other measures that can be taken to increase water availability is by reducing evaporation. In an agricultural setting, this could be achieved by optimizing irrigation management. Irrigation during the night and use of drip irrigation reduces local water loss through evaporation (Yang et al., 2020; Pool et al., 2021). Furthermore, to reduce forest evaporation a radical option could be to convert coniferous forest to deciduous forest. On a yearly base, Swank and Douglass (1974) found that coniferous trees transpire more water as they continue to transpire during the non-growing season of deciduous trees. However, Sun et al. (2008) did not find a difference in evaporation between the two types of forest based on their observations. Personally, I would advocate to include the potential impact on biodiversity and the vitality of the ecosystem in the trade-off whether a coniferous or mixed forest should be converted to deciduous trees only.

Besides attempts to reduce evaporation, other measures can be taken to increase water availability such as the decrease of water consumption or the increase of storage capacity. The latter can for instance be achieved by creating storage basins in an urban setting, or increase the capacity of lakes, but also by investing in vital soils that can retain more water. Furthermore, measures could be taken to reduce the impact of drinking water abstractions on water availability. Van Engelenburg (2020) has suggested some measures to reduce this impact on the Veluwe area in the Netherlands. These measures include the redistribution of drinking water abstraction locations and use of managed aquifer recharge.

#### 6.4.4 The future of evaporation modelling

Nowadays, there are numerous evaporation models available. These models all use a different parameterization of the evaporation process and are thus sensitive to different environmental variables. Therefore, depending on the choice for a particular model the result can be substantially different, as was shown in Chapter 3. This questions whether existing models perform well under all conditions and even more so, it questions if the best evaporation model has yet been developed or if there is still a gap in the landscape of existing models that could be filled.

Only if the impact of different drivers is included correctly in an evaporation model, will we be able to correctly estimate evaporation. This requires knowledge of the considered land cover systems and it requires the acknowledgement of the differences between systems, e.g. the difference between a water surface and a land surface. In this thesis, I looked at the differences between land cover systems rather than the similarities. Comparison of evaporation observations of sites located relatively close to each other within the same climate zone, but representing different land cover systems, provided the opportunity to link evaporation differences between sites directly to land cover. This would be less feasible based on data from FLUXNET sites only, as these are located at larger distances from each other and do not cover most land cover types. Differences found between FLUXNET sites would therefore more likely be explained by climate, rather than by differences between the systems.

In Chapter 5, the comparison of a large number of sites has revealed that land cover type can partly explain evaporation dynamics. It clearly showed that different drivers underlie evaporation from different land cover types. For instance, it was found that evaporation from urban sites is closely linked to water availability, whereas open water evaporation can largely be explained by exchange efficiency. Therefore, the performance of an evaporation model would be low if the model includes drivers which do not explain the evaporation dynamics at the intended modelled timescale. In case of an urban environment or a lake for example, it therefore makes sense that a model that is mainly driven by energy availability, like Penman's model (Penman, 1948), would not perform well. So, although Penman's model is widely used and in many studies has proved to work well, the results



of Chapter 4 have shown that it does not perform well in a land cover type that is not mainly energy-driven, namely a water body. In that case, we showed that simple empirical models perform better.

A distinction can be made between statistical and physically-based models. In Chapters 4 and 5 regression analyses were performed to develop simple evaporation models. There are some limitations to such an observation-based statistical approach. For instance, such an approach does not necessarily prove causal relationships between correlated variables within the coupled land-atmosphere system. Additionally, it remains unknown if variables that have not been observed might additionally explain causal relationships. The lack of establishing causal relationships limits the use of regression models in a changing environment, e.g. climate and land cover changes, because it only captures the dynamics of the current conditions. Furthermore, bidirectional relations between variables cannot be fully explained through a statistical approach only (Orlowsky and Seneviratne, 2010; Teuling, 2018b; Miralles et al., 2019), and long time series are required to accurately determine extreme values. Despite these limitations, statistical models are able to capture patterns in the data and provide the most important explanatory variables, even when the underlying physical mechanisms are not fully understood. Furthermore, in physically-based models, empirical relations are also included (e.g. the wind function in Dalton's and Penman's model), and parameters need to be statistically estimated.

#### 6.4.5 Let water and soil direct our decisions

Freshwater resources are found amongst others in lakes, rivers, wetlands, and aquifers. Freshwater is a valuable resource as it is one of the crucial foundations of all life on earth. However, it is a rare resource since only 2.5% of all water on earth is freshwater, of which the largest portion is even inaccessible to us because it is frozen or stored as soil moisture or deep groundwater. As a consequence, only a fraction (tenths of 1%) of all water on Earth is accessible to us, while an increasing population relies on it (Vörösmarty et al., 2005). Through climate change the pressure on water resources increases further. Some regions are faced with increasing water scarcity, potentially leading to conflicts, while other regions will see an increase of water excess (Gosling and Arnell, 2016). Besides the impact on people and society, ecosystems will also face detrimental effects of severe conditions of either water scarcity or water excess.

A question that arises, is how we deal with the management of water and its resources with the increasing extremes that we will be facing as a result of climate change. In a country like the Netherlands, where the deltaic setting already requires intensive water management and the high population density has already led to a meticulous spatial planning, we should ask ourselves from which perspective we make those plans. Currently, the Dutch government is advocating for an integral policy that is more directed by the water and the soil themselves (Rijksoverheid, 2022). Up till now, the focus of water management

in the Netherlands was targeted towards discharging water as quickly as possible. Now that extremes are occurring more frequently, a policy is required in which water can be discharged quickly in times of floods, but should be retained in times of drought. Healthy soils are crucial for the retention of water. As the government describes it: '*the land should transform from a colander to a sponge*'. With more water stored in the soil, more water will be available for extended periods of drought. There are also opportunities to store more water above the surface by increasing the capacity of reservoirs and river areas, but that will also increase open water evaporation, which we have shown in Chapter 4 to be substantial.

International initiatives such as Ecosystem Restoration Camps (ERC) (ERC, 2023) have lifted the principle of working in close connection with the soil and the water with the aim to revive ecosystem functions of degraded landscapes. The camps are used as living labs and they claim that their integral approach to restore degraded land has led to a positive effect on the water system and on local biodiversity. Instead of imposing measures on the land, the ERCs use the intrinsic vitality of the land to restore it. I think it would be very interesting to study if there would be any effects of ecosystem restoration on the local land-atmosphere interaction, on the surface temperature, on regional moisture recycling and on regional atmospheric circulation. Based on the initiative Justdiggitt, which is focusing on Sub-Saharan Africa, it was claimed that the effect of greening and the resulting increased water retention on the energy partitioning is mostly local (Van der Zaaij and Van 't Hof, 2022). The effect on regional climate remains uncertain.

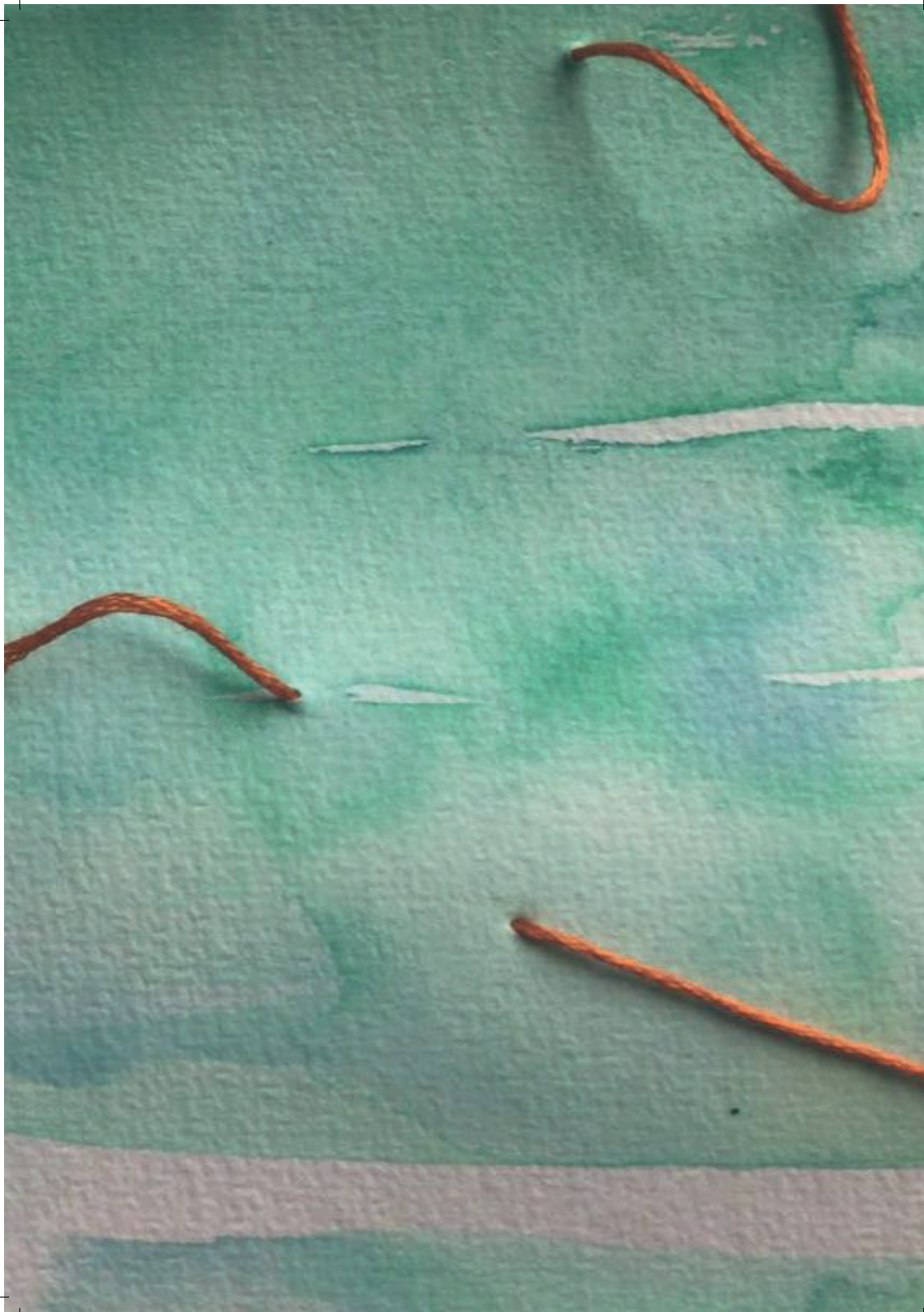
#### 6.4.6 Implication and advice for water management

In this section, I will focus on the water management situation in the Netherlands specifically. One of the main findings of this thesis that has direct implications for water management in the Netherlands is the distinct difference found in the dynamics of open water evaporation compared to terrestrial evaporation (see Chapter 5). Currently, Rijkswaterstaat uses the energy-driven Makkink equation, including a correction factor, to estimate open water evaporation in the Landelijk Hydrologisch Model (LHM). The LHM model is used for operational water level management of Lake IJssel. However, in Chapter 4 it was shown that open water evaporation at the hourly and daily timescale is driven by wind more than energy. As a result, Makkink's model was not able to correctly estimate open water evaporation at the daily timescale. Based on this information, I would recommend to implement a transport-driven model in the LHM to correctly estimate open water evaporation also at the smaller timescales. For this, the regression models developed in Chapter 4 could be used, or a similar model, such as the well-known Dalton model (Dalton, 1802). Implementing the correct parameterization of open water evaporation will be essential considering the projected increase of extreme hydrological conditions.

In Chapter 4, our observations have shown that evaporation is a large loss term in the water balance of Lake IJssel. When contemplating about potential solutions that can be taken to decrease water losses through open water evaporation we need to consider one of the main controls on open water evaporation, namely wind. One, maybe far-fetched, option to decrease wind speeds is planting trees along the dikes surrounding Lake IJssel. It would need to be studied if these trees would have any substantial effects on the open water evaporation rates on such a large water body. I could imagine that the effect would only be local and depending on atmospheric conditions. Another approach to break the wind might be obtained through installing wind turbines in the lake. Obviously, the effects of this on the total evaporation should first be studied, as well as other potential effects it might have on the ecosystem of the lake. Despite the focus on Lake IJssel in this section, I believe that the results from this thesis and recommendations given in this section can also be applied to other shallow inland water bodies. The deltaic setting of the Netherlands, however, poses extra challenges to the operational water management practice of Lake IJssel.

In the more elevated areas of the Netherlands, e.g. the Veluwe area and parts in the east and south of the Netherlands, groundwater levels are relatively deep (up to 20 meters in the Veluwe area). In the Veluwe area, where forest is the main land cover type, water availability for the trees is thus relatively limited. In Chapter 5, we found that energy and water availability are the main drivers of evaporation from the forest sites. Unlike the suggested measures for Lake IJssel, it seems more difficult to control or change the dynamics of evaporation from the forested area in the Veluwe. However, the longer-term mean evaporation, and therefore the recharge of the area, might be changed. This could be achieved by land cover conversion from coniferous to deciduous trees or to other vegetation that transpires less than trees, allowing the recharge to increase. Plant factors affecting the transpiration rate include the biomass, stand age, height, and leaf structure (Jaramillo et al., 2018; Teuling, 2018a; Teuling and Hoek van Dijke, 2020). The long-term time series of evaporation in Castricum have shown a consistent and continuous decline in average recharge with increases of tree height and biomass (Teuling, 2018a). Furthermore, Teuling et al. (2019) have shown that full-grown forests are found to move closer to the limits of the Budyko space, which describes the relation between the evaporative fraction and aridity. So, an upwards shift indicates an increase of evaporation given the same climate, which results in decreasing recharge. In terms of water availability in the area, younger vegetation with less biomass would thus be preferable. Naturally, I would again advocate to first thoroughly study the impact of land cover conversion on the ecosystem functioning as a whole before acting. However, not acting should also be considered an option.





# Appendices

# A | Additional results of Chapter 2

Table A1: Evaporation methods further explained  
(a) Information about the evaporation methods. Abbreviations of the variables and constants are explained in table A1(b).

Method	Category	Equation	Input data	Assumptions
Penman (PN)	Combination	$LE = \frac{s}{s+\gamma} Q_n + \frac{\gamma}{s+\gamma} E_a$	$T_a, R_n, u, RH, P_a$	<ol style="list-style-type: none"> <li>1) closed energy balance at water surface</li> <li>2) <math>e_{sat}</math> at surface decreases linearly to <math>e_{sat}</math> at observation height</li> <li>3) <math>r_a</math> can be estimated by a wind function</li> </ol>
De Bruin - Keijman (BK)	Combination	$LE = \alpha_{BK} \frac{s}{s+\gamma} (R_n - G) + \beta_{BK}$	$T_a, R_n$	<ol style="list-style-type: none"> <li>1) constant proportionality between radiation and aerodynamic term</li> <li>2) aerodynamic term can be described by a constant, assuming no explicit wind effects</li> <li>3) Heat storage often assumed to be negligible</li> </ol>
Makkink (MK)	Energy	$LE = 0.05 \frac{s}{s+\gamma} K_{in}$	$T_a, K_{in}$	<ol style="list-style-type: none"> <li>1) heat storage is negligible in relation to <math>R_n</math></li> <li>2) <math>R_n</math> is half of <math>K_{in}</math></li> <li>3) wind speed does not need to be accounted for explicitly</li> </ol>
Granger & Hedstrom (GH)	Wind	$E = a * u$ $a = f(\Delta T, \Delta e, X)$	$u, RH, X_{shore}, \Delta T, \Delta e$	<ol style="list-style-type: none"> <li>1) No relation between <math>E_{water}</math> and <math>R_n</math> at hourly timescales</li> <li>2) Atmospheric stability can be described by land-lake temperature contrast</li> <li>3) Non-linear over-all relation between <math>E_{water}</math> and <math>u</math> is approximated by linear relation</li> </ol>
Hargreaves (HA)	Temperature	$ET_{ref} = 0.0023 h_a (TC + 17.8) T R^{0.50}$	$T_a, R_a$	<ol style="list-style-type: none"> <li>1) <math>K_{in}</math> can be approximated using the extraterrestrial radiation</li> <li>2) Cloudiness is represented using the temperature range</li> <li>3) No heat storage since method is developed for land surfaces</li> </ol>
Flake (FL)	physical-oriented	$LE = -(q_a - q_s) \frac{u_* k}{\frac{1}{Sc_n} (\frac{1}{T_n} - \frac{1}{T_0}) + \psi_0 a(z/L)}$	$T_a, K_{in}, u, RH,$ cloudiness, $d_{lake}, X_{fetch}, \epsilon$	<ol style="list-style-type: none"> <li>1) Top layer of lake is assumed to be well mixed</li> <li>2) Thermocline in bottom layer is described with concept of self-similarity of temperature profile</li> </ol>

(b) Variables and constants needed as input data for the methods

Variable/Constant	Unit
$\alpha_{BK} = 1.1$ = De Bruin-Keijman empirically derived constant	[-]
$\beta_{BK} = 10$ = De Bruin-Keijman empirically derived constant	[W m <sup>-2</sup> ]
$\gamma$ = psychrometric 'constant'	[kPa °C <sup>-1</sup> ]
$\Delta e$ = Horizontal vapour pressure gradient, lake-land	[°C]
$\Delta T$ = Horizontal temperature gradient, land-lake	[°C]
$\epsilon$ = Light extinction coefficient	[m <sup>-1</sup> ]
$LE$ = latent heat flux	[W m <sup>-2</sup> ]
$\rho_a$ = Air density	[kg m <sup>-3</sup> ]
$\psi_q$ = Dimensionless function accounting for static stability in the surface layer	[-]
$d_{lake}$ = Lake depth	[m]
$E_a$ = drying power of air, representing water vapour transport capacity of the atmosphere	[W m <sup>-2</sup> ]
$G$ = water/ground heat flux	[W m <sup>-2</sup> ]
$k$ = Von Karman constant	[-]
$K_{in}$ = incoming shortwave radiation	[W m <sup>-2</sup> ]
$L$ = Obukhov length	[m]
$L_v$ = Latent heat of vaporization	[kJ kg <sup>-1</sup> ]
$P_a$ = Air pressure	[kPa]
$Q_n$ = available energy	[W m <sup>-2</sup> ]
$q_s$ = Saturated specific humidity at the surface	[-]
$q_z$ = Air specific humidity at height $z$	[-]
$RH$ = Relative Humidity	[-]
$R_a$ = Extraterrestrial radiation	[MJ m <sup>-2</sup> d <sup>-1</sup> ]
$R_n$ = Net radiation	[W m <sup>-2</sup> ]
$s$ = slope of the saturated vapour pressure curve	[kPa °C <sup>-1</sup> ]
$Sc_n$ = Schmidt number	[-]
$T_a$ = Temperature	[°C]
$TC$ = Temperature	[°C]
$TR$ = Temperature range	[°C]
$u$ = Wind speed	[m s <sup>-1</sup> ]
$u_*$ = Friction velocity	[m s <sup>-1</sup> ]
$X_{shore}$ = Distance to the shore	[m]
$X_{fetch}$ = Fetch distance	[m]
$z$ = Height of measurements of temperature and humidity	[m]
$z_0$ = Roughness length for specific humidity	[m]



## B | Additional results of Chapter 4

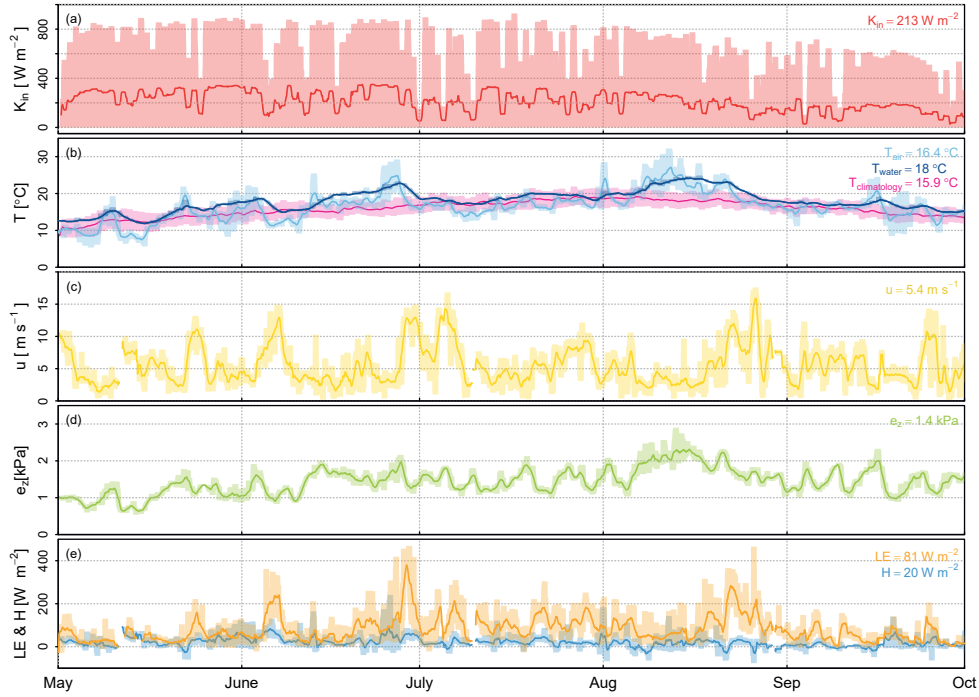


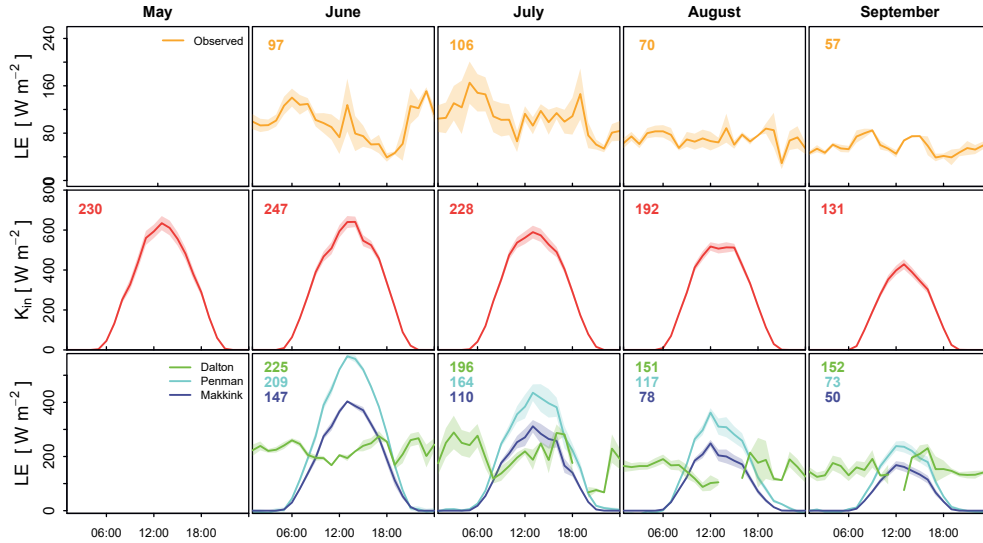
**Figure B1:** Meteorological conditions in Stavoren in 2020 showing running daily means of global radiation (a), air temperature (current and climatology) and water temperature (b), wind speed (c), vapour pressure (d), and turbulent fluxes (e). The shaded area represents the range between minimum and maximum observed values and the numbers reported at the top right of each panel provide the average values of the respective variables during the presented months.

**Table B1:** Basic statistics of the latent heat flux during the summer periods of 2019 and 2020 at both locations (i.e. Stavoren and Trintelhaven) at the hourly and daily timescale. The statistics given are mean, standard deviation, minimum, maximum, 25th and 75th quantile, and the number of observation points.

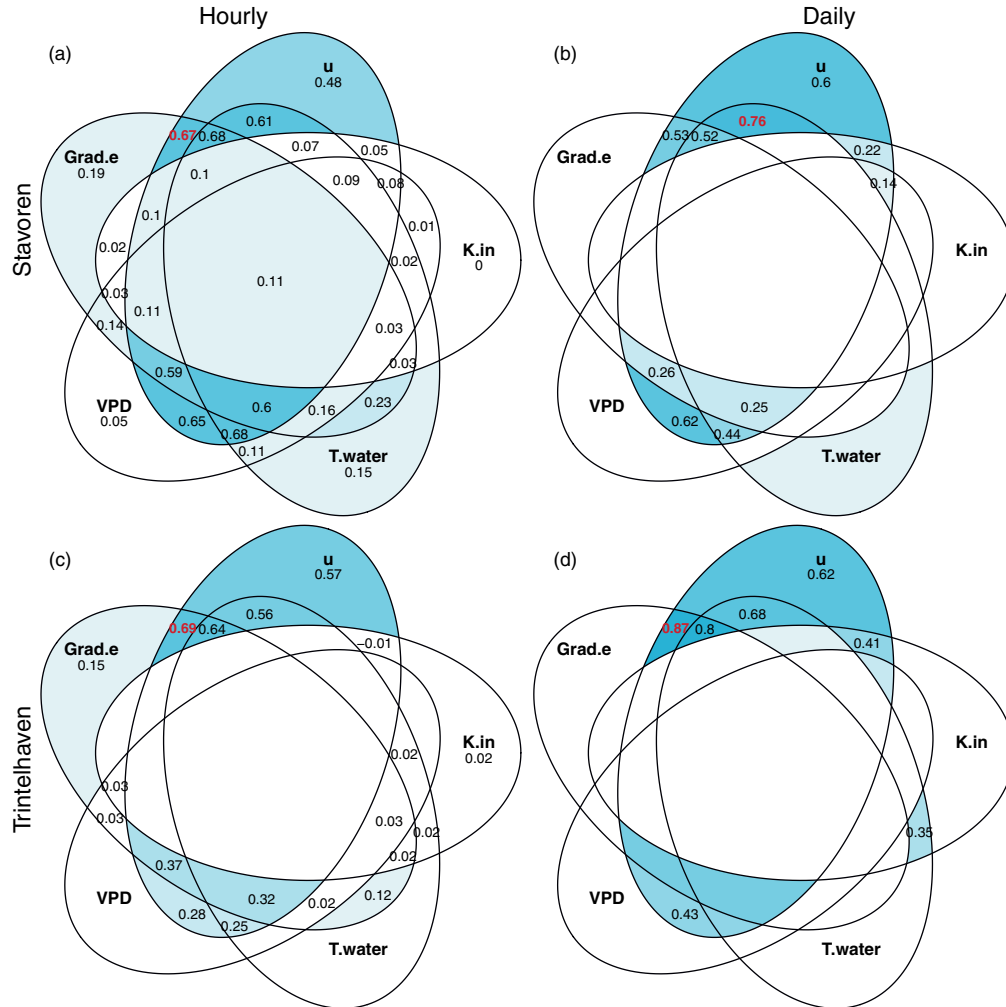
(a) Stavoren – $LE$ [ $W\ m^{-2}$ ]		Mean	Stdev	min	max	Q25	Q75	$N$
Hourly								
2019		104.1	69.2	-21.5	516.1	56.6	133.1	896
2020		128.4	87.6	-27.7	444.6	66.1	146.5	687
Daily								
2019		130.7	67.3	51.2	310.1	84.3	147.5	20
2020		168.4	85.3	55.7	364.5	111.3	215.0	18

(b) Trintelhaven – $LE$ [ $W\ m^{-2}$ ]		Mean	Stdev	min	max	Q25	Q75	$N$
Hourly								
2019		95.9	59.2	11.0	333.9	47.4	130.3	454
2020		91.6	60.2	-34.8	351.8	52.1	113.2	663
Daily								
2019		122.3	45.3	58.9	210.9	94.8	147.3	10
2020		100.5	60.1	35.1	273.8	81.9	105.4	13



**Figure B2:** An illustration of the decoupling at Trintelhaven in 2019 between the monthly average diurnal cycles of observed latent heat flux (top panels) and global radiation (middle panels), with the latter forming the basis of the frequently used evaporation models of Penman (1948) and Makkink (1957). These models are shown together with the model of Dalton (1802) in the bottom panels. Note that some variables included in the evaporation models are measured at heights above the 2 m that is prescribed (see Eqs. 4.4-4.10). Additionally, all three models are generally used on a daily basis, but they are presented here to show the underlying daily cycle. The shaded area represents the uncertainty, which is defined as the standard deviation divided by the square root of the number of observations. Average daily means of the respective variables are indicated by the number in the top left of each panel and display the average course over the summer period.



**Figure B3:** A systematic exploration of which variable or combination of variables (product) can best explain the dynamics of open water evaporation. The outer ‘leaves’ of the Venn diagram represent the single variables, whereas the combinations of products of variables are represented towards the centre of the diagram. Within each leaf, the adjusted  $R^2$  value is depicted. The higher this value, the darker blue the colour of the leaf. The red number indicates the highest  $R^2$  value, indicating the best combination found for a maximum of two variables, i.e. the best ‘simple’ model. The  $R^2$  values were removed if the model fit was found to be insignificant ( $p < 0.05$ ). The analysis is based on data from the summer of 2019 and is performed at an hourly timescale – Stavoren (a) and Trintelhaven (c) – and a daily timescale – Stavoren (b) and Trintelhaven (d).

**Table B2:** ANOVA analysis indicating the significant difference ( $p < 0.05$ ) of the hourly model coefficients found between the two measurement sites during the summer of 2019. The abbreviations used in the table are as follows: Res. df – residual degrees of freedom, RSS – residual sum of squares, df – degrees of freedom, Sum of sq – sum of squares, F – value of F statistics, and Pr – p value for F statistics. Significance is represented as follows: [0, 0.001] “\*\*\*”; [0.001, 0.01] “\*\*”; [0.01, 0.05] “\*”; and  $> 0.05$  “ ” (no symbol).

Analysis of Variance Table (ANOVA)

Model 1:  $LE \sim u\Delta e + (u\Delta e)^2$

Model 2:  $LE \sim u\Delta e + (u\Delta e)^2 * \text{Measurement site}$

Model	Res.Df	RSS	Df	Sum of Sq	F	Pr(> F)
1	559	664256				
2	556	652804	3	11452	3.2512	0.02151*

## C | Additional results of Chapter 5

**Table C1:** Measurement flux tower sites that were not included in this study because the data was not available to us.

Meaurement site	Land cover
Langbroekwetering	Grass
Uden	Grass
Fochteloërveen	Grass
Fleditebos	Forest
Kampina	Forest
Bankenbos	Forest
Utrecht	Urban
Oukoop	Peatland swamp
Stein	Peatland swamp

**Table C2:** The mean and standard deviation of the input variables of the measurement sites.

Measurement site	Kin [W m <sup>-2</sup> ]	Rn [W m <sup>-2</sup> ]	Ta [°C]	u [m s <sup>-1</sup> ]	VPD [kPa]	SM [m <sup>3</sup> m <sup>-3</sup> ]	Prec3 [mm]	Prec10 [mm]	HSP [hr]
Cabauw	220.2 ± 256.7	116 ± 175.4	16.6 ± 4.7	3.7 ± 2	0.5 ± 0.5	0.4 ± 0.1	7 ± 11.1	23.5 ± 22.7	148.7 ± 193.1
Veenkampen	213.1 ± 255.3	118.2 ± 175.5	16.9 ± 5	2.4 ± 1.5	0.3 ± 0	0.3 ± 0.1	7 ± 9.4	22.7 ± 18.1	145.7 ± 183.5
Horstermeer	209.2 ± 252.4	118.8 ± 183.1	16.8 ± 5.1	2.4 ± 1.3	0.6 ± 0.6	0.6 ± 0.1	4.5 ± 5.9	15.3 ± 12.8	191.3 ± 192.2
Loobos	202.2 ± 248.6	157.5 ± 223.7	16.2 ± 4.9	2.1 ± 1.1	0.5 ± 0.6	0.2 ± 0.1	6.3 ± 9.3	20.4 ± 19.4	253.6 ± 406.4
Oostwaard	226.7 ± 264.6	132 ± 197.2	16.4 ± 4.4	1.4 ± 0.7	0.4 ± 0.4	0.3 ± 0.1	2 ± 2.7	6.5 ± 5.7	1025.1 ± 814.5
Speulderbos	218.7 ± 269.7	145.3 ± 234.8	16.1 ± 5.1	2.9 ± 1.2	0.4 ± 0.5	0.1 ± 0.1	3.6 ± 5.1	12.3 ± 10.4	150.4 ± 129.5
Stavoren	219 ± 267.3	174.4 ± 243.3	16.5 ± 3.8	5.7 ± 3.1	1 ± 0.4	–	5.1 ± 7.4	17.5 ± 14.7	204.4 ± 200.5
Trintelhaven	209.5 ± 261.8	159.5 ± 240.2	17.8 ± 4.5	5.3 ± 2.7	1 ± 0.4	–	5.1 ± 7.3	19.5 ± 15	129.4 ± 118.5
Arnhem	201 ± 246.4	129.1 ± 220.5	17.4 ± 4.9	2.4 ± 1.1	0.6 ± 0.6	0.3 ± 0.1	4.1 ± 5.5	13.6 ± 10.5	231.2 ± 210.5
Amsterdam	233.7 ± 272.5	144.3 ± 224.5	16.2 ± 4.4	3.9 ± 1.7	0.4 ± 0.4	0.5 ± 0.1	4.5 ± 7.3	15.2 ± 15.2	308.3 ± 388.1
Dijkgraaf	179.1 ± 227.3	101.7 ± 166.8	16.8 ± 4.3	1.4 ± 0.9	0.5 ± 0.4	0.3 ± 0	1 ± 0.9	3.8 ± 1.9	1236.5 ± 253.6
Langerak	191.1 ± 232.7	107.1 ± 170.1	17.8 ± 4.4	1.5 ± 0.8	0.5 ± 0.5	0.4 ± 0	4.9 ± 5.2	18 ± 10.5	169 ± 169.4
Lutjewad	195.4 ± 241.3	114.8 ± 180.4	16.3 ± 4.4	3.2 ± 1.7	0.4 ± 0.4	0.2 ± 0.1	3.7 ± 4.6	11.6 ± 9.5	238.6 ± 267.1
Molenweg	180 ± 223	194.7 ± 195.3	16.7 ± 3.8	1.7 ± 1	0.4 ± 0.4	0.3 ± 0	3.1 ± 3.8	10.6 ± 5.9	203.6 ± 150.6
Vredepeel	196.3 ± 242.1	109.9 ± 174.3	16.8 ± 5.2	2 ± 1.3	0.6 ± 0.6	0.2 ± 0.1	3.5 ± 4.6	11 ± 11.1	304.4 ± 276.9
Zeewolde	163.2 ± 210	90.8 ± 152.8	17.8 ± 4	3 ± 0.8	0.4 ± 0.4	0.2 ± 0	2.9 ± 2.7	10.3 ± 3.5	222.9 ± 141.1
Onlanden	213.6 ± 246.6	128.5 ± 186.3	18.6 ± 5.6	2.6 ± 1.3	0.5 ± 0.6	0.3 ± 0.1	2.3 ± 3.4	5.8 ± 5.7	413.6 ± 414.1
Camphuijs	167.7 ± 214.8	105.6 ± 169.2	16.2 ± 4.9	1.8 ± 1.3	0.3 ± 0.3	0.4 ± 0	1.8 ± 2.8	6.2 ± 7.7	552.8 ± 299.8
Zegveld	301.5 ± 244.7	184.6 ± 176.9	17.9 ± 4.8	1.9 ± 1.2	0.5 ± 0.5	0.5 ± 0.1	6.4 ± 7.2	20.5 ± 12.7	143.5 ± 158.7

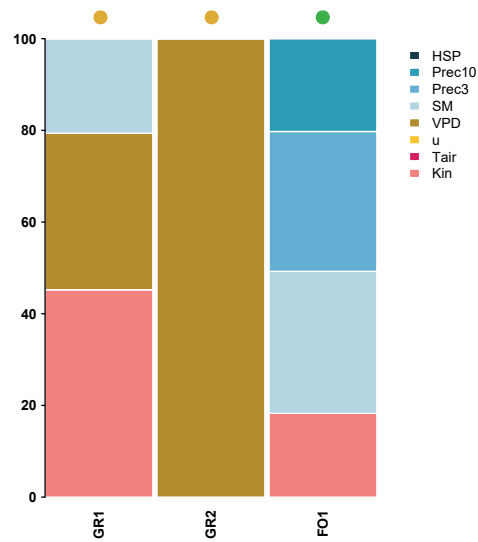


**Figure C1:** Relative contribution of the individual variables in explaining the dynamics of latent heat flux at a daily timescale for the dry year 2018. The coloured dots above the bars indicate the land cover type. HSP is the hours since precipitation, Prec10 the 10-day cumulative precipitation, Prec3 the 3-day cumulative precipitation, SM the soil moisture, VPD the vapour pressure deficit,  $u$  the wind speed,  $T_{\text{air}}$  the air temperature, and  $K_{\text{in}}$  the global radiation.

# References

- Aalbers, E. E., G. Lenderink, E. van Meijgaard, and B. J. J. M. van den Hurk (2017). “Local-Scale Changes in Mean and Heavy Precipitation in Western Europe, Climate Change or Internal Variability?” *Climate Dynamics* 50.11-12, 4745–4766. DOI: 10.1007/s00382-017-3901-9.
- Abdelrady, A. R., J. Timmermans, Z. Vekerdy, and M. S. Salama (2016). “Surface Energy Balance of Fresh and Saline Waters: AquaSEBS”. *Remote Sensing* 8.7, 583. DOI: 10.3390/rs8070583.
- Abtew, W. and A. M. Melesse (2013). *Evaporation and Evapotranspiration: Measurements and Estimations*. Springer Netherlands. 206 pages.
- Adrian, R., C. M. O'Reilly, H. Zagarese, S. B. Baines, D. O. Hessen, W. Keller, D. M. Livingstone, R. Sommaruga, D. Straile, E. Van Donk, G. A. Weyhenmeyer, and M. Winder (2009). “Lakes as Sentinels of Climate Change”. *Limnology and Oceanography* 54.6, 2283–2297. DOI: 10.4319/lo.2009.54.6\_part\_2.2283.
- Allen, R. G., L. S. Pereira, D. Raes, and M. Smith (1998). “Crop Evapotranspiration - Guidelines for Computing Crop Water Requirements - FAO Irrigation and Drainage Paper 56”. *United Nations-Food and Agricultural Organization*.
- AmeriFlux (2023). *About the Ameriflux Network*. ameriflux.lbl.gov. (Last accessed 23 January 2023).
- Anderson, M. C., W. P. Kustas, J. M. Norman, C. R. Hain, J. R. Mecikalski, L. Schultz, M. P. González-Dugo, C. Cammalleri, G. d’Urso, A. Pimstein, and F. Gao (2011). “Mapping Daily Evapotranspiration at Field to Continental Scales Using Geostationary and Polar Orbiting Satellite Imagery”. *Hydrology and Earth System Sciences* 15.1, 223–239. DOI: 10.5194/hess-15-223-2011.
- Andreas, E. L. (1989). “Two-Wavelength Method of Measuring Path-Averaged Turbulent Surface Heat Fluxes”. *Journal of Atmospheric and Oceanic Technology* 6.2, 280–292. DOI: 10.1175/1520-0426(1989)006<0280:TWMOMP>2.0.CO;2.
- Arnell, N. W. (1999). “Climate Change and Global Water Resources”. *Global Environmental Change* 9, S31–S49. DOI: 10.1016/S0959-3780(99)00017-5.
- AsiaFlux (2023). *AsiaFlux*. <https://www.asiaflux.net>. (Last accessed 23 January 2023).
- Aubinet, M., T. Vesala, and D. Papale (2012). *Eddy Covariance: A Practical Guide to Measurement and Data Analysis*. Springer Science & Business Media. 451 pp.
- Baldocchi, D., E. Falge, L. Gu, R. Olson, D. Hollinger, S. Running, P. Anthoni, C. Bernhofer, K. Davis, R. Evans, J. Fuentes, A. Goldstein, G. Katul, B. Law, X. Lee, Y. Malhi, T. Meyers, W. Munger, W. Oechel, K. T. P. U, K. Pilegaard, H. P. Schmid, R. Valentini, S. Verma, T. Vesala, K. Wilson, and S. Wofsy (2001). “FLUXNET: A New Tool to Study the Temporal and Spatial Variability of Ecosystem-Scale Carbon Dioxide, Water Vapor, and Energy Flux Densities”. *Bulletin of the American Meteorological Society* 82.11, 2415–2434. DOI: 10.1175/1520-0477(2001)082<2415:FANTTS>2.3.CO;2.



- Baldocchi, D. D. (2020). “How Eddy Covariance Flux Measurements Have Contributed to Our Understanding of Global Change Biology”. *Global Change Biology* 26.1, 242–260. DOI: 10.1111/gcb.14807.
- Bastiaanssen, W. G. M., M. Menenti, R. A. Feddes, and A. A. M. Holtslag (1998). “A Remote Sensing Surface Energy Balance Algorithm for Land (SEBAL). 1. Formulation”. *Journal of Hydrology* 212–213, 198–212. DOI: 10.1016/S0022-1694(98)00253-4.
- Beer, T., J. Li, and K. Alverson (2018). *Global Change and Future Earth: The Geoscience Perspective*. Cambridge: Cambridge University Press. 430 pages.
- Beljaars, A. C. M. and F. C. Bosveld (1997). “Cabauw Data for the Validation of Land Surface Parameterization Schemes”. *Journal of Climate* 10.6, 1172–1193. DOI: 10.1175/1520-0442(1997)010<1172:CDFTV0>2.0.CO;2.
- Bentamy, A., J. F. Piollé, A. Grouazel, R. Danielson, S. Gulev, F. Paul, H. Azelmat, P. P. Mathieu, K. von Schuckmann, S. Sathyendranath, H. Evers-King, I. Esau, J. A. Johannessen, C. A. Clayson, R. T. Pinker, S. A. Grodsky, M. Bourassa, S. R. Smith, K. Haines, M. Valdivieso, C. J. Merchant, B. Chapron, A. Anderson, R. Hollmann, and S. A. Josey (2017). “Review and Assessment of Latent and Sensible Heat Flux Accuracy over the Global Oceans”. *Remote Sensing of Environment* 201, 196–218. DOI: 10.1016/j.rse.2017.08.016.
- Beyrich, F., J. Bange, O. K. Hartogensis, S. Raasch, M. Braam, D. Van Dinter, D. Gräf, B. Van Kesteren, A. C. Van den Kroonenberg, B. Maronga, S. Martin, and A. F. Moene (2012). “Towards a Validation of Scintillometer Measurements: The LITFASS-2009 Experiment”. *Boundary-Layer Meteorology* 144.1, 83–112. DOI: 10.1007/s10546-012-9715-8.
- Blanken, P. D., W. R. Rouse, A. D. Culf, C. Spence, L. D. Boudreau, J. N. Jasper, B. Kochtubajda, W. M. Schertzer, P. Marsh, and D. Verseghy (2000). “Eddy Covariance Measurements of Evaporation from Great Slave Lake, Northwest Territories, Canada”. *Water Resources Research* 36.4, 1069–1077. DOI: 10.1029/1999WR900338.
- Blanken, P. D., C. Spence, N. Hedstrom, and J. D. Lenters (2011). “Evaporation from Lake Superior: 1. Physical Controls and Processes”. *Journal of Great Lakes Research* 37.4, 707–716. DOI: 10.1016/j.jglr.2011.08.009.
- Bosveld, F. C. and W. Bouten (2001). “Evaluation of Transpiration Models with Observations over a Douglas-fir Forest”. *Agricultural and Forest Meteorology* 108.4, 247–264. DOI: 10.1016/S0168-1923(01)00251-9.
- Bosveld, F. C., P. Baas, A. C. M. Beljaars, A. A. M. Holtslag, J. V.-G. de Arellano, and B. J. H. Van de Wiel (2020). “Fifty Years of Atmospheric Boundary-Layer Research at Cabauw Serving Weather, Air Quality and Climate”. *Boundary-Layer Meteorology* 177.2, 583–612. DOI: 10.1007/s10546-020-00541-w.
- Bosveld, F. C. and W. Bouten (2003). “Evaluating a Model of Evaporation and Transpiration with Observations in a Partially Wet Douglas-Fir Forest”. *Boundary-Layer Meteorology* 108.3, 365–396. DOI: 10.1023/A:1024148707239.
- Bouin, M.-N., G. Caniaux, O. Traullé, D. Legain, and P. L. Moigne (2012). “Long-Term Heat Exchanges over a Mediterranean Lagoon”. *Journal of Geophysical Research: Atmospheres* 117.D23. DOI: 10.1029/2012JD017857.
- Breil, M., E. L. Davin, and D. Rechid (2021). “What Determines the Sign of the Evapotranspiration Response to Afforestation in European Summer?” *Biogeosciences* 18.4, 1499–1510. DOI: 10.5194/bg-18-1499-2021.
- Bright, R. M., E. Davin, T. O’Halloran, J. Pongratz, K. Zhao, and A. Cescatti (2017). “Local Temperature Response to Land Cover and Management Change Driven by Non-Radiative Processes”. *Nature Climate Change* 7.4, 296–302. DOI: 10.1038/nclimate3250.

- Brutsaert, W. (1982). *Evaporation into the Atmosphere: Theory, History and Applications*. Springer Netherlands. 302 pp.
- Brutsaert, W. and M. B. Parlange (1998). “Hydrologic Cycle Explains the Evaporation Paradox”. *Nature* 396.6706, 30–30. DOI: 10.1038/23845.
- Brutsaert, W. and D. Chen (1995). “Desorption and the Two Stages of Drying of Natural Tallgrass Prairie”. *Water Resources Research* 31.5, 1305–1313. DOI: 10.1029/95WR00323.
- Budyko, M. I. (1974). *Climate and Life*. New York: Academic Press. 508 pp.
- Buitelaar, R., J. Kollen, and C. Leerlooijer (2015). *Rapport Operationeel Waterbeheer IJsselmeergebied - Inventarisatie Huidige Waterbeheer IJsselmeergebied Door Rijkswaterstaat En Waterschappen*. Alkmaar: Grontmij, 112 pp.
- Buzacott, A., H. Mulder, M. van den Berg, B. Kruijt, and Y. van der Velde (2022). “Quantifying the Contribution of Grassland and Paludiculture to Carbon Fluxes from a Single Eddy Covariance Tower in a Dutch Peatland”. In: EGU General Assembly 2022. Vol. EGU22-9978. Vienna, Austria: Copernicus Meetings. DOI: 10.5194/egusphere-egu22-9978.
- Charuchittipan, D., W. Babel, M. Mauder, J.-P. Leps, and T. Foken (2014). “Extension of the Averaging Time in Eddy-Covariance Measurements and Its Effect on the Energy Balance Closure”. *Boundary-Layer Meteorology* 152.3, 303–327. DOI: 10.1007/s10546-014-9922-6.
- Chen, L., P. A. Dirmeyer, Z. Guo, and N. M. Schultz (2018). “Pairing FLUXNET Sites to Validate Model Representations of Land-Use/Land-Cover Change”. *Hydrology and Earth System Sciences* 22.1, 111–125. DOI: 10.5194/hess-22-111-2018.
- Christidis, N. and P. A. Stott (2021). “The Influence of Anthropogenic Climate Change on Wet and Dry Summers in Europe”. *Science Bulletin* 66.8, 813–823. DOI: 10.1016/j.scib.2021.01.020.
- Ciais, P., M. Reichstein, N. Viovy, A. Granier, J. Ogée, V. Allard, M. Aubinet, N. Buchmann, C. Bernhofer, A. Carrara, F. Chevallier, N. De Noblet, A. D. Friend, P. Friedlingstein, T. Grünwald, B. Heinesch, P. Keronen, A. Knohl, G. Krinner, D. Loustau, G. Manca, G. Matteucci, F. Miglietta, J. M. Ourcival, D. Papale, K. Pilegaard, S. Rambal, G. Seufert, J. F. Soussana, M. J. Sanz, E. D. Schulze, T. Vesala, and R. Valentini (2005). “Europe-Wide Reduction in Primary Productivity Caused by the Heat and Drought in 2003”. *Nature* 437.7058, 529–533. DOI: 10.1038/nature03972.
- Cisneros Vaca, C., C. van der Tol, and C. P. Ghimire (2018). “The Influence of Long-Term Changes in Canopy Structure on Rainfall Interception Loss: A Case Study in Speulderbos, the Netherlands”. *Hydrology and Earth System Sciences* 22.7, 3701–3719. DOI: 10.5194/hess-22-3701-2018.
- Cleugh, H. A., R. Leuning, Q. Mu, and S. W. Running (2007). “Regional Evaporation Estimates from Flux Tower and MODIS Satellite Data”. *Remote Sensing of Environment* 106.3, 285–304. DOI: 10.1016/j.rse.2006.07.007.
- Cleveland, W. S. (1979). “Robust Locally Weighted Regression and Smoothing Scatterplots”. *Journal of the American Statistical Association* 74.368, 829–836. DOI: 10.1080/01621459.1979.10481038.
- Cogley, J. G. (1979). “The Albedo of Water as a Function of Latitude”. *Monthly Weather Review* 107.6, 775–781. DOI: 10.1175/1520-0493(1979)107<0775:TAOWAA>2.0.CO;2.
- Cronin, M. F., C. L. Gentemann, J. Edson, I. Ueki, M. Bourassa, S. Brown, C. A. Clayson, C. W. Fairall, J. T. Farrar, S. T. Gille, S. Gulev, S. A. Josey, S. Kato, M. Katsumata, E. Kent, M. Krug, P. J. Minnett, R. Parfitt, R. T. Pinker, P. W. J. Stackhouse, S. Swart, H. Tomita, D. Vandemark, A. R. Weller, K. Yoneyama, L. Yu, and D. Zhang (2019). “Air-Sea Fluxes with a Focus on Heat and Momentum”. *Frontiers in Marine Science* 6, 1–30. DOI: 10.3389/fmars.2019.00430.
- Cummings, N. W. and B. Richardson (1927). “Evaporation from Lakes”. *Physical Review* 30.4, 527–534. DOI: 10.1103/PhysRev.30.527.

- Cunliffe, A. M., F. Boschetti, R. Clement, S. Sitch, K. Anderson, T. Duman, S. Zhu, M. Schlumpf, M. E. Litvak, R. E. Brazier, and T. C. Hill (2022). “Strong Correspondence in Evapotranspiration and Carbon Dioxide Fluxes Between Different Eddy Covariance Systems Enables Quantification of Landscape Heterogeneity in Dryland Fluxes”. *Journal of Geophysical Research: Biogeosciences* 127.8, 1–13. DOI: 10.1029/2021JG006240.
- Dalton, J. (1802). “Experimental Essays on the Constitution of Mixed Gases: On the Force of Steam or Vapour from Water or Other Liquids in Different Temperatures, Both in a Torricelli Vacuum and in Air; on Evaporation; and on Expansion of Gases by Heat.” *Memoirs of the Literary and Philosophical Society of Manchester* 5, 536–602.
- De Bruin, H. A. R. (1979). *Neerslag, Openwaterverdamping En Potentieel Neerslagoverschot in Nederland, Frequentieverdelingen in Het Groeiseizoen, KNMI Report WR 79-04*. De Bilt: KNMI.
- (1982). “Temperature and Energy Balance of a Water Reservoir Determined from Standard Weather Data of a Land Station”. *Journal of Hydrology* 59.3, 261–274. DOI: 10.1016/0022-1694(82)90091-9.
- De Bruin, H. a. R., C. M. J. Jacobs, P. G. Jarvis, K. G. McNaughton, J. Milford, W. Kohsiek, P. Rowntree, J. L. Monteith, B. Gardiner, W. J. Shuttleworth, P. G. Jarvis, J. L. Monteith, W. J. Shuttleworth, and M. H. Unsworth (1989). “Forests and Regional-Scale Processes”. *Philosophical Transactions of the Royal Society of London. B, Biological Sciences* 324.1223, 393–406. DOI: 10.1098/rstb.1989.0054.
- De Bruin, H. A. R. and J. Q. Keijman (1979). “The Priestley-Taylor Evaporation Model Applied to a Large Shallow Lake in The Netherlands”. *Journal of Applied Meteorology* 18, 898–903.
- De Bruin, H. A. R. and W. N. Lablans (1998). “Reference Crop Evapotranspiration Determined with a Modified Makkink Equation”. *Hydrological Processes* 12.7, 1053–1062. DOI: 10.1002/(SICI)1099-1085(19980615)12:7<1053::AID-HYP639>3.0.CO;2-E.
- De Laat, P. J. M. and P. Varoonchotikul (1996). “Modelling Evapotranspiration of Dune Vegetation”. In: *Proceedings of the International Conference on Hydrology and Water Resources, New Delhi, India, December 1993*. Ed. by V. P. Singh and B. Kumar. Water Science and Technology Library. Dordrecht: Springer Netherlands, 19–27. DOI: 10.1007/978-94-011-0389-3\_2.
- De Lange, W. J., G. F. Prinsen, J. C. Hoogewoud, A. A. Veldhuizen, J. Verkaik, G. H. P. Oude Essink, P. E. V. van Walsum, J. R. Delsman, J. C. Hunink, H. T. L. Massop, and T. Kroon (2014). “An Operational, Multi-Scale, Multi-Model System for Consensus-Based, Integrated Water Management and Policy Analysis: The Netherlands Hydrological Instrument”. *Environmental Modelling & Software* 59, 98–108. DOI: 10.1016/j.envsoft.2014.05.009.
- De Vries, J. (2007). “Groundwater”. In: *Geology of the Netherlands*. Edited by Th.E. Wong, D.A.J. Batjes & J. de Jager. Royal Netherlands Academy of Arts and Sciences, 295–315.
- Denissen, J., A. Teuling, A. Pitman, S. Koirala, M. Migliavacca, W. Li, M. Reichstein, A. Winkler, C. Zhan, and R. Orth (2022). “Widespread Shift from Ecosystem Energy to Water Limitation with Climate Change”. *Nature Climate Change* 12. DOI: 10.1038/s41558-022-01403-8.
- Denissen, J. M., A. J. Teuling, M. Reichstein, and R. Orth (2020). “Critical Soil Moisture Derived From Satellite Observations Over Europe”. *Journal of Geophysical Research: Atmospheres* 125.6, 1–10. DOI: 10.1029/2019JD031672.
- Desai, A. R., J. A. Austin, V. Bennington, and G. A. McKinley (2009). “Stronger Winds over a Large Lake in Response to Weakening Air-to-Lake Temperature Gradient”. *Nature Geoscience* 2.12, 855–858. DOI: 10.1038/ngeo693.
- Dirmeyer, P. A. (2011). “The Terrestrial Segment of Soil Moisture–Climate Coupling”. *Geophysical Research Letters* 38.16, L16702. DOI: 10.1029/2011GL048268.

- Dolman, A. J., E. J. Moors, and J. A. Elbers (2002). “The Carbon Uptake of a Mid Latitude Pine Forest Growing on Sandy Soil”. *Agricultural and Forest Meteorology* 111.3, 157–170. DOI: 10.1016/S0168-1923(02)00024-2.
- Dolman, A. J., E. J. Moors, J. A. Elbers, and W. Snijders (1998). “Evaporation and Surface Conductance of Three Temperate Forests in the Netherlands”. *Annales des Sciences Forestières* 55.1-2, 255–270.
- Duan, Z. and W. G. M. Bastiaanssen (2017). “Evaluation of Three Energy Balance-Based Evaporation Models for Estimating Monthly Evaporation for Five Lakes Using Derived Heat Storage Changes from a Hysteresis Model”. *Environmental Research Letters* 12.2, 024005. DOI: 10.1088/1748-9326/aa568e.
- Durack, P. J., S. E. Wijffels, and R. J. Matear (2012). “Ocean Salinities Reveal Strong Global Water Cycle Intensification During 1950 to 2000”. *Science* 336.6080, 455–458. DOI: 10.1126/science.1212222.
- EasyFlux (2017). *EasyFlux DL CR6OP for CR6 and Open-Path Eddy-Covariance System - Product Manual*. Campbell Scientific, Inc.
- EddyPro (2021). *EddyPro® Software (Version 7.0) [Computer Software]*. LI-COR, Inc; Infrastructure for Measurements of the European Carbon Cycle Consortium. Lincoln, NE.
- Elbers, J., E. Moors, and C. Jacobs (2009). *Gemeten Actuele Verdamping Voor Twaalf Locaties in Nederland*. Alterra-rapport 1920. Wageningen: Wageningen UR Alterra, 36.
- Elbers, J. A., C. M. J. Jacobs, B. Kruijt, W. W. P. Jans, and E. J. Moors (2011). “Assessing the Uncertainty of Estimated Annual Totals of Net Ecosystem Productivity: A Practical Approach Applied to a Mid Latitude Temperate Pine Forest”. *Agricultural and Forest Meteorology* 151.12, 1823–1830. DOI: 10.1016/j.agrformet.2011.07.020.
- ERC (2023). *Ecosystem Restoration Camps*. <https://ecosystemrestorationcamps.org>. (Last accessed 25 January 2023).
- Euser, T., W. M. J. Luxemburg, C. S. Everson, M. G. Mengistu, A. D. Clulow, and W. G. M. Bastiaanssen (2014). “A New Method to Measure Bowen Ratios Using High-Resolution Vertical Dry and Wet Bulb Temperature Profiles”. *Hydrology and Earth System Sciences* 18.6, 2021–2032. DOI: 10.5194/hess-18-2021-2014.
- Fank, J. (2011). “Lysimeters: A Tool for Measurements of Soil Fluxes”. In: *Encyclopedia of Agrophysics*. Ed. by J. Gliński, J. Horabik, and J. Lipiec. Encyclopedia of Earth Sciences Series. Dordrecht: Springer Netherlands, 428–431. DOI: 10.1007/978-90-481-3585-1\_85.
- Feigenwinter, C., R. Vogt, and A. Christen (2012). “Eddy Covariance Measurements Over Urban Areas”. In: *Eddy Covariance: A Practical Guide to Measurement and Data Analysis*. Springer Science & Business Media, 377–397.
- Feldman, A. F., D. J. Short Gianotti, I. F. Trigo, G. D. Salvucci, and D. Entekhabi (2019). “Satellite-Based Assessment of Land Surface Energy Partitioning–Soil Moisture Relationships and Effects of Confounding Variables”. *Water Resources Research* 55.12, 10657–10677. DOI: 10.1029/2019WR025874.
- Feynman, R. (1964). “Atoms in Motion”. In: *The Feynman Lectures on Physics*. Vol. 1: Mainly mechanics, radiation, and heat. Reading: Addison–Wesley.
- Finch, J. W. (2001). “A Comparison between Measured and Modelled Open Water Evaporation from a Reservoir in South-East England”. *Hydrological Processes* 15.14, 2771–2778. DOI: 10.1002/hyp.267.
- Finch, J. and A. Calver (2008). *Methods for the Quantification of Evaporation from Lakes*. Oxfordshire: World Meteorological Organisation’s Commission for Hydrology, 41.
- Fischer, E. M. and C. Schär (2010). “Consistent Geographical Patterns of Changes in High-Impact European Heatwaves”. *Nature Geoscience* 3.6, 398–403. DOI: 10.1038/ngeo866.

- Fisher, D. K. (2012). "Simple Weighing Lysimeters for Measuring Evapotranspiration and Developing Crop Coefficients". *International Journal of Agricultural and Biological Engineering* 5.3, 35–43. DOI: 10.25165/ijabe.v5i3.627.
- Foken, T. (2008). "The Energy Balance Closure Problem: An Overview". *Ecological Applications* 18.6, 1351–1367. DOI: 10.1890/06-0922.1.
- Foken, T., M. Gockede, M. Mauder, L. Mahrt, B. Amiro, and W. Munger (2004). "Chapter 9 - Post-field Data Quality Control". In: *Handbook of Micrometeorology*. Springer Science + Business Media, Inc, 181–208.
- Foken, T., R. Leuning, S. R. Oncley, M. Mauder, and M. Aubinet (2012). "Corrections and Data Quality Control". In: *Eddy Covariance. A Practical Guide to Measurements and Data Analysis*. Dordrecht: Springer Netherlands, 85–131.
- Foken, T. and S. Oncley (1995). "Workshop on Instrumental and Methodical Problems of Land Surface Flux Measurements". *Bulletin of the American Meteorological Society* 76.7, 1191–1193. JSTOR: 26232527.
- Gates, D. M. (1968). "Transpiration and Leaf Temperature". *Annual Review of Plant Physiology* 19.1, 211–238. DOI: 10.1146/annurev.pp.19.060168.001235.
- Gokmen, M., Z. Vekerd, A. Verhoef, W. Verhoef, O. Batelaan, and C. van der Tol (2012). "Integration of Soil Moisture in SEBS for Improving Evapotranspiration Estimation under Water Stress Conditions". *Remote Sensing of Environment* 121, 261–274. DOI: 10.1016/j.rse.2012.02.003.
- Görgen, K., J. Beersma, G. Brahmer, H. Buiteveld, M. Carambia, O. de Keizer, P. Krahe, E. Nilson, R. Lammersen, C. Perrin, and D. Volken (2010). *Assessment of Climate Change Impacts on Discharge in the Rhine River Basin: Results of the RheinBlick2050 Project*. CHR Report 1 23. Lelystad: Secretariat CHR/KHR.
- Gosling, S. N. and N. W. Arnell (2016). "A Global Assessment of the Impact of Climate Change on Water Scarcity". *Climatic Change* 134.3, 371–385. DOI: 10.1007/s10584-013-0853-x.
- Granger, R. J. and N. Hedstrom (2011). "Modelling Hourly Rates of Evaporation from Small Lakes". *Hydrology and Earth System Sciences* 15, 267–277. DOI: 10.5194/hess-15-267-2011.
- Greve, P., B. Orlowsky, B. Mueller, J. Sheffield, M. Reichstein, and S. I. Seneviratne (2014). "Global Assessment of Trends in Wetting and Drying over Land". *Nature Geoscience* 7.10, 716–721. DOI: 10.1038/ngeo2247.
- Grimmond, C. S. B. and T. R. Oke (1999). "Heat Storage in Urban Areas: Local-Scale Observations and Evaluation of a Simple Model". *Journal of Applied Meteorology and Climatology* 38.7, 922–940. DOI: 10.1175/1520-0450(1999)038<0922:HSUAL>2.0.CO;2.
- Grismer, M. E., M. Orang, R. Snyder, and R. Matyac (2002). "Pan Evaporation to Reference Evapotranspiration Conversion Methods". *Journal of Irrigation and Drainage Engineering* 128.3, 180–184. DOI: 10.1061/(ASCE)0733-9437(2002)128:3(180).
- Hargreaves, G. H. (1975). "Moisture Availability and Crop Production". *Transactions of the ASAE* 18.5, 0980–0984. DOI: 10.13031/2013.36722.
- Hargreaves, G. H. and R. G. Allen (2003). "History and Evaluation of Hargreaves Evapotranspiration Equation". *Journal of Irrigation and Drainage Engineering* 129.1, 53–63. DOI: 10.1061/(ASCE)0733-9437(2003)129:1(53).
- Hartogensis, O. K., C. J. Watts, J.-C. Rodriguez, and H. A. R. De Bruin (2003). "Derivation of an Effective Height for Scintillometers: La Poza Experiment in Northwest Mexico". *Journal of Hydrometeorology* 4.5, 915–928. JSTOR: 24909272.
- Hazeleger, W., X. Wang, C. Severijns, S. Ștefănescu, R. Bintanja, A. Sterl, K. Wyser, T. Semmler, S. Yang, B. van den Hurk, T. van Noije, E. van der Linden, and K. van der Wiel (2012). "EC-Earth V2.2:

- Description and Validation of a New Seamless Earth System Prediction Model". *Climate Dynamics* 39.11, 2611–2629. DOI: 10.1007/s00382-011-1228-5.
- Held, I. M. and B. J. Soden (2006). "Robust Responses of the Hydrological Cycle to Global Warming". *Journal of Climate* 19.21, 5686–5699. DOI: 10.1175/JCLI3990.1.
- Hendriks, D. M. D., J. van Huissteden, and A. J. Dolman (2007). "The Full Greenhouse Gas Balance of an Abandoned Peat Meadow". *Biogeosciences* 4, 411–424. DOI: 10.5194/bg-4-411-2007.
- Hoek van Dijke, A. J., K. Mallick, M. Schlerf, M. Machwitz, M. Herold, and A. J. Teuling (2020). "Examining the Link between Vegetation Leaf Area and Land–Atmosphere Exchange of Water, Energy, and Carbon Fluxes Using FLUXNET Data". *Biogeosciences* 17.17, 4443–4457. DOI: 10.5194/bg-17-4443-2020.
- Hoek van Dijke, A. J., K. Mallick, A. J. Teuling, M. Schlerf, M. Machwitz, S. K. Hassler, T. Blume, and M. Herold (2019). "Does the Normalized Difference Vegetation Index Explain Spatial and Temporal Variability in Sap Velocity in Temperate Forest Ecosystems?" *Hydrology and Earth System Sciences* 23.4, 2077–2091. DOI: 10.5194/hess-23-2077-2019.
- Holmes, T. R. H., C. R. Hain, M. C. Anderson, and W. T. Crow (2016). "Cloud Tolerance of Remote-Sensing Technologies to Measure Land Surface Temperature". *Hydrology and Earth System Sciences* 20.8, 3263–3275. DOI: 10.5194/hess-20-3263-2016.
- Huisman, P. (1998). *Water in the Netherlands*. NHV-Special - 3. Delft: Netherlands Institute of Applied Geoscience. 132 pages.
- Huntington, T. G. (2006). "Evidence for Intensification of the Global Water Cycle: Review and Synthesis". *Journal of Hydrology* 319.1, 83–95. DOI: 10.1016/j.jhydro1.2005.07.003.
- Hurkmans, R. T. W. L., B. van den Hurk, M. J. Schmeits, F. Wetterhall, and I. G. Pechlivanidis (2022). "Comparing Seasonal Streamflow Forecast Systems for Management of a Fresh Water Reservoir in the Netherlands". *Hydrology and Earth System Sciences Discussions*, 1–22. DOI: 10.5194/hess-2021-604.
- ICOS (2023). *Integrated Carbon Observation System*. <https://www.icos-cp.eu> (Last accessed 23 January 2023).
- Jacobs, A. F. G., B. G. Heusinkveld, and A. A. M. Holtslag (2010). "Eighty Years of Meteorological Observations at Wageningen, the Netherlands: Precipitation and Evapotranspiration". *International Journal of Climatology* 30.9, 1315–1321. DOI: 10.1002/joc.1957.
- Jacobs, A. F. G., B. G. Heusinkveld, and A. A. M. Holtslag (2003). "Carbon Dioxide and Water Vapour Flux Densities over a Grassland Area in the Netherlands". *International Journal of Climatology* 23.13, 1663–1675. DOI: 10.1002/joc.959.
- Jacobs, C. M. J., A. F. G. Jacobs, F. C. Bosveld, D. M. D. Hendriks, A. Hensen, P. S. Kroon, E. J. Moors, L. Nol, A. Schrier-Uijl, and E. M. Veenendaal (2007). "Variability of Annual CO<sub>2</sub> Exchange from Dutch Grasslands". *Biogeosciences* 4, 803–816. DOI: 10.5194/bg-4-803-2007.
- Jacobs, C., J. Elbers, R. Brolsma, O. Hartogensis, E. Moors, M. T. Rodríguez-Carretero Márquez, and B. van Hove (2015). "Assessment of Evaporative Water Loss from Dutch Cities". *Building and Environment*. Special Issue: Climate Adaptation in Cities 83, 27–38. DOI: 10.1016/j.buildenv.2014.07.005.
- Jansen, F. A., R. Uijlenhoet, C. M. J. Jacobs, and A. J. Teuling (2022). "Evaporation from a Large Lowland Reservoir – Observed Dynamics and Drivers during a Warm Summer". *Hydrology and Earth System Sciences* 26.11, 2875–2898. DOI: 10.5194/hess-26-2875-2022.
- Jaramillo, F., N. Cory, B. Arheimer, H. Laudon, Y. van der Velde, T. B. Hasper, C. Teutschbein, and J. Uddling (2018). "Dominant Effect of Increasing Forest Biomass on Evapotranspiration: Interpretations of Movement in Budyko Space". *Hydrology and Earth System Sciences* 22.1, 567–580. DOI: 10.5194/hess-22-567-2018.

- Jarvis, P. G. (1976). “The Interpretation of the Variations in Leaf Water Potential and Stomatal Conductance Found in Canopies in the Field”. *Philosophical Transactions of the Royal Society of London. Series B, Biological Sciences* 273.927, 593–610. JSTOR: 2417554.
- Jarvis, P. G. and K. G. McNaughton (1986). “Stomatal Control of Transpiration: Scaling Up from Leaf to Region”. In: *Advances in Ecological Research*. Ed. by A. MacFadyen and E. D. Ford. Vol. 15. Academic Press, 1–49. DOI: 10.1016/S0065-2504(08)60119-1.
- Jenny, J.-P., O. Anneville, F. Arnaud, Y. Baulaz, D. Bouffard, I. Domaizon, S. A. Bocaniov, N. Chèvre, M. Ditttrich, J.-M. Dorioz, E. S. Dunlop, G. Dur, J. Guillard, T. Guinaldo, S. Jacquet, A. Jamoneau, Z. Jawed, E. Jeppesen, G. Krantzberg, J. Lenters, B. Leoni, M. Meybeck, V. Nava, T. Nôges, P. Nôges, M. Patelli, V. Pebbles, M.-E. Perga, S. Rasconi, C. R. Ruetz, L. Rudstam, N. Salmaso, S. Sapna, D. Straile, O. Tammeorg, M. R. Twiss, D. G. Uzarski, A.-M. Ventelä, W. F. Vincent, S. W. Wilhelm, S.-Å. Wängberg, and G. A. Weyhenmeyer (2020). “Scientists’ Warning to Humanity: Rapid Degradation of the World’s Large Lakes”. *Journal of Great Lakes Research* 46.4, 686–702. DOI: 10.1016/j.jglr.2020.05.006.
- Jiménez, C., B. Martens, D. M. Miralles, J. B. Fisher, H. E. Beck, and D. Fernández-Prieto (2018). “Exploring the Merging of the Global Land Evaporation WACMOS-ET Products Based on Local Tower Measurements”. *Hydrology and Earth System Sciences* 22.8, 4513–4533. DOI: 10.5194/hess-22-4513-2018.
- Jongen, H., G.-J. Steeneveld, J. Beringer, A. Christen, N. Chrysoulakis, K. Fortuniak, J. Hong, J.-W. Hong, C. Jacobs, L. Järvi, F. Meier, W. Pawlak, M. Roth, N. Theeuwes, E. Velasco, R. Vogt, and A. Teuling (2022). “Urban Water Storage Capacity Inferred From Observed Evapotranspiration Recession”. *Geophysical Research Letters* 49, 1–11. DOI: 10.1029/2021GL096069.
- Josey, S. A., S. Gulev, and L. Yu (2013). “Chapter 5. Exchanges Through the Ocean Surface”. In: *Ocean Circulation and Climate: A 21st Century Perspective*. Elsevier Inc. Chapters, 115–140.
- Jung, M., S. Koirala, U. Weber, K. Ichii, F. Gans, G. Camps-Valls, D. Papale, C. Schwalm, G. Tramontana, and M. Reichstein (2019). “The FLUXCOM Ensemble of Global Land-Atmosphere Energy Fluxes”. *Scientific Data* 6.1, 74. DOI: 10.1038/s41597-019-0076-8. (Visited on 2023).
- Jung, M., M. Reichstein, P. Ciais, S. I. Seneviratne, J. Sheffield, M. L. Goulden, G. Bonan, A. Cescatti, J. Chen, R. de Jeu, A. J. Dolman, W. Eugster, D. Gerten, D. Gianelle, N. Gobron, J. Heinke, J. Kimball, B. E. Law, L. Montagnani, Q. Mu, B. Mueller, K. Oleson, D. Papale, A. D. Richardson, O. Roupsard, S. Running, E. Tomelleri, N. Viovy, U. Weber, C. Williams, E. Wood, S. Zaehle, and K. Zhang (2010). “Recent Decline in the Global Land Evapotranspiration Trend Due to Limited Moisture Supply”. *Nature* 467.7318, 951–954. DOI: 10.1038/nature09396.
- Katul, G. G. and M. B. Parlange (1992). “A Penman-Brutsaert Model for Wet Surface Evaporation”. *Water Resources Research* 28.1, 121–126. DOI: 10.1029/91WR02324.
- Keijman, J. Q. (1974). “The Estimation of the Energy Balance of a Lake from Simple Weather Data”. *Boundary-Layer Meteorology* 7.3, 399–407. DOI: 10.1007/BF00240841.
- Keijman, J. Q. and R. W. R. Koopmans (1973). “A Comparison of Several Methods of Estimating the Evaporation of Lake Flevo”. *International Association of Hydrological Sciences Publ.* 109, 225–232.
- Kitaigorodskii, S. A. and Y. Z. Miropolskii (1970). “On the Theory of the Open Ocean Active Layer”. *Izv. Atmos. Oceanic Phys.* 6, 97–102.
- Kleidon, A. and M. Renner (2017). “An Explanation for the Different Climate Sensitivities of Land and Ocean Surfaces Based on the Diurnal Cycle”. *Earth System Dynamics* 8.3, 849–864. DOI: 10.5194/esd-8-849-2017.

- Kljun, N., P. Calanca, M. W. Rotach, and H. P. Schmid (2004). “A Simple Parameterisation for Flux Footprint Predictions”. *Boundary-Layer Meteorology* 112.3, 503–523. DOI: 10.1023/B:BOUN.0000030653.71031.96.
- (2015). “A Simple Two-Dimensional Parameterisation for Flux Footprint Prediction (FFP)”. *Geoscientific Model Development* 8.11, 3695–3713. DOI: 10.5194/gmd-8-3695-2015.
- KNMI (2015). *KNMI’14 Klimaatscenario’s Voor Nederland; Leidraad Voor Professionals in Klimaatadaptatie*. De Bilt: KNMI, 34.
- (2018). *KNMI - Zomer 2018 (Juni, Juli, Augustus)*. <https://www.knmi.nl/nederland-nu/klimatologie/maand-en-seizoensoverzichten/2018/zomer>. (Last accessed 23 November 2022).
- (2022). *KNMI - Klimaatviewer*. [https://www.knmi.nl/klimaat-viewer/grafieken-tabellen/klimaattabellen-per-station/de-bilt/klimaattabel.de-bilt\\_1991-2020](https://www.knmi.nl/klimaat-viewer/grafieken-tabellen/klimaattabellen-per-station/de-bilt/klimaattabel.de-bilt_1991-2020). (Last accessed 17 November 2022).
- Konapala, G., A. K. Mishra, Y. Wada, and M. E. Mann (2020). “Climate Change Will Affect Global Water Availability through Compounding Changes in Seasonal Precipitation and Evaporation”. *Nature Communications* 11.1, 3044. DOI: 10.1038/s41467-020-16757-w.
- Koster, R. D., S. D. Schubert, and M. J. Suarez (2009). “Analyzing the Concurrence of Meteorological Droughts and Warm Periods, with Implications for the Determination of Evaporative Regime”. *Journal of Climate* 22.12, 3331–3341. JSTOR: 26260570.
- Kruijt, B., C. Jacobs, H. Berghuis, J. Biermann, R. Letting, W. Jans, R. Hutjes, and J. Veraart (2020). “Natuurlijke Klimaatbuffers – natte natuur in noord-Nederland” (Wageningen).
- Kutner, M. H., C. J. Nachtsheim, J. Neter, and W. Li (2005). *Applied Linear Statistical Models*. 5th ed. The McGraw-Hill/Irwin Series Operations and Decision Sciences. Boston: McGraw-Hill Irwin. 1396 pp.
- Lansu, E. M., C. C. van Heerwaarden, A. I. Stegehuis, and A. J. Teuling (2020). “Atmospheric Aridity and Apparent Soil Moisture Drought in European Forest During Heat Waves”. *Geophysical Research Letters* 47.6, 1–8. DOI: 10.1029/2020GL087091.
- Lazhu, K. Yang, J. Wang, Y. Lei, Y. Chen, L. Zhu, B. Ding, and J. Qin (2016). “Quantifying Evaporation and Its Decadal Change for Lake Nam Co, Central Tibetan Plateau”. *Journal of Geophysical Research: Atmospheres* 121.13, 7578–7591. DOI: 10.1002/2015JD024523.
- Le Moigne, P., J. Colin, and B. Decharme (2016). “Impact of Lake Surface Temperatures Simulated by the FLake Scheme in the CNRM-CM5 Climate Model”. *Tellus A* 68, 31274. DOI: 10.3402/tellusa.v68.31274.
- Lee, X., M. L. Goulden, D. Y. Hollinger, A. Barr, T. A. Black, G. Bohrer, R. Bracho, B. Drake, A. Goldstein, L. Gu, G. Katul, T. Kolb, B. E. Law, H. Margolis, T. Meyers, R. Monson, W. Munger, R. Oren, K. T. Paw U, A. D. Richardson, H. P. Schmid, R. Staebler, S. Wofsy, and L. Zhao (2011). “Observed Increase in Local Cooling Effect of Deforestation at Higher Latitudes”. *Nature* 479.7373, 384–387. DOI: 10.1038/nature10588.
- Leijnse, H., R. Uijlenhoet, and J. N. M. Stricker (2007). “Hydrometeorological Application of a Microwave Link: 1. Evaporation”. *Water Resources Research* 43.4, 1–9. DOI: 10.1029/2006WR004988.
- Lenters, J. D., T. K. Kratz, and C. J. Bowser (2005). “Effects of Climate Variability on Lake Evaporation: Results from a Long-Term Energy Budget Study of Sparkling Lake, Northern Wisconsin (USA)”. *Journal of Hydrology* 308.1, 168–195. DOI: 10.1016/j.jhydrol.2004.10.028.
- Lin, H., Y. Chen, H. Zhang, P. Fu, and Z. Fan (2017). “Stronger Cooling Effects of Transpiration and Leaf Physical Traits of Plants from a Hot Dry Habitat than from a Hot Wet Habitat”. *Functional Ecology* 31.12, 2202–2211. DOI: 10.1111/1365-2435.12923.



- Liu, C. and R. P. Allan (2013). “Observed and Simulated Precipitation Responses in Wet and Dry Regions 1850–2100”. *Environmental Research Letters* 8.3, 034002. DOI: 10.1088/1748-9326/8/3/034002.
- Liu, H., P. D. Blanken, T. Weidinger, A. Nordbo, and T. Vesala (2011a). “Variability in Cold Front Activities Modulating Cool-Season Evaporation from a Southern Inland Water in the USA”. *Environmental Research Letters* 6.2, 024022. DOI: 10.1088/1748-9326/6/2/024022.
- Liu, H., Y. Zhang, S. Liu, H. Jiang, L. Sheng, and Q. L. Williams (2009). “Eddy Covariance Measurements of Surface Energy Budget and Evaporation in a Cool Season over Southern Open Water in Mississippi”. *Journal of Geophysical Research: Atmospheres* 114.D4, 1–13. DOI: 10.1029/2008JD010891.
- Liu, S. M., Z. W. Xu, W. Z. Wang, Z. Z. Jia, M. J. Zhu, J. Bai, and J. M. Wang (2011b). “A Comparison of Eddy-Covariance and Large Aperture Scintillometer Measurements with Respect to the Energy Balance Closure Problem”. *Hydrology and Earth System Sciences* 15.4, 1291–1306. DOI: 10.5194/hess-15-1291-2011.
- Lobos-Roco, F., O. Hartogensis, J. Vilà-Guerau de Arellano, A. de la Fuente, R. Muñoz, J. Rutllant, and F. Suárez (2021). “Local Evaporation Controlled by Regional Atmospheric Circulation in the Altiplano of the Atacama Desert”. *Atmospheric Chemistry and Physics* 21.11, 9125–9150. DOI: 10.5194/acp-21-9125-2021.
- Loridan, T. and C. S. B. Grimmond (2012). “Characterization of Energy Flux Partitioning in Urban Environments: Links with Surface Seasonal Properties”. *Journal of Applied Meteorology and Climatology* 51.2, 219–241. DOI: 10.1175/JAMC-D-11-038.1.
- Lucatero, D., H. Madsen, J. C. Refsgaard, J. Kidmose, and K. H. Jensen (2018). “On the Skill of Raw and Post-Processed Ensemble Seasonal Meteorological Forecasts in Denmark”. *Hydrology and Earth System Sciences* 22.12, 6591–6609. DOI: 10.5194/hess-22-6591-2018.
- MacIntyre, S., J. P. Fram, P. J. Kushner, N. D. Bettez, W. J. O’Brien, J. E. Hobbie, and G. W. Kling (2009). “Climate-Related Variations in Mixing Dynamics in an Alaskan Arctic Lake”. *Limnology and Oceanography* 54 (6part2), 2401–2417. DOI: 10.4319/lo.2009.54.6\_part\_2.2401.
- Maes, W. H., P. Gentile, N. E. C. Verhoest, and D. G. Miralles (2019). “Potential Evaporation at Eddy-Covariance Sites across the Globe”. *Hydrology and Earth System Sciences* 23.2, 925–948. DOI: 10.5194/hess-23-925-2019.
- Makkink, G. F. (1957). “Testing the Penman Formula by Means of Lysimeters”. *Journal of the Institution of Water Engineers* 11.3, 277–288.
- Mammarella, I., A. Nordbo, Ü. Rannik, S. Haapanala, J. Levula, H. Laakso, A. Ojala, O. Peltola, J. Heiskanen, J. Pumpanen, and T. Vesala (2015). “Carbon Dioxide and Energy Fluxes over a Small Boreal Lake in Southern Finland”. *Journal of Geophysical Research: Biogeosciences* 120.7, 1296–1314. DOI: 10.1002/2014JG002873.
- Martens, B., R. de Jeu, N. Verhoest, H. Schuurmans, J. Kleijer, and D. Gonzalez Miralles (2018). “Towards Estimating Land Evaporation at Field Scales Using GLEAM”. *Remote Sensing* 10.11, 1–25. DOI: <http://dx.doi.org/10.3390/rs10111720>.
- Masoner, J. R. and D. I. Stannard (2010). “A Comparison of Methods for Estimating Open-Water Evaporation in Small Wetlands”. *Wetlands* 30.3, 513–524. DOI: 10.1007/s13157-010-0041-y.
- Massman, W. J. (2000). “A Simple Method for Estimating Frequency Response Corrections for Eddy Covariance Systems”. *Agricultural and Forest Meteorology* 104.3, 185–198. DOI: 10.1016/S0168-1923(00)00164-7.
- Mauder, M., M. Cuntz, C. Drüe, A. Graf, C. Rebmann, H. P. Schmid, M. Schmidt, and R. Steinbrecher (2013). “A Strategy for Quality and Uncertainty Assessment of Long-Term Eddy-Covariance Measurements”. *Agricultural and Forest Meteorology* 169, 122–135. DOI: 10.1016/j.agrformet.2012.09.006.

- Mauder, M. and T. Foken (2004). *Documentation and Instruction Manual of the Eddy Covariance Software Package TK2*. Arbeitsergebnisse 26. Universität Bayreuth, Abt. Mikrometeorologie, 44.
- Mauder, M., T. Foken, and J. Cuxart (2020). “Surface-Energy-Balance Closure over Land: A Review”. *Boundary-Layer Meteorology* 177.2, 395–426. DOI: 10.1007/s10546-020-00529-6.
- McGloin, R., H. McGowan, D. McJannet, F. Cook, A. Sogachev, and S. Burn (2014). “Quantification of Surface Energy Fluxes from a Small Water Body Using Scintillometry and Eddy Covariance”. *Water Resources Research* 50.1, 494–513. DOI: 10.1002/2013WR013899.
- McJannet, D. L., F. J. Cook, R. P. McGloin, H. A. McGowan, and S. Burn (2011). “Estimation of Evaporation and Sensible Heat Flux from Open Water Using a Large-Aperture Scintillometer”. *Water Resources Research* 47.5, 1–14. DOI: 10.1029/2010WR010155.
- McMahon, T. A., B. L. Finlayson, and M. C. Peel (2016). “Historical Developments of Models for Estimating Evaporation Using Standard Meteorological Data”. *WIREs Water* 3.6, 788–818. DOI: 10.1002/wat2.1172.
- McMahon, T. A., M. C. Peel, L. Lowe, R. Srikanthan, and T. R. McVicar (2013). “Estimating Actual, Potential, Reference Crop and Pan Evaporation Using Standard Meteorological Data: A Pragmatic Synthesis”. *Hydrology and Earth System Sciences* 17.4, 1331–1363. DOI: 10.5194/hess-17-1331-2013.
- McPherson, R. A. (2007). “A Review of Vegetation—Atmosphere Interactions and Their Influences on Mesoscale Phenomena”. *Progress in Physical Geography: Earth and Environment* 31.3, 261–285. DOI: 10.1177/0309133307079055.
- McVicar, T. R., M. L. Roderick, R. J. Donohue, L. T. Li, T. G. Van Niel, A. Thomas, J. Grieser, D. Jhajharia, Y. Himri, N. M. Mahowald, A. V. Mescherskaya, A. C. Kruger, S. Rehman, and Y. Dinpashoh (2012). “Global Review and Synthesis of Trends in Observed Terrestrial Near-Surface Wind Speeds: Implications for Evaporation”. *Journal of Hydrology* 416, 182–205. DOI: 10.1016/j.jhydrol.2011.10.024.
- Meijninger, W. M. L., O. K. Hartogensis, W. Kohsiek, J. C. B. Hoedjes, R. M. Zuurbier, and H. A. R. De Bruin (2002). “Determination of Area-Averaged Sensible Heat Fluxes with a Large Aperture Scintillometer over a Heterogeneous Surface – Flevoland Field Experiment”. *Boundary-Layer Meteorology* 105.1, 37–62. DOI: 10.1023/A:1019647732027.
- Melsen, L. A., N. Addor, N. Mizukami, A. J. Newman, P. J. J. F. Torfs, M. P. Clark, R. Uijlenhoet, and A. J. Teuling (2018). “Mapping (Dis)Agreement in Hydrologic Projections”. *Hydrology and Earth System Sciences* 22.3, 1775–1791. DOI: 10.5194/hess-22-1775-2018.
- Metzger, J., M. Nied, U. Corsmeier, J. Kleffmann, and C. Kottmeier (2018). “Dead Sea Evaporation by Eddy Covariance Measurements vs. Aerodynamic, Energy Budget, Priestley–Taylor, and Penman Estimates”. *Hydrology and Earth System Sciences* 22.2, 1135–1155. DOI: 10.5194/hess-22-1135-2018.
- Middelkoop, H., K. Daamen, D. Gellens, W. Grabs, J. C. J. Kwadijk, H. Lang, J. Schulla, and K. Wilke (2001). “Impact of Climate Change on Hydrological Regimes and Water Resources Management in the Rhine Basin.” *Climatic Change* 49, 105–128. DOI: 10.1023/A:1010784727448.
- Miralles, D. G., W. Brutsaert, A. J. Dolman, and J. H. Gash (2020). “On the Use of the Term “Evapo-transpiration””. *Water Resources Research* 56.11, 1–5. DOI: 10.1029/2020WR028055.
- Miralles, D. G., T. R. H. Holmes, R. A. M. D. Jeu, J. H. Gash, A. G. C. A. Meesters, and A. J. Dolman (2011). “Global Land-Surface Evaporation Estimated from Satellite-Based Observations”. *Hydrology and Earth System Sciences* 15.2, 453–469. DOI: 10.5194/hess-15-453-2011.
- Miralles, D. G., P. Gentile, S. I. Seneviratne, and A. J. Teuling (2019). “Land–Atmospheric Feedbacks during Droughts and Heatwaves: State of the Science and Current Challenges”. *Annals of the New York Academy of Sciences* 1436.1, 19–35. DOI: 10.1111/nyas.13912.

- Miralles, D. G., A. J. Teuling, C. C. van Heerwaarden, and J. Vilà-Guerau de Arellano (2014). “Mega-Heatwave Temperatures Due to Combined Soil Desiccation and Atmospheric Heat Accumulation”. *Nature Geoscience* 7.5, 345–349. DOI: 10.1038/ngeo2141.
- Mironov, D. V. (2008). *Parameterization of Lakes in Numerical Weather Prediction – Description of a Lake Model*. COSMO Technical Report No. 11. Offenbach am Main, Germany: Deutscher Wetterdienst, 41.
- Moene, A. F. and J. C. van Dam (2014). *Transport in the Atmosphere-Vegetation-Soil Continuum*. New York: Cambridge University Press. 436 pp.
- Moncrieff, J., R. Clement, J. Finnigan, and T. Meyers (2004). “Averaging, Detrending, and Filtering of Eddy Covariance Time Series”. In: *Handbook of Micrometeorology: A Guide for Surface Flux Measurement and Analysis*. Ed. by X. Lee, W. Massman, and B. Law. Atmospheric and Oceanographic Sciences Library. Dordrecht: Springer Netherlands, 7–31. DOI: 10.1007/1-4020-2265-4\_2.
- Monteith, J. L. (1965). “Evaporation and Environment”. *Symposia of the Society for Experimental Biology* 19, 205–234.
- Moors, E., H. (Dolman, J. Elbers, A. Hensen, J. Duyzer, P. Kroon, E. Veenendaal, Ko, K. Van Huissteden, F. Bosveld, C. Jacobs, W. Jans, P. Kuikman, L. Nol, and C. Beek (2012). *Integrated Observations and Modelling of Greenhouse Gas Budgets at the Ecosystem Level in The Netherlands*. KvR 055/12: National Research Programme Climate changes Spatial Planning, 61.
- Moors, E. J. (2012). “Water Use of Forests in The Netherlands”. PhD thesis. Amsterdam: Vrije Universiteit Amsterdam.
- Muñoz Sabater, J. (2021). *ERA5-Land Hourly Data from 1950 to 1980*. Copernicus Climate Change Service (C3S). DOI: 10.24381/cds.e2161bac.
- Nordbo, A., S. Launiainen, I. Mammarella, M. Leppäranta, J. Huotari, A. Ojala, and T. Vesala (2011). “Long-Term Energy Flux Measurements and Energy Balance over a Small Boreal Lake Using Eddy Covariance Technique”. *Journal of Geophysical Research: Atmospheres* 116.D2, 1–17. DOI: 10.1029/2010JD014542.
- Oki, T. and S. Kanae (2006). “Global Hydrological Cycles and World Water Resources”. *Science* 313.5790, 1068–1072. DOI: 10.1126/science.1128845. pmid: 16931749.
- Orlowsky, B. and S. I. Seneviratne (2010). “Statistical Analyses of Land–Atmosphere Feedbacks and Their Possible Pitfalls”. *Journal of Climate* 23.14, 3918–3932. DOI: 10.1175/2010JCLI3366.1.
- Penman, H. L. (1956). “Evaporation: An Introductory Survey.” *Netherlands Journal of Agricultural Science* 4.1, 9–29. DOI: 10.18174/njas.v4i1.17768.
- Penman, H. L. (1948). “Natural Evaporation from Open Water, Bare Soil and Grass”. *Proceedings of the Royal Society of London. Series A. Mathematical and Physical Sciences* 193.1032, 120–145. DOI: 10.1098/rspa.1948.0037.
- Perrault, P. (1674). *De l’origine des fontaines*. Paris: Pierre Le Petit. 353 pp.
- Pielke, R. A. and R. Avissar (1990). “Influence of Landscape Structure on Local and Regional Climate”. *Landscape Ecology* 4.2, 133–155. DOI: 10.1007/BF00132857.
- Pinker, R. T., A. Bentamy, K. B. Katsaros, Y. Ma, and C. Li (2014). “Estimates of Net Heat Fluxes over the Atlantic Ocean”. *Journal of Geophysical Research: Oceans* 119.1, 410–427. DOI: 10.1002/2013JC009386.
- Pool, S., F. Francés, A. Garcia-Prats, M. Pulido-Velazquez, C. Sanchis-Ibor, M. Schirmer, H. Yang, and J. Jiménez-Martínez (2021). “From Flood to Drip Irrigation Under Climate Change: Impacts on Evapotranspiration and Groundwater Recharge in the Mediterranean Region of Valencia (Spain)”. *Earth’s Future* 9.5, 1–20. DOI: 10.1029/2020EF001859.

- Potes, M., R. Salgado, M. J. Costa, M. Morais, D. Bortoli, I. Kostadinov, and I. Mammarella (2017). “Lake–Atmosphere Interactions at Alqueva Reservoir: A Case Study in the Summer of 2014”. *Tellus A: Dynamic Meteorology and Oceanography* 69.1, 1272787. DOI: 10.1080/16000870.2016.1272787.
- Priestley, C. H. B. and R. J. Taylor (1972). “On the Assessment of Surface Heat Flux and Evaporation Using Large-Scale Parameters”. *Monthly Weather Review* 100.2, 81–92. DOI: 10.1175/1520-0493(1972)100<0081:OTAOSH>2.3.CO;2.
- Prinsen, G., F. Sperna Weiland, and E. Ruijgh (2015). “The Delta Model for Fresh Water Policy Analysis in the Netherlands”. *Water Resources Management* 29.2, 645–661. DOI: 10.1007/s11269-014-0880-z.
- Pruitt, W. and D. Angus (1960). “Large weighing lysimeter for measuring evapotranspiration”. *American Society of Agricultural and Biological Engineers* 3.2, 13–15. DOI: 10.13031/2013.41105.
- Renner, M., C. Brenner, K. Mallick, H.-D. Wizemann, L. Conte, I. Trebs, J. Wei, V. Wulfmeyer, K. Schulz, and A. Kleidon (2019). “Using Phase Lags to Evaluate Model Biases in Simulating the Diurnal Cycle of Evapotranspiration: A Case Study in Luxembourg”. *Hydrology and Earth System Sciences* 23.1, 515–535. DOI: 10.5194/hess-23-515-2019.
- Rijksoverheid (2022). *Kamerbrief over rol Water en Bodem bij ruimtelijke ordening*. <https://www.rijksoverheid.nl/documenten/kamerstukken/2022/11/25/water-en-bodem-sturend>. (Last accessed 25 January 2023).
- Rosenberry, D. O., T. C. Winter, D. C. Buso, and G. E. Likens (2007). “Comparison of 15 Evaporation Methods Applied to a Small Mountain Lake in the Northeastern USA”. *Journal of Hydrology* 340.3, 149–166. DOI: 10.1016/j.jhydrol.2007.03.018.
- Running, S. W., D. D. Baldocchi, D. P. Turner, S. T. Gower, P. S. Bakwin, and K. A. Hibbard (1999). “A Global Terrestrial Monitoring Network Integrating Tower Fluxes, Flask Sampling, Ecosystem Modeling and EOS Satellite Data”. *Remote Sensing of Environment* 70.1, 108–127. DOI: 10.1016/S0034-4257(99)00061-9.
- Savenije, H. H. G. (2004). “The Importance of Interception and Why We Should Delete the Term Evapotranspiration from Our Vocabulary”. *Hydrological Processes* 18.8, 1507–1511. DOI: 10.1002/hyp.5563.
- Schär, C., P. L. Vidale, D. Lüthi, C. Frei, C. Häberli, M. A. Liniger, and C. Appenzeller (2004). “The Role of Increasing Temperature Variability in European Summer Heatwaves”. *Nature* 427.6972, 332–336. DOI: 10.1038/nature02300.
- Schilperoort, B., M. Coenders-Gerrits, W. Luxemburg, C. Jiménez Rodríguez, C. Cisneros Vaca, and H. Savenije (2018). “Technical Note: Using Distributed Temperature Sensing for Bowen Ratio Evaporation Measurements”. *Hydrology and Earth System Sciences* 22.1, 819–830. DOI: 10.5194/hess-22-819-2018.
- Schmid, M. and O. Köster (2016). “Excess Warming of a Central European Lake Driven by Solar Brightening”. *Water Resources Research* 52.10, 8103–8116. DOI: 10.1002/2016WR018651.
- Schotanus, P., F. Nieuwstadt, and H. De Bruin (1983). “Temperature Measurement with a Sonic Anemometer and Its Application to Heat and Moisture Fluxes”. *Boundary-Layer Meteorology* 26.1, 81–93. DOI: 10.1007/BF00164332.
- Senay, G. B., S. Kagone, and N. M. Velpuri (2020). “Operational Global Actual Evapotranspiration: Development, Evaluation, and Dissemination”. *Sensors* 20.7, 1915. DOI: 10.3390/s20071915.
- Seneviratne, S. I., T. Corti, E. L. Davin, M. Hirschi, E. B. Jaeger, I. Lehner, B. Orlowsky, and A. J. Teuling (2010). “Investigating Soil Moisture–Climate Interactions in a Changing Climate: A Review”. *Earth-Science Reviews* 99.3, 125–161. DOI: 10.1016/j.earscirev.2010.02.004.

- Seneviratne, S. I., I. Lehner, J. Gurtz, A. J. Teuling, H. Lang, U. Moser, D. Grebner, L. Menzel, K. Schrott, T. Vitvar, and M. Zappa (2012a). “Swiss Prealpine Rietholzbach Research Catchment and Lysimeter: 32 Year Time Series and 2003 Drought Event”. *Water Resources Research* 48.6, 1–20. DOI: 10.1029/2011WR011749.
- Seneviratne, S. I., D. Lüthi, M. Litschi, and C. Schär (2006). “Land–Atmosphere Coupling and Climate Change in Europe”. *Nature* 443.7108, 205–209. DOI: 10.1038/nature05095.
- Seneviratne, S. I., N. Nicholls, D. Easterling, C. M. Goodess, S. Kanae, J. Kossin, Y. Luo, J. Marengo, K. McInnes, M. Rahimi, M. Reichstein, A. Sorteberg, C. Vera, X. Zhang, M. Rusticucci, V. Semenov, L. V. Alexander, S. Allen, G. Benito, T. Cavazos, J. Clague, D. Conway, P. M. Della-Marta, M. Gerber, S. Gong, B. N. Goswami, M. Hemer, C. Huggel, B. van den Hurk, V. V. Kharin, A. Kitoh, A. M. K. Tank, G. Li, S. Mason, W. McGuire, G. J. van Oldenborgh, B. Orlowsky, S. Smith, W. Thiaw, A. Velegrakis, P. Yiou, T. Zhang, T. Zhou, and F. W. Zwiers (2012b). “Changes in Climate Extremes and Their Impacts on the Natural Physical Environment”. In: *Managing the Risks of Extreme Events and Disasters to Advance Climate Change Adaptation*. Ed. by C. B. Field, V. Barros, T. F. Stocker, and Q. Dahe. Cambridge: Cambridge University Press, 109–230. DOI: 10.1017/CB09781139177245.006.
- Solcerova, A., F. van de Ven, and N. van de Giesen (2019). “Nighttime Cooling of an Urban Pond”. *Frontiers in Earth Science* 7, 1–10. DOI: 10.3389/feart.2019.00156.
- Steenefeld, G. J., L. F. Tolk, A. F. Moene, O. K. Hartogensis, W. Peters, and A. a. M. Holtslag (2011). “Confronting the WRF and RAMS Mesoscale Models with Innovative Observations in the Netherlands: Evaluating the Boundary Layer Heat Budget”. *Journal of Geophysical Research: Atmospheres* 116.D23, 1–16. DOI: 10.1029/2011JD016303.
- Steenefeld, G.-J., S. Horst, and B. Heusinkveld (2020). “Observing the Surface Radiation and Energy Balance, Carbon Dioxide and Methane Fluxes over the City Centre of Amsterdam”. In: EGU General Assembly. DOI: 10.5194/egusphere-egu2020-1547.
- Stelling, E. (1882). “Ueber Die Abhängigkeit Der Verdunstung Des Wassers von Seiner Temperatur Und von Der Feuchtigkeit Und Bewegung Der Luft (Vorgelegt 1881)”. *Österreichische Gesellschaft für Meteorologie* 17, 372–373.
- Su, Z. (2002). “The Surface Energy Balance System (SEBS) for Estimation of Turbulent Heat Fluxes”. *Hydrology and Earth System Sciences* 6.1, 85–100. DOI: 10.5194/hess-6-85-2002.
- Sumner, D. M. and J. M. Jacobs (2005). “Utility of Penman–Monteith, Priestley–Taylor, Reference Evapotranspiration, and Pan Evaporation Methods to Estimate Pasture Evapotranspiration”. *Journal of Hydrology* 308.1, 81–104. DOI: 10.1016/j.jhydrol.2004.10.023.
- Sun, G., A. Noormets, J. Chen, and S. G. McNulty (2008). “Evapotranspiration Estimates from Eddy Covariance Towers and Hydrologic Modeling in Managed Forests in Northern Wisconsin, USA”. *Agricultural and Forest Meteorology*. Chequamegon Ecosystem–Atmosphere Study Special Issue: Ecosystem–Atmosphere Carbon and Water Cycling in the Temperate Northern Forests of the Great Lakes Region 148.2, 257–267. DOI: 10.1016/j.agrformet.2007.08.010.
- Swank, W. T. and J. E. Douglass (1974). “Streamflow Greatly Reduced by Converting Deciduous Hardwood Stands to Pine”. *Science* 185.4154, 857–859. DOI: 10.1126/science.185.4154.857.
- Swinbank, W. C. (1951). “The Measurement of Vertical Transfer of Heat and Water Vapor by Eddies in the Lower Atmosphere”. *Journal of Atmospheric Sciences* 8, 135–145. DOI: 10.1175/1520-0469(1951)008<0135:TM0VTO>2.0.CO;2.
- Tanny, J., S. Cohen, S. Assouline, F. Lange, A. Grava, D. Berger, B. Teltch, and M. B. Parlange (2008). “Evaporation from a Small Water Reservoir: Direct Measurements and Estimates”. *Journal of Hydrology* 351.1, 218–229. DOI: 10.1016/j.jhydrol.2007.12.012.

- Teuling, A. J., M. Hirschi, A. Ohmura, M. Wild, M. Reichstein, P. Ciais, N. Buchmann, C. Ammann, L. Montagnani, A. D. Richardson, G. Wohlfahrt, and S. I. Seneviratne (2009). “A Regional Perspective on Trends in Continental Evaporation”. *Geophysical Research Letters* 36.2, 1–5. DOI: 10.1029/2008GL036584.
- Teuling, A. J., S. I. Seneviratne, C. Williams, and P. A. Troch (2006). “Observed Timescales of Evapotranspiration Response to Soil Moisture”. *Geophysical Research Letters* 33.23, 1–5. DOI: 10.1029/2006GL028178.
- Teuling, A. J. (2018a). “A Forest Evapotranspiration Paradox Investigated Using Lysimeter Data”. *Vadose Zone Journal* 17.1, 1–7. DOI: 10.2136/vzj2017.01.0031.
- (2018b). “A Hot Future for European Droughts”. *Nature Climate Change* 8.5, 364–365. DOI: 10.1038/s41558-018-0154-5.
- Teuling, A. J., E. A. G. de Badts, F. A. Jansen, R. Fuchs, J. Buitink, A. J. Hoek van Dijke, and S. M. Sterling (2019). “Climate Change, Reforestation/Afforestation, and Urbanization Impacts on Evapotranspiration and Streamflow in Europe”. *Hydrology and Earth System Sciences* 23.9, 3631–3652. DOI: 10.5194/hess-23-3631-2019.
- Teuling, A. J. and A. J. Hoek van Dijke (2020). “Forest Age and Water Yield”. *Nature* 578.7794, E16–E18. DOI: 10.1038/s41586-020-1941-5.
- Teuling, A. J., S. I. Seneviratne, R. Stöckli, M. Reichstein, E. Moors, P. Ciais, S. Luyssaert, B. van den Hurk, C. Ammann, C. Bernhofer, E. Dellwik, D. Gianelle, B. Gielen, T. Grünwald, K. Klumpp, L. Montagnani, C. Moureaux, M. Sottocornola, and G. Wohlfahrt (2010). “Contrasting Response of European Forest and Grassland Energy Exchange to Heatwaves”. *Nature Geoscience* 3.10, 722–727. DOI: 10.1038/ngeo950.
- Teuling, A. J., A. F. Van Loon, S. I. Seneviratne, I. Lehner, M. Aubinet, B. Heinesch, C. Bernhofer, T. Grünwald, H. Prasse, and U. Spank (2013). “Evapotranspiration Amplifies European Summer Drought”. *Geophysical Research Letters* 40.10, 2071–2075. DOI: 10.1002/grl.50495.
- Thorntwaite, C. W. (1948). “An Approach toward a Rational Classification of Climate”. *Geographical Review* 38.1, 55–94. DOI: 10.2307/210739. JSTOR: 210739.
- TNO (2022). *DINOloket - Data and Information on the Dutch Subsurface*. <https://www.dinoloket.nl/> (Last accessed 18 November 2022).
- Trenberth, K. E., A. Dai, G. van der Schrier, P. D. Jones, J. Barichivich, K. R. Briffa, and J. Sheffield (2014). “Global Warming and Changes in Drought”. *Nature Climate Change* 4.1, 17–22. DOI: 10.1038/nclimate2067.
- Van der Ent, R. J., H. H. G. Savenije, B. Schaeffli, and S. C. Steele-Dunne (2010). “Origin and Fate of Atmospheric Moisture over Continents”. *Water Resources Research* 46.9, 1–12. DOI: 10.1029/2010WR009127.
- Van der Laan, S. (2010). “Validation of the Greenhouse Gas Balance of the Netherlands. Observational Constraints on CO<sub>2</sub>, CH<sub>4</sub> and N<sub>2</sub>O from Atmospheric Monitoring Station Lutsjewad.” PhD thesis. Groningen: University of Groningen.
- Van der Velde, Y., S. W. Lyon, and G. Destouni (2013). “Data-Driven Regionalization of River Discharges and Emergent Land Cover–Evapotranspiration Relationships across Sweden”. *Journal of Geophysical Research: Atmospheres* 118.6, 2576–2587. DOI: 10.1002/jgrd.50224.
- Van der Zaan, T. and S. Van ‘t Hof (2022). “Regeneration of Degraded Land with Nature-based Solutions (NBS)”. In: *Design for Regenerative Cities and Landscapes: Rebalancing Human Impact and Natural Environment*. Ed. by R. Roggema. Contemporary Urban Design Thinking. Cham: Springer International Publishing, 173–196. DOI: 10.1007/978-3-030-97023-9\_8.

- Van Emmerik, T., A. Rimmer, Y. Lechinsky, K. Wenker, S. Nussboim, and N. van de Giesen (2013). “Measuring Heat Balance Residual at Lake Surface Using Distributed Temperature Sensing”. *Limnology and Oceanography: Methods* 11.2, 79–90. DOI: 10.4319/lom.2013.11.79.
- Van Engelenburg, J. (2020). “Towards Sustainable Drinking Water Supply in the Netherlands”. PhD thesis. Wageningen: Wageningen University. 230 pp.
- Van Meijgaard, E., L. H. Van Ulft, W. J. Van de Berg, F. C. Bosveld, B. J. J. M. Van den Hurk, G. Lenderink, and A. P. Siebesma (2008). *The KNMI Regional Atmospheric Climate Model RACMO, Version 2.1*. Technical Report TR-302. De Bilt: KNMI, 50.
- Van Dijk, A. I. J. M., J. H. Gash, E. van Gorsel, P. D. Blanken, A. Cescatti, C. Emmel, B. Gielen, I. N. Harman, G. Kiely, L. Merbold, L. Montagnani, E. Moors, M. Sottocornola, A. Varlagin, C. A. Williams, and G. Wohlfahrt (2015). “Rainfall Interception and the Coupled Surface Water and Energy Balance”. *Agricultural and Forest Meteorology* 214–215, 402–415. DOI: 10.1016/j.agrformet.2015.09.006.
- Venäläinen, A., M. Frech, M. Heikinheimo, and A. Grelle (1999). “Comparison of Latent and Sensible Heat Fluxes over Boreal Lakes with Concurrent Fluxes over a Forest: Implications for Regional Averaging”. *Agricultural and Forest Meteorology* 98–99, 535–546. DOI: 10.1016/S0168-1923(99)00100-8.
- Verburg, P. and R. E. Hecky (2009). “The Physics of the Warming of Lake Tanganyika by Climate Change”. *Limnology and Oceanography* 54 (6part2), 2418–2430. DOI: 10.4319/lo.2009.54.6\_part\_2.2418.
- Vercauteren, N., E. Bou-Zeid, H. Huwald, M. B. Parlange, and W. Brutsaert (2009). “Estimation of Wet Surface Evaporation from Sensible Heat Flux Measurements”. *Water Resources Research* 45.6, 1–7. DOI: 10.1029/2008WR007544.
- Verhagen, F., T. Spek, F. Witte, B. Voortman, E. Moors, E. Querner, G. Eertwegh, and J. van Bakel (2014). “Expertdialog de Veluwe. Begrijpen We Het Watersysteem?” *Stromingen* 20.3, 49–64.
- Vermeulen, M. H., B. J. Kruijt, T. Hickler, and P. Kabat (2015). “Modelling Short-Term Variability in Carbon and Water Exchange in a Temperate Scots Pine Forest”. *Earth System Dynamics* 6.2, 485–503. DOI: 10.5194/esd-6-485-2015.
- Vesala, T., J. Huotari, Ü. Rannik, T. Suni, S. Smolander, A. Sogachev, S. Launiainen, and A. Ojala (2006). “Eddy Covariance Measurements of Carbon Exchange and Latent and Sensible Heat Fluxes over a Boreal Lake for a Full Open-Water Period”. *Journal of Geophysical Research: Atmospheres* 111.D11, 1–12. DOI: 10.1029/2005JD006365.
- Vickers, D. and L. Mahrt (1997). “Quality Control and Flux Sampling Problems for Tower and Aircraft Data”. *Journal of Atmospheric and Oceanic Technology* 14.3, 512–526. DOI: 10.1175/1520-0426(1997)014<0512:QCAFSP>2.0.CO;2.
- Vilà-Guerau de Arellano, J., O. Hartogensis, I. Benedict, H. de Boer, P. J. M. Bosman, S. Botía, M. A. Cecchini, K. A. P. Faassen, R. González-Armas, K. van Diepen, B. G. Heusinkveld, M. Janssens, F. Lobos-Roco, I. T. Luijkx, L. A. T. Machado, M. R. Mangan, A. F. Moene, W. B. Mol, M. van der Molen, R. Moonen, H. G. Ouwersloot, S.-W. Park, X. Pedruzo-Bagazgoitia, T. Röckmann, G. A. Adnew, R. Ronda, M. Sikma, R. Schulte, B. J. H. van Stratum, M. A. Veerman, M. C. van Zanten, and C. C. van Heerwaarden (2023). “Advancing Understanding of Land–Atmosphere Interactions by Breaking Discipline and Scale Barriers”. *Annals of the New York Academy of Sciences* Online version before inclusion in an issue. DOI: 10.1111/nyas.14956.
- Voortman, B. R., R. P. Bartholomeus, S. E. A. T. M. van der Zee, M. F. P. Bierkens, and J. P. M. Witte (2015). “Quantifying Energy and Water Fluxes in Dry Dune Ecosystems of the Netherlands”. *Hydrology and Earth System Sciences* 19.9, 3787–3805. DOI: 10.5194/hess-19-3787-2015.
- Vörösmarty, C. J. (2000). “Global Water Resources: Vulnerability from Climate Change and Population Growth”. *Science* 289.5477, 284–288. DOI: 10.1126/science.289.5477.284.

- Vörösmarty, C. J., C. Lévéque, and C. Revenga (2005). “Chapter 7: Fresh Water”. In: *Ecosystems and Human Well-being: Current State and Trends*. Washington, DC: Island Press, 165–207.
- Voskamp, T. (2018). “The Evaporation of Lake IJssel - Comparison of the FLake Model with Standard Methods at Multiple Timescales for Estimating Evaporation Rates”. MSc thesis report. Wageningen: Wageningen University.
- Wang, L., S. P. Good, and K. K. Caylor (2014a). “Global Synthesis of Vegetation Control on Evapotranspiration Partitioning”. *Geophysical Research Letters* 41.19, 6753–6757. DOI: 10.1002/2014GL061439.
- Wang, W., X. Lee, W. Xiao, S. Liu, N. Schultz, Y. Wang, M. Zhang, and L. Zhao (2018). “Global Lake Evaporation Accelerated by Changes in Surface Energy Allocation in a Warmer Climate”. *Nature Geoscience* 11.6, 410. DOI: 10.1038/s41561-018-0114-8.
- Wang, W., W. Xiao, C. Cao, Z. Gao, Z. Hu, S. Liu, S. Shen, L. Wang, Q. Xiao, J. Xu, D. Yang, and X. Lee (2014b). “Temporal and Spatial Variations in Radiation and Energy Balance across a Large Freshwater Lake in China”. *Journal of Hydrology* 511, 811–824. DOI: 10.1016/j.jhydrol.2014.02.012.
- Wang-Erlandsson, L., R. J. van der Ent, L. J. Gordon, and H. H. G. Savenije (2014). “Contrasting Roles of Interception and Transpiration in the Hydrological Cycle &ndash; Part 1: Temporal Characteristics over Land”. *Earth System Dynamics* 5.2, 441–469. DOI: 10.5194/esd-5-441-2014.
- Wannasin, C., C. C. Brauer, R. Uijlenhoet, W. J. van Verseveld, and A. H. Weerts (2021). “Daily Flow Simulation in Thailand Part II: Unraveling Effects of Reservoir Operation”. *Journal of Hydrology: Regional Studies* 34, 100792. DOI: 10.1016/j.ejrh.2021.100792.
- Webb, E. K., G. I. Pearman, and R. Leuning (1980). “Correction of Flux Measurements for Density Effects Due to Heat and Water Vapour Transfer”. *Quarterly Journal of the Royal Meteorological Society* 106.447, 85–100. DOI: 10.1002/qj.49710644707.
- Weisman, R. N. and W. Brutsaert (1973). “Evaporation and Cooling of a Lake under Unstable Atmospheric Conditions”. *Water Resources Research* 9.5, 1242–1257. DOI: 10.1029/WR009i005p01242.
- Wieringa, J. (2019). *Metingen van het Flevo-1967 verdampingsonderzoek*. Technical Report. De Bilt: KNMI, 1–9.
- Wilczak, J. M., S. P. Oncley, and S. A. Stage (2001). “Sonic Anemometer Tilt Correction Algorithms”. *Boundary-Layer Meteorology* 99.1, 127–150. DOI: 10.1023/A:1018966204465.
- Williams, C. A. and J. D. Albertson (2004). “Soil Moisture Controls on Canopy-Scale Water and Carbon Fluxes in an African Savanna”. *Water Resources Research* 40.9, 1–14. DOI: 10.1029/2004WR003208.
- Williams, C. A., M. Reichstein, N. Buchmann, D. Baldocchi, C. Beer, C. Schwalm, G. Wohlfahrt, N. Hasler, C. Bernhofer, T. Foken, D. Papale, S. Schymanski, and K. Schaefer (2012). “Climate and Vegetation Controls on the Surface Water Balance: Synthesis of Evapotranspiration Measured across a Global Network of Flux Towers”. *Water Resources Research* 48.6, 1–13. DOI: 10.1029/2011WR011586.
- Williams, I. N., J. M. Lee, J. Tadić, Y. Zhang, and H. Chu (2020). “Modeling Spatial Heterogeneity in Surface Turbulent Heat Flux in the U.S. Southern Great Plains”. *Journal of Geophysical Research: Atmospheres* 125.13, 1–19. DOI: 10.1029/2019JD032255.
- Wilson, K., A. Goldstein, E. Falge, M. Aubinet, D. Baldocchi, P. Berbigier, C. Bernhofer, R. Ceulemans, H. Dolman, C. Field, A. Grelle, A. Ibrom, B. E. Law, A. Kowalski, T. Meyers, J. Moncrieff, R. Monson, W. Oechel, J. Tenhunen, R. Valentini, and S. Verma (2002a). “Energy Balance Closure at FLUXNET Sites”. *Agricultural and Forest Meteorology*. FLUXNET 2000 Synthesis 113.1, 223–243. DOI: 10.1016/S0168-1923(02)00109-0.
- Wilson, K. B., D. D. Baldocchi, M. Aubinet, P. Berbigier, C. Bernhofer, H. Dolman, E. Falge, C. Field, A. Goldstein, A. Granier, A. Grelle, T. Halldor, D. Hollinger, G. Katul, B. E. Law, A. Lindroth, T. Meyers, J. Moncrieff, R. Monson, W. Oechel, J. Tenhunen, R. Valentini, S. Verma, T. Vesala, and S. Wofsy



- (2002b). “Energy Partitioning between Latent and Sensible Heat Flux during the Warm Season at FLUXNET Sites”. *Water Resources Research* 38.12, 1–11. DOI: 10.1029/2001WR000989.
- Wilson, K. B., P. J. Hanson, and D. D. Baldocchi (2000). “Factors Controlling Evaporation and Energy Partitioning beneath a Deciduous Forest over an Annual Cycle”. *Agricultural and Forest Meteorology* 102.2, 83–103. DOI: 10.1016/S0168-1923(00)00124-6.
- Witte, J.-P. M., B. Voortman, K. Nijhuis, M. van Huijgevoort, and S. Rijpkema (2019). “Met het historische landschap verdween er water van de Veluwe”. *Stromingen* 33.1, 91–108.
- Woolway, R. I., B. M. Kraemer, J. D. Lenters, C. J. Merchant, C. M. O’Reilly, and S. Sharma (2020). “Global Lake Responses to Climate Change”. *Nature Reviews Earth & Environment* 1.8, 388–403. DOI: 10.1038/s43017-020-0067-5.
- Woolway, R. I., P. Verburg, J. D. Lenters, C. J. Merchant, D. P. Hamilton, J. Brookes, E. de Eyto, S. Kelly, N. C. Healey, S. Hook, A. Laas, D. Pierson, J. A. Rusak, J. Kuha, J. Karjalainen, K. Kallio, A. Lepistö, and I. D. Jones (2018). “Geographic and Temporal Variations in Turbulent Heat Loss from Lakes: A Global Analysis across 45 Lakes”. *Limnology and Oceanography* 63.6, 2436–2449. DOI: 10.1002/lno.10950.
- Xiao, J., Q. Zhuang, B. E. Law, D. D. Baldocchi, J. Chen, A. D. Richardson, J. M. Melillo, K. J. Davis, D. Y. Hollinger, S. Wharton, R. Oren, A. Noormets, M. L. Fischer, S. B. Verma, D. R. Cook, G. Sun, S. McNulty, S. C. Wofsy, P. V. Bolstad, S. P. Burns, P. S. Curtis, B. G. Drake, M. Falk, D. R. Foster, L. Gu, J. L. Hadley, G. G. Katul, M. Litvak, S. Ma, T. A. Martin, R. Matamala, T. P. Meyers, R. K. Monson, J. W. Munger, W. C. Oechel, U. K. T. Paw, H. P. Schmid, R. L. Scott, G. Starr, A. E. Suyker, and M. S. Torn (2011). “Assessing Net Ecosystem Carbon Exchange of U.S. Terrestrial Ecosystems by Integrating Eddy Covariance Flux Measurements and Satellite Observations”. *Agricultural and Forest Meteorology* 151.1, 60–69. DOI: 10.1016/j.agrformet.2010.09.002.
- Xu, R., Y. Li, A. J. Teuling, L. Zhao, D. V. Spracklen, L. Garcia-Carreras, R. Meier, L. Chen, Y. Zheng, H. Lin, and B. Fu (2022). “Contrasting Impacts of Forests on Cloud Cover Based on Satellite Observations”. *Nature Communications* 13.1, 670. DOI: 10.1038/s41467-022-28161-7.
- Yang, D., S. Li, S. Kang, T. Du, P. Guo, X. Mao, L. Tong, X. Hao, R. Ding, and J. Niu (2020). “Effect of Drip Irrigation on Wheat Evapotranspiration, Soil Evaporation and Transpiration in Northwest China”. *Agricultural Water Management* 232, 106001. DOI: 10.1016/j.agwat.2020.106001.
- Yuan, K., Q. Zhu, S. Zheng, L. Zhao, M. Chen, W. J. Riley, X. Cai, H. Ma, F. Li, H. Wu, and L. Chen (2021). “Deforestation Reshapes Land-Surface Energy-Flux Partitioning”. *Environmental Research Letters* 16.2, 024014. DOI: 10.1088/1748-9326/abd8f9.
- Zhan, S., C. Song, J. Wang, Y. Sheng, and J. Quan (2019). “A Global Assessment of Terrestrial Evapotranspiration Increase Due to Surface Water Area Change”. *Earth’s Future* 7.3, 266–282. DOI: 10.1029/2018EF001066.
- Zhang, K., J. S. Kimball, Q. Mu, L. A. Jones, S. J. Goetz, and S. W. Running (2009). “Satellite Based Analysis of Northern ET Trends and Associated Changes in the Regional Water Balance from 1983 to 2005”. *Journal of Hydrology* 379.1, 92–110. DOI: 10.1016/j.jhydro1.2009.09.047.
- Zhou, W., L. Wang, D. Li, and L. R. Leung (2021). “Spatial Pattern of Lake Evaporation Increases under Global Warming Linked to Regional Hydroclimate Change”. *Communications Earth & Environment* 2.1, 1–10. DOI: 10.1038/s43247-021-00327-z.

# Statement of authorship contribution

The general research direction of this thesis was proposed by my promotors, Bart van den Hurk, and other applicants of the SWM-EVAP project (Smart Water Management - EVAPoration). The research topic was rooted in the need expressed by water managers in the Netherlands and therefore this research project also received their support. Based on the ideas proposed in the SWM-EVAP project, I formulated the research plan and specific research questions. I wrote the introduction (Chapter 1) and the synthesis (Chapter 6), with minor suggestions from my promotors. Chapter 2 provides a description of the study area, data and measurement methods from the core Chapters 3–5. Therefore, Chapter 2 has the same author contributions as the listed contributions to Chapters 3–5 below. An overview of the author contributions to the core Chapters 3–5 is listed below. Names have been abbreviated in the following way:

FJ = Femke Jansen (WUR)

AB = Alexander Buzacott (VU)

BK = Bart Kruijt (WUR)

CJ = Cor Jacobs (WEnR)

EM = Eddy Moors (VU/IHE)

GS = Gert-Jan Steeneveld (WUR)

MM = Michiel van der Molen (WUR)

RU = Remko Uijlenhoet (TUD)

BH = Bert Heusinkveld (WUR)

BV = Bernard Voortman (MM)

CT = Christiaan van der Tol (UT)

FB = Fred Bosveld (KNMI)

HJ = Harro Jongen (WUR)

RT = Ryan Teuling (WUR)

YV = Ype van der Velde (VU)

## Chapter 3

Conceptualization:

FJ, RT

Data collection:

FJ

Data analysis and interpretation:

FJ in consultation with RT

Writing of manuscript:

FJ

Revision of manuscript and approval for publication:

RT

**Chapter 4**

Conceptualization:	CJ, FJ, RT, RU
Data collection:	FJ, RT, supported by Pieter Hazenberg (WUR)
Data analysis and interpretation:	FJ in consultation with CJ, RT, RU
Writing of manuscript:	FJ
Revision of manuscript and approval for publication:	CJ, RT, RU

**Chapter 5**

Conceptualization:	FJ, HJ, RT, RU
Data collection:	AB, BH, BK, CJ, CT, EM, FB, FJ, GS, HJ, MM, RT, YV
Data analysis and interpretation:	FJ in consultation with HJ, RT, RU
Writing of manuscript:	FJ with contributions from RT
Revision of manuscript and approval for publication:	AB, BH, BK, BV, CJ, CT, EM, FB, GS, HJ, MM, RT, RU, YV

# Acknowledgements

‘Weaving dissolves the illusion of separation  
It makes the invisible interconnectiveness between All visible  
It gives life to the image of connectiveness  
It connects space and time,  
life and death,  
it connects bodies of the Earth  
We are weaving bodies connected through the weaving water that moves in us’

---

Water is constantly moving and transforming and I feel similar about my journey through this PhD trajectory. Throughout these years, I have faced many challenges, and have gone through phases of strong resistance, but I also experienced moments of joy for instance when I was high up in the air to install our measurement installations and during all the brightening laughs I had with my fellow PhD colleagues. During these years life unfolded and I grew. What I learned most is to follow my nature and the wildness inside. Life is too short to ignore that. I am curious where this will bring me. I would like to take this opportunity to thank the people who have joined and helped me on this journey through (PhD) life.

First of all, I would like to thank my supervisors Ryan and Remko. Thank you for giving me the opportunity to start this project and for providing support on both a professional and personal level all the way to the end. Ryan, thank you for your daily supervision and our Arboretum walking meetings during Covid times. I have appreciated the clarity you gave whenever I was not sure which way to move forward in the project. This always helped me to gain renewed energy and to keep the bigger picture in mind. Remko, thank you for your always positive, constructive and detailed feedback and suggestions on my work. This has made me enthusiastic to try out additional analyses, which often led to interesting results. Not to forget, thanks to your detailed comments on my manuscripts, I found myself at the top of our office’s *highest number of comments per chapter/paper* ranking (471 comments on a piece of text was no exception). Much appreciated!

Besides my promotors, I would like to thank some other people who were crucially important to bring this project to a successful conclusion. Cor Jacobs, thank you for being involved almost from the start of my project. All my co-authors, for your ideas, input and

feedback. Ruud Hurkmans, thanks for managing the SWM-EVAP project which my PhD project was part of. Furthermore, I would like to thank Wim Werkman and Bas de Jong for being involved in the SWM-EVAP project from the perspective of Rijkswaterstaat, as well as Klaas Groen and Charlotte Schmidt from Rijkswaterstaat for seeing the value and importance of conducting proper open water evaporation measurements. Considering my fieldwork, this would not have been possible without the kind help and cooperation of the managers of the harbour in Stavoren, the volunteers and employees from Natuurmonumenten and Boskalis for sailing us to the Marker Wadden, and the employees from Rijkswaterstaat and Novec who helped us to get access to Trintelhaven.

In addition, I received a lot of practical help from within HWM as well to conduct the fieldwork. Pieter and Jelte, you both have been invaluable. Without your help the observations of open water evaporation would not have been there. Thank you for the numerous *gezellige* car trips to Stavoren and Trintelhaven, building the scaffolding every time again to reach up high! And a big thank you to my other HWM colleagues who helped me numerous times with my fieldwork, no matter what the weather was like (cold and windy weather are no joke if you are used to tropical conditions).

It has been amazing to have experienced how HWM has grown and transformed into a more international group. I feel very rich to interact on a daily basis with colleagues from all over the world coming from different backgrounds. I especially would like to thank my dear office mates Linda, Rahel, Janneke, Sjoukje, Marjanne, and Tessa when around. What a joy it has been sharing the office with you ladies and ‘what happens in the ladies office, stays in the ladies office!’. It is for a reason that on many occasions the entire hallway (Iris, Joris, Jelte, Judith, Mo, Henk, Ruben, Rose *The Queen*) could hear our laughter. But I also appreciate the deeper and honest conversations that we have had. Thank you! Let’s always stay Young and Hot. Furthermore, I would like to thank Harro for your support and ideas working towards my last paper, and Tamara for your kind presence and support with all the administrative paperwork along the way.

Dearest Daphne and Geerte, my fairytale paranympths, your light and supporting presence and friendship is very dear to me. Thank you for that. Daphne, I love your craziness and humour, it is very contagious. Whenever and wherever we meet, there is always time for a silly dance. Think of it as a friendly greeting, but in our own crazy way. I have enjoyed our yearlong bushcraft course together so much. It was you who actually introduced me to this course, and what an amazing adventure this resulted into. To spend time together in the woods has been very important to me as a counterbalance to this PhD project. Geerte, I find it so amazing to have such a lovely friendship that seems to have been there forever. I always enjoy it when we are sharing time and space together (be it in the dance studio or outside). It feels like home. Thank you for your joyful energy, honest questions and feedback throughout these years. This has supported me to start seeing what is important

to me. Dear paranymphs, with both of you I feel a deep and natural connection. Thank you for being my wings during the defence ceremony!

To be honest, I do not think I could have completed this PhD journey, if I would not have been dancing and ‘bushcrafting’ alongside my work on this PhD thesis. Marisa, having you as my dance teacher and my friend has made me tap into my fire, vitality and wild nature again. Thank you so much! I am grateful that you started the ELAP program in collaboration with Iris, my other great dance teacher. This program has served as a ground to move on and provided a space to go through resistances, so I could transform and grow deeper to rise more rooted. Thanks to all ELAPers for the journey we took and a special thanks to our amazing cook Raül, you are very dear to me. Antípodas, it is great to meet in the studio and weave through! Beke and René, thank you for sparking the vital fire in me and teach me so many bushcraft skills. Moreover, thank you for supporting my autonomy and self-sufficiency in connection with nature (inside and outside). I have spend two years in the woods with you together with the wonderful JO and VO groups. It has been so amazing and I am looking forward to all the adventures yet to come.

I would like to thank a couple of more people. Susan, thank you for all our walks and talks, sharing about life unfolding, and thank you for using your wonderful art skills to draw up a summary of this thesis. My housemates, it has been great to share home office during corona time. Furthermore, I would like to thank all the dear people that I got to know through our connection with my dearest friend Ronja. Around Ronja’s sudden illness and death, such a strong and loving web of connection was created. Thank you, Bärbel and Martin for allowing us to be so close to you and your daughter in this time. Matthias and Lotte, I could not have wished for more beautiful people to have shared this intense and precious time with (with a lot of chocolate to keep us going). Now I wish to continue this web of support for you Matthias. Wishing you, Aldona and your son all the strength!

Lastly, I would like to thank my parents and brother. You have supported me throughout my life in all my decisions and you always showed genuine interest in the PhD work I was doing, even if it sometimes felt challenging to give the full picture of what it actually was that I was working on. Thank you for standing with me. And of course, last but not least, I would like to thank my dearest partner Marijn. Thank you for always being there and for your support all the way through this sometimes challenging journey. I look forward to continuing feeding our fire.



*Netherlands Research School for the  
Socio-Economic and Natural Sciences of the Environment*

# D I P L O M A

*for specialised PhD training*

The Netherlands research school for the  
Socio-Economic and Natural Sciences of the Environment  
(SENSE) declares that

***Femke Anouk Jansen***

born on 17 August 1991, Huizen, The Netherlands

has successfully fulfilled all requirements of the  
educational PhD programme of SENSE.

Wageningen, 7 June 2023

Chair of the SENSE board



Prof. dr. Martin Wassen

The SENSE Director



Prof. Philipp Pattberg

*The SENSE Research School has been accredited by the Royal Netherlands Academy of Arts and Sciences (KNAW)*



K O N I N K L I J K E N E D E R L A N D S E  
A K A D E M I E V A N W E T E N S C H A P P E N



The SENSE Research School declares that **Femke Anouk Jansen** has successfully fulfilled all requirements of the educational PhD programme of SENSE with a work load of 42.1 EC, including the following activities:

#### SENSE PhD Courses

- o Environmental research in context (2017)
- o Research in context activity: 'Organizing stakeholder workshop and creating video impression on Smart Water Management – Evaporation' (2019)

#### Other PhD and Advanced MSc Courses

- o Research data management, Wageningen Graduate Schools (2017)
- o Brain friendly working and writing, Wageningen Graduate Schools (2018)
- o Scientific writing, Wageningen Graduate Schools (2018)
- o Workshop Eddy Covariance – on the principles, technique and use of EC equipment and processing tools, CaTeC (2019)
- o Project and time management, Wageningen Graduate Schools (2019)
- o Training on the use and calibration of IRGASON measurement equipment, Wageningen University (2021)

#### Management and Didactic Skills Training

- o Organize GEWEX ET 2nd workshop (2021)
- o Organize writing week chairgroup HWM (2022)
- o Supervising two MSc students and one BSc student with thesis (2018-2021) and one MSc student with the internship (2018)
- o Assisting practicals in the BSc courses 'Water 1' (2017-2021) & 'Water Quality and Quantity' (2020)
- o Assisting practical and excursion in the MSc course 'Urban Hydrometeorology' (2020-2021)
- o Assisting practicals in the MSc courses 'Catchment and Climate Hydrology' (2020-2021) & 'Interdisciplinary Topics in Earth and Environment' (2022)
- o Co-author of Deltafact 'Verdamping', STOWA (2020)

#### Oral Presentations

- o *Openwaterverdamping*. Water Science for Impact, 18 October 2018, Wageningen, The Netherlands
- o *SWM-EVAP Openwaterverdamping*. NKWK, 14 May 2019, Delft, The Netherlands
- o *ET workshop – State of the art and future challenges*. GEWEX, 10- 12 February 2021, Wageningen, The Netherlands
- o *Evaporation from a large lowland reservoir – observed dynamics during a warm summer*. EGU, 29 April 2021, Online

SENSE coordinator PhD education

Dr. ir. Peter Vermeulen



The research presented in this thesis is part of the SWM-EVAP project financially supported by the Dutch Research Council (NWO) under grant number ALWTW.2016.049 of the *Topsector Water Call* Research Programme. Additional funding for the measurement campaign of open water evaporation was provided by Rijkwaterstaat - Water, Verkeer en Leefomgeving under grant number 31141561 (Open-waterverdamping IJsselmeer). The research was carried out at the Hydrology and Quantitative Water Management Group, Department of Environmental Sciences, Wageningen University & Research (Wageningen, the Netherlands).

Financial support from Wageningen University for printing this thesis is gratefully acknowledged.

Cover design:	Femke Jansen and Geerte de Koe
Layout design:	Femke Jansen, using $\text{\LaTeX}$
Printed by:	ProefschriftMaken on FSC-certified paper

